New copolymers based on poly(dopamine) for the sustained delivery of active pharmaceutical ingredient to the eye by intravitreal administration

Floriane Bahuon

THÈSE POUR OBTENIR LE GRADE DE DOCTEUR DE L'UNIVERSITÉ DE MONTPELLIER

En Chimie et Physico-Chimie des Matériaux

École doctorale Sciences Chimiques Balard (ED 459)

Unité de recherche : Institut des Biomolécules Max Mousseron (IBMM-UMR 5247)

Nouveaux systèmes polymères à base de poly(dopamine) pour la délivrance prolongée de principes actifs par administration intravitréenne

Présentée par Floriane BAHUON

Le 30 Septembre 2021

Sous la direction de Benjamin NOTTELET et Vincent DARCOS

Devant le jury composé de

Christine JEROME, PU, Université de Liège	Rapporteure
Joël LYSKAWA, MCU, Université de Lille	Rapporteur
Amélie BOCHOT, PU, Université Paris-Saclay	Examinatrice
Emmanuel BELAMIE, Directeur d'étude, EPHE	Examinateur
Benjamin NOTTELET, PU, Université de Montpellier	Directeur de thèse
Vincent DARCOS, IR, CNRS	Co-directeur de thèse
Jean COUDANE, PUEm, Université de Montpellier	Encadrant
Grégoire SCHWACH, PhD, F.Hoffmann-La Roche	Encadrant

Remerciements

Je souhaite adresser mes sincères remerciements au jury qui m'a fait l'honneur d'évaluer mes travaux : les rapporteurs, Pr. Christine Jérôme du CERM à l'Université de Liège, Dr. Joël Lyskawa de l'équipe ISP de l'Université de Lille et les examinateurs, Pr. Amélie Bochot de l'Institut Galien Paris-Saclay, et Emmanuel Belamie, Directeur d'études à l'Ecole Pratique des Hautes Etudes, ICGM.

Je tiens sincèrement à remercier le Dr. Grégoire Schwach pour m'avoir fait confiance sur ce projet de thèse. Merci également pour les échanges scientifiques que nous avons eus, pour tes conseils judicieux et pour l'apport de ton point de vue industriel qui m'ont permis de mener à bien ce projet.

Mes remerciements vont ensuite au Pr. Jean Coudane pour m'avoir accueillie au sein du laboratoire département PHBM (Polymers for Health and Biomaterials) de l'IBMM. Je te remercie pour toutes les discussions enrichissantes que nous avons eues, les nombreux calculs et les tableaux Excel ! Merci pour tous les bons moments passés au laboratoire ou autour d'un verre.

Je tiens à exprimer mes remerciements les plus chaleureux et ma profonde gratitude à mon directeur de thèse le Pr. Benjamin Nottelet. Merci pour ta disponibilité, tes conseils, ton optimisme. Merci d'avoir compris mon fonctionnement et de m'avoir guidée tout au long de ces presque 4 années, tant sur l'aspect scientifique que personnel. Merci d'avoir eu confiance en moi et de m'avoir donné confiance jusqu'au bout.

J'exprime mes remerciements et ma reconnaissance les plus sincères à mon co-directeur de thèse le Dr. Vincent Darcos. Merci pour le tout le temps passé avec moi à la paillasse, au bureau, pour tes précieux conseils et pour m'avoir également guidée pendant cette thèse. Merci pour la confiance que tu m'as accordée, et celle que j'ai ainsi pu développer. Une mention spéciale pour le dessiccateur le premier jour au laboratoire que l'on ne reverra jamais !

Je tiens également à remercier l'ensemble des personnes avec lesquelles j'ai pu travailler ou que j'ai rencontrées chez F.Hoffmann-La Roche. Je remercie tout particulièrement les Drs. Sulabh Patel et Sima Rahimian pour leurs conseils scientifiques et Zana Marin pour sa contribution aux manipulations.

Tout ce travail n'aurait pu s'effectuer sans l'extraordinaire équipe du laboratoire. Je vous remercie tous pour le soutien, les encouragements, les conseils, la joie que vous m'avez apportée. Je pense aussi à tous les moments que nous avons passés ensemble, les séances de sports, les activités de team-building, les soirées, les moments partagés au quotidien.

Je tiens ainsi à remercier Xavier pour son sens de la communication, Hélène, Cédric, Carine, Coline pour son initiation à l'HPLC et ses conseils sur l'organisation, Sylvie pour tous ses conseils sur la GPC à n'importe quelle heure de la journée (ou de la nuit !), Audrey pour son temps passé sur la biologie et Stéphane pour son aide précieuse au laboratoire (1 euro !).

Mille mercis aux doctorants, post-doctorants, stagiaires, ingénieurs qui sont, ou sont passés, au laboratoire. Samantha, ma binôme dans la folie ; Elo, ma panama girl ; Carlos, mi guapo; Mathilde G ; Mathilde M ; Gabriele ; Hadda, les craquages musicaux après 18h ; Victor M ; Salomé ; Clémence ; Werner ; Eloise ; Marie M. ; Christopher ; Prescillia, ma coloc de paillasse de première année ; Victor D. dit papi ; Louis ; Karima ; Teddy ; Mickaël ; Baptiste. Vous avez chacun illuminé mes journées.

Je voudrais chaleureusement remercier tous mes amis quimpérois, lorientais, nantais bordelais, montpellierains, et d'ailleurs qui ont été présents pendant ces années pour votre soutien sans faille et pour nos échappées, nos escapades, nos soirées, nos week-ends sportifs et moins sportifs. Vous êtes fabuleux et j'ai hâte de repartager des moments avec vous. Je pense particulièrement à Anaïs ma chérie & Antoine ; Dorian B. mon frère ; Sylvain partenaire de mixte ; Lorie ; Jules ; Yann ; Romain ; Alexia ; Oliver ; Théo ; Alice ; Sophie ; Camille-Anne ; Tim ; Thierry ; Roxane ; Vincent mon fils ; Carole ma maman ; Chloé ; Mathilde ; Lise ; Alice ; le MBC, ABIL & tous les autres clubs !

Evidemment, je tiens à remercier ma famille, mes parents et ma petite sœur pour leur soutien au quotidien, leurs encouragements, la confiance et la fierté que vous me portez depuis tant d'années. Merci d'avoir toujours été là pour moi, à l'écoute à tout moment de la journée et de la nuit, et ce malgré la distance. Je vous aime.

Grace à vous tous, j'ai pu porter ce projet jusqu'au bout.

J'ai tant appris, scientifiquement et humainement.

Encore une fois, merci.

Table of content

Main abbreviations

Polymers, products and solvents

API	active pharmaceutical ingredient
BPO	benzoyl peroxide
DEX	dexamethasone
CIP.HCl	ciprofloxacin hydrochloride
CL or CL-I	ε-caprolactone or iodinated ε-caprolactone
FITC-BSA	Fluorescein isothiocyanate labelled bovine serum albumin
LDA	lithium diisopropylamide
PCL	poly(ε-caprolactone)
PCL X	poly(ε-caprolactone) with a total molecular weight of X $g.mol^{-1}$
PCL-I	iodinated poly(ε-caprolactone)
PCL-*g*-PDA	poly(ε-caprolactone)-*graft*-poly(dopamine)
PLGA	poly(lactic-*co*-glycolic acid)
PEG	poly(ethylene glycol)
PEG X also PEG_x	poly(ethylene glycol) with a total molecular weight of X $g.mol^{-1}$
PCL-*b*-PEG-*b*-PCL	poly(ε-caprolactone)-*block*-poly(ethylene glycol)-*block*-poly(ε-caprolactone)
PCL_Y-PEG_X-PCL_Y also y-x-y	PCL-*b*-PEG-*b*-PCL with a PCL molecular weight of Y $g.mol^{-1}$ and PEG of X $g.mol^{-1}$
T	PCL-*b*-PEG-*b*-PCL
(PCL-I)-*b*-PEG-*b*-(PCL-I)	Iodinated poly(ε-caprolactone)-*block*-poly(ethylene glycol)-*block*-poly(ε-caprolactone)
T-I	(PCL-I)-*b*-PEG-*b*-(PCL-I)
PDA	poly(dopamine)
(PCL-*g*-PDA)-*b*-PEG-*b*-(PCL-*g*-PDA)	(poly(ε-caprolactone)-*graft*-poly(dopamine))-*block*-poly(ethylene glycol)-*block*-(poly(ε-caprolactone)-*graft*-poly(dopamine))
T-PDA	(PCL-*g*-PDA)-*b*-PEG-*b*-(PCL-*g*-PDA)
PMDETA	*N*,*N*,*N'*,*N'*,*N''*-pentamethyldiethylenetriamine
$Sn(Oct)_2$	tin(II) 2-ethylhexanoate
DMSO	dimethylsulfoxide
DMF	dimethylformamide
THF	tetrahydrofuran
PBS	phosphate buffer solution
HBS	histidine phosphate buffer solution
VH	vitreous humor
mAb	Monoclonal antibody
L929	mouse fibroblast cell

ARPE-19	Adult human retinal epithelial cell

Analytical techniques

NMR	nuclear magnetic resonance
^{1}H-NMR or DOSY-NMR	proton or diffusion ordered NMR
DSC	differential scanning calorimetry
TGA	thermogravimetric analysis
HPLC	high- performance liquid chromatography
SEC	size exclusion chromatography
IOP-OES	inductively coupled plasma optical emission spectrometry
UV	ultraviolet

Physico-chemical characteristics

Ti	degree of substitution by iodine
$M_{moitiesinPCL\text{-}I}$	number average molecular weight of a unit in an iodinated PCL chain
M_w	weight average molecular weight
M_n	number average molecular weight
$Đ$	dispersity
DL	drug loading
DR	drug released
w_i	initial weight
$w_{w,t}$ or $w_{d,t}$	wet or dry weight after t time
ΔH	enthalpy of fusion
χ	degree of crystallinity
T_g	glass transition temperature
T_m	melting temperature

Others

IVT	intravitreal
FDA	Food and Drug Administration
ExVit-HS	Ex vivo intravitreal horizontal stability

List of Figures

CHAPTER I. CONTEXT AND STRATEGIES

CHAPTER II. INJECTABLE IMPLANT SYSTEMS BASED ON GRAFT COPOLYMERS CONTAINING PCL AND PDA (PCL-g-PDA) FOR SUSTAINED DRUG RELEASE

CHAPTER III. INJECTABLE GELLING SYSTEMS BASED ON COPOLYMERS CONTAINING PCL, PEG AND PDA ((PDA-g-PCL)-b-PEG-b-(PCL-g-PDA)) FOR SUSTAINED RELEASE OF BIOLOGICS

List of Tables

CHAPTER I. CONTEXT AND STRATEGIES

CHAPTER II. INJECTABLE IMPLANT SYSTEMS BASED ON GRAFT COPOLYMERS CONTAINING PCL AND PDA (PCL-g-PDA) FOR SUSTAINED DRUG RELEASE

CHAPTER III. INJECTABLE GELLING SYSTEMS BASED ON COPOLYMERS CONTAINING PCL, PEG AND PDA ((PDA-g-PCL)-b-PEG-b-(PCL-g-PDA)) FOR SUSTAINED RELEASE OF BIOLOGICS

List of Schemes

CHAPTER I. CONTEXT AND STRATEGIES

CHAPTER II. INJECTABLE IMPLANT SYSTEMS BASED ON GRAFT COPOLYMERS CONTAINING PCL AND PDA (PCL-g-PDA) FOR SUSTAINED DRUG RELEASE

CHAPTER III. INJECTABLE GELLING SYSTEMS BASED ON COPOLYMERS CONTAINING PCL, PEG AND PDA ((PDA-g-PCL)-b-PEG-b-(PCL-g-PDA)) FOR SUSTAINED RELEASE OF BIOLOGICS

GENERAL INTRODUCTION

The ocular diseases refer to any condition or disorder that interferes with the ability of the eye to function properly and/or that negatively affects the visual clarity. In 2015, around 216.6 million people were visually impaired and another 36 million people were estimated to be blind worldwide [1], thus ocular diseases are a major public health issue. Among them, the retinal diseases are a particular class of posterior segment eye diseases, which include the age-related macular degeneration (AMD), the diabetic retinopathy (DR) and diabetic macular edema (DME).

Intravitreal administration (IVT) refers to the administration of a dosage formulation or a medical device in the vitreous cavity and is, up to now, the most efficient method to deliver active pharmaceutical ingredients (APIs) to the retina. While becoming routine thanks to the breakthrough of biologics for the treatment of AMD and DME, IVT administration bears some risks, and a lack of compliance is one of the main reasons for sub-efficient treatments. The other main challenges are the tolerability of longer acting treatments in terms of biologics storage and biocompatibility of the formulation. A decrease in injection frequency is thought to be a way to improve patient compliance and adherence to the treatment by developing formulations or devices allowing the retention of the APIs. Formulations (solid, solution, suspension) based on polymer technology are marginal and recent. Scientists are focusing their efforts on developing biocompatible, (bio)degradable or not, formulations providing long and sustained delivery of APIs with a minimal surgery operation in order to increase the well-being of patients and to reach therapeutic level to treat efficiently the ocular diseases.

Poly(dopamine) (PDA) is a synthetic analogue of melanin [2] which is naturally present in the retinal cells. The interest in PDA is quite recent and the science of PDA is young. It has already been used for medical application in imaging and cancer therapy [3] thanks to its interesting properties of biocompatibility, degradability, photo-thermal conversion and drug-binding affinity, to name of few. [4] The use of PDA is marginal in medical applications, and PDA has never been studied for ophthalmic applications. The introduction of PDA moieties in already existing polymers, suitable for introduction into the eye, and its effect regarding the release kinetics of APIs would be major innovations.

The FDA has approved the use of non-degradable [5–10] (Vitrasert®, Retisert™, Iluvien™) and degradable [7,11] (Ozurdex™) implants for the delivery of low molecular weight (small) hydrophobic drugs. They can either surgically placed and attached to the edges of the vitreous cavity (non-degradable implants) or injected with a 22-27G needle (non-degradable and degradable implants). In both cases, the solid implants showed interesting properties for sustained delivery (from 3 months to 3 years depending on the composition) and storage capacity. However, the implantation and even injection are more invasive techniques and can lead to severe complications, cataract formation, retinal detachment and infections.

Currently, the delivery of biologics using a formulation based on polymer technology has not received viable and FDA-approved solution yet. Indeed, biologics are often denatured [12] and tend to interact with the drug vehicle. However, biologics are efficient in the treatment of retinal diseases, particularly AMD and DR. According to the estimated 230 million people suffering from AMD in 2030 [13,14], the delivery of biologics represents a major breakthrough.

The work of this thesis was carried out at the *Polymer for Health and Biomaterials Department at IBMM (Montpellier, France)* and at department of the Pharmaceutical Development, PTD Biologics Europe in F.Hoffmann-La Roche *(Basel, Switzerland)*. The topic of the thesis was to investigate the potential and the benefits of including PDA units in synthetic copolymers for ophthalmology. The main objective of the project was the design of new polymers for the sustained delivery of APIs (small or large molecules) into the vitreous by exploiting the PDA and drug interactions. The products specifications were drawn at the beginning of the project. The APIs vehicle must be under solid form or under liquid form to inject it through fine needles. For each strategy of administration, the formulation must be biocompatible, degradable to avoid repetitive surgical operations and composed at least partly of poly(dopamine). Finally, the formulation must show sustained release of APIs, small hydrophobic drug or biologics, for a period from 1 to 6 months.

The project presented in the manuscript focused on the synthesis of grafted copolymers based on poly(ethylene glycol) (PEG) and/or poly(ε-caprolactone) (PCL) functionalized with PDA. PCL was chosen because (1) it is accepted by the Food and Drug Administration for medical application (not ophthalmology yet), (2) it biodegrades slowly, (3) functionalization is possible and (4) it is commercially available. PEG was chosen because (1) it is accepted by the Food and Drug Administration for ophthalmology, (2) it is commercially available, (3) the synthesis of amphiphilic block copolymer with PCL is possible providing an aqueous environment favouring the stability of biologics and (4) its gelation properties can be modulated. PDA was selected as functional group of the PCL and or PCL/PEG copolymers to exploit the presence of catechol and amine and their interactions with APIs to enhance the release over longer period of time.

The manuscript is divided into three chapters.

Chapter I is a bibliographic research study on the anatomy of the eye, the possible disorders and the strategies to treat them. This bibliographic part also includes the synthesis of PDA-based materials and their use for medical applications. This chapter also presents the commercial solid implantable/injectable systems and the research ongoing for the development of injectable liquid formulation. From the collected information, specifications and strategies will be finally outlined.

Chapter II is dived into two sections dedicated to the design of degradable implants based on synthetic aliphatic polyester PCL and PDA. Section 1 deals with the synthesis and the properties of the grafted copolymer PCL-*g*-PDA. Section 2 deals with the preparation of drug-unloaded and loaded films of PCL-*g*-PDA. Their thermal properties, their structure evolution during degradation and their biological properties are evaluated. Section 3 deals with the evaluation of the kinetics of *in vitro* release of APIs. The choice of APIs and the composition of the polymer matrix are discussed.

Chapter III is divided into three sections dedicated to the design of *in situ*-gelling system based on PCL, PEG and PDA. Section 1 deals with the synthesis and the properties of the grafted amphiphilic copolymer of PCL/PEG and PDA. Section 2 deals with the elaboration a formulation suitable for injection through a fine needle and maintaining the stability of biologics. The choice of a cosolvent, the solubility of the compounds and the composition of the formulations are discussed. Section 3 deals with the formation and the formulation of an *in-situ* forming depot and the evaluation of the kinetics of *in vitro* release of biologics.

CHAPTER I.

CONTEXT AND STRATEGIES

1. Structure of the eye and emergence of strategies dedicated to the treatment of ocular diseases

1.1 Structure of the eye

The eye is a unique organ that reacts to lights and allows vision. The eye can be divided in two segments: anterior and posterior. The anterior segment is composed of the cornea, the iris, the pupil, the lens and the aqueous humor. The posterior segment is composed of the retina, the choroid, the sclera and the vitreous humor (**Figure 1**). [15]

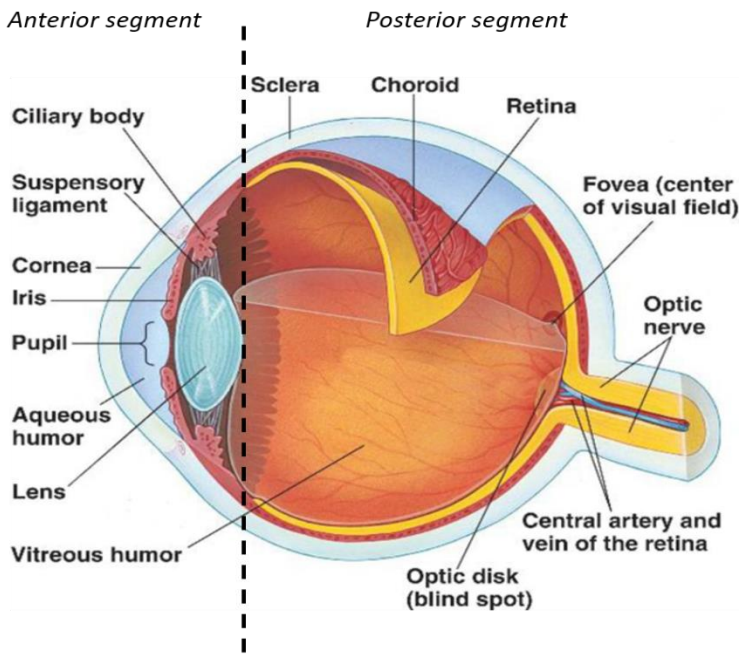

Figure 1. Schematic representation of a human eye [15]

For people with normally functioning eyes, ray light enters the eye through the cornea, converges, passes through the aqueous humor and enter the pupil that regulates the amount of light by varying its size. Subsequently, the ray lights reach the lens which bends the light by varying its thickness, they pass tough the vitreous humor and converge to the back of the eye to hit one particular point of the retina, called fovea/macula. Then, the retina translates light into electrical impulses thanks to the action of light-sensitive retinal receptors (cones and rods). Those electrical impulses are carried out to the brain thanks to the optic nerve and the visual cortex of the brain interprets these impulses as what we see. If any part or any function of the eye is damaged, the light and electrical pathways are compromised, which cause vision problems.

1.2 Ocular Diseases, disorders and drugs to treat them

In 2015, around 36 million people were estimated to be blind and another 216.6 million visually impaired worldwide. Most of them were people over 50 years old. The main causes of partial and total visual loss come from uncorrected refractive error (RE) (myopia, hypermetropia, astigmatism and presbyopia), from cataract and glaucoma in anterior segment of the eye, and age-related macular degeneration (AMD), diabetic retinopathy (DR) and the uveitis in the posterior segment. (**Figure 2**). [1,16]

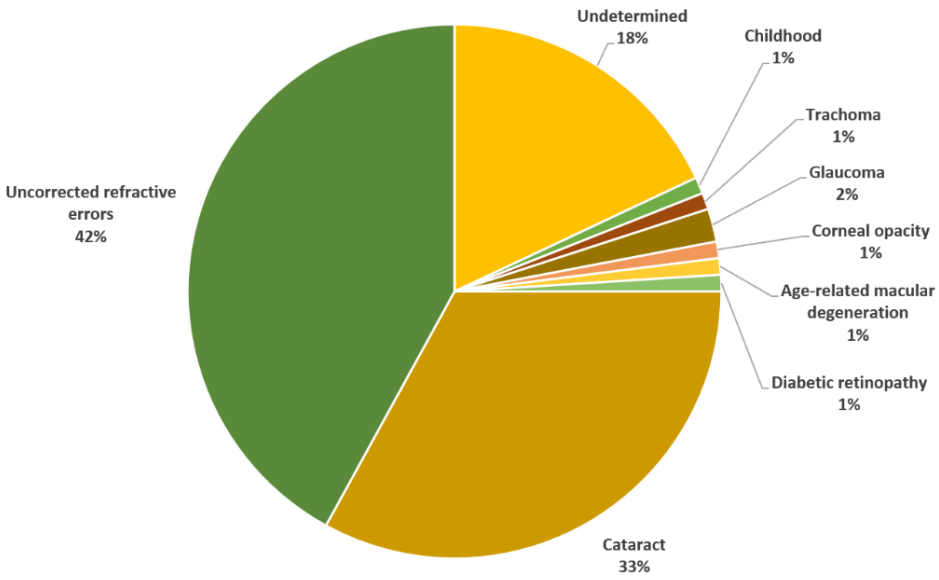

Figure 2. Global causes of visual impairments, blindness included, around the world in 2010 [1]

1.2.1 Anterior segment diseases

Cataract is the opacification of the crystalline lens leading to a progressive vision loss and blindness. Type of cataract differs from the localisation and from the cause. It can be partial or complete, stable or progressive, soft or hard. It is commonly due to aging but may also occur due to trauma, genetic inheritance, skin diseases, diabetes, alcohol or tobacco consumptions, radiation exposure or use of corticoids.

Glaucoma results from the progressive degeneration of the optic nerve leading to irreversible vision loss then blindness. Causes of glaucoma include increased pressure in the eye, hypertension or high blood pressure, genetics and prolonged use of steroids. In open-angle glaucoma pathology, the angle formed by iris and cornea intersection is as opened as it should be. However, the slow degeneration and obstruction of draining canals (trabecular meshwork), whose function is to eliminate aqueous humour from the eye to anterior chamber, increases the intraocular pressure (IOP) and damages the optic nerve. In closed-angle glaucoma pathology, the angle formed by iris and cornea intersection differs from the normal value, the iris blocks the draining canals that accumulate liquid resulting in a sudden increase of intra ocular pressure and pain.

1.2.2 Posterior segment diseases

Age-related macular degeneration (AMD) is a retinal disease induced by the progressive degeneration of the macula, the central part of the retina. Typical signs and symptoms include a decrease of visual acuity and a distorted vision or blurred vision. Around the world, over 6 million people are affected, most of them over 50 years old. The early-stage AMD is characterized by the presence of medium-sized drusen, which are extracellular materials, in the retina. In intermediate stage AMD, the drusen are larger and retinal abnormalities appear. The advanced stage AMD can be qualified as dry or wet. Dry AMD is non-neovascular and regroups early and intermediate stages and geographic atrophy that lead to irreversible loss of retinal cells and visual functions. Dry AMD can progress to a wet form, a neovascular condition which leads to vision loss due to abnormal blood vessel growth in the retina. Those blood vessels, which are more fragile than healthy ones, may cause bleeding, leaking of blood proteins and irreversible damages to photoreceptors. This leads to a macular oedema, a thickening of the macula (i.e., the central portion of the retina) and causes vision loss.

Diabetic retinopathy (DR) is a retinal disease induced by an over accumulation of glucose damaging blood vessels and neurons of the retina. It affects more than 80% of diabetic people from the age of 20 and almost 100% of them risk developing it over 30. The early stage of DR is qualified as non-proliferative diabetic retinopathy (non-PVR), no signs and symptoms are detectable. The second stage of DR is qualified as proliferative diabetic retinopathy (PVR) in which abnormal blood vessels grow and bleed. DR can either lead to macular oedema, as AMD, or ischemia, which is a restriction of blood supply to tissue.

Uveitis is the inflammation of the uvea which is composed of the iris, the ciliary body and the choroid. Such inflammations are called the anterior, intermediate and posterior uveitis, respectively. In case of inflammation of all the layers, it is called panuveitis. Main signs and symptoms are blurred vision in all cases, redness of the eye, photophobia and headaches for anterior uveitis, presence of dark sports floating in the visual fields (floaters) for intermediate uveitis, floaters and flashing lights for posterior uveitis. Uveitis is commonly associated with other medical disorders such as infectious, non-infectious or autoimmune causes and systemic diseases.

Cytomegalovirus (CMV) retinitis is a viral retinal disease associated with the acquired immunodeficiency syndrome (AIDS) and immunosuppressive therapies. Main signs and symptoms are blurred vision due to floaters or blind spots without photophobia, progressing from one eye to the other. It infects the retina and lead to necrosis, causing blindness, and retinal breaks and detachments.

1.2.3 Small molecule drugs and proteins used for the treatment of ocular diseases and disorders

The most common small molecule drugs and proteins approved by the FDA or used off-label to treat ocular diseases are listed in **Table 1**. Typically, anterior segment diseases are treated with small molecules. Concerning the posterior segment of the eye diseased, the wet AMD is treated with biologics such as anti-Vascular Endothelium Growth Factor agent (anti-VEGF agent), and the diabetic retinopathy and the diabetic macular oedema are treated both with biologics and small molecules.

Table 1. FDA approved and off-label (*) small molecule drugs and biologics used for the treatment of ocular diseases and disorders.

Name	Molecular weight **	Water solubility (mg/mL) ***	Route of administration	Therapy	Clinical phase
Small molecule drugs					
Ganciclovir (GVC)	255.2 $g.mol^{-1}$	11.5	IVT, IV, topical	CMV retinitis, herpetic keratitis	FDA-approved (1989)
Cyclosporine A (CsA)	1202.7 $g.mol^{-1}$	<0.01	Topical	Inflammations, uveitis, dry eye	FDA-approved (2002)
Tacrolimus (FK-506)	804 $g.mol^{-1}$	<0.01	Topical, scleral	corneal graft rejection*, scleritis*, uveitis*	off-label
Dexamethasone (DEX)	392.5 $g.mol^{-1}$	0.05	Topical, IVT	Inflammations, uveitis, DME*	FDA-approved (2004)
Fluocinolone acetonide (FA)	452.5 $g.mol^{-1}$	<0.01	IVT	Inflammations, uveitis, DME	FDA-approved (1995)
Ciprofloxacin (CIP)	331.1 $g.mol^{-1}$	1.35	Topical	Inflammation*, uveitis*, bacterial keratitis*	off-label
Biologics					
Bovine serum albumin (BSA)	66 kDa	40	N/A	N/A	Model
Ranibizumab	48 kDa	Freely soluble	IVT	Wet AMD, DME, DR*	FDA-approved (2006)
Bevacizumab/ Avastin ®	149 kDa	Freely soluble	IVT	Wet AMD*, DR*, DM*	Off label

Aflibercept	115 kDa	>100 mg/mL	IVT	Wet AMD, DME, DR	FDA-approved (2011)
Brolucizumab	26 kDa	Freely soluble	IVT	Wet AMD	FDA-approved (2019)

N/A: not available; ** Physico-chemical parameters found on DrugBank; *** Predicted properties; IVT: intravitreal; IV: intravenous

1.3 Route of administration, advantages and associated limiting barriers

Designing an ocular system to deliver drug to a specific target tissue is a challenging task due to the complex anatomy of the eye. Several routes of drug delivery into ocular systems exist (**Figure 3**) and their advantages and challenges are summarized in **Table 2**. [17] In general, the selection of the route depends mostly on the target tissue and the type of drug used, taking into account the exiting physiological and anatomical barriers.

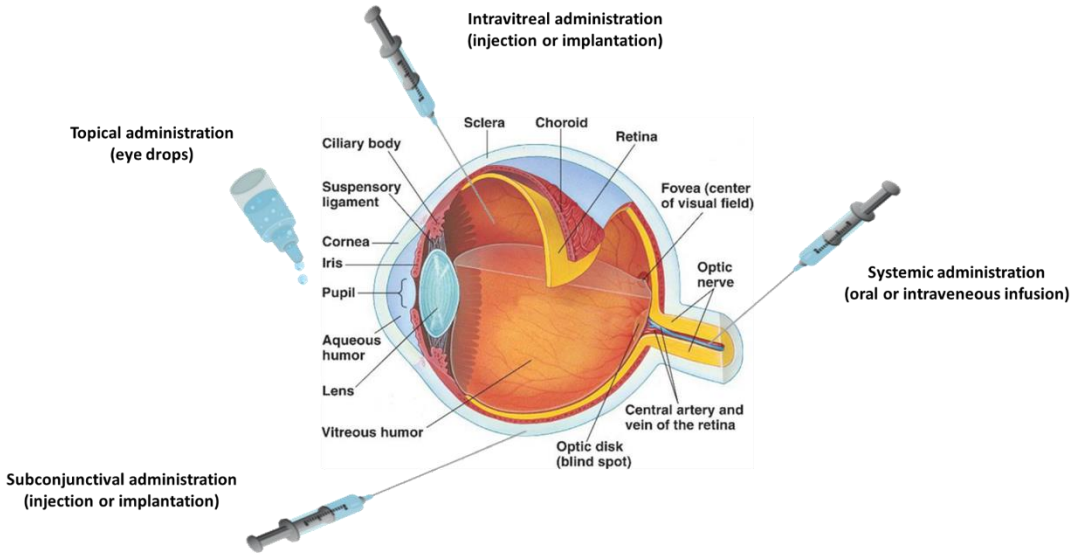

Figure 3. Schematic representation of the eye and the administration routes. Adapted from [15]

Table 2. Summary of the diverse routes of administration, their advantages, challenges and application in the treatment of diseases.

Route	Dosage form	Advantages of the route of administration	Challenges of the route of administration	Application
Anterior eye segment administration				
Topical	Eye drops solution	High patient compliance, non-invasive, self-administrable	Precorneal and corneal barrier which decrease BA under 5%	Keratitis, uveitis, conjunctivitis, scleritis, episcleritis, blepharitis, glaucoma
Blood administration				
Systemic	Solution (intravenous or oral), solid (oral)	Patient compliance, non-invasive	BAB, BRB, high dosing causes toxic effect, BA under 2%	Scleritis, episcleritis, CMV retinitis, posterior uveitis
Posterior eye segment administration				
Subconjunctival	Solution or solid implant	Delivery to anterior and posterior segment, implant preferred, avoid cornea barrier	Conjunctival and choroidal blood or lymphatic flows, BRB, needle size	Glaucoma, CMV retinitis, AMD, posterior uveitis
Intravitreal	Solution, suspension or solid implant	Direct access to vitreous and retina, avoid BRB, sustained delivery with microparticles and implant formulations, small and large molecules	Retinal detachment, haemorrhage, cataract, endophthalmitis, patient compliance because of surgery, injection volume limiting the dose, needle size, viscosity	AMD, posterior uveitis, BRVO, CRVO, DME, CME, UME, CMV retinitis

BRVO = branched retinal vein occlusion; CRVO = central retinal vein occlusion, CME = cystoid macular oedema; UME = uveitic macular oedema; BRB = Blood Retinal Barrier ; BAB = Blood Aqueous Barrier

1.3.1 Topical ocular administration

Topical ocular administration, such as eye drops solutions, is the most convenient method to treat the anterior segment diseases (dry eye, glaucoma). Indeed, this method is non-invasive and easy to apply. Two pathways exist for the entry of drugs into the eye after topical administration: the corneal route and the conjunctival/sclera route. The corneal route is assumed to be the principal pathway. The cornea is a clear transparent epithelial membrane and a mechanical barrier that protects ocular tissues by limiting exotic substance permeation. It is composed of three layers: the epithelium, the stroma and the endothelium. Each layer is rate-limiting for drugs permeation. The proprieties of the drug (solubility, molecular weight, ionization) and the properties of the formulation (size of particles in suspension, concentration) affect corneal permeation. [18–22] Generally, drugs which cross the corneal layers are hydrophobic, or at least amphiphilic, and small. The conjunctival/sclera route [23], also known as the non-corneal route is the pathway for some part of the drug such as large hydrophilic molecules which were unable to pass the epithelium barrier. They can pass the conjunctiva that is more permeable than the sclera and the cornea. [24] The drug can reach the anterior chamber by vessel uptake, lateral diffusion into the cornea or by direct diffusion though the conjunctival, sclera and ciliary body. However, the presence of several blood vessels dissipates the drug into the systemic circulation, decreasing the bioavailability. As a result, due to the presence of the precorneal factors (tear drainage, blinking, tear film and tear turnover) and the various layer of the cornea and the blood flows, only a small fraction, typically 1 to 7%, of the applied dose reaches the ocular tissues. [17] Even if the topical route is the most efficient for anterior segment of the eye treatment, this method is in general not suitable for posterior segment.

1.3.2 Systemic administration

Upon oral administration or intravenous infusion, the systemic administration, also known as the parental route in the case of intravenous infusion, is used to treat both segments of the eye. Oral delivery is non-invasive and well tolerated by patients. However, there is a limited access to target tissues. High dosage of oral medication is necessary to increase the bioavailability of the drug and to observe therapeutic efficacy but can lead to severe systemic toxicity. [17] For large molecules, parenteral injection is mostly recommended. The major barriers for drugs permeation to the anterior segment and the posterior segment are the blood-aqueous-barrier (BAB) and the blood-retinal-barrier (BRB), respectively.

1.3.3 Ocular blood barriers

The BAB is composed of thigh junctional complexes in two discrete cells layers (the endothelium of the iris/ciliary blood vessels and the non-pigmented ciliary epithelium) and restrict the entry of drugs into the intraocular environment such as the aqueous humour. [25 26 27]

The BRB is located between the retina and the choroid (**Figure 4**) [28]. It limits the entry of drugs from blood (in the choroid) to retina and therefore the posterior segments (choroid-to-retina direction) and from the posterior segment to the choroid (retina-to-choroid direction). The BRB is essential in maintaining retinal homeostasis, regulating fluids and movements, and preventing leakage of macromolecules or possible harmful species. It is composed of an inner and an outer component. The inner BRB [29] (iBRB) is formed by the thigh junctions between endothelial cells of the retinal capillaries (RCE), pericytes and Müller cells. The outer BRB (oBRB) [30 31 32] is formed by the junctional complexes of the polarised retinal pigment epithelial cells (RPE). It participates to biochemical functions, controls and selects the traverse of nutriments or compounds and maintains the visual system. The thight jonctions of the RPE restrics the entry of large and small molecules. Besides, the interaction of the molecules with the proteins and organic component of the RPE also restrics the permeability.

The shape and nature integrities of the BAB and the BRB can be modified, even partiarly desintegated, in the case of old eyes or eye presenting diseased described in the previsous parts.

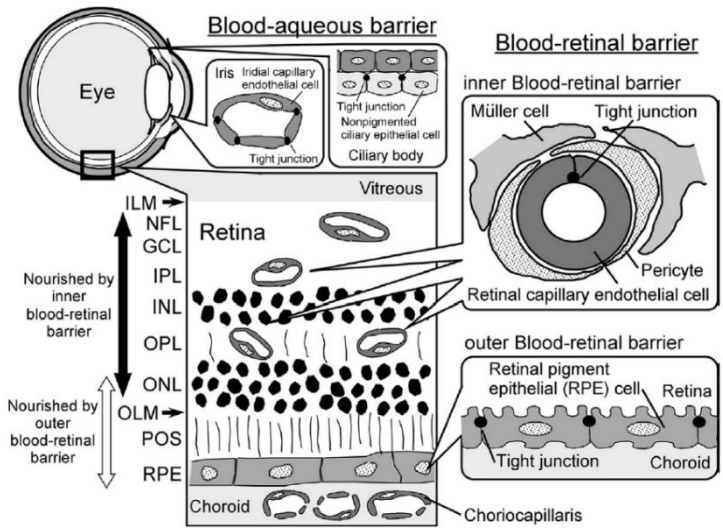

Figure 4. Schematic Blood-Aqueous-Barrier (BAB) and Blood-Retinal-Barrier (BRB) [28]

1.3.4 Subconjunctival administration

The subconjunctival administration has been used to treat both anterior and posterior segments of the eye. This method reduces the administration dose frequency, helps to maintain a sustained drug release, prevents systemic side-effect and is surgically safer than other periocular route. [33,34] Subconjunctival administration method bypasses the cornea-conjunctiva barrier, which provides for the drug a direct access to the sclera. Drug can reach the anterior and posterior segments by three routes: transscleral route (predominant pathway), hematogenic route and anterior route. [33,35,36] After administration, part of the drug is rapidly eliminated by dynamic barriers like conjunctival blood and lymphatic flows leading to the decrease of the bioavailability of the drugs of direction penetration of the sclera. The transscleral route refers to this direct penetration of the remaining part of the drug through the sclera. The sclera is more permeable than the cornea and its permeability mostly depends on the molecular radius (compared to the cornea and conjunctival layers whose permeability only depends on lipophilicity). [32,37] After sclera permeation, drugs can penetrate through the choroid. However, the choroid is highly vascularised and drugs are rapidly cleared. To deliver to the retina the fraction remaining in the choroid must penetrate through the RPE, the outer BRB component, which is highly rate-limiting. For this reasons, few amount of drug is able to reach the retinal tissue at the end. [17]

1.3.5 Intravitreal administration

Intravitreal administration (IVT) offers the advantage of a direct access to the vitreous and is the most efficient method (compared to topical, intravenous and subconjunctival [38]) to deliver drugs to the posterior segment up to now, especially from the vitreous to the retina. However, the delivery of drug from vitreous to the choroid is more limited because of the presence of BRB. [17] IVT administration has limitations like being surgically invasive and can lead to serious complications such as lens opacification, retinal detachment, cataract, vitreous haemorrhage and endophtalmitis, depending on the dosage forms. [33] However, the benefit-risk balance of this method of injection and delivery system has been qualified as favourable.

1.3.5.1 Drug diffusion in the vitreous

The vitreous is a gel-like component composed of water (99%), collagen fibrils, hyaluronic acid and ions. The vitreous occupies the posterior segment, between the lens and retina, and maintains the 3D-structure and shape of the eye. The hyaluronic acid, also sometimes called hyaluronan, is not uniformly distributed into the vitreous, the highest concentration is found in the posterior segment of the eye. Consequently, the vitreous is more viscous in the back of the eye than in the centre. The mesh size of the vitreous humour network is estimated around 500 nm and the viscosity is around 300-2000 cP (or cSt). [39] In older eyes, dissociation of the collagen and hyaluronan occurs and age-dependent increase in hyaluronan leads to a liquefaction of the vitreous, losing its viscoelastic behaviour. In diseased eyes, the blood barriers can lose shape and nature integrities, also modified the viscoelastic behaviour of the behaviour.

After IVT injection, the administrated drug diffuses throughout the vitreous, distributes into the ocular tissue. Typically, the small molecules and the large molecular weight molecules, such as anti-VEGF agent frequently used, have a radius under 10 nm in the vitreous. According to the estimated mesh size of the vitreous, the vitreous should not be a restrictive barrier of the dissolved drugs. [40] Nevertheless, the vitreous is considered as electronegatively charged network due to hyaluronan. It is understandable that a cationic drug could interact with the vitreous and its diffusion would be restricted. [32,40,41]

1.3.5.2 Drug clearance from the vitreous

Drug elimination from the vitreous can occur via biotransformation, which means by **metabolic drug elimination** by enzyme action, due to the presence of a low number of metabolic enzymes in the vitreous humour. Due to the low amount of metabolic enzyme, this mechanism is considered as minor mechanism for drug elimination and has not been deeply studied up to now. [40]

The second mechanism, and the most preponderant, of drug elimination is the **physical elimination** of drug to the blood circulation thought the anterior route or the posterior route. The anterior route elimination consists in diffusion through the vitreous to the anterior chamber and elimination by aqueous turn over and blood flow. This anterior route is assumed to be a route of elimination for all type of drugs. On the other hand, the posterior route consists in diffusion through the vitreous and permeation across retina and the BRB and also permeation to the BAB. Due to the restrictive

permeation properties previously described in the chapter, the posterior route is assumed to be the preferable route of elimination for the small drug exhibiting lipophilic properties. (**Figure 5**) [42–44]

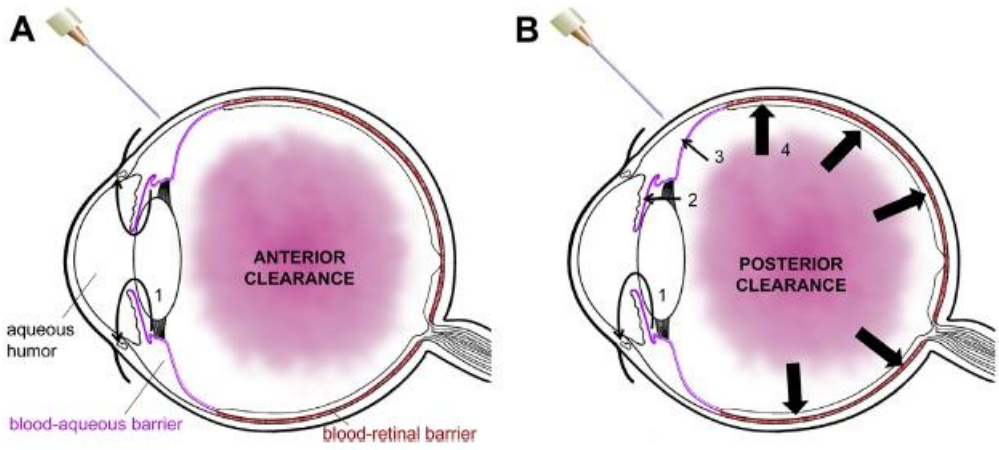

Figure 5 Schematic representation of exit pathway from the vitreous to plasma via (A) anterior elimination route and (B) posterior elimination route. [44] Drug elimination by (1) aqueous humour flow, (2) blood flow , (3) anterior segment route across the vitreous into the anterior chamber thought blood aqueous barrier or (4) posterior segment route through the blood retinal barrier.

The half-life of a drug in the vitreous represents the period of time that it takes for the concentration of the drug in the vitreous to be reduced by exactly one half on the initial concentration due to drug elimination. The small drugs have low retention half-life in the vitreous (few hours) while large molecules have higher retention half-life (hours to days). [45] The half-life of a drug is linked in a minor way to volume of distribution of the drug, which is the factor relating drug concentration in plasma to drug amount in the body. It is representative of drug distribution, and is linked to the clearance rates, which is representative for drug elimination. It has been calculated that the clearance rate of small molecules is 50 times higher than the one of large molecules and that the clearance of small molecules preferably occurred through posterior route. Del Amo and al. drawn an *in silico* model to predict the pharmacokinetics of the small drug in the vitreous of rabbits. [45] They concluded that the clearance of small molecules through the blood barriers was linked to permeability of the membrane with respect to the physico-chemical parameters of the drug such as the hydrogel binding and the *logD* at physiological pH, but not the molecular weight.

1.3.5.3 Consensus recommendations for intravitreal injection in human eye

Intravitreal therapy is one of the most common performed wordwild procedure across all the medical and surgical specialities, qualified as cornerstone of ocular and particularly retinal care. A recent study reported that an estimated 5.9 million of IVT injections were received by American people in 2016. [12] It showed the evidence in practical needs to reduce the potential risks, complications or discomfort for patient related to IVT administration.

The IVT therapy is used to administrate solution/suspension formulations or solid formulations into the vitreous. For a given formulation, the needle depth, the needed size, the speed of injection and the angle of injection have a significant influence on the drug distribution and the drug elimination in the vitreous because of diffusion, flows and eye movements for example. This is particularly true for solution/suspension formulations, less for solid formulations. Also, the quality of the vitreous plays a role in system movement or drug diffusion. [46]

Consensus recommendations have been adapted to provide standardized approaches. Regarding the form of the drug delivery systems administrated (solution/suspension or solid) and even the type of drug used (liquid or viscous), the needle size varied. Typically, the diameter varies from 27 gauge (equivalent to 0.36 mm) to 30 gauge (0.255 mm), and even to 32 gauge (0.202 mm) in particular case and the needle length is between 13 and 18 mm. Smaller needle should be preferred to reduce the force for sclera penetration and increase the patient compliance, and to prevent the drug reflux in the case of liquid formulation which would cause decrease in bioavailability of the drug. The injection volume is commonly between 50 to 200 µL for liquid formulation and the mass is commonly between 1 to 5 mg for solid formulation (corresponding to less than 20 µL) to prevent a significant increase in intraocular pressure.

1.4 Drug delivery systems design and challenges to deliver active components to the posterior segment

As described in the previous part, the delivery of drug to the posterior segment is challenging because of the presence of the two major blood barriers (blood aqueous barrier and blood retinal barrier) that restrict the entry of the drug into the tissues. Consensus recommendations have been drawn to standardize the procedures of intraocular administrations of potential drug delivery systems, and the type and nature of drugs affect largely their design.

On the one hand, up to now, the delivery of small drug to the posterior segment has been extensively studied and some long-term delivery systems have been approved by the FDA. These systems will be further described in part 3 and part 4 of this literature review. However, some systems may migrate into the vitreous humour, they also may lack of degradation or on the opposite degrade too quickly and some those system can also produce acidic by-products that can affect the local environment.

On the other hand, the long-term delivery of biologics is more complicated. Indeed, biologics have complex structure and have stability issues due to protein aggregation and/or fragmentation that lead to loss of activity and in some cases to unwanted immune responses. [47] Moreover, biologics have a tendency to interact with the drug vehicle. At present, ophthalmologists treat the patient with frequent bolus injections containing protein but the therapeutic dose level to the retina is not maintained. [39] Considering that the biologics, especially anti-VEGF agents that focused most attention, are efficient to cure the retinal diseases (AMD and DR), that over 16 million of Europeans and American people are affected by the AMD, which represent a global cost of $6.9 billons in 2018, and that the prediction of people affected by AMD worldwide in 2030 is estimated around 230 million [13,14], it is urgent to developed sustained-delivery systems of biologics. The FDA-approved systems and the pre-clincal ones will be further described in part 3 and part 4 of this literature review.

Therefore, there still remains a challenge to develop drug delivery systems for both small drugs and biologics/proteins that are biocompatible and non-toxic, that deliver the API in a sustained manner without affecting the API properties and allow to reach therapeutic dose levels for the target tissue with a minimal invasive technique for the well-being of patients.

To deal with these challenges, it will be interesting to developed polymeric systems based on biocompatible polymers already existing in the eye to ensure safe and biocompatible properties in addition to drug-binding properties to enhance the retention time of drug in the vitreous cavity and/or in the eye tissue.

Melanin is a natural polymer that exhibits all of the properties required (biocompatibility, biodegradability, produced by retinal cells, drug-binding properties) and consequently is a good candidate. The synthetic analogue of melanin, the poly(dopamine) is also a good candidate to build drug delivery systems, and particularly for the eye. Given this, the following part (part 2) will be dedicated to melanin and poly(dopamine), their synthesis, their properties, the acute interest of poly(dopamine) for pharmaceutical and biomedical applications and its potency for ophthalmic applications.

2. Melanin and melanin inspired synthetic biopolymers, their applications as biomaterials and for release of drugs

2.1 Melanin: structure and properties

2.1.1 Melanin and pigmentation

Melanin is a macromolecule responsible for pigmentation. It is located into pigment cells of the skin, hair, brain and eye. In the eye, high concentration of melanin is found. More than 60% of ocular melanin is located into posterior ocular tissues (RPE and choroid, see part I) and 40% in anterior ocular tissues (ciliary body and iris). Both segments form a continuous pigmented envelope **(Figure 6).** Two types of cells are able to produce ocular melanin: the pigmented epithelial cells and the uveal melanocytes. The pigmented epithelial cells are located into the pigmented epithelium tissue composed of RPE, iris pigment epithelium (IPE) and pigmented ciliary epithelium (PCE). The uveal melanocytes are located into uveal tract composed choroid, iris stroma and ciliary stroma. [48,49]

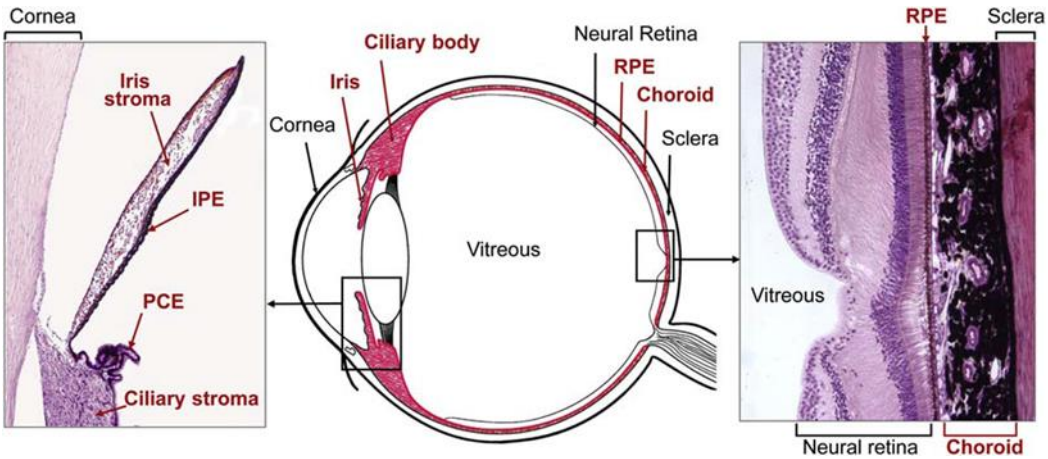

Figure 6. Schematic representation of the eye showing the pigmented enveloped (in pink) composed of pigmented epithelia tissue (RPE, IPE, PCE) and uveal tract (choroid, iris stroma and ciliary stroma). [49]

Melanin is synthesized from the amino acids tyrosine and cysteine via enzymatic and spontaneous reactions within melanosome (**Figure 7**) [49] Two types of melanin are produced: brown-black eumelanin and yellow-reddish pheomelanin. The ratio between both depends on tyrosine and cysteine activities and availabilities. **Eumelanin** is mainly found in pigmented epithelial cells. Its content is independent on the population, the age and the animal race.[50] Eumelanin and pheomelanin are found into uveal melanocytes. The ratio of eumelanin and pheomelanin is related to the pigmentation of the eye: the higher the ratio is, the browner the iris is.[51,52] The same correlation between quantity and type of melanin has been done with skin and hair coloration.[53,54] Therefore, albino (non-pigmented) animals differ from pigmented animals by the non-synthesis of melanin due to the absence of tyrosinase.

The macromolecular structure of eumelanin is unclear. It should consist of 3.4 Å-spaced stacked oligomers of 4 to 8 monomer units of 5,6-dihydroxyndole (DHI), 5,6-dihydroxyindole-2-carboxyl acid (DHICA) and their respective oxidized forms as quinone-like 5,6-indolquinone (IQ) and indole-2-carboxylic acide-5,6-quinone (IQCA) or as semi-quinone. [55,56] Eumelanin is usually considered as water-insoluble component [57], and due to the presence of free carboxyl, phenolic and quinonoid groups, the density charge is influenced by pH.

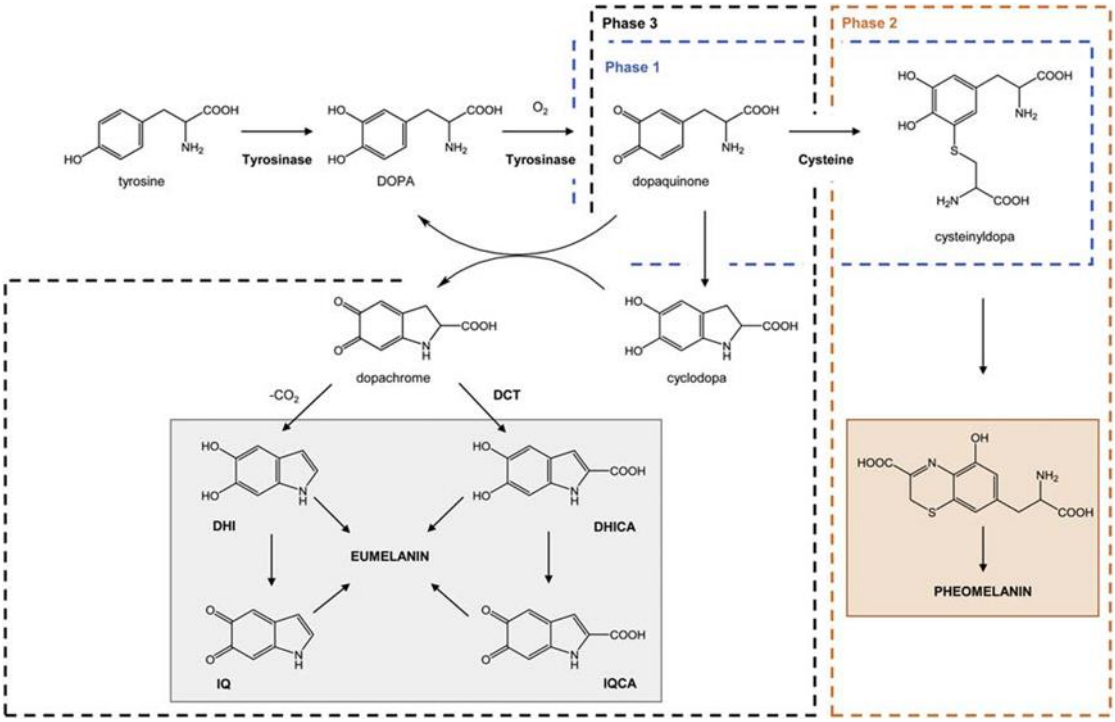

Scheme 1. Biosynthesis of eumelanin and pheomelanin from amino acid tyrosine. [49]

2.1.2 Melanin as protective macromolecule for the eye

Ocular melanin plays a role in photo-screening, biophysics and biochemistry. Melanin protects the eye from light by absorbing light from ultraviolet to near-infrared wavelengths. In the iris, melanin protects the eye from ultraviolet to visible light. The amount of light entering in the eye is reduced, thus protecting the eye from harmful effects. Light that escapes absorption reaches the posterior segment. In the RPE, melanin also absorbs light and minimizes reflection. The retina is protected from intensive and extended light exposure. [58] Melanin also acts as an antioxidant to protect the eye against reactive oxygen species (ROS) which damage the cells. Indeed, ROS are formed by normal metabolism of oxygen but UV light or heat exposure increase the ROS level leading to toxic effect (oxidative stress). Melanin exhibits ROS scavenging [59] and metal chelation [60] capacities, the latter decreasing the ROS formation induced by free metal catalyst.

2.1.3 Melanin as drug-binder in pigmented tissues

2.1.3.1 Drug accumulation, pharmacology and adverse effects in ocular tissues

Drug accumulation was observed in the ocular tissue of pigmented animal and not in non-pigmented animal. Therefore, eumelanin is assumed to be responsible for drug accumulation which affects the pharmacodynamics (PD) and pharmacokinetics (PK) of some drugs.[61] Melanin and therefore particularly eumelanin acts as a **reservoir-binding**. The reservoir-binding property increases the amount of a given drug into ocular tissue, which extends the half-life of the drug because protected from clearance. The melanin-bound fraction is slowly released and the free drug can reach the target tissue. The whole reservoir-binding mechanism extends therapeutic action of the given drug. Meanwhile, the reservoir-binding properties can also play a role in the reduction of pharmacodynamics response, meaning a faster response of the organism after drug administration. It depends on the balance between PK and PD for a given drug. [62–64] Not only drug and melanin structures affect the *in vivo* pharmacology, other factors exist that make the prediction even more complex. The resulting ocular PK is a chemical interplay between drug structure, melanin type, drug-melanin affinity, permeability of cell or melanosome membranes and clearance rates. [49,65–67]

It has been reported that some drugs that are able to binding with melanin could lead to ocular toxicity. However, this ocular toxicity should come from the cytotoxicity of the drug or related adverse effect of accumulation, but not from the drug-melanin binding itself. [49]

2.1.3.2 Model of prediction of drug binding affinity

With the aim to study the drug binding to melanin, *in vitro, ex vivo* and *in vivo* methods can be drawn. Simply, the *in vitro* study can be carried out employing different sources of ocular pigment (synthetic or natural melanin, melanosome, tissue section, cells) and employing different processes and analytics techniques. It is the most frequently tool to investigate the melanin binding. The *in vivo* study can be carried out using imaging methods, using dosage of drug concentration in excised tissue or observing the pharmacology effect in albinos *vs.* pigmented animals.

A variety of drugs is expected to bind with melanin, depending on their physico-chemical properties (acid/basic status, pKa, binding energy, *log*P). In general, the drugs exhibiting a high binding capacity *in vitro* are **small, basic, hydrophobic, composed of aromatic rings**. For example, at physiological pH (7.4), basic drugs are cationic and able to interact with the negative charged 5,6-dihydroxyindole-2-carboxyl acid (DHICA) units and the aromatic rings mimic the supposed stacking structure of melanin. Thus, the melanin-drug binding is a combination of several interactions: electrostatic, hydrophobic, charge transfer and hydrogen bounding. [68–72]

With the aim to predict the strength (low or high) of binding of drug to melanin, many *in silico* models,[73–76] also known as computational models have been drawn. Rimpelä *el al.* [49] have drawn a qualitative classification from a data set of 50 compounds using partial least square discriminant analysis (PLS-DA) (**Figure 7**). Recently, Jakubiak *el al.* [65] performed *in vitro* melanin binding affinity study using isolated melanin and compared the result to the *in silico* model they drawn. The model showed good predictivity and precision for 91% of the compounds experimentally classified as high and very high binders but the model was considered non precise for compound experimentally classified as mid and low binders. Besides, the model pointed the correlation between the number of aromatic rings (≥3), the ionization category (basic at pH 7.4), the hydrophobicity (2 < log D <3) and the binding affinity, thus confirming the existence of several interactions involved in the drug-melanin binding.

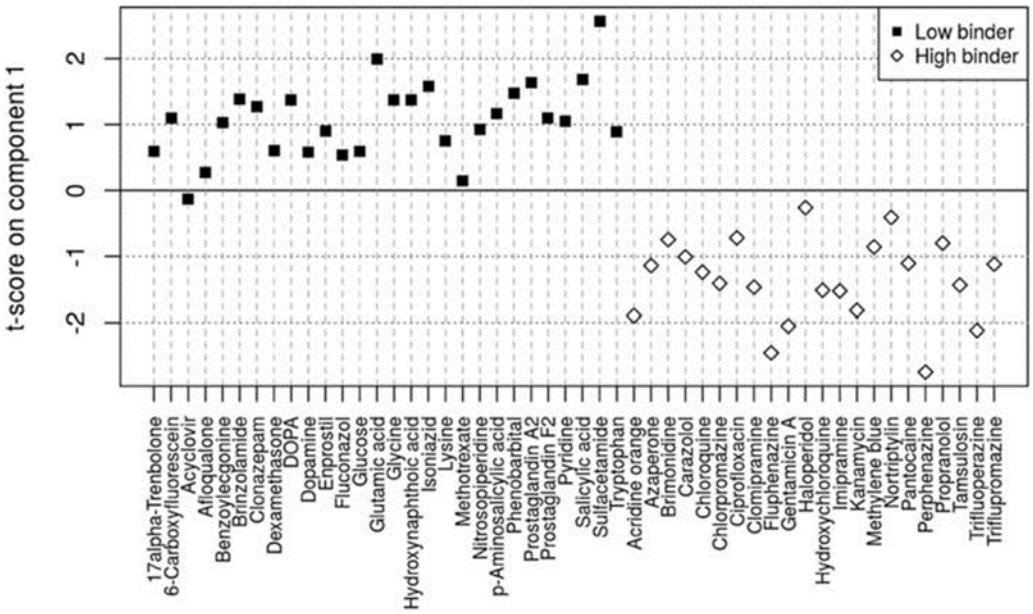

Figure 7. Qualitative classification of 50 compounds taking into account polarizability and electrostatic interactions as key parameters for melanin-binding using PLS-DA method. [49]

2.1.4 Conclusion

Melanin plays an important role in protection of the eye and has shown interesting and promising properties of drug binding to extend the pharmaceutical activity of a drug in the ocular tissue. Therefore, it would be interesting to use melanin in the drug delivery formulation to extend the release rate of the drug. Melanin itself is an amorphous compound insoluble in water and exhibiting limited solubility is organic solvent, which restricts the use of analytic analysis and the application in biomaterials [77] . Also, the varieties of source of melanin (mammalian, cuttlefish, synthetic) change the physico-chemical characteristics of drug-binding.[66]. In order to develop drug delivery systems on an industrial scale, it would be beneficial to synthetize melanin using a synthetic pathway that mimic the structure and the properties of the natural melanin without the extraction process from the eye and the possible non-reproducibility in batches. In the following part, we will focus of the synthetic melanin and its applications in drug delivery.

2.2 Polydopamine: synthesis and structure

2.2.1 Dopamine

In nature, mussels exhibit a strong adherence capacity to surfaces, such as wood and stones, despite the continuous shear stress induces by water flow. It has been shown that the secret of this strong adhesion lies in the composition of proteins they secrete. The proteins contain a considerable amount of 3,4-dihydroxyphenylalanine (DOPA), which is also a precursor for eumelanin synthesis as described previously. Therefore, the DOPA, containing a catechol and an amine groups, is considered as the key factor in adhesive properties of mussel to material. [78] **Dopamine** is a neurotransmitter synthesized in the brain and in kidneys. Dopamine is derived from DOPA by removing the carboxylic groups though the action of the enzyme DOPA decarboxylase (primary pathway of synthesis, **Scheme 2**). It still contains catechol and amine groups suggestive the potency of dopamine to exhibit adhesive properties. Dopamine is commercially available, especially dopamine hydrochloride, and is used as a precursor for polydopamine synthesis.

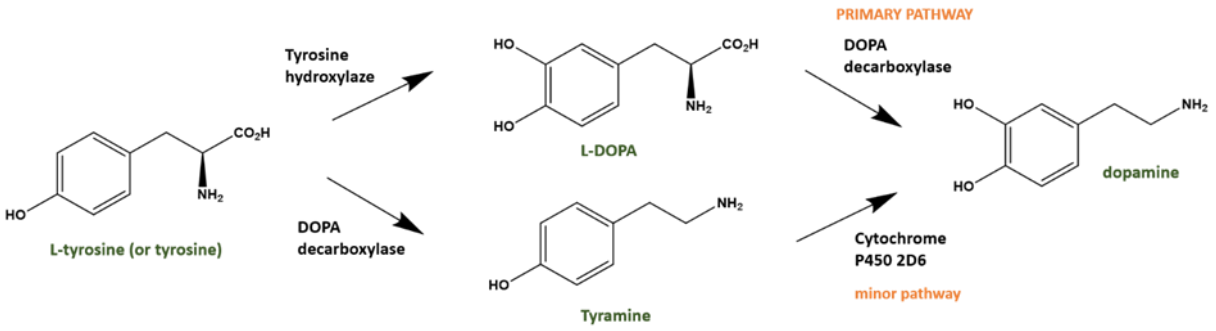

Scheme 2. Synthesis of dopamine from L-tyrosine

2.2.2 Polymerization process to synthesize polydopamine

Regarding the similar composition of reactive units, polydopamine (PDA) is traditionally qualified in literature as mussel-inspired material and a synthetic analogue of melanin, particularly of eumelanin. PDA can be synthesized by three different polymerization mechanism processes using dopamine as monomer: the oxidation polymerization under alkaline conditions, the enzyme-catalysed oxidative polymerization and the electro-polymerization. The advantages and limitations of each technique are listed in **Table 3**

Table 3. Processes of polymerization of dopamine to synthesize synthetic polydopamine (PDA)

Polymerization	PDA material	Conditions	Advantages	Limitations
oxidative polymerization in alkaline conditions	Films, nanoparticles	Oxygen In solution pH>7.5	Easy, thickness or size driven by experimentation conditions (time, concentration...), mild conditions	Lack of thickness (50 nm for films deposition), insolubility of PDA in aqueous and many organic solvents
oxidative polymerization using enzymatic catalysis	Films, nanoparticles	Oxygen In solution Enzyme	Easy process, environmentally friendly, enzymatic activity	Lack of studies, insolubility of PDA in aqueous and many organic solvents
Electro-polymerization	Film	Oxygen-free In solution	Considerable thickness	Electrically conductive materials as support, insolubility of PDA in aqueous and many organic solvents

In the **oxidative polymerization under alkaline conditions,** dopamine spontaneously polymerises at pH > 7.5 with oxygen as oxidant in aqueous or organic solution. Indeed, dopamine is sensitive to pH and to oxidation due to catechol and amine moieties [4,79] (pKa (phenol) = 9.27 and pKa (amine) = 10.01).

The mechanism of polymerization is still unclear due to the complex redox process and a high number of oxidized and cyclized intermediates generated during the reaction. In the early stage of research, the formation of PDA is assumed to be similar to the **biosynthetic pathway of eumelanin**. Typically, dopamine is first oxidized to form a quinone, followed by cyclization via intramolecular rearrangement to form leucodopaminechrome, then oxidized in dopaminechrome followed by rearrangement to form 5,6-hydroxyindole then oxidized to form 5,6-indolequinone (**Scheme 3**). The final structure is still on debate and will be discussed further. The major advantage of this technique is the use of the mild conditions for synthesis. However, the insolubility of PDA in water and in almost all organic solvents impede its use in formulation [80] (creams or lotion for examples), and chemical modification or treatment, or copolymerization with reactive monomers or polymers are two approaches to developed water-soluble PDA-based material.

The polymerization process can also be assisted by enzymes such as lactase or urease in an **enzyme-catalysed oxidative polymerization** process [81,82]. Alternatively or in combination with the oxidative polymerization, the **electro-polymerization** allows the polymerization of dopamine in oxygen-free solution and direct deposition of the film on the electrode [81].

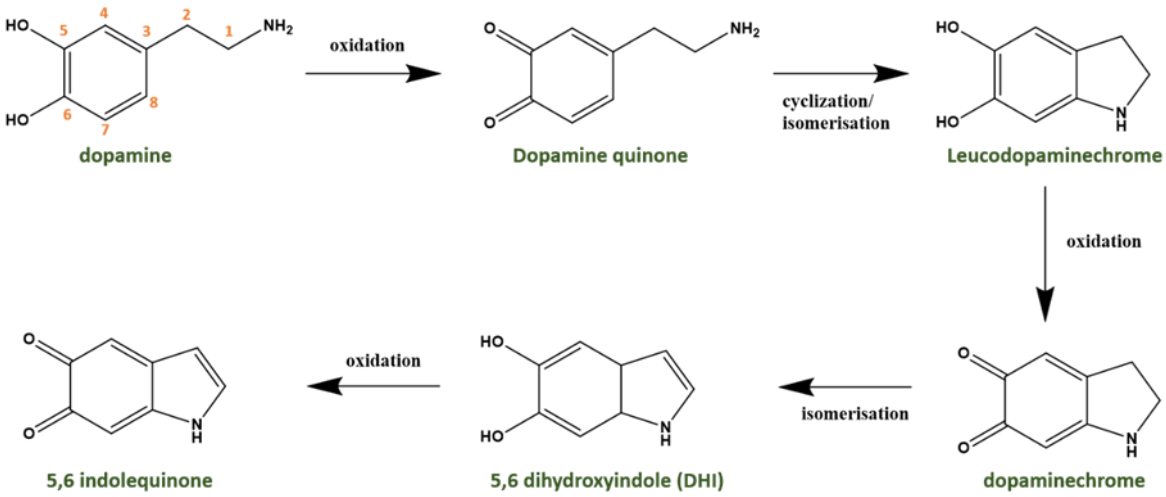

Scheme 3. Dopamine and its reaction intermediates after successive oxidation and rearrangement/isomerisation.

2.2.3 Structure of polydopamine

Since 2012, many authors have started to elucidate the structure of PDA. Up to now the precise structure is still a subject of debate. Dreyer *et al.* [83] proposed a model based on non-covalent forces like charge transfer, π-stacking and H-bonding interactions between 5,6-dihydroxyndole (DHI) monomer units. This model disagreed with the one proposed by Liebscher *et al.* [84] in which the authors proposed π-π stacking aggregation of tetramers and octamers of DHI and its tautomeric forms covalently linked in 4,7 position in phenyl groups. (**Scheme 4**)

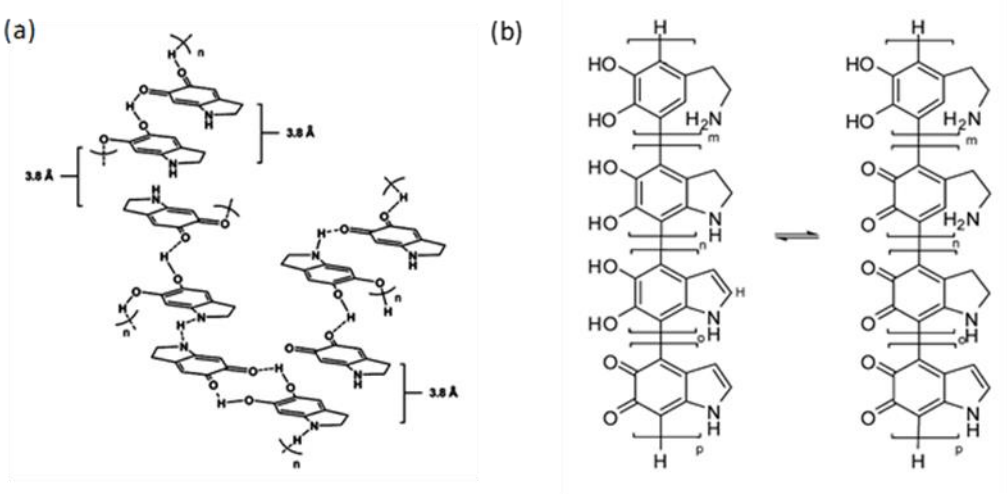

Scheme 4. Model of (a) H-bonding defended by Dreyer et al and (b) 4,7-monomer linkage between DHI units and its tautomeric forms defended by Liebscher et al. Adapted from [83,84]

Recently, Chen *et al.* [85] established an information model to predict the more stable conformations of dimer, trimer and tetramer of DHI units. They selected the 12 and 16 more stable conformations for trimers and tetramers respectively, over all the conformations generated by the algorithm. The most stable forms include 1,4-, 1,7- and 1,1-monomer linkages, the less stable forms include 4,7-monomer linkages. They also showed that planar conformation of DHI oligomers is more likely to exist due to low energy conformation and their self-assembly into aggregated layers. (**Scheme 5**). However, this model didn't take into account all the redox forms due to computational limitation. In agreement with this model, Cîrcu *et al.* [86] showed by $^{13}C/^{1}H/^{2}H$ solid-state NMR that the majority of phenyl and indole rings are rigid and that phenyl rings are protonated in the final material. They also proved that 1,4-, 1,7- and 1,1-monomer linkages are predominant over 4,7-monomer previously described in literature, and that π-π stacking is the driving force to tetramers aggregation.

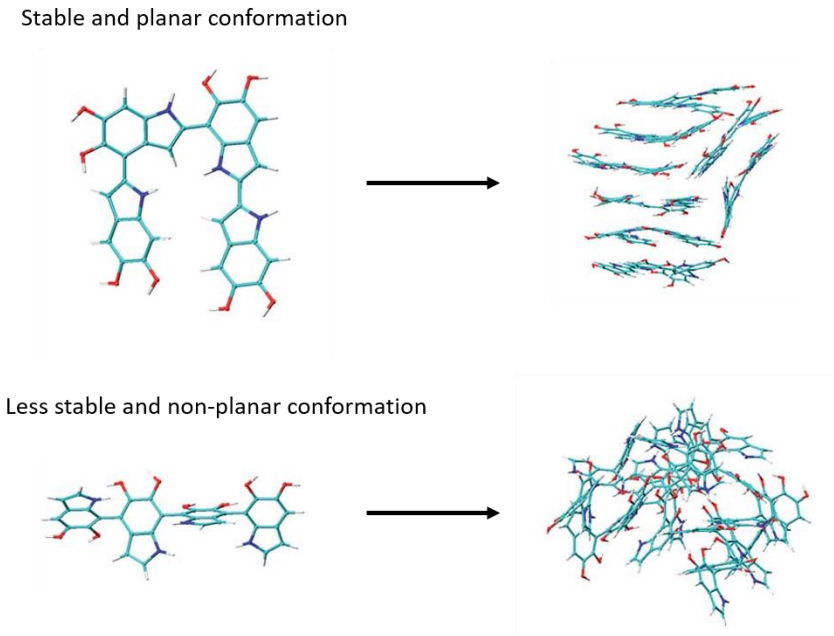

Scheme 5. Molecular and aggregated structure of stable and less stable tetramers of DHI units. [85]

Therefore, up to the last structural studies, PDA is described **as π-stacked supramolecular aggregates of covalently bound mixture of oligomers (mostly up to tetramers) of DHI with different redox form**s (quinone or catechol and uncyclized ethyleneamine or cyclized indole or cyclized indoline).

2.2.4 Properties of polydopamine and applications

PDA synthetic polymers offer a wide range of biological and chemical properties, similar to melanin due to the analogous structure, as described in two recent reviews [3,4,87]. The main properties are described below. Polydopamine (PDA) has garnered particular interest in diverse applications since 2007, as listed in two recent reviews, including water treatment, biosensors, energy and the biomedical field, particularly for toxicity attenuation, antimicrobial, tissue engineering and drug delivery applications. [87,88]

PDA exhibits **biocompatibility** during *in vitro* [4,89] evaluations performed onto fibroblast [90], osteoblast [90], neurons [90], endothelial cells [90], cervical cancer cells [89], endocrine cells [91] and smooth muscle cells [91]. Also, PDA shows biocompatibility after intravenous injection in rat [89] during which no abnormalities was observed in neurological functions and in histopathological examination.

PDA absorbs in the IR-UV-visible regions [92] of the light spectrum (**Figure 8**-A) and exhibits **high photothermal conversion** upon the application of near infrared light stimuli [92] (**Figure 8**-B) with almost 40% of light-to-heat conversion efficiency [89] due to the nature of the monomeric units, the conformation of the oligomers and their stacking [4,85].

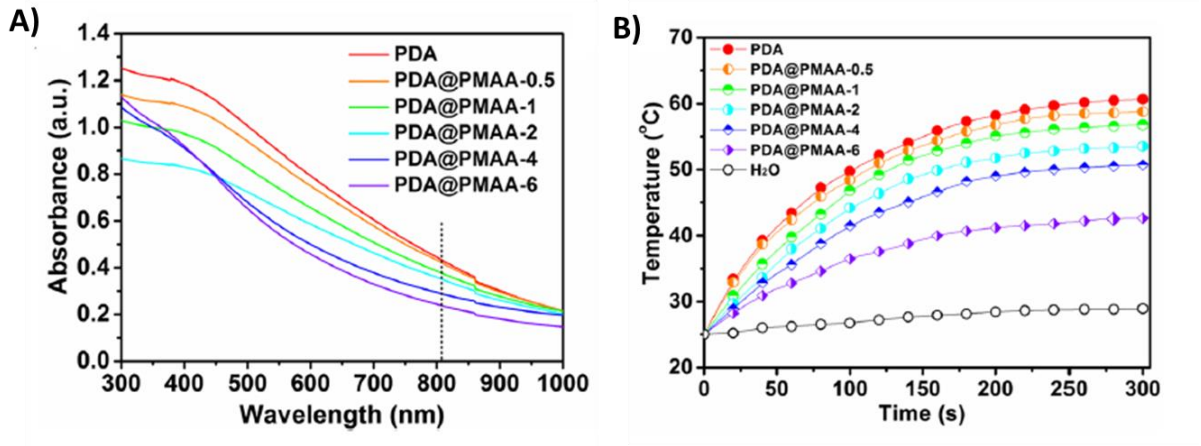

Figure 8. A) UV-visible spectra of PDA at a concentration of 0.1 mg/mL in aqueous solution and B) photothermal effect of PDA after laser irradiation at 808 nm. [92]

PDA is an **amorphous** [93] compound (**Figure 9**-A) which offers **stability in physiological conditions** [4] and which can **endure elevated temperature** [4,93,94] before suffering from decomposition above 200°C (**Figure 9**-B).

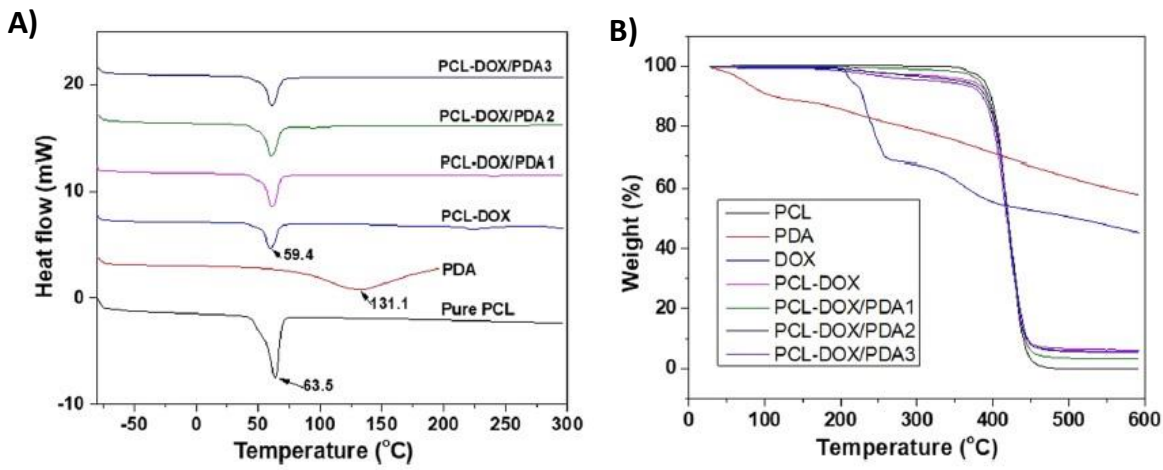

Figure 9. Thermal characterisations of PDA by A) DSC and B) TGA. [93]

Despite its great resistance toward degradation in vitro, PDA exhibits **degradability** by oxygen-induced process [4,89], by alkalinity-driven process [95] and by micro-organism [96]. When in presence of oxidative reactive species, the color fading and the diminution in diameter of PDA is observed [4,97] suggesting degradation. Moreover, melanin implants has been proved to degrade after 8 weeks in rat muscles [98] with the formation of pyrrole-2,3,5-tricarboxylic acid and pyrrole-2,3-diacarboxyic acid oligomers by redox reaction [4,97]. Once gathered, all the information shows the potency of polydopamine to degrade in vivo. The enzymatic degradation is assumed to be a potential process [4,89] for biodegradation in vivo, especially by NADPH oxidase [99] which are distributed into many organs and which are able to generate active oxygen species. The capacity of PDA to be degraded by oxidative species result from the ability of PDA to act as a scavenge the free radical species [100] (**ROS scavenging properties**) conferring anti-oxidant effect.

Due to the presence of amino-like and catechol-like groups, PDA is zwitterionic [101,102] with a isoelectric point around 4. Under a pH value of 4, PDA is positively charged because of protonation of amino-groups, and above, PDA is negatively charged because of deprotonation of phenolic group. Therefore, PDA is **pH-sensitive**, also its sensitivity can play a role into the capacity of loading [90] and the release [90] of drugs.

Moreover, still resulting from presence of amino-like and catechol-like groups, PDA exhibits **binding capacity** towards the functional groups of wide range of molecules or surfaces via physical (electrostatic, hydrophobic, hydrogen bounding – previously described for melanin binding capacity to drug) or chemical interactions. One of the most widely investigated chemical reaction is the reaction of PDA via its catechol groups with thiol- and/or amine- containing molecules under basic conditions- Michael addition is most likely to occurs for thiols-containing molecules while Michael addition or Schiff base reaction can occur for amine-containing molecules. It has been shown that PDA-based films are able to interact with proteins [103–105] thanks to a combination of physical and chemical interaction. In fact, the protein attachment capacity and value are governed by the conditions of pH [104] and of the composition of the buffer media [104] during the synthesis of the PDA film, and by the concentration [103,104] , the molecular weight [103,104] and the isoelectric point [103] of the proteins. Also, in the presence of free amine or imide groups in PDA, the chemical reaction between these groups and other functional groups is possible as well.

As a result, when combining the pH-sensitivity with the physical or chemical drug binding capacity, it is possible to modulate drug absorption/loading/release properties.

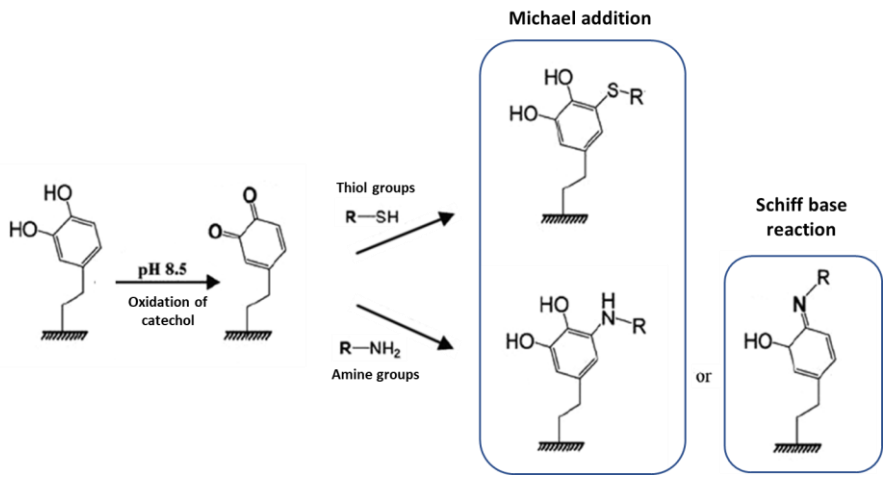

Scheme 6. Reaction of catechol functional group with thiol- or amine- containing molecules via Michael addition and Schiff base reaction

2.3 PDA-based material for coating and drug delivery applications

2.3.1 Dopamine-based material

Dopamine and its derivatives have been investigated in many fields of applications and particularly as adhesive [106], self-healing [107] or wound healing hydrogels [108] and memory shape hydrogels [109] in field of biomedical applications, and even as potential drug delivery vehicle.[110,111] The key factors for the success of dopamine-based materials (dopamine either as free molecule or as end-chain or side-chain units) are the reversible and strong bonds that catechol units form to metal oxide [106] and also the intermolecular covalent cross-liking of the oxidized form of dopamine [106] or the reversible association of hydrophobic form of dopamine [109] that confer strong adhesion by substrate and enhanced mechanical properties.

2.3.2 PDA-based copolymers for coating applications

Polydopamine came into consideration as coating material in biomedical application due to its strong adhesion to surface (metal or soft tissues), its anti-microbial and its molecules anchoring capacities. [88] In the early time of research, polydopamine was deposited on the substrate via an oxidation polymerization process of dopamine in aqueous solution, which corresponds to a *grafting from* process, and the kinetics and thickness of the polydopamine layer deposition was dependant on the conditions of polymerization (pH, time, oxidant type, concentration of monomer). [112,113] This layer could be further modified with polymer, metals or molecules of interest depending on the targeted application. [88]

In order to open a new chapter on the coating applications, we will focus on varied examples encountered in the literature with different strategies of deposition process (*grafting from* vs. *grafting onto* and dip coating vs. spin coating) and the nature of the copolymer deposited on the substrate (post-modification of the PDA layer vs. copolymer containing dopamine or PDA). A particular interest was taken in the synthesis of a copolymer containing dopamine or PDA in order to evaluate the possibility to extend the methods of polymerization to other types of polymers, including polymers for biomedical application.

Sundaram *et al.* [114,115] developed universal anti-fouling coatings for either hydrophobic or hydrophilic surfaces based on the *"grafting onto"* technique of zwitterionic poly(sulfobetaine methacrylate) (PBSMA) or poly(carboxybetaine methacrylate) (PCBMA) functionalized with a chain-end DOPA moiety assisted by dopamine polymerization. DOPA-PSBMA or DOPA-PCBMA were obtained similarly. Firstly, the synthesis of DOPA-PCBMA polymers was made by atom transfer radical polymerization (ATRP) of carboxybetaine methacrylate (CMBA) monomer using brominated DOPA (DOPA-Br) as initiator. Secondly, the coating process was carried out into TRIS solution containing the functionalized polymer and dopamine hydrochloride. (**Figure 10**-A)

Similarly, Zhai *et al.* [116] prepared amphiphilic diblock AB and triblock ABA copolymers composed of a hydrophilic block A based on poly(dopamine methacrylamide) (PDMA) and a hydrophobic block B based on poly[(sulfobetaine methacrylate)-*co*-(2-(dimethylamino) ethyl methacrylate)] (P(SBMA-*co*-DMAEMA)). The PDMA-*b*-P(SBMA-*co*-DMAEMA) (AB-type) and PDMA-*b*-P(SBMA-*co*-DMAEMA)-*b*-PDMA (ABA-type) copolymers were prepared by (i) ATRP of thiethylsilane-protected dopamine methacrylate (DMA) using brominated 2-(dimethylamino)ethyl methacrylate as macro-initiator, followed by (ii) betainization of the PDMAEMA block to obtain P(SBMA-*co*-DMAEMA) central block. The *"grafting onto"* process (in TRIS solution, pH 8.5, 25°C, overnight) of ABA copolymer showed glossier coating and enhanced anti-fouling properties due to difference in spatial organisation of the micelle (smooth coating, P(SBMA-*co*-DMAEMA) on the top surface, PDMA under, no protein absorption) compared to the AB copolymer. (**Figure 10**-B)

To palliate the low grafting density and low adhesive end-group concentration of already-made copolymers through "*grafting onto*" process, especially diblock copolymers, Sheiko *et al*. [117] developed microgels using an easy and coating-thickness-controlled method. The PDA-*co*-PSBMA microgels were prepared by one-pot dispersion free radical polymerization of DMA and SBMA using AIBN as initiator, poly(vinylpyrrolidone) (PVP) as stabilizer and N,N'-methylenebisacrylamide (MBA) as cross-linker. The controlled formulation and addition of crosslinker at a specific time after nucleation resulted in well-defined and monodisperse microgels. The coating preparation was a three-step process, firstly the deposition of microgels dispersed in solution (ethanol/water) onto the substrate, secondly the film formation upon ethanol evaporation under specific humidity level, thirdly the stabilization of the film when the desired thickness and morphology are achieved by oxidation and cross-linking of catechol moieties using TRIS solution and strong oxidant species. (**Figure 10**-C)

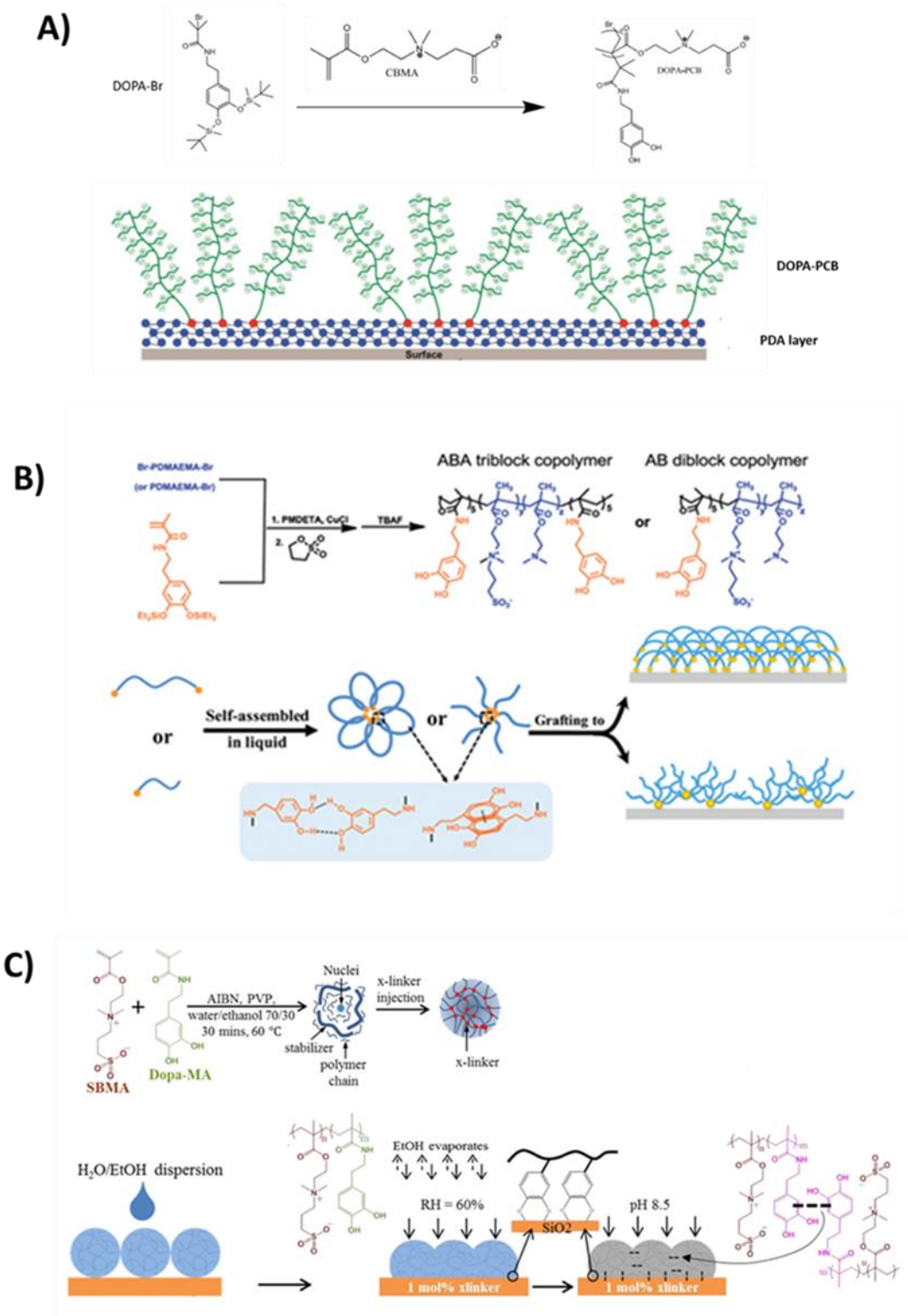

Figure 10. Synthesis of three PDA-based materials. (A) Synthesis of DOPA-PCB and coating illustration of DOPA-PCB through incorporation of PDA layer. [97] (B) Synthesis of PDMA-b-P(SBMA-co-DMAEMA) and PDMA-b-P(SBMA-co-DMAEMA)-b-PDMA copolymers and grafting onto a substate. [116] (C) Synthesis of PDAMA-co-PSBMA microgels and coating process onto a substrate. [117]

In the example detailed above, the copolymers contained units of dopamine and the polymerization of the dopamine was further carried out into TRIS buffer (aqueous solution). Cho *et al.* [118] prepared a series of diblock and triblock copolymers based on poly(methyl methacrylate) (PMMA) and PDA using an organic solution approach. The synthesis is a two-step process, (i) the synthesis of chain-end modified PMMA with bromide (PMMA-Br or Br-PMMA-Br), (ii) the grafting of PDA to prepare PMMA-*b*-PDA and PDA-*b*-PMMA-*b*-PDA by polymerization *via* an oxidative process of dopamine using brominated-PMMA as macroinitiator (**Scheme 7**). In this study, the authors used a solution of dimethylsulfoxide (DMSO) containing sodium carbonate to regulate the pH (alkaline conditions), benzoyl peroxide (BPO) to generate the radicals, *N,N,N',N',N''*-pentamethyldiethylenetriamine (PMDETA) and copper(I) bromide (CuBr) to allow chain end transfer. The content of PDA in diblock and triblock copolymer was estimated around 7.8 and 9.3 % w/w by thermogravimetric analysis, showing poor reaction conversation due to limited solubility of growing polydopamine in organic solvent, but sufficient to demonstrate enhanced thermal stability (compared to PMMA itself) (**Figure 11**). Moreover, the copolymers showed enhanced solubility in variety of organic solvents (compared to PDA itself, only soluble in DMSO and DMF), hydrophilicity, stability and antifouling properties (compared to PMMA itself).

The advantage of this synthesis is the obtaining of the block copolymer containing PDA in powder form and the possibility of storage of the copolymer before the coating deposition by spin coating process. Besides, it seems that this synthesis is transferable to other hydrophobic polymers, which could be advantageous for biomedical applications.

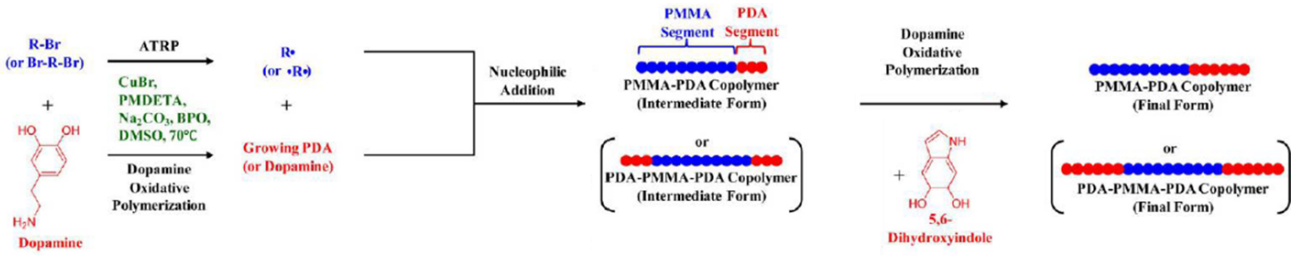

Scheme 7. Synthesis of PMMA-b-PDA and PDA-b-PMMA-b-PDA copolymers by nucleophilic addition and dopamine oxidative polymerisation in an alkaline solution of DMSO. [118]

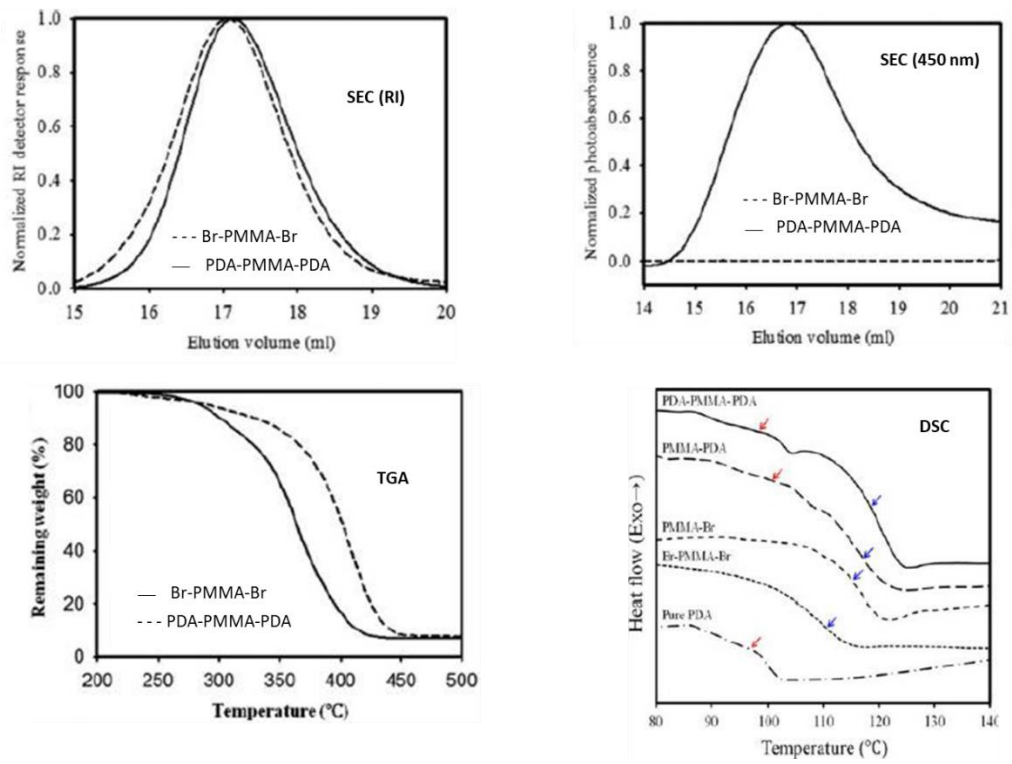

Figure 11. Characterisations (SEC, TGA, DSC) of Br-PMMA-Br and PDA-b-PMMA-b-PDA copolymers. Adapted from [118]

2.3.3 PDA-based nanomaterial for drug delivery applications in cancer therapy

Few years after the discovery of the potency of PDA to coat several kinds of substrates and the numerous advantageous properties of this coating, a particular attention has been paid to the development of nanomaterial of PDA for biomedical applications. PDA nanomaterials for drug delivery application have been widely studied over the last decade, including the cancer therapy [3,79,119,120], particularly in **photothermal-chemotherapy (PTT-CT).** PTT-CT combines NIR irradiation and heat production with the release of an anticancer drug, driven by pH changes or the presence of reactive oxygen species to efficiently kill cancer cells, thanks to the biocompatibility, the pH-responsiveness and the NIR light-to-heat conversion efficiency.

The nano systems are classified as: PDA-coating of nanoparticles (NPs) also known as core@shell PDA NPs, PDA hollow NPs, PDA NPs or self-assembled PDA NPs. The therapeutic agent is either encapsulated into the core matrix, contained into or between multiple layers composing the shell or physically attached to the surface by adsorption or covalent binding. The different schematics representation of the PDA-based nano-systems, the endocytosis and the mechanism of drug release is represented in **Figure 12**.

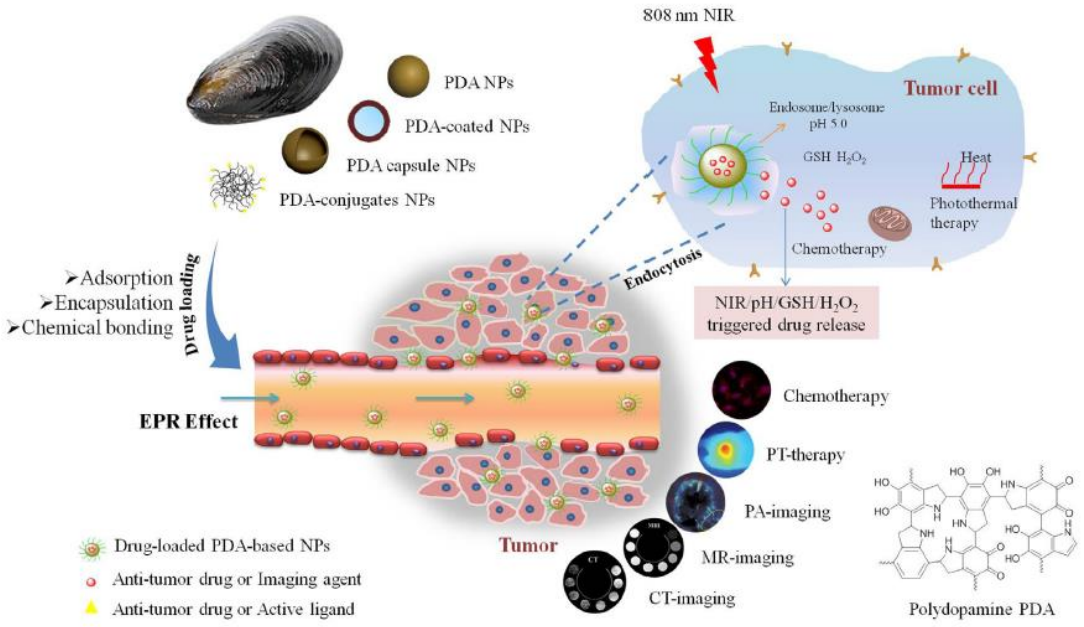

Figure 12. Poly(dopamine)-based nanomaterials and their applications in tumor/cancer therapy. [3]

The synthesis of PDA core@shell nanoparticles consists of an organic or inorganic core coated with a layer of PDA obtained mainly by oxidative polymerization of dopamine in aqueous and alkaline solution. The thickness of the PDA layer [113,112] (deposited on planar or on colloidal surfaces in this particular case) mainly depends on the type of oxidant involved in the reaction, for example O_2 or Cu^{2+}, the type of buffer media, for example Tris or PBS, the pH value, the concentration of dopamine in solution and the time of reaction. The advantages of core@shell nanoparticles are the ability to obtain various structures by modifying the composition of the core and by post-modifying the shell in order to drive the kinetics of release and the biological properties. Due to combined properties of the core

and the shell, the core@shell nanoparticles are non-toxic, exhibit enhanced cellular uptake and efficiency kill the cancer cells by drug release stimulated by pH and also triggered by application of NIR light.

He *et al.* [121] developed a biodegradable NIR- and pH-sensitive nanomaterial based on PLGA (M_n= 16 000 g/mol) nanoparticles containing doxorubicin and coated with PDA through hydrophobic interaction. The PDA shell was further functionalized with PEG-SH (M_n= 2 000 g/mol) by covalent bonding and cetuximab as a targeting ligand and inhibitor of EGFR in head and neck cancer treatment and chemothermal agent enhancer. (**Figure 13**-A)

Zhang *et al.* [122] developed self-assembled micelles based on 1,2-Distearoyl-*sn*-glycero-3-phosphoethanolamine-N-[methoxy-(polyethylene glycol)-2000] (DSPE-PEG) amphiphilic copolymer loaded with doxorubicin and coated on the surface with PDA conjugates. The dual drug release was triggered by acidic pH buffer and NIR irradiation and the DSPE-PEG@PDA nanocarrier showed biocompatibility, enhanced cellular uptake and effective breast cancer cell killing. (**Figure 13**-B)

Xue *et al.* [123] developed a nanomaterial based on Fe_3O_4 core coated with PDA layer further functionalized with PEG-SH and loaded with doxorubicin physically adsorbed on the PDA surface via hydrophobic and π-π interaction. The application of a magnetic field considerably increased the photothermal effect and the endocytosis of Fe_3O_4@PDA/PEG-SH NPs, leading to a combined magnetic targeting-, photo-and chemo- therapeutic systems. (**Figure 13**-C)

Lei *et al.* [124] developed a nanomaterial based on mesoporous silica nanoparticles (MSN) containing doxorubicin and coated with PDA layer via disulfide bonds (MNS-SS/PDA or MNS@PDA). PDA layer enhanced the stability and acted as a “gatekeeper” for the drug. (**Figure 13**-D)

Wang *et al.* [125] developed pH- and NIR- responsive gold nanorods (GNR) coated with PDA further functionalized with PEG and loaded with doxorubicin at the surface. The GNR-PDA nanomaterial showed excellent biocompatibility, cancer cells killing and antitumoral effect *in vivo*. (**Figure 13**-E)

Hollow nanoparticles are typically prepared as core@shell nanoparticles with PDA coating by oxidative polymerization of dopamine, and include an additional chemical or physical treatment, i.e., an etching step, to remove the sacrificial template. The original advantage of hollow nanoparticles is the low density, high surface area and high loading capacity due to the intern void left. By combining the advantages of hollow nanoparticle with the advantages of PDA itself, the material is biocompatible, pH- and NIR-responsive [126,127]

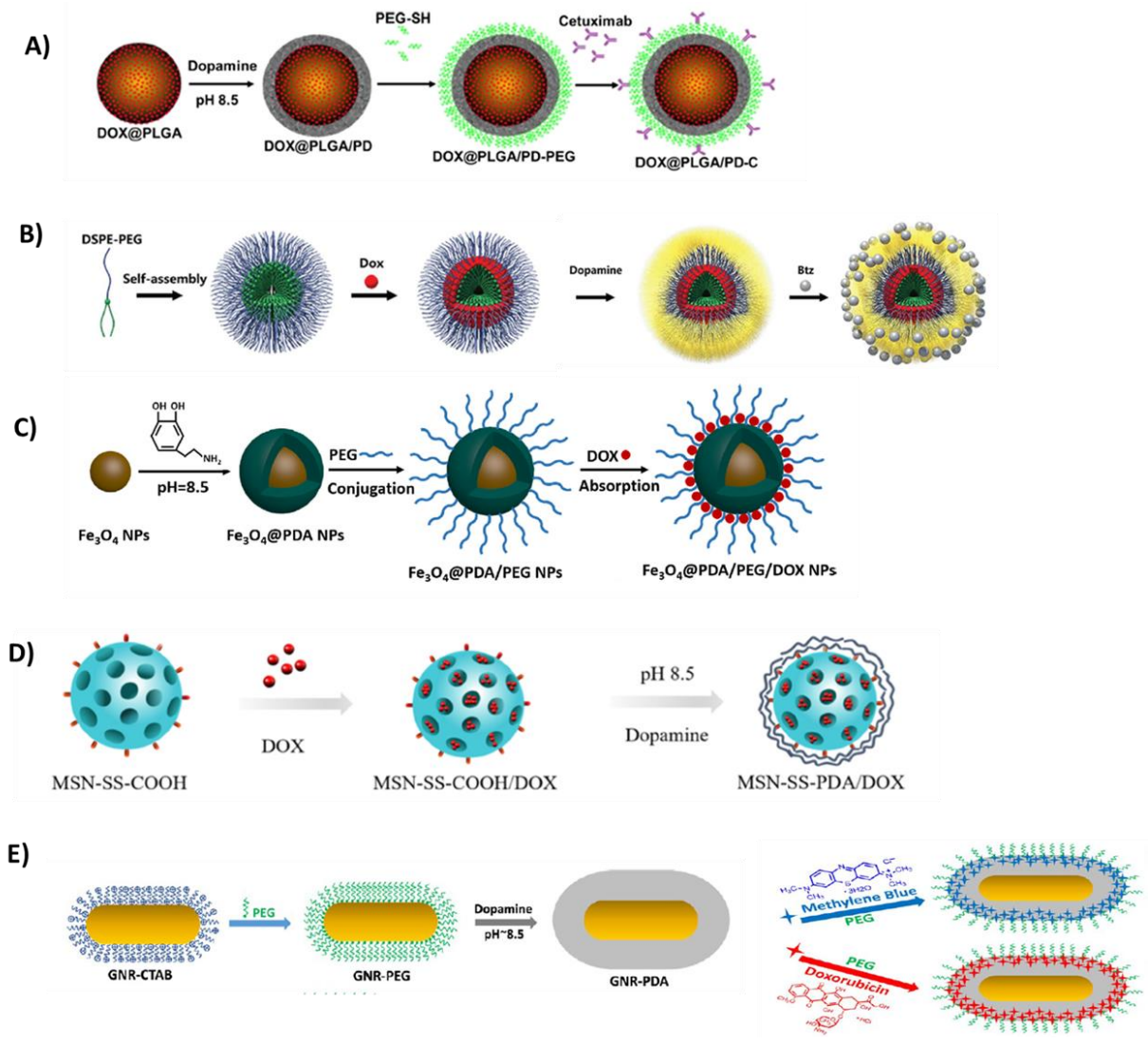

Figure 13. Different structures and morphologies of core@shell nanoparticles coated with PDA and functionalized on the surface. [121–125]

Similarly to the core@shell nanoparticles coated with PDA**, the synthesis of PDA nanoparticles** is typically obtained by polymerization of dopamine hydrochloride in basic aqueous solution using TRIS or NaOH. The size and the shape of NPs also mainly depend on the concentration of basic component, pH, temperature, reaction time and concentration of dopamine in solution. [100,128]

Wang *el al.* [129] developed PDA nanoparticles produced by polymerization of dopamine in ammonia aqueous solution, further functionalized with PEG-NH_2 and loaded with doxorubicin or 7-ethyl-10-hydroxycamptothecin (SN38) physically adsorbed on the PDA surface. The size of unloaded and loaded PDA/PEG-NH_2 NPs was around 98 nm. *In vivo,* the system was injected intravenously and showed biocompatibility, ability to reduce the volume of tumors and even suppress them. (**Figure 14Figure 13**-A)

Similarly, Wang *et al.* [130] developed PDA nanoparticles modified with COOH moieties and further functionalized by hydrophilic block copolymers composed of poly(2-methacryloyloxyethyl phosphorylcholine) and poly((2-dimethylamino)ethyl methacrylate) (PMPC-*b*-PDMAEMA) to enhance their colloidal stability, extend the blood circulation time and a obtain a pH- and NIR- responsive nanomaterial. The size of PDA NPs was around 198 nm, then around 270-297 nm for PDA/PMPC-*b*-PDMAEMA NPs depending on the PMPC-*b*-PDMAEMA composition, and around 296-323 nm after drug loading. *In vitro,* the PDA/PMPC-*b*-PDMAEMA loaded systems efficiently kills the cells after NIR irradiation proving its potency for *in vivo* application. (**Figure 14**-B)

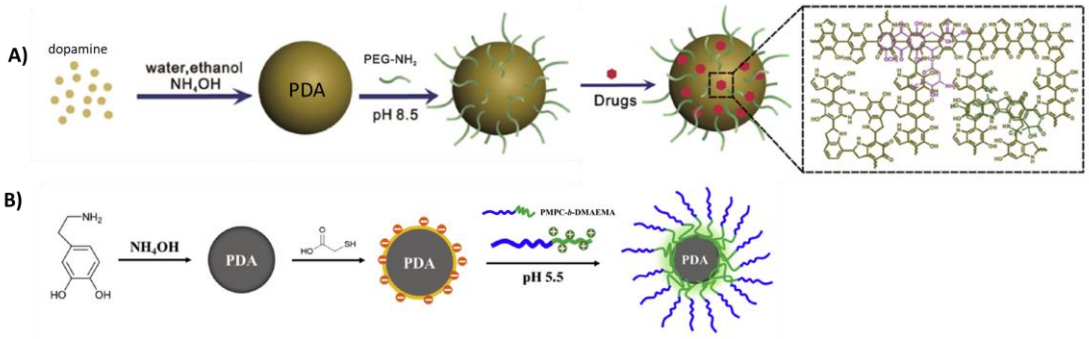

Figure 14 Different structures of nanoparticles of PDA functionalized on their surface. [129,130]

Incorporating **PDA nano systems into gelling systems** can promote the cell adhesion, the pH- and NIR-responsiveness, biocompatibility and tumor cell killing efficiency upon NIR irradiation. It also promotes the slowdown of the release rate of the loaded drug compared to drug-loaded hydrogels or drug-loaded NPs taken separately. PDA NPs have been incorporated into natural polymeric matrices [131–133] such as alginate and nanocellulose and into synthetic polymeric matrices such as PNIPAAM, 4-arms PEG-SH [134–136] for application in drug delivery.

2.3.4 Promising applications of PDA-based material for the drug delivery in ophthalmology

In cancer therapy described above, the drug loaded in the polymeric matrix is always a small molecule, especially doxorubicin. Moreover, despite the huge interest of PDA and the similarities of PDA with melanin, none of those PDA-based material was tested for ocular application, neither in vitro or in vivo. Besides, the potency of PDA nanoparticles as carriers for targeted delivery of biologics remained unknown despite the urgent need in delivery systems for treatment of retinal diseases.

Recently, Jian *et al.* [97] were the first to develop PDA-based nanoparticles loaded with bevacizumab (anti-VEGF agent, off labelled for AMD treatment) for the suppression of angiogenesis. The release rate of the biologics and the biodegradation of the PDA nanoparticles were triggered by oxidative response of the dismutation of hydrogen peroxide to create ROS species which is typically found in the ocular system after the development of AMD. The authors mentioned that after 6 months the PDA nanoparticles were not fully degraded. Therefore, the loaded-PDA nanoparticles showed excellent promising application for the delivery of biologics in the eye under the oxidative stress to slow down the progression of AMD for example, and excellent ROS scavenging properties of PDA to protect the eye over additional damage. Additional data, and more particularly *in vivo* data about the movement of particles into the vitreous humour and the retina are required to ensure the safety and the potency of the biologics-loaded PDA nanoparticles to cure retina diseases.

2.4 Conclusion about the poly(dopamine)-based systems and potency as sustained drug delivery systems for ocular applications

To sum up, the obtaining of a copolymer containing polydopamine was possible using two methods, (i) the functionalisation of a polymer by dopamine and polymerisation of dopamine in aqueous solution or (ii) the polymerization of dopamine and the simultaneous grafting of polydopamine onto the reactive polymer in organic solution. It appears that the choice of the methods depends on the hydrophobic/hydrophilic balance of the reactive polymer and the form of product targeted (coating by dip coating process, powder form). As shown all along the examples and up to now, attention was paid to the development of nanoparticles of PDA for the cancer therapy. Polydopamine exhibits a huge potency in drug delivery application with a promising success for ocular drug delivery and eye protection.

Regarding all the advantages of using PDA, we hypothesize that it would be of interest to use PDA in ocular drug delivery systems in order to create new drug delivery PDA-based systems. Those systems would exhibit biocompatible and degradable properties. Moreover, the systems would provide sustained drug delivery for small drug and for biologics over long period of time due to the interesting binding properties of PDA toward drugs. Therefore, it would be possible reach the therapeutics level of drug dosage and overcome the limits of the current systems.

Therefore, in the next part, we will describe the commercial (clinically used, approved by the FDA) implantable and injectable drug delivery systems and the one that are in pre-clinical or clinical phase trials for ophthalmic applications.

3. Implantable drug delivery systems in the posterior segment of the eye

The term 'implantable drug delivery system' refers to solid formulation shaped as pellets, discs, rod, sheets or plugs. The implantable systems can be classified as a **reservoir-type** (device) in which the active substance composes the core and is surrounded by a polymeric membrane that composes the shell or as **matrix-type** (solid formulation/implants), in which the active substance is dispersed into a polymeric network. When the active substance is homogeneously dispersed, the formulation refers to monolithic-type. When the active substance is bonded to the polymer by chemical and ionic bonds, it refers to binding-type. In this part we will describe the ocular implants that have been developed for delivery to the back of the eye. The implants are surgically implanted into the vitreous humour (IVT implants), the sclera (scleral implants) or in the conjunctiva (subconjunctival implants). They can be divided into two main categories regarding the type of polymer used: non-biodegradable and biodegradable.

3.1 Non-biodegradable ocular implants for posterior segment of the eye

Non-biodegradable polymeric implants have been developed since 1970. [137] The most common non-degradable polymers used are polyimide (PI), poly(ethylene-*co*-vinyl acetate) (EVA), silicone and poly(vinyl alcohol) (PVA) (**Scheme 8**). EVA and silicone are hydrophobic polymers used as membrane with limited permeability. PVA is hydrophilic and more permeable to drugs. It is water-soluble, so it is often used in combination with EVA and/or silicone. PI is either hydrophilic and/or hydrophobic depending of the composition of the main chain (R_1) and the functional group (R_2).

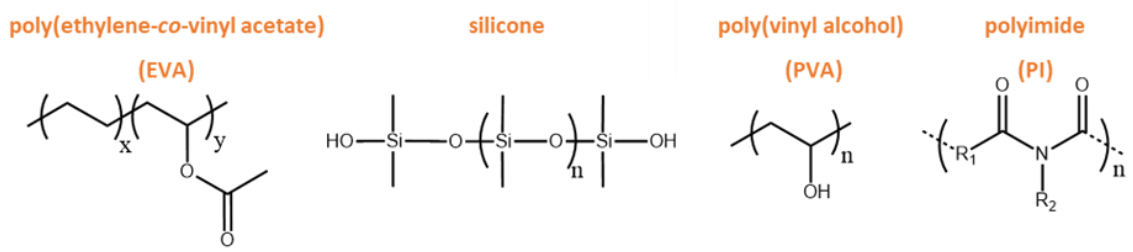

Scheme 8. Non-biodegradable polymers used as ocular implant for posterior segment diseases treatment.

3.1.1 The commercial and pre-clinal strategies to deliver small molecules to the posterior segment

In 1996, the Food and Drug Administration approved the use of **Vitrasert®** [138,139] for the treatment of CMV retinitis. The implants are composed of the ganciclovir (GCV) pellet (diameter = 2.5 mm; weight = 6 mg). The pellet is coated with prepressed EVA films on the sides and a 3-mm EVA disc coated with 10% PVA on the top in order to obtain a constant low release rate of drug of 2 µg/L, sufficient to reach therapeutical level dose over 2.5 months without any drug-related toxicity or complications. The device is implanted surgically and sutured to the sclera thanks to a PVA suture tag (**Figure 15**). Vitrasert® was removed from the marketplace in 2004 due to the decrease in number of patient suffering from CMV retinitis.

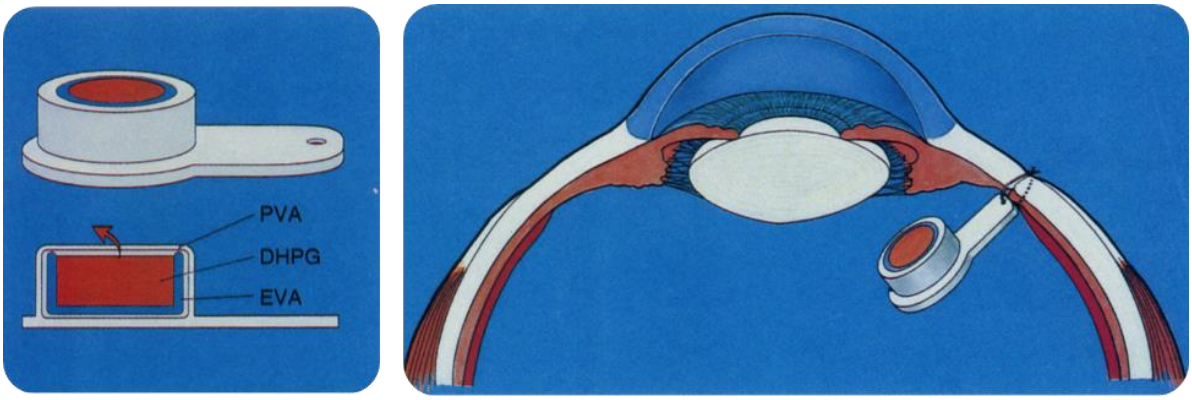

Figure 15. Schematic representation of a EVA/PVA device implanted into the vitreous and attached to the sclera. [138]

Other PVA/EVA-based solid implants were studied and tested in preclinical studies. For example, Cheng *et al.* [140] developed intravitreal solid PVA/EVA implant containing dexamethasone (DEX) for the treatment of uveitis in rabbit and also for the treatment of proliferative vitreoretinopathy (PVR) [141].The implant is composed of a pellet containing dexamethasone coated with successive layers of PVA (M_n = 78 000 g/mol) and EVA and a suture tag is added to anchor the implant to the sclera. This device showed efficiency in the treatment of uveitis in rabbit eye model. The drug was released over 3.5 months. The induced inflammation was suppressed, the integrity of both BAB and BRB were preserved and complication developments such as corneal neovascularization, retinal detachment and cataract were limited. However, the pressure inside the eye cavity, also known as the intraocular pressure (IOP), rose and risk of cataract increased. Ashton *et al.* [142,143] tested the PVA/EVA implant using cyclosporine A (CsA) as active principle for the treatment of uveitis. The drug was detected at therapeutic levels for

9 years into non-inflamed rabbit eyes and for at least 6 months into inflamed rabbit eyes. The difference possibly came from solubility properties, CsA being better soluble in intravitreal serum resulting from the breakdown of BRB of inflamed eye, than in vitreous humour of a non-inflamed one. The CsA-loaded implant showed toxicity in rabbit eyes but not in monkey eyes and the retina/choroid sections appeared normal compared to non-treated inflamed eye. Finally, Okabe *et al*. [144] developed trans-sclera implants as an alternative to intravitreal implants and efficient route in achieving therapeutic concentration of drug in the posterior segment of the eye. [145] The implant was composed of a pellet containing a blend of betamethasone (BM) and PVA at a ratio 3:1. The pellets (diameter: 3 mm; thickness: 0.5 mm) were coated on one side by EVA disc (diameter: 4 mm; thickness: 1 mm). The concentration of drug in the retina and the choroid was maintained over the therapeutic level during a month without inducing any toxicity. Assuming the fact that the large molecules penetrate the retina thought the trans-sclera route, due to the higher permeability of the sclera regarding large molecules [23] compared to other ocular tissue, this device should be promising for the delivery of biologics. However, the EVA/PVA membrane is not really permeable to large and hydrophilic molecules and interaction of biologics such as protein with the membrane could affect the protein stability.[146]

In 2005, the Food and Drug Administration (FDA) approved **Retisert™,** developed by Bausch & Lomb, for the treatment of chronic non-infectious uveitis. Retisert™ is composed of a central compressed core containing 0.59 mg of a fluocinolone acetonide (FA), which is coated with a silicone elastomer layer containing an orifice for the drug release. Between both elements, a semi permeable membrane of PVA controls the release rate (**Figure 16**). The reservoir-type device (length: 5 mm; width: 3mm; thickness: 2 mm) is inserted through a *pars plana* incision and anchored to the sclera. The drug is delivered up to 3 years. [147,148] The visual acuity was stabilized but led to severe complications like the increase of the intraocular pressure IOP for 60% of patients and 7% of them required surgical operation to reduce it. Cataract development was reported in 13% of implanted eyes, 10% of them leading to surgical operation. [149]

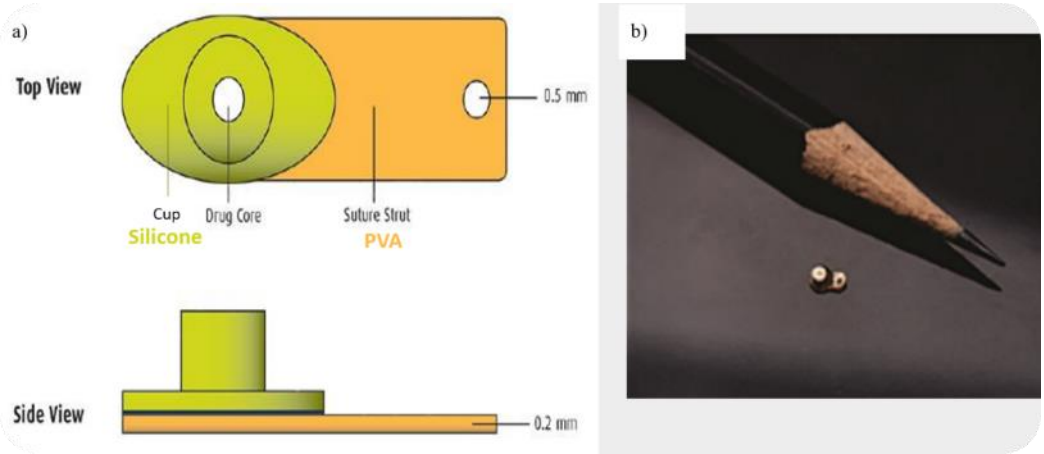

Figure 16. (a) Schematic view of Retisert reservoir-type device [147] and (b) Retisert implant dimension compare to a pencil. [148]

In 2014, the FDA approved the use of **Iluvien™** for the treatment of DME and is currently in clinical phase II and III for the treatment of macular edema and wet AMD respectively. It is used as an alternative to current insufficiently responding laser or anti-vascular endothelial growth (anti-VEGF) treatments. [150,151] Iluvien™ is composed of 0.19 mg FA loaded into a PVA matrix into a polyimide tube (length: 3.5 mm; diameter: 0.37 mm) with a silicone impermeable membrane cap at one end and a PVA permeable membrane cap at the other. Thanks to its small size, when compared to Retisert, the implant is directly injected into the vitreous with a 25-gauge needle (**Figure 17**). The drug is released up to 3 years at an initial release rate of 0.25 µg/day [9,150], the inflammation was reduced and the diabetic retinopathy severity grade decreased but the IPO increased [152,153].

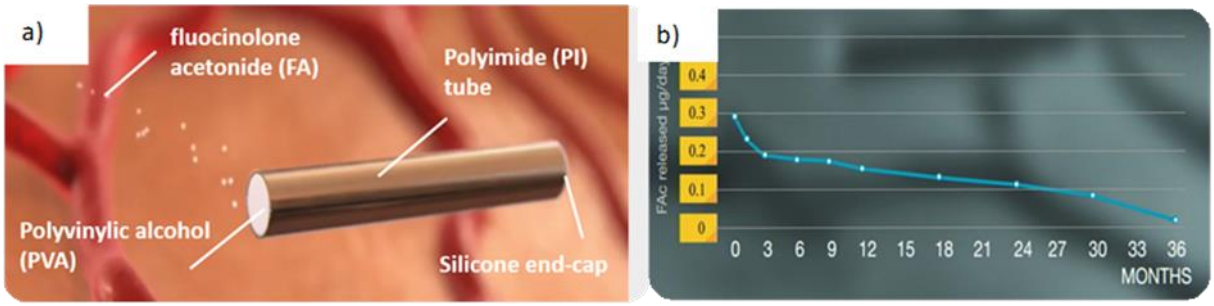

Figure 17. (a) Representation of Iluvien ® and (b) in vitro release. [9]

In 2018, the Food and Drug administration approved the use of **Yutiq®** for the treatment of chronic non-infectious uveitis. Yutiq® has a similar composition with Iluvien. It is composed of a polyimide tube containing 0.18 mg of FA. The drug is released across the end-cap composed of the permeable PVA at a rate of 0.25 µg/day. This implant is preferred to Retisert® for the lower dose of corticosteroid deliver reducing the elevation of IOP and the risk of cataract.

3.1.2 The clinical strategies to deliver biologics to the posterior segment

In the examples described above, all the polymeric systems approved by the FDA aim to deliver small molecules over long period of time. None of them contained biologics. Recently, Genentech reported the development of a new implantable and refillable device called the **Port Delivery System (PDS)** [10,154,155], currently in phase 3 of clinical trial for the delivery of ranibizumab in the treatment of neovascular AMD. The PDS consists in a polysulfone (PSU) body, an extra-flange, a self-sealing septum in silicone to give access to the reservoir without the need to remove the implant for the replenishment process, and a porous metal control element designed to release ranibizumab slowly (**Figure 18**). The PDS is surgically implanted in the vitreous chamber through a small incision in the sclera, the flange is against the sclera and the release control element is in the vitreous chamber. The PDS is filled with 20 µL of solution at varied concentrations of ranibizumab in solution with a promising application for the concentration of 100 mg/mL of ranibizumab in solution to reach relevant therapeutic level during at least 6 months. This technology is promising and would be revolutionary in field of the sustained and sufficient delivery of proteins to cure retinal disease with preservation of the protein characteristics (structure, activity…).

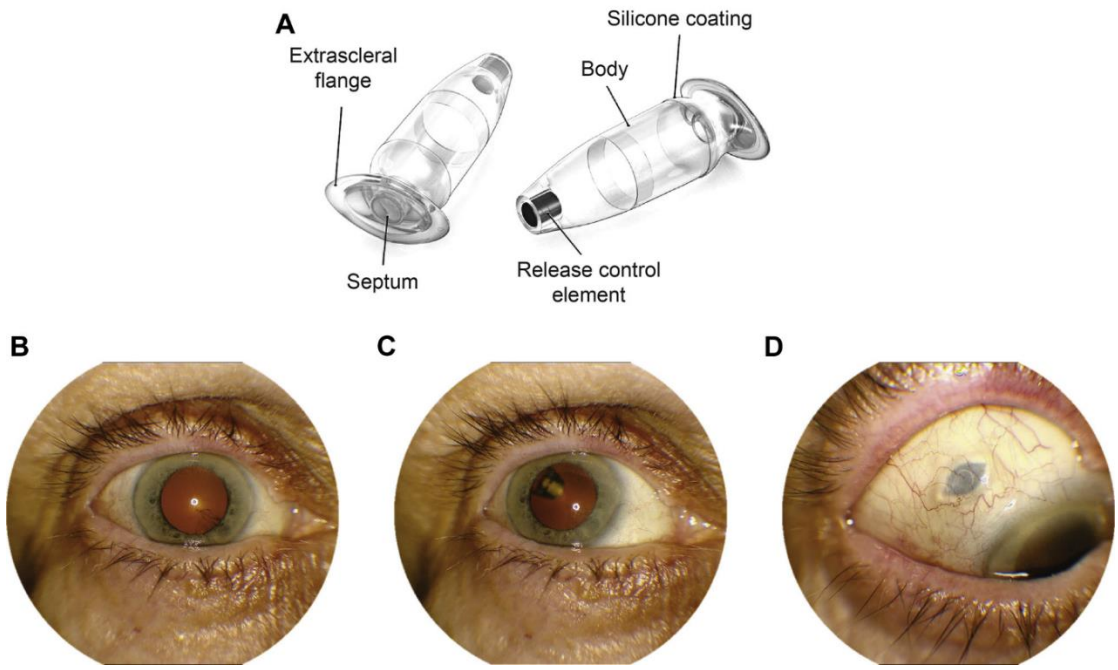

Figure 18. Schematic representation of the Port Delivery System (PDS) with ranibizumab and images of the PDS surgically implanted into human eye. [10]

3.1.3 Conclusion

In conclusion, the major advantage of non-degradable polymeric reservoir-type implants is the zero-order drug release over extended period of time. It is useful for uveitis and DME treatments. They present also several drawbacks, like repeated (except of the refillable PDS) surgical operations to place and remove the implant, and complications, like retinal detachment and infections. Therefore, degradable implants are also considered.

3.2 Degradable ocular implants for posterior segment of the eye

The degradation of polymer includes all changes in the chemical structure and physico-chemical properties of the polymer (for example shape, colour, molecular weight, tensile strength) under the processing or environmental conditions. Particularly, biodegradable polymeric systems are composed of biocompatible polymers that degrade into nontoxic by-products such as carbon dioxide and water thanks to the action of the micro-organism environment. The biodegradable polymeric systems are a sub-branch of biomaterials and have been used in medicine and recently in ecological applications.

In this part, we will focus on the degradable and biocompatible polymers. Two major families of degradable polymers are described in the literature: natural and synthetic polymers. Natural polymers suffer from expensive cost and working conditions, batch-to-batch variation, can lead in some cases to immunogenic response, to complex purification and characterisation processes. [39] Scientists have to explore synthetic biodegradable polymer such as poly(amino-acids), polyorthoesters and polyesters to overcome these disadvantages. For biomedical applications, aliphatic polyesters are commonly used. Therefore, in the following part we will focus on the synthesis and properties of polyesters, their characteristic of degradation of and on the commercial and pre-clinical implants for the delivery of drug to the posterior segment of the eye.

3.2.1 Degradation processes of polymeric systems

The degradation mechanisms of polymeric biomaterials can be divided into 4 types: (i) hydrolytic, which is the scission of specific bonds by water, (ii) enzymatic, which is the scission of specifics bonds by enzyme catalysis, (iii) oxidative, which is caused by radical degradation supported by peroxide during inflammatory reactions, and (iv) physical, which corresponds to swelling-deswelling, the physical stress applied for example. For synthetic biomaterials, hydrolytic degradation is preferred.[156–158]

3.2.1.1 Hydrolytic degradation of polyesters

Hydrolytic degradation is a combination of water diffusion into the network and resulting random cleavage of unstable bonds. Two main mechanisms of hydrolytic degradation exist: the surface erosion and the bulk erosion (also known as bulk degradation). (**Figure 19**)

Surface erosion occurs when hydrolysis is faster than the diffusion of water into the matrix. When immersed into the degradation medium, the material immediately and progressively loses weight (erosion) but keeps its initial molecular weight (no degradation) and its initial shape all along. Typically this type of degradation is encountered with sensitive biomaterials like polyanhydrides or polyorthoesters. [159]

Bulk erosion occurs when the diffusion of water into the matrix is faster than the hydrolysis rate. When immersed, no significative change in the physico-chemical parameters of the material is observed. After some time, the polymer chains start to degrade with simultaneous degradation of both the chains at the surface and in the core. In some specific cases where the degradation rate and the diffusion allow it (*e.g.* PLA), after an incubation period the molecular weight of the polymer chains in the bulk decreases faster than the molecular weight of the polymer chains at the surface (degradation). This is because chain cleavage leads to carboxylic acid by-products which auto-catalyse the system in the inner core leading to non-homogenous degradation and a bimodal molecular weight distribution. After a critical degree of degradation, the network is porous and the oligomers and monomers diffuse through and are released. The material loses weight (erosion). The material progressively degrades and erodes from the centre to the surface. This is the typical mechanism for aliphatic polyesters . [158–164]

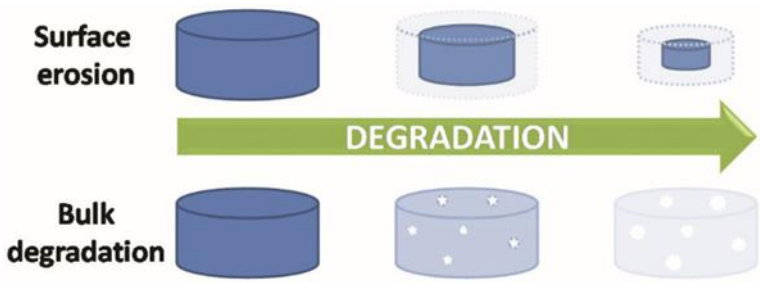

Figure 19. Hydrolytic degradation mechanism of polymeric systems by surface erosion or bulk degradation. [161]

The dominant mechanism between surface or bulk degradation depends therefore mainly on the relation between (i) the time required for the degradation of the polymer chain (defined by the bond energies), (ii) the time required for the diffusion of water into the polymeric matrix (dependent on the intrinsic physico-chemical parameters of the polymer), and (iii) the dimensions of the matrix with maximal critical dimensions being defined for all hydrolysable polymers. [161] In general, the dimensions of ocular matrix are under these matrix maximal critical dimensions, which means that, in the case of polyester-based polymers, the degradation mechanism remains as a bulk degradation mechanism. Moreover, formulations for ocular systems are so small that no autocatalytic degradation is observed. [165]

3.2.1.2 Parameters influencing the degradation of polyesters

Crystallinity refers to the structural order in solid and is influenced by the composition, molecular weight and tacticity. Crystallinity impacts the hydrolytic degradation. Generally, in a semi-crystalline copolymer, the more amorphous the copolymer is, the less ordered the copolymer is, the easier water penetrates, the faster amorphous regions are degraded compared to crystalline regions. [164,166,167]

The hydrophilicity/hydrophobicity balance of polymer impacts the degradation rate. Indeed, the more hydrophilic, the faster is the degradation. [160,164]

Molecular weight generates three factors impacting the hydrolysis rate: the mobility of the chains, the ability of water to penetrate and the concentration in acidic chain-ends. Mobility of the chain decreases when chain length increases. High molecular chain length induces steric hindrance which results in lower amount of water able to penetrate to degrade the chains. Then, the longer the polymer is, the less the concentration of chain-ends catalysing the reaction is, the slower the degradation rate is. [161,168]

The nature of chain end-group affects the *in vitro* degradations. If the chain-end originally composed of carboxylic end-groups (non-end-capped) is modified in order to obtain lactic-acid-ethyl-ester end-groups (end-capped material) for example, the non-end capped material would start to degrade sooner after immersion than the end-capped materials due to the autocatalysis mechanism. [161] Moreover, the non-end-capped materials are more hydrophilic than the end-capped ones.

Temperature is a key factor, degradation is faster upon high media temperature due to higher mobility of the chain, a possible change in material state (glass transition for example) and degradation of the linkage.

The pH value governs the degradation mechanism because ester hydrolysis occurs through acidic or basic catalysis mechanism. Typically, degradation of PCL (M_w = 43 000 -50 000 g/mol) discs in acidic conditions (pH= 1) lead to bulk degradation [169,170]. No gradient of pH was observed in acidic conditions, additional factors may play a role in the bulk erosion mechanism but they are still unknown. On the opposite, alkaline conditions (pH=13) lead to surface erosion [169,170]. Similar characteristics have been observed for PLA as well [171] . This pH-dependence mechanism makes interesting to study the degradation polymer over shorter period of time. Especially, the acidic conditions appear as a suitable model for the accelerated conditions of PCL [158] due to similarities in morphological outcomes.

3.2.1.3 Drug release profile from degradable implants

The release of a pharmaceutical ingredient through a biodegradable matrix is governed by the diffusion of the pharmaceutical ingredient and the degradation of the matrix. The release profile is generally composed of 1, 2 or 3 steps [172] over time and represented in **Figure 20**:

- Phase I: burst effect due to presence of drug at the surface (optional)
- Phase II: constant drug release. The drug diffuses through the implant at a quasi-constant rate without or with slow rate degradation process.
- Phase III: burst effect due to the complete degradation of the implant releasing the remaining amount of drug (optional)

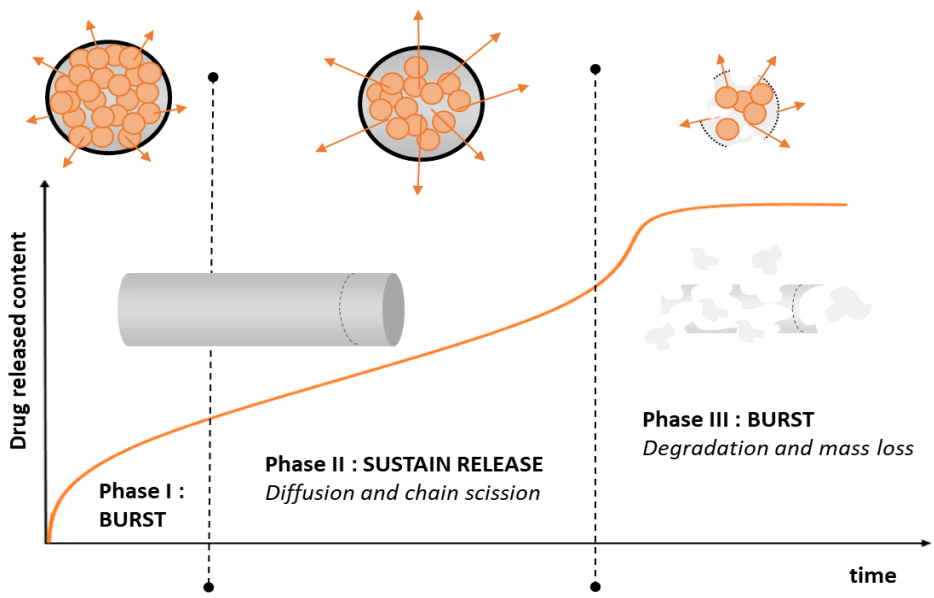

Figure 20. Drug release mechanism and kinetic from biodegradable implants

The physico-chemical properties of the drug (hydrophilic balance, solubility, and molecular weight), the composition of drug/polymer matrix (drug loading, polymer type, polymer molecular weight) and the working conditions (polymer concentration, release media choice) impact the kinetics of the release.

3.2.2 Polyesters used in biomedical and pharmaceutical applications

For biomedical applications, the most commonly used polyesters are aliphatic polyesters such as poly(lactic acid) (PLA), poly(glycolic acid) (PGA) or their copolymers (PLGA), and poly(ε-caprolactone) (PCL) (**Scheme 9**).

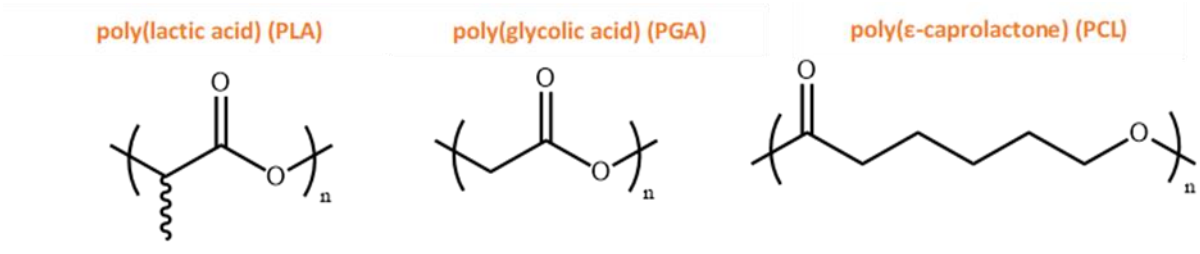

Scheme 9 Common biodegradable polyesters used in the biomedical field.

3.2.2.1 Poly(lactic acid)

PLA is a linear aliphatic polyester. It is hydrophobic and its properties depends on its stereochemical structure and its molecular weight. It is obtained either by ring-opening polymerization of lactide in presence of a catalyst, typically Tin (II) 2-ethylhexanoate (stannous octanoate) or by step growth polymerization (polycondensation) of lactic acid (**Scheme 10**). Due to the presence of two asymmetric carbons, PLA is a chiral polymer and can be under three stereoisomer forms: D-lactide, L-lactide and DL-lactide. (**Scheme 11**)

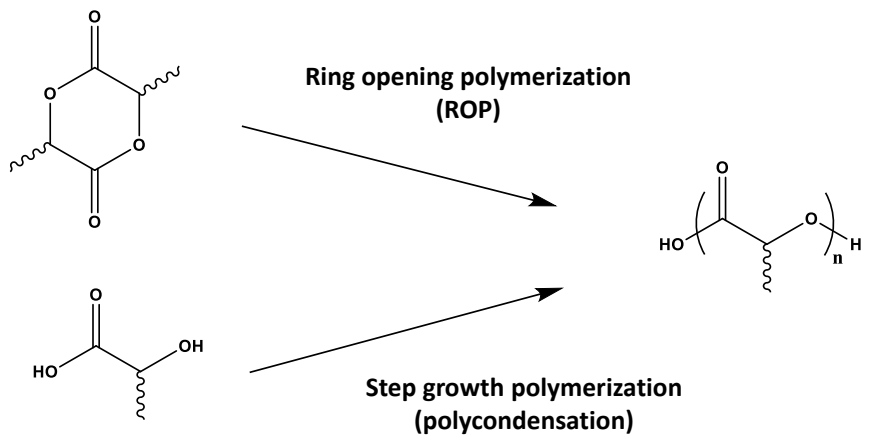

Scheme 10. Synthesis pathways to synthesize poly(lactic acid) (PLA).

PLA ranges from amorphous to high crystalline polymer depending on its stereochemistry. When PLA is either composed of an equal mix of D-lactide and L-lactide or composed of DL-lactide (PDLLA), the PLA is amorphous and the glass transition is around 50°C. When PLA is only composed of D-lactide or L-lactide (PDLA and PLLA respectively), the PLA is semi-crystalline (from mid to high crystallinity), the glass transition is between 55-65°C and the melting temperature is between 130-180°C. PLA degrades by non-specific chain scission of the ester backbone into lactic acid. Depending of the type of PLA (amorphous or crystalline), the molecular weight and the structure of the implant, the implants take between 6 months to 5 years for total resorption. [173,174] Due to its interesting mechanical, biocompatible and slow rate degradation properties, PLA is widely use in tissue engineering [175,176] and as drug delivery carriers [175,176]. Moreover, the release rate of the drug incorporated into a PLA-based system can be triggered by a mix of PLA with various molecular weights and structures [177,178].

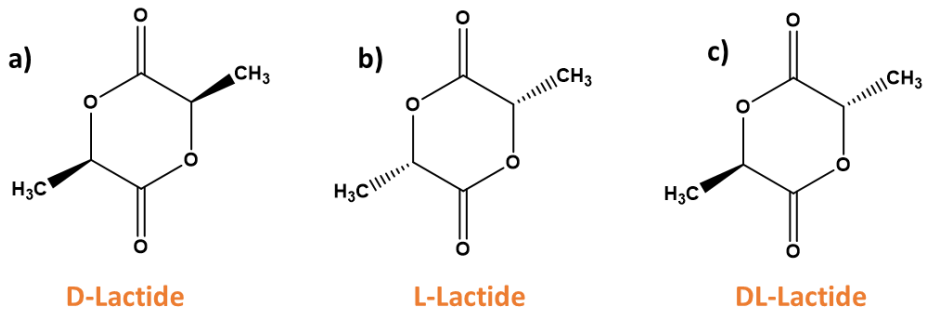

Scheme 11 Chemical structure of lactide stereoisomers: (a) D-lactide, (b) L-lactide, (c) DL-lactide

3.2.2.2 Poly(lactic acid-co- glycolic acid)

PGA is a linear and hydrophobic polyester. It is obtained by the polycondensation of glycolic acid, by ring-opening polymerization of glycolide or by solid-state polycondensation. PGA is crystalline (around 45-55%), the glass transition is between 35-40°C and the melting temperature is between 225-230°C. It is relatively sensitive to water and therefore hydrolytically unstable. It degrades by non-specific scission of the ester backbone into acidic by product, losing mechanical properties within a month and is fully resorbed within a year. To overcome these disadvantages (particularly the high rate of degradation), PGA is often associated with PLA, thus forming a family of **PLGA** copolymers (also written PLAGA copolymers). PLGA is a linear and hydrophobic polyester obtained by the copolymerization of lactic acid and glycolic acid by ring opening polymerization. According to the nomenclature, PLA_XGA_Y refers to X the percentage of L-lactic units and Y the percentage of glycolic acid units.[160] The degree of crystallinity and the characteristic temperatures of PLGA, and by extension to the rate of degradation, depend on the LA/GA ratio, the proportion of PLLA and the molecular weight [179–181]. Therefore, PLGA is a very interesting copolymer with tailored properties for biomedical applications and drug delivery applications. [182–186] However, the acidic degradation of the PLGA gives by products that could lead to change in the pH of the environmental media [187] and cause inflammation reactions [188].

3.2.2.3 Poly(ε-caprolactone)

PCL is a linear aliphatic polyester, the most hydrophobic of all aliphatic polyester. It is obtained by ring-opening polymerization of ε-caprolactone (**Scheme 12**). PCL is a semi-crystalline polymer with a glass transition of -60°C and a melting temperature of 60°C. PCL is biodegradable and degrades by non-specific chain scission of the ester backbone. Due to its structure, PCL is highly crystalline and highly hydrophobic, which confers very slow degradation rate (2-3 years) [174]. Depending on the molecular weight and the structure of the implant, PCL is estimated to take between 2 and 8 years for total resorption [189]. PCL is approved by the Food and Drug Administration in specific application such as drug delivery implant [174,190–192], surgical suture [174] and in tissue engineering [174,193,194]. Compare to PLGA, the PCL degradation products are not acidic, or probably less, and PCL is potentially safe for the micro-environment and particularly for the eye [195] .

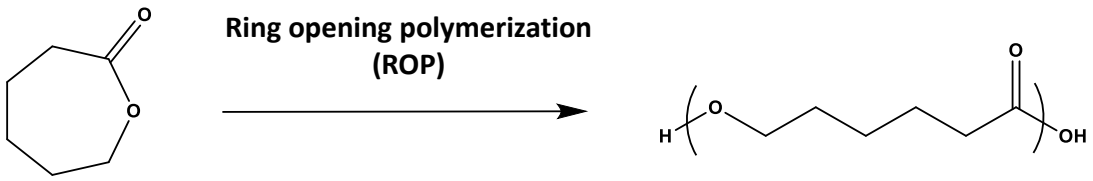

Scheme 12. Synthesis pathway to synthesize poly(ε-caprolactone) (PCL)

3.2.3 The commercial and clinical strategies to deliver small molecules to the posterior segment

3.2.3.1 PLGA-based solid implants

In 2009, the Food and Drug Administration approved the use of **Ozurdex™ (ex Posurdex ™)** for the treatment of macular edema and branch or central retinal vein occlusion (BRVO and CRVO respectively) and, recently in 2014, for the treatment of DME and of non-infectious uveitis. Ozurdex is a biodegradable rod-shaped (length: 6 mm; diameter: 0.46 mm) intravitreal implant composed of a PLGA matrix based on a mix of ester-terminated PLGA (50:50) and acid-terminated PLGA (50:50) loaded with 700 µg of DEX. It is inserted into the vitreous through pars plana incision with a 22-gauge needle. (**Figure 21**) [148] In monkey eyes, DEX is released into 2 stages either in the vitreous or the retina and the implant became smaller and fragmented around day 210 without influencing the release. The therapeutic level is reached and maintained during 6 months. In human eye, tests have been performed for Ozurdex™-type implant. [196–200] The intraocular pressure and the improvements of visual accuracy (VA) are correlated to the DEX release, increasing during the first 2 months then decreasing.

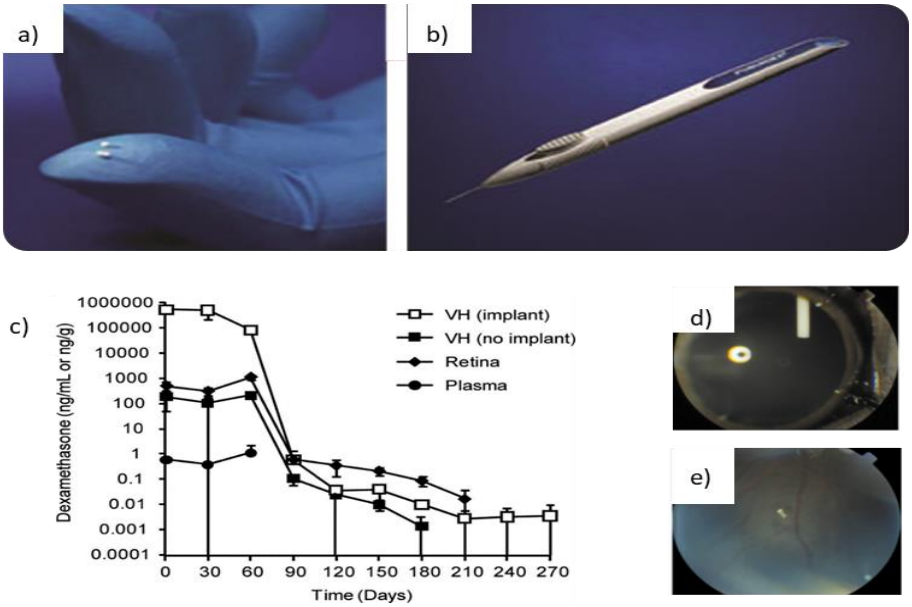

Figure 21. a) Ozurdex™ (b) its 22-gauge needle microinjector. (c) Concentration of dexamethasone in the vitreous, the retina and in the plasma after intravitreal administration into monkey eyes. Photographs showing the implant (d) in its original shape at day 3 and (e) degraded at day 180. [196]

Today, other PLGA-based implants are in clinical trial, particularly the PLGA-based implant developed by Allergan containing brimonidine tartrate, an adrenergic agonist drug, called **Brimo DDS**, currently in phase II for the treatment of dry AMD. [201]

Other PLGA-based solid implants were studied and are tested in preclinical studies. For example, Ikada *et al.* [177,202] developed PLGA-based scleral implants prepared by heat compression. The implant was composed of $PLA_{37.5}GA_{25}$–121 000 g/mol and 25% (w/w) of ganciclovir. In vitro, the release was triphasic and was completed at day 90. In vivo, the concentration of GCV was maintained in the therapeutic range for 3 months in the vitreous and for 5 months in the retina/choroid. The implant started to disintegrate 3 months after implantation and was completely degraded after 5 months. The plug, fragmented or not, was well tolerated by the eye during the study. No retinal detachment or severe inflammations in ocular tissues were observed. Similarly, Fialho *et al.* [203] developed intravitreal $PLA_{25}GA_{50}$ (M_w = 28 -54 000 g/mol) implant (diameter = 1 mm, length = 4 mm, weight = 4.5 mg) containing 28 wt% of the dexamethasone acetate. *In vitro,* 75% of dexamethasone was released after 25 weeks. *In vivo,* 60 % of the drug was released over 8 weeks in an effective concentration range in the vitreous cavity. The implant and its fragmented parts were non-toxic for the retina. [204,205] Also, Sakurai *et al.* [206] developed intravitreal $PLA_{25}GA_{50}$ (M_w = 63 000 g/mol) implant loaded with 1% of FK506

for the treatment of uveitis. *In vitro*, FK506 was slowly released to reach 35% at 35 days without burst effect. *In vivo*, the concentration of FK506 in the vitreous of rabbits was maintained from 350 to 480 ng/g for 35 days. The implant was efficient in reducing/suppressing the inflamed cells without any toxic side-effect and in preserving the architecture of ocular tissues in the rabbit model. Similarly, Souza *et al.* [86] showed that a FK506-loaded (10%) PLGA (75:25) implant was safe to rabbit eye and deliver adequate concentrations of drug in the vitreous.

3.2.3.2 PCL-based solid implants

Despite all the advantages of PCL previously exposed, there is no PCL-based implant approved by the FDA at present to treat posterior segment diseases. Only pre-clinical interesting and promising applications will be detailed in this part.

Fialho *et al.* [207,208] studied the release of DEX (25 wt.%) from PCL (M_w = 14 000 g.mol^{-1}) disc implants made by compression technique. *In vitro*, they showed that 25% of drug was released over 21 weeks. They expected at least a 1-year period of release thanks to the slow degradation and good stability of PCL and thanks to the hydrophobicity of DEX which prevents fast diffusion. *In vivo*, the concentration was maintained within the therapeutic range during 55 weeks. In return, IOP was higher in eye containing the DEX-loaded implant but no cataract was induced due to the low dose slowly released.

Sun *el al.* [192] developed episcleral multi-layered PCL films for the prevention and the treatment of PVR. The film (thickness = 300-400 µm) was composed of successive sprayed layers of PCL (M_w = 80 000 g/mol) and triamcinolone acetonide. *In vitro*, they showed that 75% of the drug was progressively released during the 90-day study. In vivo, the degradation of the film was detected 3 months after surgery implantation and the sustained released of TA over 4 months was observed in an appropriate concentration range. The film was well tolerated by the rabbit eye without any severe adverse effects.

The previous example treated the delivery of small molecules. In order to palliate the lack of delivery of biologics over long period of time to the posterior segment of the eye, Lance *et al.* [209,210] developed a nanostructure membrane (~20 nm) of PCL (Mn = 80 000 g.mol^{-1}) to deliver ranibizumab. The thin structure allows the sustained delivery of the biologics during 16 weeks *in vitro* and during 12 weeks in the vitreous cavity of rabbits without immune response and absorption of protein on PCL layer but some protein aggregation occurred inside the implant.

3.3 Conclusion about the implantable drug delivery systems

The majority of the implantable systems were designed for the delivery of small molecules due to their stability regarding the manufacture process and the polymeric matrix compared to biologics. The implantable ocular systems allow the sustained release of the drug from 3 months to 3 years regarding their composition. The majority of the ocular implants studied and approved by the FDA is composed of PLGA and a huge potency of PCL systems has been observed for drug delivery applications. Therefore, there is still a need in ocular delivery to overcome the invasive surgical procedure and extends the therapeutic action of large molecules for the treatment of retinal diseases. A resume of the implantable systems is drawn in **Table 4**.

Table 4. Implantable polymeric systems approved by the FDA or under clinical and pre-clinal studies for drug delivery to the posterior segment of the eye

Commercial Brand	Route of administration	Polymer	Drug	Drug loading	Release rate	Therapy recommended	Clinical phase	Major advantages	Major limitations	
					Non degradable					
Vitrasert	IVT	EVA/PVA	ganciclovir	6 mg	2.5 months (in vivo)	CMV retinitis	FDA-approved (1996)	-	Invasive surgical procedure (implantation and removal)	138,139
Retisert	IVT	Silicone/PVA	fluocinolone acetonide	0.59 mg	3 years	uveitis	FDA-approved (2005)	-	Invasive surgical procedure (implantation and removal)	147,148
Iluvien	IVT	PI/PVA	fluocinolone acetonide	0.19 mg	3 years	DME, wet AMD	FDA-approved (2004), (phase III)	25G needle injector	-	9,150
Yutiq	IVT	PI/PVA	fluocinolone acetonide	0.18 mg	2.5-3 years	uveitis	FDA-approved (2018)	Less IOP elevation compare to Retisert	-	
PDS	IVT	PSU/Silicone	ranibizumab	2 mg in 20 uL	6-15 months for refill	AMD	Phase III	The only non-biodegradable system for delivery of biologics	Stability only for ranibizumab	10,154, 155
					Degradable					
Ozurdex	IVT	PLGA	dexamethasone	700 mg	6 months	MD, CRVO, DME, uveitis	FDA-approved (2009)	Biodegradable long-term release	PLGA acid degradation products IOP elevation	148 196–200

Brimo DDS	IVT	PLGA	brimonidine tartrate	132-400 mg	N/A	Dry AMD	Phase II	No elevation of IOP	-	201
-	scleral	PLGA	ganciclovir	25%	3 months (in vitro)	Model for retinal disease	Pre-clinical	-	-	177,202
-	IVT	PLGA	dexamethasone	1.26 mg (28%)	75% in 25 week (in vitro), 60% in 8 weeks (in vivo)	Model for retinal disease	Pre-clinical	-	-	203
-	IVT	PCL	dexamethasone	25%	25% in 21 weeks (in vitro), therapeutic level in 55 weeks (in vivo)	Model for retinal disease	Pre-clinical	Sustained and long-term release	IOP elevation	207,208
-	sclera	PCL	fluocinolone acetonide	6-12 mg	75% in 3 months (in vitro), therapeutic level in 4 weeks (in vivo)	PVR	Pre-clinical	-	-	192
-	IVT	PCL	ranibizumab	0.17-0.19 mg	12 weeks (in vivo)	AMD		The only biodegradable system for delivery of biologics	Protein aggregation in the device	209,210

4. Injectable *in situ*-gelling medical formulation in the posterior segments of the eye

The term "injectable" refers to a solution able to form (i) a suspension of micelles, liposomes, nano- or micro-capsules, nano- or micro-spheres for example or to form in-situ (ii) semi-solid depot/gel.

4.1 The particulate strategy for delivery of drugs

The first category is **the particulate strategy**. It includes polymeric micelles, liposomes, polymersomes, micro- or nano-capsules, nano- or micro-spheres, dendrimers and complex conjugates. [211] By definition, the size of the nano-systems ranges from 1-1000 nm and the micro-systems from 1-1000 µm. (**Figure 22**)

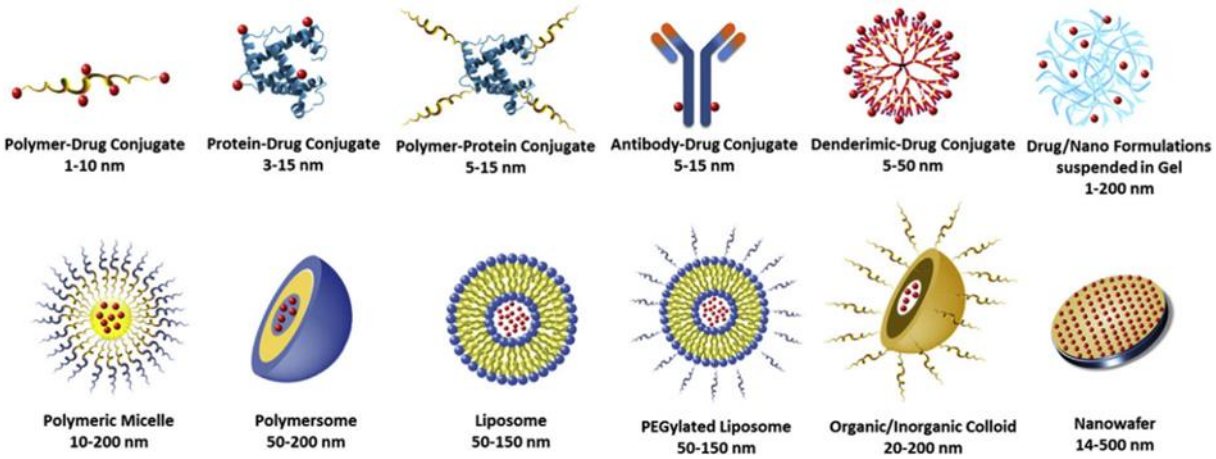

Figure 22. Schematic representation of nanomedicine formulations used in ocular delivery [211]

Polymeric micelles and liposomes are potential good candidates for the delivery of molecules due to their compatibility, the possibility to entrap hydrophobic and hydrophilic drugs, and small size (< 300 nm) but they suffer from rapid degradation and clearance rate [212], which is not suitable for long sustained delivery of drug to the posterior segment but showed interest for anterior segment disorders [213]. The **solid micro- and nano- systems** offer great advantages like high surface area to volume which make them capable of encapsulate or interact with targeting moieties. Moreover, they can be engineered in a wide range of size, shapes and surface properties using very simple methods.[212] Given

that, this technology helps to improve the solubility and the stability of a drug, increase the residence time of the drug into the tissues, enhance the cellular uptake by active or passive transport [214] and decrease the potential toxicity of the drug and in a less invasive and painful technique compare to implants. The particulate strategy has been widely studied for the treatment of ocular diseases in the anterior as well as in the posterior eye segment. [211,212,214–217] However, the micro and nano-systems present several drawbacks. Regarding their size/composition, the particulate system will be washed away due to the presence of anatomical barriers and liquid movements in the eye or will be immobilized in the vitreous (reminder: negatively charged, mesh size around 500 µm). This would interrupt the treatment. Moreover, spreading, sedimentation and aggregation can occur [214], which could blur the vision. Besides, many scientists reported the non-toxicity or the relatively low toxicity of the particulate systems to ocular cell line. However, studies performed *in vivo* showed acute immune response due to the toxicity of intravitreal injection of unloaded particulate systems. [218] The toxicity could come from the shape of the particles, their size and also from the residual solvent of the chemical particles' synthesis. For industrial perspectives, product scale-up and reproducibility in the production of ocular compounds is also a limiting step. [214] Concerning the delivery of drug to the posterior segment, only Visudyne ®, a liposomal injection containing verteporfin as small drug, was approved in 2000 for the treatment of wet AMD. The IVT injection of liposomes or microspheres for DME treatment and microparticles for the treatment of wet AMD are currently in clinical phase II. [219]

4.2 The in-situ forming depot/gelling strategy for the delivery of drugs

Regarding the need in alternative less invasive, biocompatible, degradable and custom-made polymeric strategies, the **injectable in situ depot/gelling strategy** emerged. It consists in a liquid-viscous monomeric or polymeric solution that undergoes physico-chemical changes (swelling/deswelling of the network, cross-linking, precipitation) upon administration in response to environmental variations (temperature, pH, ionic strength, solvent composition). [220,221] This strategy has grown interest for biomedical applications such as in tissue engineering [222] and particularly in ophthalmic application such as lens replacement [223–225] or as vitreous substitute [223,226–228]. It also showed potency in drug delivery applications via parental delivery administration [229,230], and eye anterior chamber or intravitreal administrations [231]. In the literature, the terms depot systems or gelling systems may be interchangeable and can simply be named as in situ forming systems.

4.2.1.1 Advantages and challenges of the in-situ forming strategy

The injectable in situ depot/gelling strategy allows the **ease of administration** through small diameter needle thus improving the patient compliance with less invasive surgical procedure compared to implantable systems [231]. Moreover, it has been reported that the gelling systems allow **high payload** [232] of various drugs [233] (hydrophilic or hydrophilic, small or large) making them promising candidates for the drug delivery to the posterior segments of the eye. Besides, thanks to its macroscopic size, the depot or the gel is **less exposed to diffusion** through the vitreous and rapid clearance compared to particulate systems, depending on the mechanical properties of the in situ formed object.

However, several critical parameters have to be taken into account for the design of such injectable in situ forming objects. First, the **viscosity** of the solution is a critical parameter. Indeed, the concentration of the polymer in solution or the **cross-linking density** of the network should be sufficient to allow sustained release of a large amount of drug once administrated but compatible with a viscosity allowing the passage thought the needle (around 30G, see chapter I-part I-3-5). Subsequently, the **time transition of liquid-viscous sol to a gel-like** object should be fast to prevent the burst release effect of the drug but not too fast to prevent gelation inside or at the tip of the needle that would block the entry. The system should not obstruct the vision. Also, the **sterilization** methods [39,234,235] of the systems can alter the properties of degradability of the polymers and cause structural changes for polymer and drug-loaded polymer. Besides, the system should preserve the **stability and the activity of the active ingredient** (mostly proteins, due to the presence of reactive NH2 and SH functional groups) during the preparation, the storage and the release. Moreover, in term of industrial point of view, the number of chemical steps involved and the batch-to-batch variation are very challenging, not be cost-effective and therefore rate-limiting of the industrial production.

As a result, and due to the recent interest in the field, the injectable in situ depot/gelling strategy of ocular drug delivery is still under pre-clinical phase.

The in-situ forming-systems can be classified regarding the type of cross-linking network, the nature of the polymer matrix, the nature of the stimuli involved and their effects on change in properties of the polymeric network. In the following parts, we will go through the different classifications listed and we will give example of the pre-clinical studies of injectable in-situ forming-systems used for the delivery of drug to the posterior segments.

4.2.1.2 Types of cross-linked networks

The chemically cross-linked networks are known as permanent networks. They are held by covalent bounding and are generated by photopolymerization, organic reactions (Michael addition, Schiff base formation, Diels–Alder reaction, click chemistry) or enzymatic reactions. [236] The chemically cross-linked network exhibits strong mechanical properties but the potentially residual components used during their synthesis (cross-linker agent for example) and the by-products may damage the cells and the bioactive principle incorporated, limiting their biological application. (**Figure 23**-a) **Physically cross-linked polymer networks** are known as non-permanent networks. They are held mainly by molecular entanglements, charge interactions, hydrophobic interactions and hydrogen bonding. [237,238] They are safer than the chemically cross-linked ones because no cross-linking agents are required, they are however less robust and degrade faster. (**Figure 23**-b)

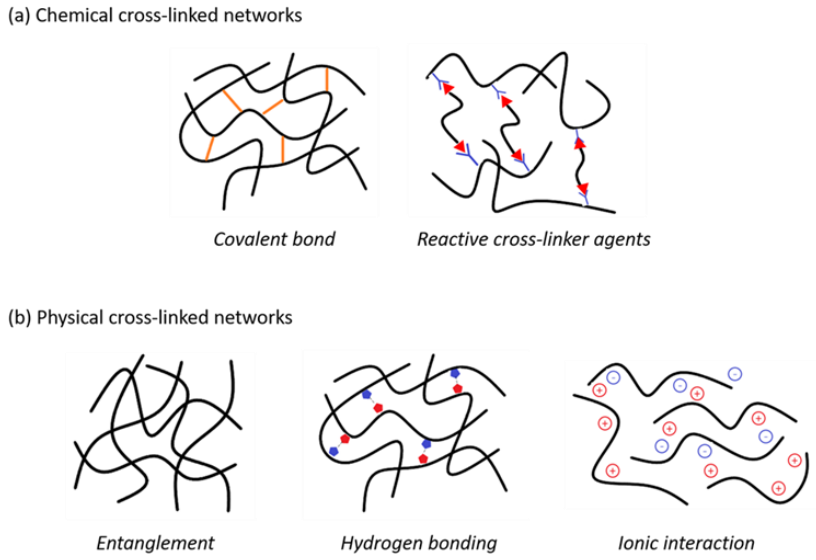

Figure 23. Representation of chemical (a) and physical (b) cross-linked hydrogel networks

4.2.1.3 The mechanism of formation of in situ forming systems

Previously we listed the various stimuli that induce a change in the physico-chemical properties of the networks. In this part, in accordance with the work described in the following chapters, we will only focus on the mechanisms involving thermo-responsiveness of aqueous polymer solutions and to the gelation/depot induced by solvent-exchange process.

The first thermo-gelation mechanism is the **coil to globule transition** which consists in a change in solvation state (swollen vs shrunken) at a specific temperature called the lower critical solution temperature (LCST) and the upper critical solution temperature (UCST). The second thermo-gelation mechanism is the **micelles packing and entanglement** which consist in the packing and entanglement of the amphiphilic copolymers above specific concentration, called critical gelation concentration (CGC), and temperature, called lower or upper critical gelation temperature (LCGT and UCGT). The temperature of transition is a combination between the composition, the molecular weight, the hydrophilic/hydrophobic balance and the concentration of copolymer in water. [238–240] The third thermo-gelation mechanism is the **coil to helix transition** which consists in the polymer chains aggregation, formation of a rigid 3D network (gel) and random polymer chain conformation (liquid) when raising the temperature.

The **solvent-exchange mechanism** consists in the dissolution of polymer in an organic solvent followed by the penetration of water resulting in a progressive diffusion of the organic solvent when immersed in an aqueous media, allowing gel formation due to hydrophobic effect. [241]

In situ gelation by thermo-responsive mechanism

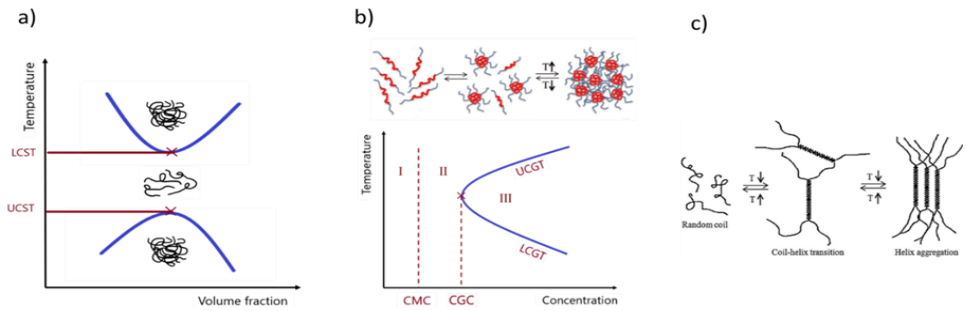

In situ gelation by solvent-exchange mechanism

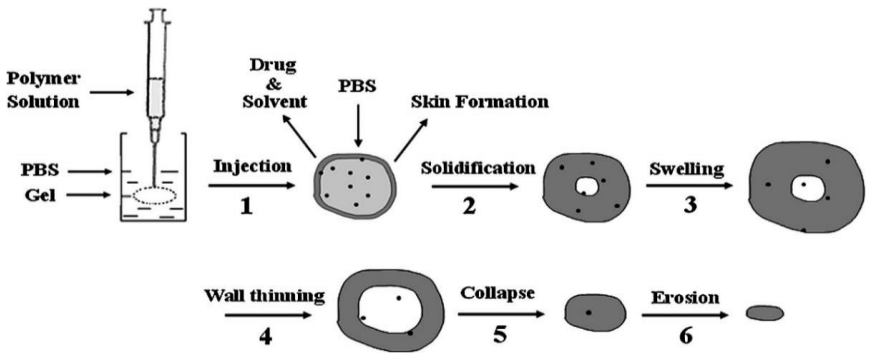

Figure 24. Schematic representation of the in situ gelation mechanism by thermo-responsive mechanism of a) coil to globule transition, b) micelle packing and entanglement [238] c) coil to helix transition [238]and by solvent-exchange mechanism [241]

4.2.1.4 Mechanisms of API release from gelling and depot systems

The release of an API from gelling systems is classified into three mechanisms. The diffusion controlled and the chemically controlled mechanism, as for implants systems are described in Chapter 1 Part 3.2.1.3. In the case of depot/gelling systems, the swelling controlled mechanism is added. The release mechanism depends on the gel formation process (thermally or solvent-exchange induced), and both polymeric network (mesh size, porosity, degradability) and API (radius, hydrophobicity) characteristics [233].

- **Diffusion controlled**: the release of the drug is proportional to the square root of time.
- **Chemically controlled:** combination of diffusion and of erosion/degradation of the polymeric network.
- **Swelling controlled**: the diffusion of the drug is enhanced thanks to the swelling of the polymer.

The gelling systems can be composed of natural or synthetic polymers or a combination of both to control and adjust the toxicity of the matrix, the kinetics of gelation and the degradation of the matrix and consequently the release profile of the pharmaceutical ingredient incorporated.

4.3 Pre-clinical strategies to delivery molecules to the anterior and posterior segments using injectable in-situ forming systems

Several strategies to deliver drug, particularly small drugs, to the anterior segment by topical application using natural [231,242–244] or synthetic in situ gelling systems [245–248] or a combination of both, with the presence of particulate systems or not, were described over the past decade. These systems are under pre-clinical study, they deal with the sol-to-gel transition but not with the injectable notion we are looking for.

The treatment of the anterior diseases through injection in the anterior chamber and the treatment of posterior diseases through vitreous or subconjunctival administration of in-situ forming systems is one of the major research fields today due to the urgent need in alternative treatments (less invasive procedure, stability and sustained release of biologics).

4.3.1 Natural polymeric matrix

The natural polymers display several advantages like good cell adhesion, stimuli-responsiveness, and biodegradability. [39] Among the natural polymers, we can distinguish one particular family called polysaccharides, derived from plants extraction, animal or microbial sources, and exhibit excellent biocompatibility properties.

Hyaluronic acid (HA) is an anionic polysaccharide naturally present in the human body, and particularly in the vitreous humour. [249,250] It is a polymer of disaccharides composed of D-glucuronic acid and N-acetyl-D-glucosamine, linked via alternating glycosidic bond, β-(1→4) and β-(1→3) [249,250]. It is biocompatible, biodegradable , endogenous and non-immunogenic and thus suitable for biomedical application. [249,250] However, hyaluronic acid does not allow gelation on its own. Therefore, chemical modification of hyaluronic acid or addition of cross-linking agents or gelling agents is necessary to obtain HA-based hydrogels. HA-based hydrogels are often is combination with **dextran (DEX)**, another polysaccharide derived from glucose that also exhibits biocompatible, biodegradable, non-toxic and bio-adhesive properties. [251] For example, Yu *et al* [252] developed an *in situ*- gelling hydrogel composed of HA functionalized with vinylsulfone (HA-VS) chemically cross-linked to a thiolated dextran (DEX-SH) without any catalyst agent, making the biomedical application safer, and containing bevacizumab to treat age-related macular degeneration (AMD) and diabetic retinopathy (DR). The solution was injected into the vitreous of rabbit's eyes via *pars plana* incision and formed a bevacizumab encapsulated transparent gel. No opacification of the lens, retinal detachment or inflammation were observed. The authors did not mention the time required for gelation. *In vivo*, the concentration of bevacizumab in the vitreous is superior to the therapeutic concentration (50 ng/mL) and decreased from 50 000 ng/mL to 100 ng/mL after 6 months. The authors established a simulation and concluded that the concentration in the vitreous at the end of the study is 7 times higher than the concentration obtained after bolus injection.

Chitosan (CS) is a linear amino-polysaccharide obtained from the treatment of chitin shells of crustaceans, mostly shrimps. It is composed of randomly distributed D-glucosamine deacetylated units and *N*-acetyl-D-glucosamine acetylated units. [253] Chitosan is a natural cationic polymer having biocompatible, biodegradable, mucoadhesive, permeation enhancement, anti-bacterial and antifungal properties. [254] Chitosan is soluble in aqueous solution at pH below 6.2 but forms a hydrated gel-like precipitate at neutral and alkaline pH value. Chitosan cationic polysaccharide is combined to polyol anionic salt to prevent chitosan precipitation or is chemically modified to obtain a water-soluble form**.** To form gelling-systems and to improve chitosan properties such as stability, chitosan is crosslinked

(physically or chemically). [253] Chemical modifications or interaction with other polymers also help in the formation of a stronger network for the sustained delivery of drug. [253] For example, Cheng *et al.* [242] developed an *in situ*- gelling hydrogel composed of chitosan, gelatine to reduce the sol-to-gel transition and β-glycerophosphate. *In vitro*, the release of latanoprost is constant without initial burst, and reaches almost 70% at the end of the 28-day study. *In vivo,* the solution was injected into the sub-conjunctival space using a 30G needle into rabbits' eyes. The concentration of drug in the aqueous humour is stable during almost a month in a sufficient therapeutic dose.

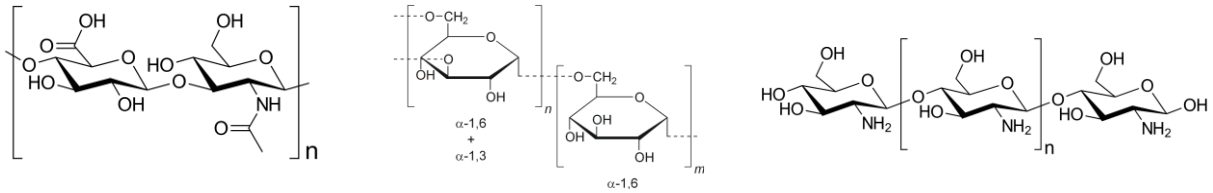

Scheme 13. Natural polymers commonly used in the drug delivery to the posterior segment of the eye

4.3.2 Synthetic polymeric matrices

4.3.2.1 Thermo-responsive in situ forming systems based on amphiphilic copolymers

Poly(ethylene glycol) (PEG) is a water-soluble polymer approved by the FDA [39] for many pharmaceutical clinal uses. In the literature, PEG is also describe as poly(ethylene oxide) (PEO), the term are interchangeable. PEG tends to accumulate into the tissues and the organs. After intravenous administration, PEG is eliminated from the body by kidney filtration (renal excretion) when the molecular weight is below 20 000 g.mol^{-1} making it bio-eliminable [255] whereas above this value, the elimination is not guaranteed. After intravitreal administration, PEG may accumulate in the retinal cells (RPE) [256], therefore careful attention should be provided. In order to form gelling systems, PEG can be crosslinked [257] (physically or chemically). However those systems may require the use of toxic products [257] which limits the use of ocular applications and they may rapidly form the cross-linked network which limits their application for intravitreal injection. PEG can also be used for the synthesis of crosslinked copolymer networks or the synthesis of block and star-shaped copolymers.

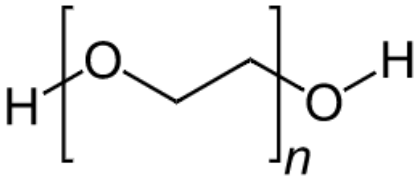

Scheme 14. Chemical formula of poly(ethylene glycol) (PEG)

Poly(*N*-isopropylacrylamide) (PNIPAAm) is a synthetic non-degradable polymer obtained from the polymerization of *N*-isopropylacrylamide by radical, redox or ionic polymerisation. [258] PNIPAAm is thermosensitive and exhibits a lower critical solution temperature (LCST) in water around 32°C. The LCST can be modulated by copolymerization of NIPAAm with other monomers or by external factors (pH, solvent nature, electrolytes for example). [259] For example, Drapala *et al.* [260] developed a PNIPAAm-based hydrogel chemically cross-linked with poly(ethylene glycol) diacrylate (PEG-DA) by polymerization of NIPAAM and PEG-DA. The 8mM PEG-PDA cross-linked PNIPAAm hydrogel showed good consistency for its ease of injection as being not too rigid (16 mM crosslinker concentration) and not too liquid (4 mM crosslinker concentration) with a temperature of transition around 32°C. The *in vitro* release tests showed that almost 80% of Bovine Serum Albumin (BSA) was released after 5 days at 37°C. **(Figure 26)** Turturro *et al.* [261] injected the same 8mM-PEG-DA/PNIPAAm solution into the vitreous of rats. They showed that NIPAAm/PEG-DA hydrogel was safe for the retina and retinal function and showed potential as drug delivery vehicle for posterior segment application. Despite its potential, the toxicity of PNIPAAm systems is still under discussion and therefore the PNIPAAm systems are not approved by the FDA up to now.

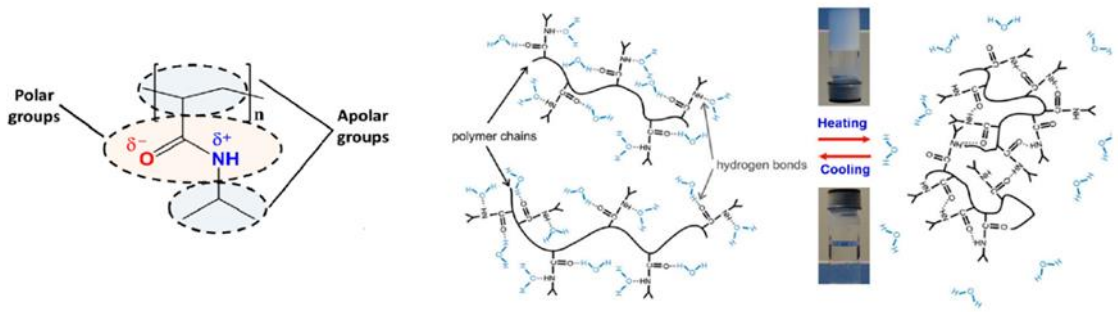

Figure 25 Chemical formula of PNIPAAm and representation in its swollen and shrunken state. [259]

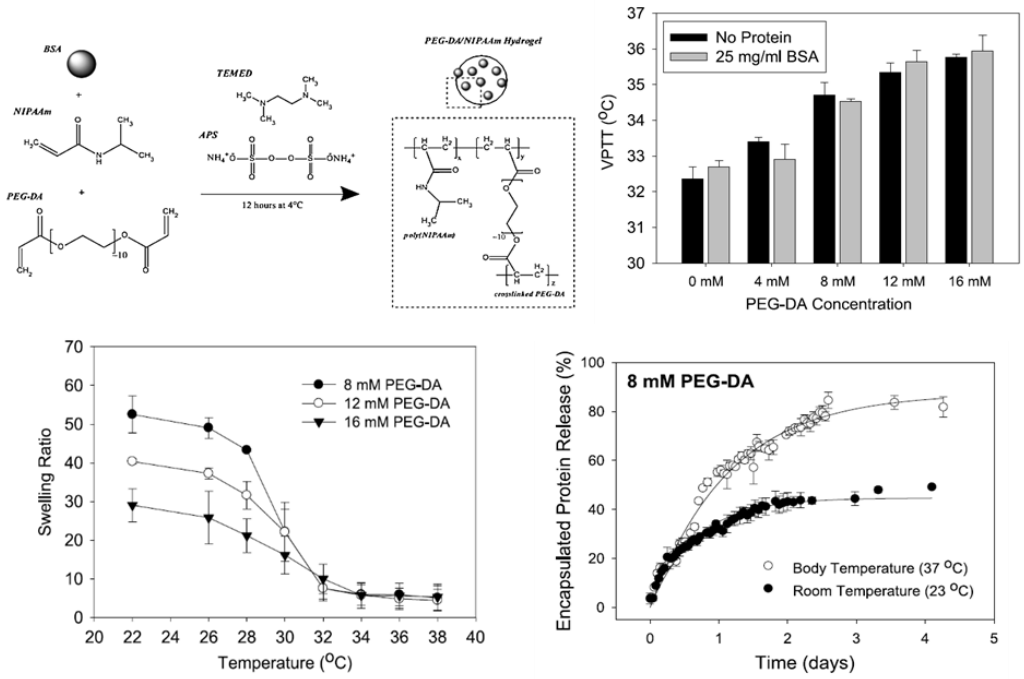

Figure 26. Synthesis and characteristics (VPTT and swelling ratio) of PEG-DA/PNIPAAm hydrogel and in vitro cumulative release of BSA encapsulated. [260]

Poloxamers, also known as Pluronics®, are linear amphiphilic triblock copolymers approved by the FDA for cosmetic and pharmaceutical applications. They are composed of a hydrophobic poly(propylene oxide) (PPO) central block and hydrophilic poly(ethylene oxide) (PEO) side chains [262–267]. However, PEO-PPO-PEO systems showed short residence time, weak mechanical properties and retinal toxicity, especially after intravitreal injection of Pluronic F127 [268,269] when the concentration exceed 20 wt.% in water, which limits its use for a drug delivery carrier to the posterior segment**.**

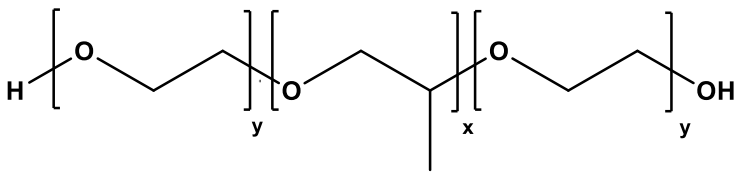

Scheme 15 Chemical formula of PEO-*b*-PPO-*b*-PEO copolymer

Poly(lactic-*co*-glycolic acid) (PLGA) and poly(ε-caprolactone) (PCL) are biocompatible, biodegradable and hydrophobic polymers described in the previous parts. They are used in combination with hydrophilic polymers, such as PEG, to obtain amphiphilic copolymers susceptible exhibiting stimuli-responsive gelling systems. [239,270]

PLGA–PEG–PLGA triblock copolymers are synthesize by ring opening polymerization of lactide and glycolide in presence of PEG as initiator and catalyst in dried conditions (**Scheme 16**). These copolymers have been widely investigated in diverse applications due to their adjustable gel performance [271] and controllable biodegradation rate. For example, ReGel® is composed of PLGA-PEG-PLGA copolymer with a central block of 1000 g.mol^{-1} and lateral blocks of 1500 g.mol^{-1} each with a LA:GA ratio of 3:1. [272] It degrades in 4 weeks and allow the sustained release of small drug from 1 to 6 weeks [272] and of protein up to 2 weeks [273] . It is approved by the FDA. However, ReGel® shows a sol to gel transition around 20°C which is not suitable for the administration of the polymer though small diameter needle into the vitreous. By increase the molecular weights of each blocks, the PLGA-PEG-PLGA copolymer composed of a central block of 1500 g.mol^{-1} and lateral blocks of 1800 g.mol^{-1} with a LA:GA ratio of 3:1 (1800-1500-1800, LA:GA ratio = 3:1) exhibit sol to gel transition around 30°C which allow intravitreal administration at room temperature. [274] The release of dexamethasone from this system can be extended to 30 days in vitro and the subconjunctival application of the drug-loaded gelling systems showed reduction is neovascularisation induced in corneal neovascularization disease in rats' eyes. [274,275] The PLGA-PEG-PLGA copolymers have also been studied for the delivery of macromolecules. Particularly, the PLGA-PEG-PLGA (1800-1500-1800, LA:GA ratio = 96:4) allow the sustained release of a given antibody during 20 days *In vitro* and the antibody was found to be stable during the encapsulation and release processes [276].

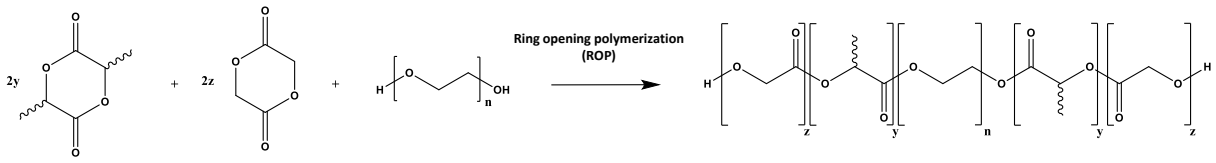

Scheme 16. Synthesis pathway of poly(lactic-*co*-glycolic acid)-*b*-poly(ethylene glycol)-*b*-poly(lactic-*co*-glycolic acid) (PLGA-*b*-PEG-*b*–PLGA) copolymer

Instead of containing only PLGA-PEG-PLGA copolymers, formulations can be prepared from a mix of copolymers. For example, the PLGA-PEG-PLGA block copolymer can be prepared from mixing PEG1000

and PEG1500 at a ratio 1/1, and containing bevacizumab for intravitreal injection. [277] *In vitro,* bevacizumab was released over 14 days without initial burst with a plateau between 10-20%. *In vivo,* 1.5 µL of solution is injected intravitreally and a gel was formed immediately and was progressively degraded to disappear after 8 weeks. No apparent toxicity to the retina and no inflammation were observed. Also, the PLGA-PEG-PLGA block copolymer can be prepared from a mixture of copolymer with distinct compositions. Two copolymers with block lengths of 1510-1000-1510 (copolymer insoluble in water) and 1270-1500-1270 (copolymer soluble in water but not able to form a gel) were mixed at different ratios (2/1, 1/1 or 1/2) to form thermal-induced gel formation at body temperature. [278] The copolymer solution was loaded with dexamethasone. Typically, for a higher dexamethasone content (4 mg/mL), 60 % of drug were released from the more hydrophobic system (ratio 2:1) while more than 70% were released from the system composed of 1/1 ratio up to 18 days, without significant burst release. *In vivo,* 100 µL of the mixture containing 1mg/mL of DEX was injected thought 26G needle, the concentration of DEX in the vitreous remained above the effective concentration during 9 days.

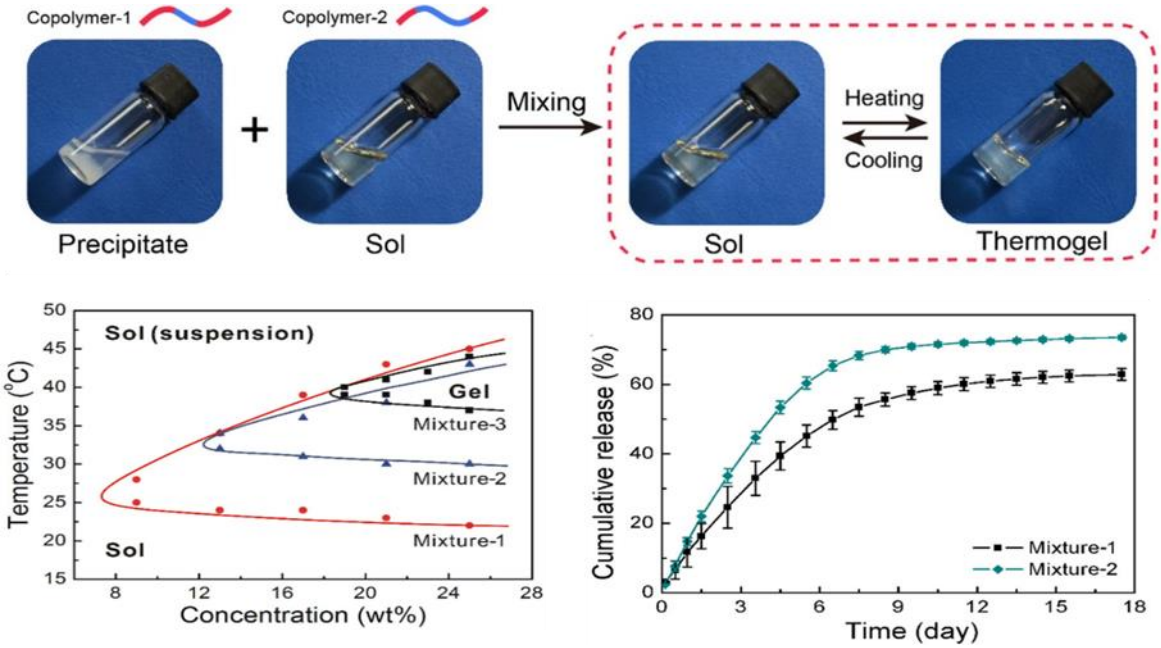

Figure 27. Sol-gel behaviour of PLGA-PEG-PLGA mixtures composed of 1510-1000-1510 and 1270-1500-1270 in different ratios (mixture 1: 2/1, mixture 2: 1/1, mixture 3: 1/2) and in vitro cumulative release of DEX for mixture of PLGA-PEG-PLGA at 25% in water with an initial drug concentration of 4 mg/mL Adapted from [278]

PCL-PEG-PCL triblock copolymers are prepared also by ring opening polymerization of ε-caprolactone in presence of PEG as initiator and catalyst in dried conditions. Gong *et al.* [279,280] developed thermo-responsive systems composed of PCL-*b*-PEG-*b*-PCL triblock copolymer hydrogels with PEG/PCL mass ratios ranging from 0.77 to 1.94 and calculated molecular weight from 2 500 to 4 500 g/mol. The formulation composed of 30 wt.% of PCL-*b*-PEG-*b*-PCL (1500-1500-1500) progressively degraded with 60% of molecular weight loss after 63 days of immersion. *In vitro,* the formulation composed of 30 wt.% of PCL-*b*-PEG-*b*-PCL (1000-1000-1000) allowed the release of 40% and 30% of honokiol hydrophobic drug and BSA protein, respectively. *In vivo,* the formulation composed of 20 wt.% PCL-*b*-PEG-*b*-PCL (1000-1000-1000) was injected and was progressively degraded and disappeared after 21 days (**Figure 28**)

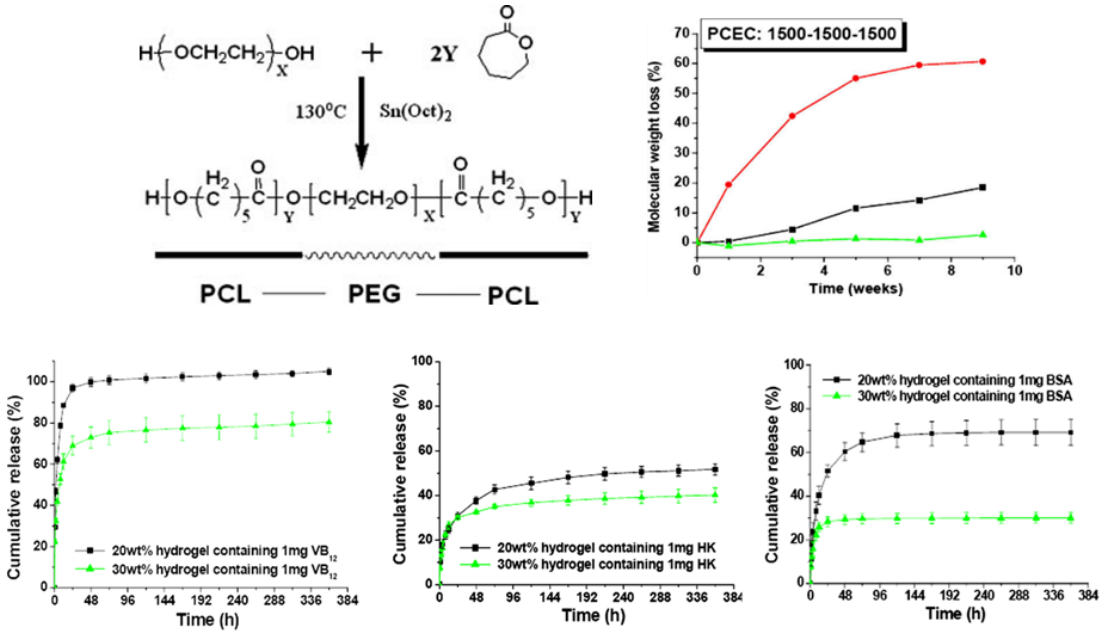

Figure 28. Synthesis, phase transition, hydrolytic degradation and *in vitro* released of hydrophilic, hydrophobic and model protein from PCL-*b*-PEG-*b*-PCL (1000-1000-1000) hydrogels.

Similarly, Ma *et al.* [281] developed PCL-*b*-PEG-*b*-PCL triblock copolymer hydrogels with PEG/PCL mass ratios ranging from 1.30 to 1.77 and calculated molecular weight from 2 600 to 4 560 g/mol. *In vitro*, the formulation composed of 20 wt.% of copolymer and containing 10 wt.% of BSA (corresponding to 20 mg) allowed sustained proteins released, particularly for PCL-*b*-PEG-*b*-PCL 1250-1500-1250 with 60% of protein released after 30 days. *In vivo,* this unloaded hydrogel was progressively degraded and disappeared after 45 days. As a substitute to PEG and to allow possibility of drug conjugation, poly(2-ethyl-2-oxazaline) (PEOz) is can be used. *In vitro*, the **PEOz-PCL-PEOz** gelling systems maintained

structural integrity for about 50 days before numerous and large pores were observed. The PEOz-PCL-PEOz loaded-hydrogel containing 20 % (w/v) of copolymer and 6% (w/w) of bevacizumab allowed the sustained release of the protein with a cumulative release of 80% in 20 days. *In vivo,* the PEOz-PCL-PEOz hydrogel was injected into the vitreous of rabbit's eye and showed no ocular toxicity. [268,282]

PEG–PCL–PEG triblock copolymers are prepared by 2 successive chemical reactions in presence of a coupling agent which may enhance the potential toxicity of the copolymer for biomedical application compared to PCL-PEG-PCL copolymers. Gong *et al*. [283,240,284] developed a series of thermo-responsive PEG-*b*-PCL-*b*-PEG triblock copolymer hydrogels with PEG/PCL mass ratios ranging from 0.39 to 2.1 and molecular weight from 2000 to 8200 g/mol. Particularly, the formulation composed of 30 wt% of PEG-*b*-PCL-*b*-PEG (550-2200-550) in water formed an opaque gel at body temperature and progressively degraded with 30% of molecular weight loss after 50 days of immersion. The drug-loaded hydrogel allows the sustained and constant release of honokiol hydrophobic drug and BSA protein, with a cumulative release of around 39% and 27% after 14 days, respectively. The PEG-*b*-PCL-*b*-PEG (550-2200-550) hydrogel was injected through a 30G needle into the anterior chamber of the eye of rats. The 5 wt.% PEG-*b*-PCL-*b*-PEG hydrogel showed good biocompatibility without inflammatory or hypersensitive responses, the 10 and 15 wt.% PEG-*b*-PCL-*b*-PEG hydrogel showed drastic intraocular pressure (IOP) elevation and slight toxicity. (**Figure 29**)

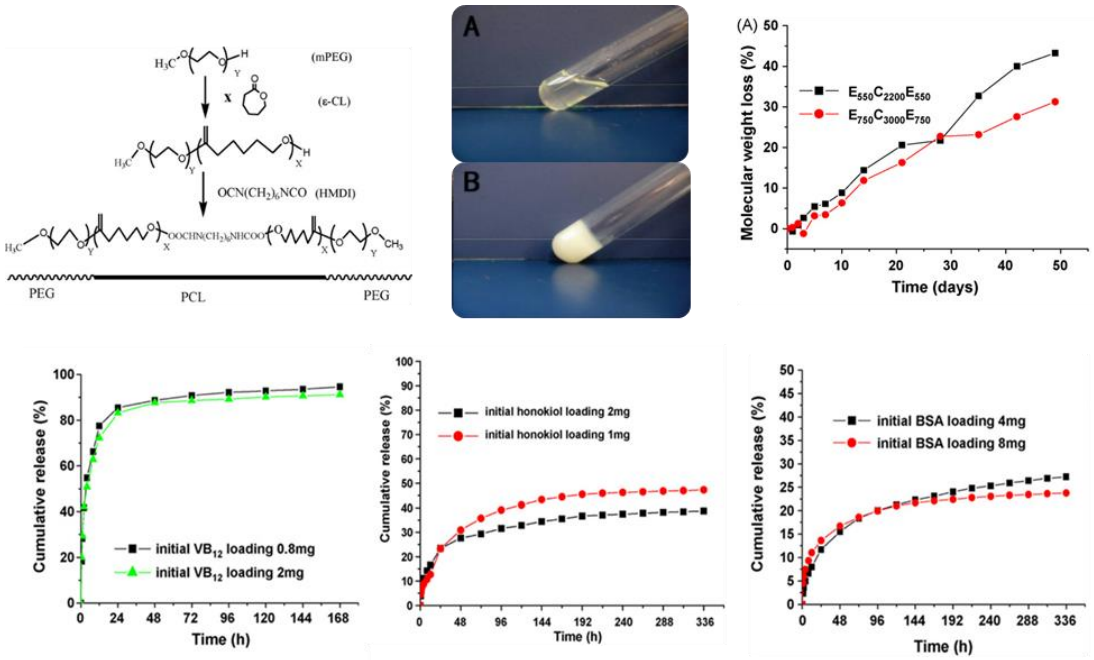

Figure 29. Synthesis, phase transition, hydrolytic degradation and *in vitro* released of hydrophilic, hydrophobic and model protein from PEG-*b*-PCL-*b*-PEG (550-2000-550, 30wt.% in water) hydrogels. Adapted from [283,240,284]

4.3.2.2 Solvent-exchange induced in situ forming systems based on hydrophobic polymers

The solvent-exchange process in based on the phase inversion of the polymer in solution. This technique gathers the injectability properties using a liquid formulation for ease of application and the potency of hydrophobic polymer, mostly PLA and PLGA as FDA-approved polymer and used as long-term delivery of drug when shaped as implantable systems. However, this technique showed a relative high burst release [285] of the drug (10 to 30%). This is due to the rate of phase inversion of the polymer (**Figure 30**) governed by the hydrophobicity of the matrix (depending on the composition and the molecular weight of PLGA), the higher the hydrophobicity the faster in the phase inversion. Moreover, the additional limitation of those systems are the drastic decrease of pH over time due to acidic by-product formed [285] and the lack of study concerning the potential toxicity of the solvent used for dissolution, typically NMP [286] and DMSO (although accepted for subcutaneous administration) for the human vitreous and the surrounding tissues.

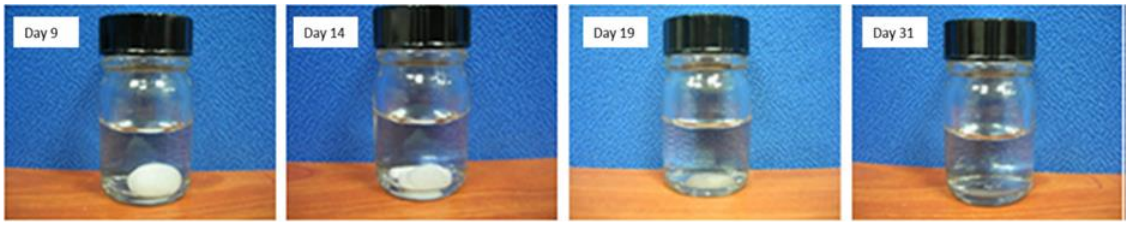

Figure 30. In-situ forming implant ($PLA_{25}GA_{50}$, Mw = 15 000) and degradation over time. [285]

4.3.2.3 Thermo-responsive in situ forming systems based on hydrophobic polymers

To gather the injectability properties and the potency of hydrophobic polymer for long term delivery without any organic solvent involved in the formulation, a PLA derivative, hexylsubstituted poly(lactic acid) written hexPLA was used as biocompatible [287] liquid formulation suitable for injection through 30G-needle. Indeed, in the hexPLA, all the methyl groups along the PLA-backbone are substituted by hexyl groups which increase the length of the aliphatic side chains, decrease the glass transition of PLA and lead to a viscous liquid solution at room-temperature with higher hydrophobicity. It also increases the PLA hydrophobicity thus leading to improved interactions and higher loadings with hydrophobic

drugs. The hex-PLA liquid formulation allows the stability, the storage and the sustained release of proteins (antibody) for 6 weeks in vitro [288] and sustained release of small drug for 4 weeks in the posterior segment of rats' eyes [289] to treat a certain form of retina disease.

4.4 Conclusion about the injectable systems

The solutions are injected into the targeted tissues *via* 30G-needle to reduce the pain of the patient during administration, but those systems lack of prolonged release and frequent administration would be necessary to reach a therapeutic level. The injectable in-situ forming ocular systems allow the sustained release of the drug from few days to 2 months *in vitro* for synthetic-based systems. The *in vivo* distribution has been poorly studied, and the therapeutic level can be maintained *in vivo* up to 6 months with natural-based systems. The degradability and the induced toxicity of certain polymers are still under discussion, the toxicity relative to the solvent used as dissolution medium and the stability of the proteins also. A summary of the injectable in-situ forming objects is drawn in **Table 5**.

Table 5. Injectable situ- forming polymeric systems for the drug delivery into the eye.

Structure	Route of administration	drug	Release rate	Therapy recommended	Cross-linking	Major advantages	Major limitations	
			Natural					
HA-VS/DEX-SH	IVT	Bevacizumab	Therapeutic level for 6 months (in vivo)	model	chemical	Long term release and activity preserved, no cross-linking agent		252
CS/gelatine	Anterior chamber	Latanoprost	70% in 28 days (in vitro), therapeutic level during 6 moths	glaucoma	Physical	Therapeutic level maintained	Lack of studies of posterior applications	242
			Synthetic					
PLGA-*b*-PEG-*b*-PLGA	Subconjunctival	Dexamethasone	30 days (in vivo)	Corneal neovascularisation	Physical	Mild conditions for synthesis, no coupling reagent	-	274, 275
PLGA-*b*-PEG-*b*-PLGA	IVT	Bevacizumab	20% in 14 days (in vitro)	Model	physical	Mild conditions for synthesis, no coupling reagent	Possible interaction of protein with systems, limiting the release	277
PLGA-*b*-PEG-*b*-PLGA	IVT	Dexamethasone	60-70% in 18 days (in vitro), therapeutic level maintained during 9 days (in vivo)	Model	Physical	Mild conditions for synthesis, no coupling reagent	-	278

PCL-*b*-PEG-*b*-PCL	subconjunctival	BSA	60% in 30 days (in vitro)	model	physical	Mild condition for synthesis, no coupling reagent	-	279, 280
PEOz-*b*-PCL-*b*-PEOz	IVT	Bevacizumab	80% in 20 days (in vitro)	Model	physical	Biocompatible	-	268, 282
PEG-*b*-PCL-*b*-PEG	Anterior chamber	Honokiol, BSA	39% and 27% after 14 days (in vitro)	model	Physical	-	Coupling agent require, slighly toxic above 5% of copolymer	283, 240, 284
PLGA	In vitro	Metosalt, dexamethasone	30-70 days (in vitro)	model	physical	Long term release, biocompatible, biodegradable	Brust release, possible solvent-relative toxicity	285, 286
Hex-PLA	In vitro	antibody fragment ESBA90	100-700 mg in 6 weeks (in vitro)	Retinal diseases	physical	biocompatible, proteins stability, solvent-free	Plateau due to inaccessibility of water to diffuse in and out	288
Hex-PLA	IVT	Spironolactone	10-20% in 65 days (in vitro)	Retinal diseases	physical	Biocompatible, solvent-free	Plateau due to inaccessibility of water to diffuse in and out	289

HA: hyaluronic acid: DEX: dextran, PLGA: poly(lactic-co-glycolic acid); PEG: poly(ethylene glycol); PBL: poly(γ-butyrolactone); PCL: poly(ε-caprolactone); PEOz: poly(2-ethyl-2-oxazaline); BSA: bovine serum albumin, Hex-PLA : hexyl substituted poly(lactic acid), IVT : intravitreal

5. Strategies of the PhD work

In ocular drug delivery, new investigations have been done to design biocompatible and biodegradable biomaterials providing long and sustained delivery of an API with a minimal surgery operation in order to increase the well-being of patients and to reach therapeutic level to treat efficiently the ocular diseases. However, there is still a need in developing a system that gather all the properties.

In order to develop suitable drug delivery systems to the ocular tissues, the drug vehicle should have the following characteristics:

- **Provide controlled and sustained release of drug** from at least two months (for proteins) and at least six months (for small drugs)
- **Biocompatible** with intraocular tissues with no irritation or rise of intraocular pressure
- **Degradable** or biodegradable
- Ease of administration with a **minimal invasive technique**
- **Respect** the local environment
- **Do not obstruct the vision** after administration
- **Maintain the drug activity**, and particularly protein activity, during preparation, storage and release
- **Allow easy manufacturing** for industrial perspective (sterilization procedure, scaling up, GMP production, cost-effectiveness)

Specifically related to our PhD study, the drug delivery system must **contain polydopamine (PDA)** to provide biocompatibility, degradability and drug binding properties to extend the release rate of drug loaded in the polymeric matrix.

We distinguish two types of ocular systems that will define the two strategies encountered in this work: the degradable implantable systems and the injectable degradable in situ forming gelling systems. The strategies are represented in **Figure 31**

The first strategy (Chapter II) is dedicated to the design of degradable injectable implant systems based on synthetic aliphatic polyester PCL and PDA. The polymeric systems are architected as graft copolymers based on a PCL backbone with PDA pendant chains (**PCL-*g*-PDA**), using oxidative polymerisation of dopamine in alkaline conditions and coupling with the macroinitiator of PCL. Several types of characterisations are performed to ensure the grafting of PDA and to quantify the amount of PDA in the copolymer. Then, two selected hydrophobic drugs are incorporated in PCL and PCL-*g*-PDA by hot melted compression to generate loaded-films. The thermal properties of unloaded and drug-loaded films as well as the kinetics of degradation and the cytotoxicity of unloaded-films are evaluated. Furthermore, the *in vitro* release study is performed in order to evaluate the potency of PCL-*g*-PDA copolymer to extend the release rate of drug compared to PCL and the potency of modulating the release rate with PCL and PCL-*g*-PDA mixtures by varying the PCL/PCL-*g*-PDA ratio. These results are compared to an *ex-vivo* intravitreal model and the viability of the model is discussed.

The second strategy (chapter III) is dedicated to the design of an injectable in situ-gelling system based on PCL, PEG and PDA. The synthesis of the amphiphilic copolymer PCL-*b*-PEG-*b*-PCL by ring opening polymerization and its properties of gelation are discussed. Then, the polymeric systems PCL-*b*-PEG-*b*-PCL with grafted pendant chains of PDA (**(PDA-*g*-PCL)-*b*-PEG-*b*-(PCL-*g*-PDA)**) are synthesized, architected and characterized in a similar way to chapter II. The ease of administration/injection and the potency of non-PDA- and PDA-modified copolymers to form in situ- forming systems by varying the copolymer ratios in water, without or with the addition of a co-solvent, are discussed. In parallel, the stability of a model protein and of an antibody provided by F.Hoffmann-La Roche in the pre-formulations are evaluated under different conditions. Finally, *in vitro* release studies is performed and discussed with a selected formulation of antibody and (PDA-*g*-PCL)-*b*-PEG-*b*-(PCL-*g*-PDA).

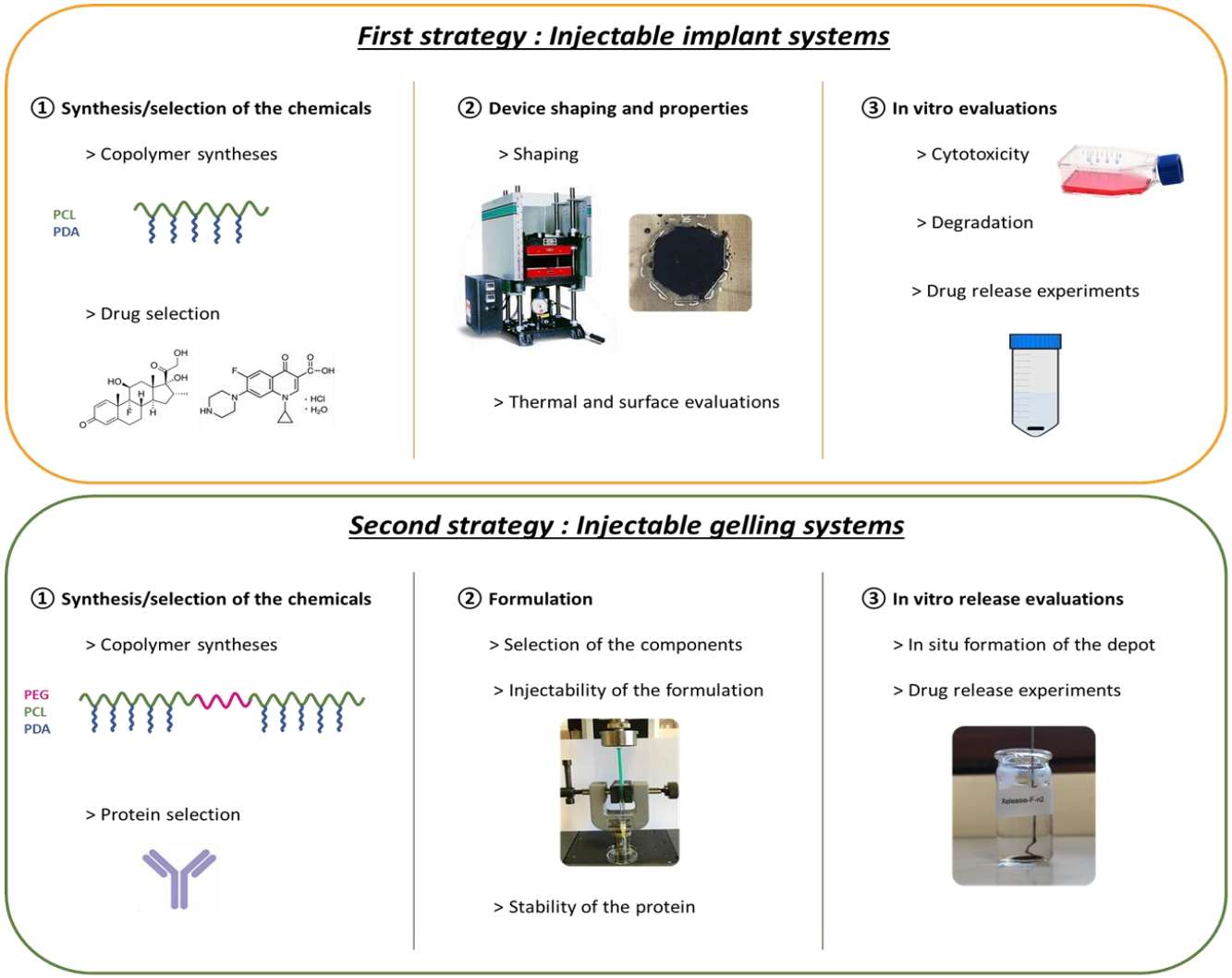

Figure 31. Graphical abstract of the strategies of the PhD

CHAPTER II.

INJECTABLE IMPLANT SYSTEMS BASED ON GRAFT COPOLYMERS CONTAINING PCL AND PDA (PCL-*g*-PDA) FOR SUSTAINED DRUG RELEASE

1. Introduction

As described in Chapter I, the investigations in the intravitreal ocular drug delivery field demonstrate the interest for a (bio)degradable polymeric material to provide sustained delivery of an active pharmaceutical ingredient (API) and minimise surgical interventions.

Poly(dopamine) (PDA) is considered as the synthetic analogue of melanin, a macromolecule naturally present in the skin, the hair and in the eye and responsible for pigmentation and photoprotection. PDA is biocompatible, thermally stable, degradable and showed pH-responsiveness and excellent binding affinity – physical or chemical binding - toward APIs and polymer thanks to the presence of catechol and amine moieties. PDA-based material has already been used for medical application in imaging and cancer therapies. [3,4,87]

Among all the polymers – natural or synthetic – presenting biocompatible properties, only a few of them are designed as (bio)degradable implantable systems approved by the FDA or under clinical studies. The majority of those implantable systems are composed of PLGA, notably the rod-shaped intravitreal implant Ozurdex™ [148] containing dexamethasone, a corticosteroid. [11,148] Recent advances showed a potency of PCL – another biodegradable polyester - for ocular and drug delivery applications proving the ability of PCL to be manufactured as an ocular drug delivery system. [209,210,290–292]

Typically, the synthesis of a PDA-based material is assessed in oxidative and alkaline conditions. Unlike PCL, PLGA degraded in these conditions. Thus, PCL was kept as preferential material. Moreover, PCL shows lower kinetics of degradation and probably lower toxicity of the acid function upon degradation, which are key factor for the design of long-acting release and safe ocular formulations.

As a result, the aim of this chapter is to develop a drug delivery system composed of PCL and PDA that would provide biocompatibility, (bio)degradability, stability and sustained release of APIs. To succeed, we split the subject into two parts. The first part (**section 1**) consists in the synthesis of PCL grafted with chains of PDA (PCL-*g*-PDA). Grafted copolymers are selected over their linear block counterparts in order to maximize the amount of PDA and expect higher drug retention. Firstly, commercial PCL of high molecular weight is functionalized with iodine (PCL-I). Then, the lability of the C-I bond is exploited to initiate the polymerization of dopamine to yield poly(dopamine) side chains resulting in the targeted PCL-*g*-PDA. The grafting of PDA onto PCL is evaluated by NMR, UV spectrometry, SEC, DSC and TGA and the content of PDA in the PCL-*g*-PDA copolymer is evaluated by UV spectrometry and TGA. PCL and PCL-*g*-PDA are processed as thin films to evaluate their thermal properties, degradation and cytotoxicity. The second part (**section 2**) consists in the preparation of drug-loaded PCL and PCL-g-PDA

implants. Dexamethasone and ciprofloxacin hydrochloride are chosen for their therapeutic action and PDA-binding affinity, respectively. The thermal properties of the drug loaded implants are evaluated and compared to the properties of the non-loaded ones. The kinetics of drug release are performed under classical *in vitro* conditions in order to evaluate the ability of PCL-*g*-PDA to temporarily retain the drug and to be used as a potential drug delivery system.

2. Experimental section

2.1 Materials

Poly(ε-caprolactone) (PCL, M_n=45 000 or 80 000 g.mol^{-1}), tetrahydrofuran (THF), iodine, hydrochloric acid (HCl, 37%), lithium diisopropylamide (LDA), sodium thiosulfate, dimethyl sulfoxide (DMSO), dopamine hydrochloride, benzoyl peroxide (BPO), copper(I) bromide, *N*,*N*,*N*',*N*',*N*''-pentamethyldiethylenetriamine (PMDETA), methanol, dichloromethane, ammonium chloride and ciprofloxacin hydrochloride (CIP.HCl) were purchased from Sigma-Aldrich (St Quentin Fallavier, France).

2.2 Instrumentation

2.2.1 Nuclear magnetic resonance (NMR)

^{1}H-NMR

Proton nuclear magnetic resonance spectroscopy (^{1}H-NMR) was carried out using a Bruker AMX-400 MHz spectrometer at room temperature. The solvents used were deuterated chloroform ($CDCl_3$) or deuterated dimethyl sulfoxide (DMSO-d_6), sample concentration was 15 mg/mL, chemical shifts were expressed in ppm with respect to tetramethylsilane (TMS)

DOSY-NMR

Diffusion ordered spectroscopy NMR (DOSY-NMR) was carried out using a Bruker AMX-600 MHz spectrometer at room temperature. The solvent used were deuterated chloroform (CDCl3) or deuterated dimethyl sulfoxide (DMSO-d_6), sample concentration was 15 mg/mL, chemical shifts were expressed in ppm with respect to tetramethylsilane (TMS).

2.2.2 Size Exclusion Chromatography (SEC)

The number-average and weight-average molar masses (M_n and M_w, respectively) and dispersity ($Đ$, M_w/M_n) of the polymers were determined by SEC. The samples (5 mg.mL^{-1}) were filtrated through a 0.45 µm PTFE Millipore filter and analyzed using a Shimadzu (Japan) apparatus equipped with a RID-

20A refractive index signal detector coupled to a SPD-20A UV/VIS detector and to a PLgel MIXED-C guard column (Agilent, 5µm, 50 x 7.5 mm) and two PLgel MIXED-C columns (Agilent, 5µm, 300 x 7.5 mm). The mobile phase was THF in the case of THF SEC line or was DMF + 0.1% LiBr in the case of DMF SEC line. The flow rate was 1.0 $mL.min^{-1}$ and the injection volume was 100 µL. The average molecular weight and dispersity (*Đ*) were express according to calibration using polystyrene (PS) standards.

2.2.3 Differential Scanning Calorimetry (DSC)

Thermal properties were analyzed using a Mettler Toledo DSC 3. Samples (from 1 to 10 mg) of each copolymer were placed in an aluminum pan and heated from -80°C to 100°C at 10°C/min, then cooled from 100°C to -80°C at 10°C/min, then heated from -80°C to 300°C at 10°C/min. The glass transition temperature (T_g) and melting temperature (T_m) of each sample were determined during the second heating ramp.

2.2.4 Thermogravimetric analysis (TGA)

Thermal decomposition was studied using a thermogravimetric analyser (TGA Q500 v20.13 build 39). Samples were heated from 30°C to 700°C at 20°C/min under nitrogen atmosphere. The degradation temperature ($T_{degradation}$) was determined at the inflexion point of the mass decrease, also known as the minimum of the curve of the derive function.

2.2.5 High-performance liquid chromatography (HPLC)

Samples were filtrated through a 0.45 µm PTFE Millipore filter and analyzed using a Shimadzu (Japan) apparatus equipped with a SPD-M20A diode array detector. A HPLC C18 column (Kinetex, 2.6 µm, 100A, 100×4.6 mm) was used. The column temperature was maintained at 37°C and the samples were stored in an autosampler at ambient temperature. Chromatographic separation was carried out using isocratic elution at a flow rate of 1 $mL.min^{-1}$. The mobile phase was a mixture of acetonitrile containing 0.1% of TFA and water containing 0.1 % of TFA. For the detection of DEX, the mobile phase was composed of 40% ACN (0.1% TFA) and 60% H2O (0.1% TFA), and the wavelength was set at λ = 254

nm. For the detection of CIP, the mobile phase was composed of 13% ACN (0.1% TFA) and 87% H2O (0.1% TFA), and the wavelength was set at λ = 278 nm.

2.2.6 Hydraulic press

Powder was placed in the centre of a PTFE custom-made mold, placed between two PTFE sheets and pressed during 15 minutes under 4 tons at 100°C with an hydraulic press (Carver, 4120-CE, USA).

2.3 Synthesis of initiators and copolymers

2.3.1 Synthesis of the diethylene glycol bis(2-bromoisobutyrate)

In a typical experiment, diethylene glycol (1g, 9.42 mmol), triethyl amine (3.94 mL, 28.3 mmol) and dry THF (40 mL) were added in a dry three-neck round-bottom flask and placed in an ice bath. Then, isobutyryl bromide (3.49 mL, 28.3 mmol) was slowly added into the flask through a dropping funnel. A guard tube filled with calcium chloride was placed to keep anhydrous conditions. Solution was left under stirring overnight. Solution was filtrated over diatomaceous earth and concentrated by evaporating THF. The crude product was dissolved in a mix of water and dichloromethane. The product was extracted from the solution by washing three times with dichloromethane using a separative funnel. The organic phase was dried using $MgSO_4$ powder, filtrated and dried under reduced pressure. The product was purified by filtration over silica using a mix of ethyl acetate:heptane (30:70) as solvent. Fractions were collected and evaporated under reduced pressure. Pure fractions were gathered and stocked at 4°C for further use.

Yield: 100 mol.%

^{1}H NMR (300 MHz, $CDCl_3$): δ = 4.28 (t, R-C*H*$_2$-O-CO), 3.73 (t, O-C*H*$_2$-R), 1.89 (s, R-C*H*3)

2.3.2 PDA oligomers

In a typical experiment, dopamine hydrochloride (1.5 g, 7.91 mmol), PMDETA (130 µL, 0.63 mmol), Na_2CO_3 (402.0 mg), BPO (1.92 g, 7.91 mmol), and DMSO (76 mL) were added. Solution was left under

stirring and argon flux for 4 hours. Then, oxygen was removed by three freeze-pump thaw cycles. Diethylene glycol bis(2-bromoisobutyrate) (0.13g, 0.32 mmol) and copper(I) bromide (0.09 mg, 0.63 mmol) were added. The flask was then dived in an oil bath at 70°C and the reaction was carried out under vigorous stirring for 48 hours. Reaction was stopped by cooling in a liquid nitrogen bath. Solution was then concentrated by evaporating DMSO at 70°C under vacuum. Finally, the polymer was precipitated, filtrated and dried under vacuum.

Yield: 17 wt.%

^{1}H NMR (600 MHz, DMSOd$_6$): δ = 6.30-7.00 ppm (m, PDA)

2.3.3 Functionalization of PCL by iodine

In a typical experiment, PCL (3 g, $M_{n,SEC,THF,}$= 65 000 g.mol^{-1}, 26.3 mmol of CL units) and anhydrous THF (300 mL) were introduced into a dry conic reactor, and put under argon atmosphere until complete polymer dissolution. The solution was then cooled down at -50°C by diving it into a liquid nitrogen/ethanol mixture before addition of LDA (13.16 mL, 1 eq. with respect to εCL unit, 26.3 mmol) under argon. After 30 minutes of reaction, a solution of iodine (6.68 g, 1 eq. with respect to εCL unit, 26.3 mmol) in a minimum amount of anhydrous THF was injected with a syringe through a septum and the mixture was kept at -50°C under stirring and argon atmosphere. After 30 minutes the reaction was stopped by addition of an aqueous solution of NH_4Cl (2 M, 200 mL) and the temperature was increased to 0°C prior to addition of HCl(aq) (37%) to reach neutral pH. The polymer was extracted from the solution by washing three times with dichloromethane (3×200 mL) in a separating funnel. Organic phases were collected, washed three times with a solution of $Na_2S_2O_3$ (0.3 M, 3×100 mL), dried using $MgSO_4$ powder, filtrated and concentrated under reduced pressure. The polymer was precipitated in cold methanol, filtrated and dried under vacuum.

Substitution: 10 mol.%

Yield: 76 %

^{1}H NMR (300 MHz, CDCl$_3$): δ = 4.30 (m, R-C*H*I-CO-O), 4.05 (t, R-C*H*$_2$-O-CO), 2.30 (t, R-C*H*$_2$-CO-O), 2.00 (t, R-C*H*$_2$-CHI), 1.64 (m, R-C*H*$_2$-CH$_2$-CO), 1.38 (m, R-C*H*$_2$-R)

SEC (THF, RI, PS): M_n = 28 000 g.mol^{-1}, $Đ$ = 2.87

2.3.4 Synthesis of PCL-*g*-PDA

In a typical experiment, in a Schlenk flask A, iodinated PCL (1.5 g, 1.18 mmol of iodinated CL units) and DMSO (20 mL) were added. In a Schlenk flask B, dopamine hydrochloride (5.62 g, 25 eq. with respect to iodinated CL unit, 29.6 mmol), PMDETA (370 µL, 1.5 eq. with respect to iodinated CL unit, 1.78 mmol), Na_2CO_3 (300.0 mg), BPO (7.18 g, 25 eq. with respect to iodinated CL unit, 29.6 mmol), and DMSO (37 mL) were added. Solutions were left under stirring and argon flux for 4 hours. Then, oxygen was removed by three freeze-pump thaw cycles. Iodinated PCL solution was transferred to the flask B and copper(I) bromide (255 mg, 1.5 eq. with respect to iodinated CL, 1.78 mmol) was added. The flask was then dived in an oil bath at 70°C and vigorous stirring during 48 hours. Reaction was stopped by cooling in a liquid nitrogen bath. Solution was concentrated by evaporating DMSO at 70°C under vacuum. The polymer was precipitated three time in methanol, filtrated and dried under vacuum.

Yield: 4%

^{1}H NMR (600 MHz, DMSOd$_6$): δ = 4.53 (m, R-C*H*(PDA)-CO), 3.94 (t, R-C*H*$_2$-O-CO), 2.23 (t, R-C*H*$_2$-CO-O), 1.90 (m, R-CH$_2$-C*H*(PDA)), 1.80 (m, R-CH$_2$-C*H*(PDA)), 1.50 (m, R-C*H*$_2$-C-CO), 1.26 (m, R-C*H*$_2$-R)

SEC (DMF, RI, PS): M_n = 17 000 g.mol^{-1}, $Đ$ = 3.12

2.4 Preparation of unloaded and drug-loaded discs

2.4.1 Preparation of the films by hot melt compression

The unloaded film of PCL and PCL-*g*-PDA were prepared in a one-step process. The PCL or PCL-*g*-PDA powders were pressed using hydraulic press to obtain thickness around 400 ± 50 µm. The drug-loaded films of PCL and of PCL-*g*-PDA were prepared in a two-step process. PCL or PCL-*g*-PDA (210 mg) and appropriate amounts of DEX or CIP.HCl were dispersed in DMSO (30 mL) to allow intimate mixing. DMSO was removed at 100°C under vacuum to yield a copolymer/drug thin film. The resulting film was pressed using hydraulic press to obtain thickness around 400 ± 50 µm. The films were further cut into small pieces (10 mm x 4 mm) and used for the release experiments *in vitro*.

2.4.2 Efficiency of drug loading

To quantify the amount of drug incorporated in the film during the encapsulation process, thermogravimetric analysis (TGA) was performed. The drug content was calculated from a calibration curve based on the resulting weight of a mix of copolymer and drug at various known ratios.

2.5 In vitro evaluation of copolymer degradation

The kinetics of degradation were studied *in vitro* on polymer films in standard (PBS at pH=7.4) and accelerated conditions (aqueous solution of HCl (2M) at pH=1) for 75 days at 37°C. Films were cut into implants (dimensions = 10 x 4 mm, thickness = 0.3-0.5 mm), weighted (15 mg, $w_{dry,t0}$) and immersed into 0.75 mL of media under stirring according the ISO-10993-13. At predetermined time points, implants were removed from the medium, washed with water, wiped and weighted to determine the wet mass ($w_{wet,tx}$) then dried under vacuum to constant mass to determine the dry mass ($w_{dry,tx}$). These experiments were carried out in triplicates. The water uptake was calculated from equation (1), the remaining weight from equation (2) and the remaining molecular weight from equation (3). The thermal characteristics of the films were analyzed by DSC as previously described. The pH was evaluated using a pH-meter at 20°C.

$$\%wateruptake, tx = \frac{(w_{wet,tx} - w_{dry,tx})}{w_{dry,tx}} * 100 \quad (1)$$

$$\%massresidual, tx = \left(1 - \frac{(w_{dry,t0} - w_{dry,tx})}{w_{dry,t0}}\right) * 100 \quad (2)$$

$$\%Mnresidual, tx = \left(1 - \frac{(M_{n,0} - M_{n,tx})}{M_{n,0}}\right) * 100 \quad (3)$$

2.6 *In vitro* drug release evaluation

The films were cut into implants of rectangular shape with dimensions corresponding to a final weight of 5.0±0.1 mg. The drug/polymer implants were dived in 20 mL of phosphate buffer solution (PBS) containing 0.05 % of Tween 20 (PS20) at 37°C under constant orbital shaking (100 rpm). At specific time points, the entire release medium was removed and replaced with fresh buffer solution. The collected samples were analyzed by HPLC as previously described. The quantification of the drugs was calculated from a calibration curve previously established in PBS from 0.1 to 50 $mg.L^{-1}$.

2.7 Cytotoxicity studies

2.7.1 Fibroblast cells

The films were cut into discs (diameter = 6 mm, thickness = 0.3-0.5 mm). The cytotoxicity of PCL and PCL-*g*-PDA discs was investigated on mouse fibroblast cell line, L929 (NCTC-Clone 929, ECACC 85011425). L929 cells were cultured at 37°C under humidified 5% CO2 in a Dulbecco's Modified Eagle Medium 4.5g/L D-glucose supplemented with 1mM L-glutamine, 5% v/v Fetal Bovine Serum, and 100 U per mL penicillin and streptomycin 100 µg per mL. Polyurethane film containing 0.25% zinc dibuthyldithiocarbamate (ZDBC) (Hatano Research Institute, Food and Drug Safety Center, Japan, batch B-173K) was used as positive reference material (RM) and high-density polyethylene film (Hatano Research Institute, Food and Drug Safety Center, Japan, batch C-161) was used as negative RM. The cells were seeded into 24-well plate at a density of 60 000 cell per well and were incubated overnight at 37°C under humidified 5% CO2. PCL, PCL-*g*-PDA discs and the RM controls were irradiated at λ=254 nm for 2 minutes, twice on each face for decontamination. Discs were added into wells and incubated with cells for 24 hours. The discs were removed and the medium was replaced by 500 µL of a PrestoBlue® solution (10% in culture cell medium) and incubated for 30 minutes. PB assay was carried out using fluorescence (λex = 558 nm, λem = 593 nm). Each experiment was performed in triplicate.

2.7.2 Human retinal cells

The cytotoxicity of PCL and PCL-*g*-PDA discs (diameter = 7 mm, thickness = 0.3-0.5 mm) was analysed on human retinal epithelial cell line ARPE-19 (ATCC, CRL-2302). ARPE-19 cells were cultured at 37°C under humidified 5% CO2 in a Dulbecco's Modified Eagle Medium/Nutrient Mixture F-12 (DMEM:F-12, ATCC 30-2006) supplemented with 10% v/v Fetal Bovine Serum. Polyurethane film containing 0.1% zinc diethyldithiocarbamate (ZDEC) (Hatano Research Institute, Food and Drug Safety Center, Japan, batch A-202K) was used as positive reference material (RM) and high-density polyethylene film (Hatano Research Institute, Food and Drug Safety Center, Japan, batch C-141) was used as negative RM. The cells were seeded into 24-well plate at a density of 20 000 cells per well and were incubated overnight at 37°C under humidified 5% CO2. PCL and PCL-*g*-PDA discs and the RM controls were irradiated at λ=254 nm for 2 minutes, twice on each face for decontamination. The discs were added into wells and incubated with cells for 48 hours. The discs were removed and the medium was replaced by a PrestoBlue® solution (10% in cell culture medium) and incubated for 30 minutes. PrestoBlue assay

was carried out using fluorescence (λex = 558 nm, λem = 593 nm). Each experiment was performed in quadruplicate.

3. Section 1: Properties of functionalized PDA-copolymers

3.1 Synthesis of the PCL-*g*-PDA copolymers

According to the literature presented in Chapter I, dopamine (DA) can polymerize into poly(dopamine) (PDA) through oxidative polymerization in alkaline conditions, enzyme-catalysed oxidative polymerization and electro-polymerization. Among these polymerizations, oxidative polymerization in alkaline conditions is the most used. This polymerization has been studied either in aqueous or in organic conditions. In particular, Cho *et al.* [118] have shown that, by combining the reversible activation of bromo-terminated PMMA (PMMA-Br) under ATRP-like conditions and the oxidative polymerization of DA, it was possible to graft DA units or oligo-PDA on the polymer chain via a nucleophilic addition of the radical and to further grow PDA to finally generate PMMA-PDA block copolymers. With the aim to synthesize PCL-*g*-PDA copolymers, the functionalization of PCL with a halogen seems required. We chose to functionalize PCL with iodine with the protocol described and published in our lab. [293] Then, the lability of the C-I bond will be exploited to initiate the polymerization of the dopamine in the similar conditions of Cho *et al.*

3.1.1 Synthesis of iodinated PCL and characterisations

Iodinated PCL can be obtained by ring-opening polymerization of iodo-substituted lactone monomers or by post modification of PCL by iodine. In the first method developed in our laboratory and described by El Habnouni *et al.* [294], the reaction was carried out in solution and the substitution rate was controlled from 0 to 100% depending of the feed molar ratio of lactone and iodo-lactone. The molecular weights of the polymers ranged from 3 600 to 6 200 g.mol^{-1}, the lower molecular weights and conversions were obtained with the higher molar fraction of iodo-lactone. Therefore, this technique is interesting to functionalize PCL at high functionalization degree but not suitable to obtain high molecular weights functionalized PCL. However, the mechanical and degradation properties of PCL are mainly governed by the molecular weight. Films prepared with low molecular weight PCL (10 000 g.mol^{-1} for example) are brittle while films prepared with high molecular weight PCL (above 45 000 g.mol^{-1} for example) are robust and flexible. With the aim to develop degradable solid formulations combining synthesis feasibility and good mechanical properties, we chose to functionalize high molecular weight PCL by post modification.

The post modification method of functionalisation of PCL is based on the work of Nottelet *et al.* [293]. The method consists in a two-step one-pot reaction described in **Scheme 17**. The first step is the anionic activation of PCL in presence of LDA, the second step is the electrophilic substitution of iodine.

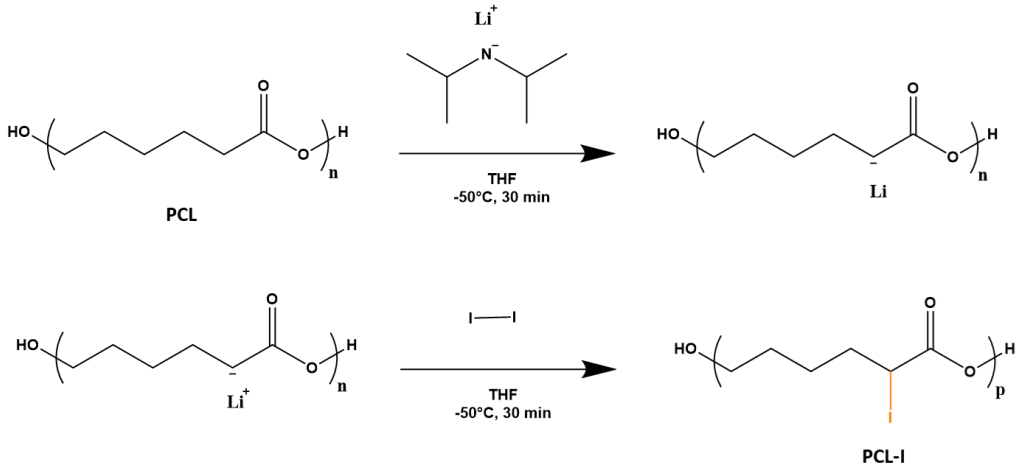

Scheme 17. Synthesis scheme of iodized PCL (PCL-I)

Starting from commercial PCL, a series of iodinated PCL were prepared by targeting different molecular weights and copolymer masses, and were characterized by SEC and ^{1}H NMR. The results are summarized in **Table 6**.

Table 6. Characterizations of iodinated PCL (PCL-I) prepared in THF by anionic activation using LDA and electrophilic substitution using iodine.

	PCL			**PCL-I obtained after reaction**				
Assay	M_n [a] (g.mol^{-1})	$Đ$ [a]	Mass of PCL (g)	M_n [a] (g.mol^{-1})	$Đ$ [a]	Mass of PCL-I (g)	Iodation ratio (T_I) [b] (mol%)	Molar yield (η_x) (g)
I1	43 100	1.62	5	17 100	2.56	3.9	11	70
I2	127 000	1.61	5	27 000	3.60	4.2	11	75

[a] determined by SEC in THF using PS standards for calibration; [b] determined by ^{1}H NMR in $CDCl_3$ and using equation 4

The SEC chromatograms in THF of PCL and PCL-I for assay I1 are presented in **Figure 32**. They showed a decrease in molecular weight of the PCL-I (M_n = 17 100 g.mol^{-1}) compared to PCL (commercial, M_n = 43 100 g.mol^{-1}) and an increase in dispersity from 1.61 to 2.65. These results are characteristic of the chain scission occurring during the anionic activation step. The grafting of iodine can be observed using UV detection in SEC analysis. Iodine exhibits a strong absorbance at 290 nm. The chromatogram clearly showed an intense absorbance at 290 nm at the retention time of the polymer after functionalization while no absorbance was observed before functionalisation, which confirmed the success of the functionalization of the PCL.

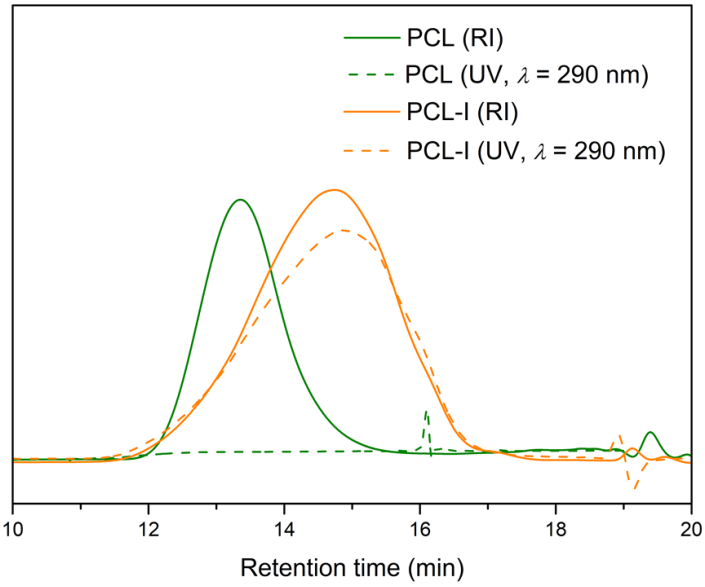

Figure 32. SEC traces of PLC and PCL-I using RI and UV (λ= 290 nm) detection for the assay I1

The ^{1}H-NMR spectra of PCL and PCL-I for the assay I1 are presented in **Figure 33**. The peaks at 4.05 ppm (peak a) and 2.30 ppm (peak d) are triplets which correspond respectively to the signals of the protons R-C$\underline{H}_2$-O-CO and R-C$\underline{H}_2$-CO-O of the PCL backbone. The peaks at 1.64 ppm (peak b+b') and 1.38 ppm (peak c) are multiplets which correspond respectively to the signal of the protons R-C$\underline{H}_2$-CH$_2$-CO and R-C$\underline{H}_2$-R of the PCL backbone as well. The appearance of the peaks at 4.30 ppm (peak e) and at 2.00 ppm (peak f) corresponds respectively to the signal of the proton R-C$\underline{H}$I-CO-O and R-C$\underline{H}_2$-CHI, which confirms the modification of the environment of the protons of the PCL backbone. The residual presence of the characteristic signal of R-C$\underline{H}_2$-CO-O at 2.30 ppm confirmed that the functionalization was partial. The degree of substitution is calculated by comparing the intensity of the signal of the

proton coupled with iodine (R-C*H*I-CO-O) at 4.30 ppm and the signal of (R-CH_2-O-CO) at 4.05 ppm, according to the equation (4). The degree of substitution was around 10% in each experiment.

$$T_I\,(\%) = 2 * \frac{I_{4.30\,ppm}}{I_{4.05\,ppm}} * 100 \qquad (4)$$

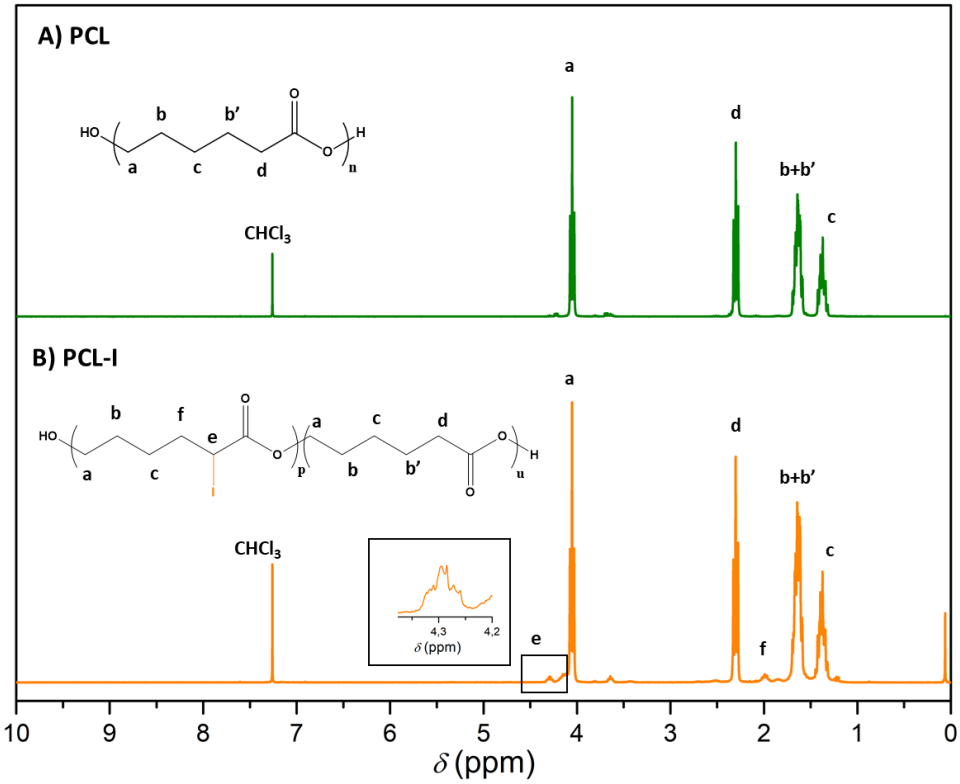

Figure 33. ^{1}H-NMR spectra of PCL and PCL-I in $CDCl_3$

With the aim to design implants with suitable mechanical properties, targeting highest molecular weight possible of functionalized polymers is preferable. Two commercial PCLs of distinct molecular weights have been tested (M_n = 43 000 g.mol^{-1} and 127 000 g.mol^{-1}) corresponding to assay I1 and I2, respectively. Using the same conditions, the SEC analyses clearly showed that the molecular weight decreased from 127 000 g.mol^{-1} to 27 000 g.mol^{-1} and the dispersity increased from 1.61 to 3.60 for the assay I2 which corresponds to 4.7 chain cuts. Meanwhile the molecular weight decreased from 43 000 g.mol^{-1} to 17 100 g.mol^{-1} and the dispersity increased from 1.61 to 2.65 for the assay I1 which corresponds to 2.5 chain cuts. It seems that the proportion of chain cuts is higher in the case of I2 but the higher molecular weight of the functional PCL-I is obtained in the assay I2. The degree of

substitution was the same, around 11%, and similar yields, between 88-94%, were obtained according to equations (5)-(7).

$$M_{moitiesinPCL-I} = T_I \times 239.9 + (100 - T_I) \times 114 \quad (5)$$

$$m_{th,PCL-I} = m_{PCL} \times \frac{M_{moitiesinPCL-I}}{M_{moitiesinPCL}} \quad (6)$$

$$\eta = \frac{m_{PCL-I}}{m_{th,PCL-I}} \times 100 \quad (7)$$

Based on these results, the conditions of the assay I2 were selected for the rest of this work to yield the macromolecular precursor PCL-I.

3.1.2 Synthesis and characterisation of PCL-g-PDA

As described previously, Cho et al [118] have shown that by combining the reversible activation of bromo-terminated PMMA (PMMA-Br) under ATRP-like conditions and the oxidative polymerization of DA, it was possible to graft DA units or oligo-PDA on the polymer chain via a nucleophilic addition of the radical, and to further grow PDA to finally generate PMMA-PDA block copolymers.

We therefore hypothesized that the carbon-iodine bond in PCL-I – previously synthesized in Chapter II part 3.1.1 – could play the role of the dormant macroinitiator that could similarly yield nucleophilic PCL radicals after removal of the iodine along the backbone, allowing the grafting of PDA side chains. Consequently, the conditions of Cho et al. were applied with PCL-I as macroinitiator, as illustrated in **Scheme 18**.

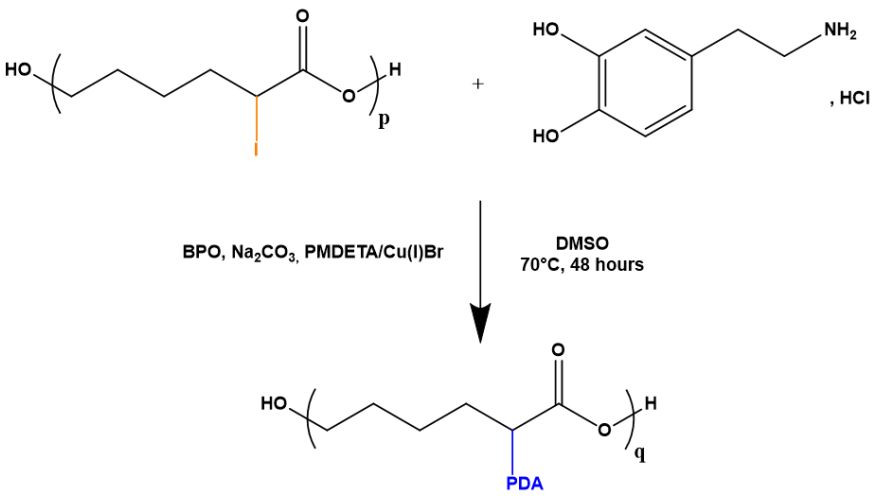

Scheme 18. Synthesis of PCL-*g*-PDA based according to the conditions adapted from Cho et al. [118]

Dopamine was introduced in a Schlenk flask containing DMSO, sodium carbonate, BPO and PMDETA at room temperature. Sodium carbonate is used to obtain basic conditions. BPO is an organic peroxide frequently used as radical initiator to induce chain-growth polymerization, PDMETA (also written PMDTA) is a tridentate ligand which can bind to metallic cation to form a complex. Rapidly after introduction of all those components (in less than one minute), the solution turned from white to black, suggesting the oxidative polymerization of dopamine. Meanwhile, PCL-I was solubilized in DMSO at room temperature. The solutions were stirred during 4 hours. The PCL-I macroinitiator solution was transferred to the first solution, and copper(I) bromide was added. Copper (I) bromide is a metallic agent that binds to the ligand and allows, like in ATRP, to activate the PCL-I dormant macroinitiator to generate a free radical PCL which was coupled with dopamine monomer or already grown PDA. The solution was heated at 70°C during 48 hours, then cooled by diving into liquid nitrogen. The majority of the solvent was removed by evaporation, then the solution was precipitated in methanol to collect the final copolymer. During precipitation, methanol turned black suggesting the presence of non-grafted PDA in the solution of DMSO, and that non-grafted PDA compounds were further solubilized in methanol.

The ^{1}H-NMR spectra of PCL-I and PCL-PDA in DMSO-d_6 are presented in **Figure 34**. For PCL-I (**Figure 34**-A), the shifts reported previously in $CDCl_3$, were slightly modified in DMSO-d_6. The characteristic signals of the protons of PCL-I were found at 4.41 ppm (R-C*H*I-CO-O | peak e), at 3.94 ppm (R-CH_2-O-CO | peak a), at 2.23 ppm (R-CH_2-CO-O | peak d), at 1.82 ppm (R-CH_2-CHI | peak f), at 1.50 ppm (peak R-CH_2-CH_2-CO | b+b') and at 1.26 ppm (R-CH_2-R | peak c). For PCL-*g*-PDA (**Figure 34**-B), the disappearance of the peak at 4.41 ppm (peak e) and 1.82 ppm (peak f), characteristic of the functionalization by iodine, showed that the chemical environment of the polymer is modified after the introduction and the

polymerization of dopamine. The characteristic peaks are represented with the black dashed rectangles.

To confirm that the changes of the chemical shifts could be attributed to an effective grafting of PDA side chains onto the PCL backbone, diffusion ordered NMR spectroscopy (DOSY NMR) analyses were performed. DOSY NMR is a powerful technique to characterise complex mixtures according to their diffusion coefficient, which is function of the temperature, the viscosity of the solution and the hydrodynamic radius of the polymer. DOSY NMR was conducted on PCL-I and PCL-*g*-PDA, in $DMSOd_6$ at a concentration of 15 $mg.mL^{-1}$ at room temperature (**Figure 35**). It is clearly shown that the peaks at 4.53 ppm, at 1.90 ppm and at 1.80 ppm on **Figure 35**-B have the same diffusion coefficient ($D = 2.34 \times 10^{-11}$ $m^2.s^{-1}$) than the peaks attributed to the PCL backbone, proving the effective grafting of PDA on the PCL backbone.

On the contrary, the peaks at 7.82 ppm, at 7.63 ppm and at 7.53 ppm ($D = 3.98 \times 10^{-10}$ $m^2.s^{-1}$) and the peaks at 6.54 ppm and at 6.46 ppm ($D = 1.62 \times 10^{-10}$ $m^2.s^{-1}$), represented with red dashed rectangle in **Figure 34** and **Figure 35**, have diffusion coefficients that differ from the PCL-*g*-PDA. They corresponded to non-grafted by-products of the reaction with a hydrodynamic radius smaller than the PCL-*g*-PDA copolymers, and were defined as impurities. As we will see later, these peaks might correspond to by-products of BPO, dopamine and PDA (Chapter II part 3.1.4.1, **Figure 43**) and the removal of these impurities was found to be critical to ensure the non-cytotoxicity of PCL-*g*-PDA (Chapter II part 3.3.2.3, **Figure 51**).

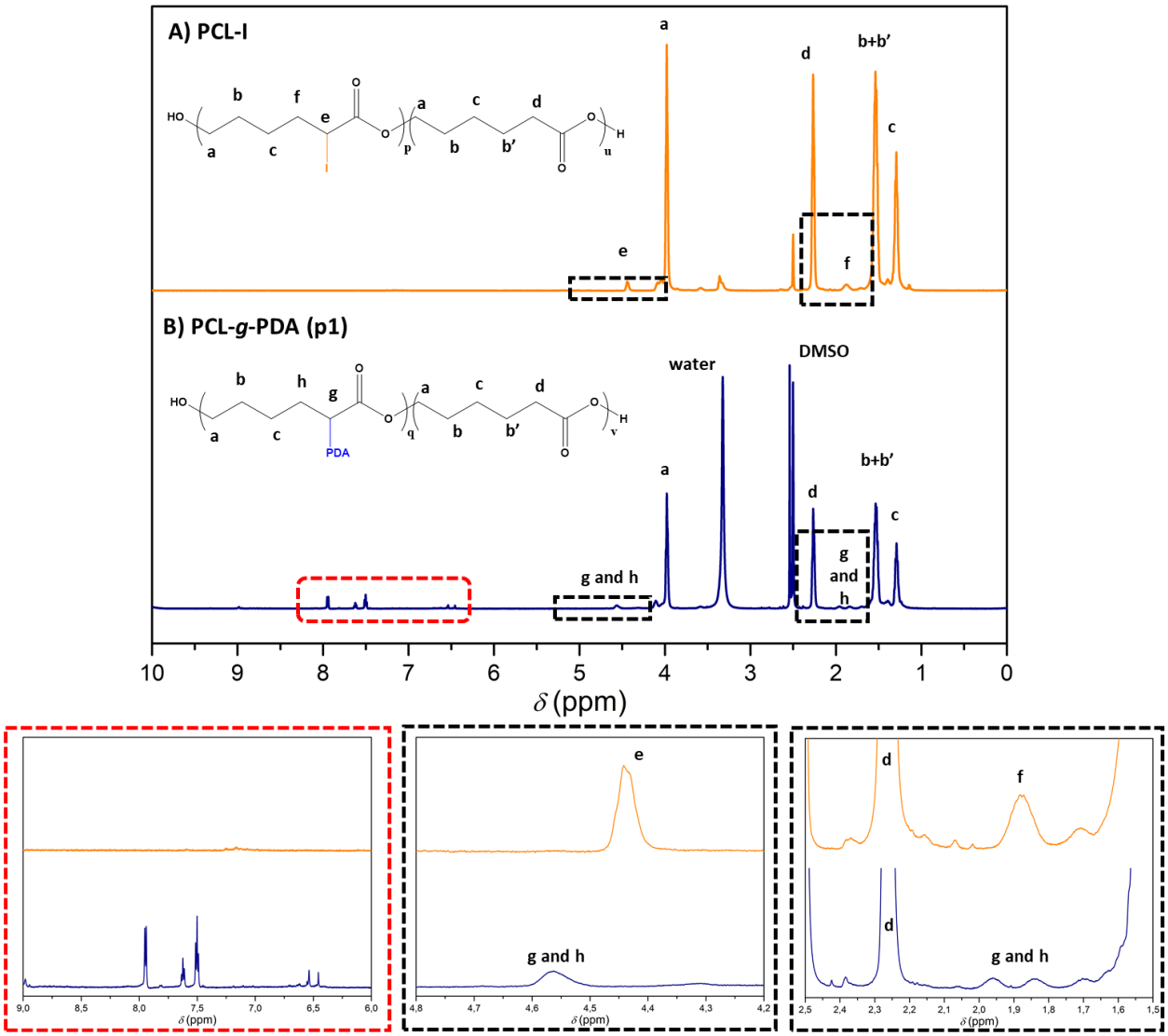

Figure 34. ^{1}H-NMR spectra of A) PCL-I and B) PCL-*g*-PDA after one step of purification (p1) in DMSO-d6 (bottom row corresponds to insets)

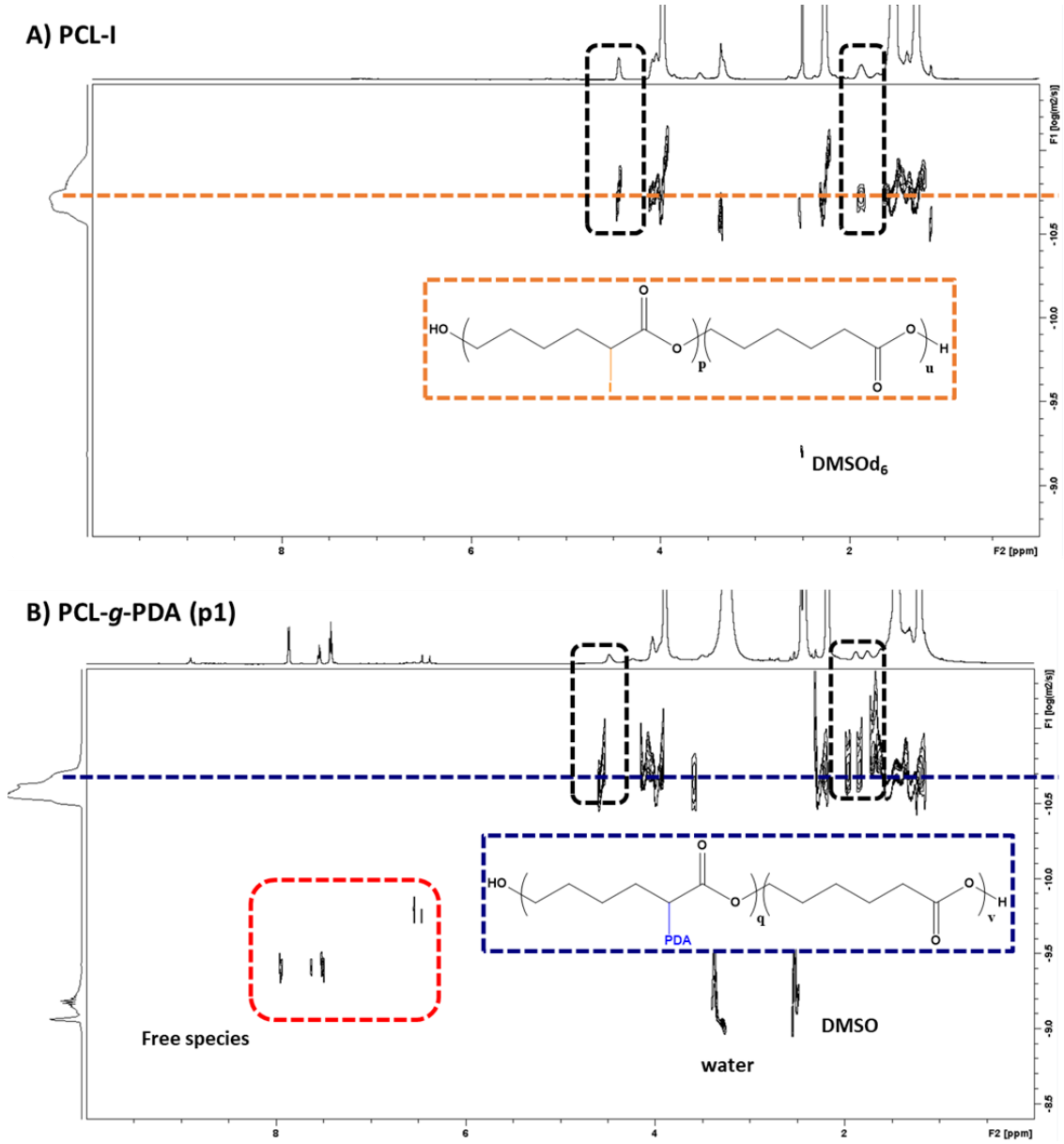

Figure 35. DOSY-NMR in $DMSOd_6$ of A) PCL-I and B) PCL-g-PDA after one step of purification (PCL-*g*-PDA (p1))

To determine the adequate purification method of PCL-*g*-PDA, two types of purification were tested: the direct precipitation (the one presented for the first purification of PCL-*g*-PDA in **Figure 34**) and the fractional precipitation. In both cases, the DMSO solution containing the crude product is concentrated by evaporation of the two third of the solvent at 70°C under. In the first technique, the concentrated solution of crude product is precipitated by slowly diving in 300 mL of cold methanol, and then filtrated. In the second technique, a precipitate is obtained by slowly adding cold methanol to the crude solution. The precipitates were dried and analysed by NMR (**Figure 62**). The comparison of ^{1}H-NMR spectra of

PCL-*g*-PDA purified by direct precipitation (DP) or by fractional precipitation (FP) showed similar proton signals and similar intensities from 8 to 6 ppm, previously defined as the region of the impurities. The two techniques showed similar efficiency to remove the free by-products. During fractional precipitation, the final product was stuck to the edges of the round-bottom flask. Therefore, the direct precipitation (DP) was kept as preferential purification technique thanks to its easier process to collect the final product.

In order to remove the last traces of residual by-products, two or three successive purification steps were performed. The removal of impurities was followed by DOSY-NMR. The crude product (**Figure 36**-A) showed all the species in solution before purification. After one precipitation (**Figure 36**-B), impurities were still present. After three precipitation steps (**Figure 36**-C) the impurities were totally removed, only PCL-*g*-PDA was remaining. The ^{1}H-NMR spectra of the PCL-g-PDA purified 3 times is presented in **Figure 37**. The mass yield was calculated according the equation (8) and was estimated around 4%. The low value suggested the low degree of polymerization of dopamine and the low grafting density of PDA in the given conditions

$$\eta = \frac{m_{PCL-g-PDA}}{m_{PCL-I} + m_{dopamine}} * 100 \quad (8)$$

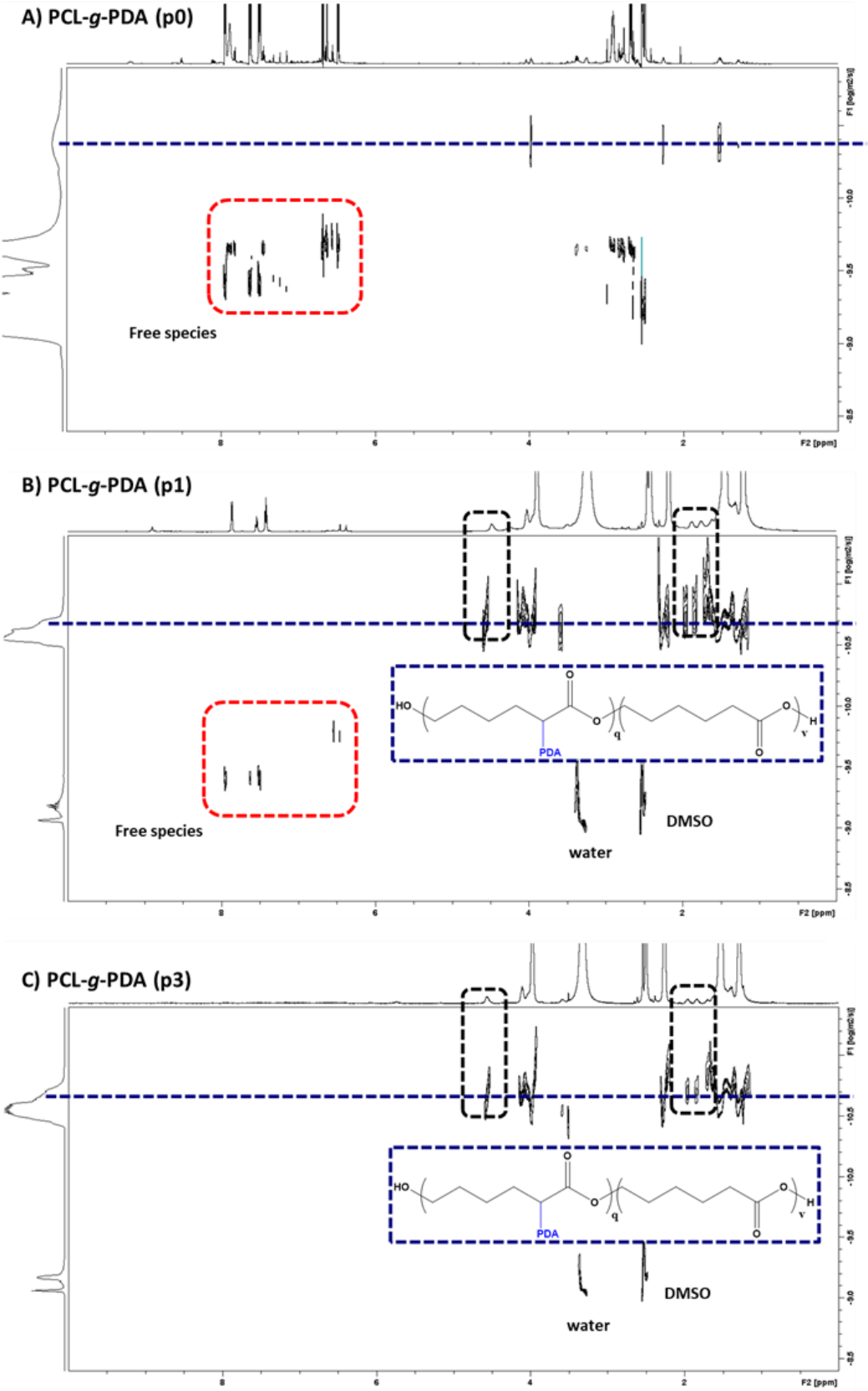

Figure 36. DOSY-NMR of the PCL-g-PDA A) before purification and after purification by B) one and C) three precipitations steps

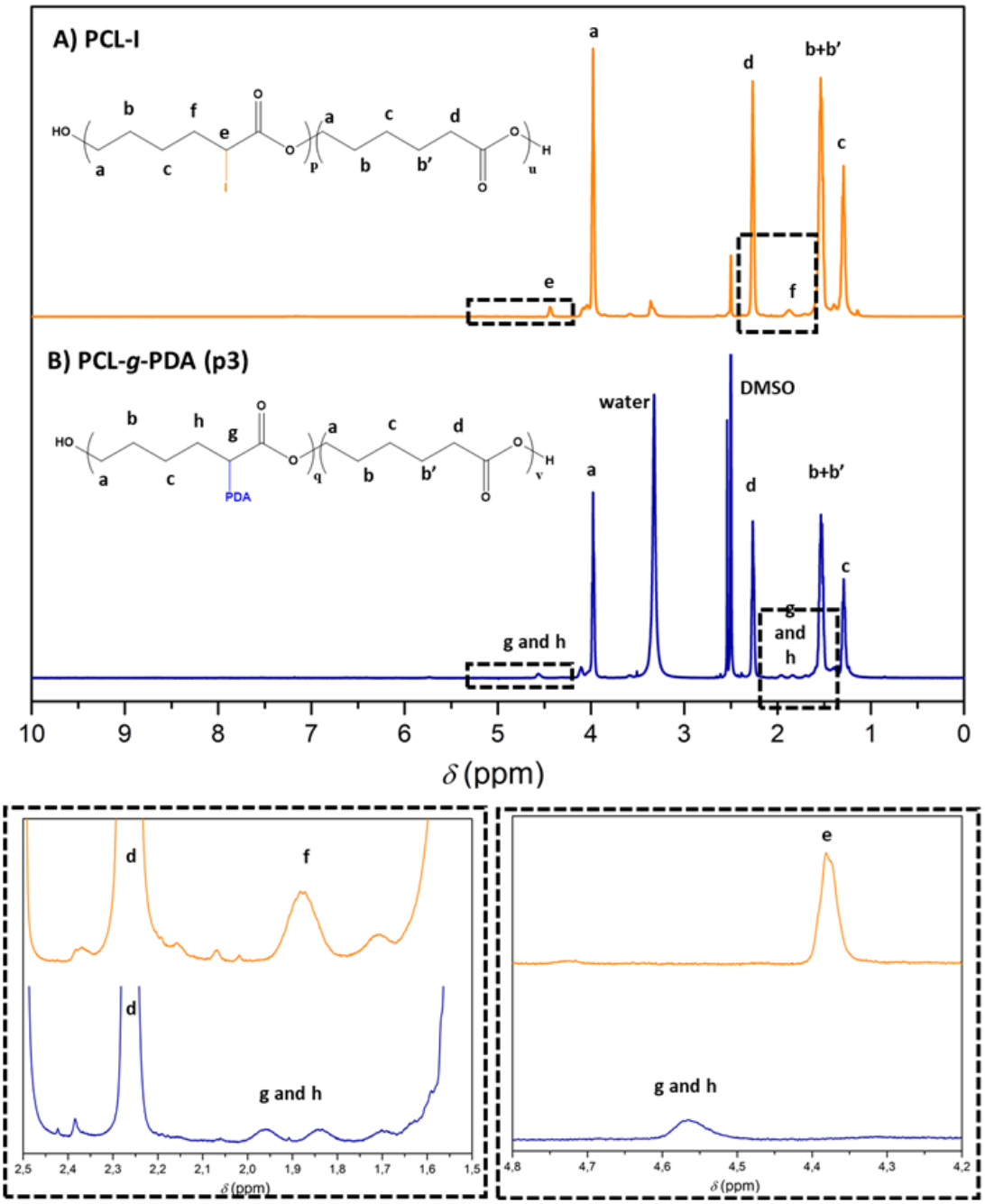

Figure 37. ^{1}H-NMR spectra of A) PCL-I and B) PCL-*g*-PDA after three steps of purification (p3) in DMSO-d6 (bottom row corresponds to insets)

The removal of impurities was also visually observed. The powders obtained after each step of purification are shown in **Figure 38** . From the first step to the third step of purification, the colour progressively shaded from dark black powder to light grey powder. It suggested that a given amount

of free PDA (black compound) was removed during the precipitation steps, which was in agreement with the NMR analysis. The successive purification steps allowed also the removal of the copper bromide involved in the chemical synthesis. The content of residual copper in the PCL-*g*-PDA copolymers was determined by ICP-OES analysis and the results are shown in **Table 7**. In a typical synthesis, the amount of copper introduced in the reactive media is 7595 ppm (theoretical value). This quantity decreased to 624 ppm after one purification and to 272 ppm after three purifications. This copper removal is of importance as the lower the quantity of residual copper, the safer for medical applications.

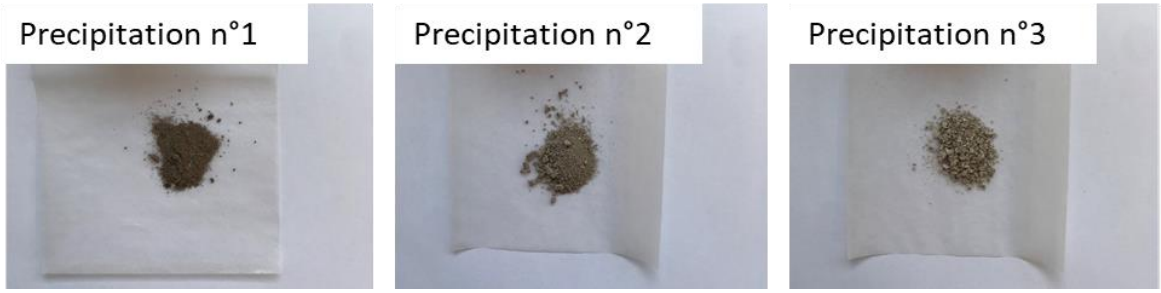

Figure 38. Photographs of the dried powder of PCL-*g*-PDA after the first, the second and the third purification in methanol.

Table 7. Residual copper content determined by ICP-OES analysis

	Before purification	One purification	Three purifications
Cu (ppm)	5168	624	272

Then, PCL, PCL-I and PCL-*g*-PDA copolymers were analyzed by SEC in DMF. The chromatograms are presented in **Figure 40** and the molecular characteristics are reported in **Table 8**.

Table 8. Characteristics of polymers by SEC analysis (PS standards used for calibration)

	In THF		In DMF	
	M_n (g.mol^{-1})	*Đ*	M_n (g.mol^{-1})	*Đ*
PCL	127 000	1.61	190 000	1.43
PCL-I	20 500	3.02	49 000	2.45
PCL-*g*-PDA	Not soluble		46 000	2.73

The chromatograms using RI detection (**Figure 40**-A) showed a decrease in number average molecular weight (M_n) from 190 000 to 49 000 g.mol^{-1} and an increase of dispersity *Đ* from 1.44 to 2.45 for PCL-I compared to PCL, in accordance with the SEC results obtained in THF. Chromatograms of PCL-*g*-PDA showed a slight decrease in *M*n (from 49 000 to 46 000 g.mol^{-1}) and an increase of *Đ* (from 2.45 to 2.73). One could have expected an increase of molecular weight upon grafting. However, the addition of PDA in the polymer modifies the chemical environment, therefore affects the solubility leading to changes in hydrodynamic radius that affect the determination of the molecular weight.

In order to select the appropriate wavelength to perform SEC analysis using UV detection, the individual components were characterized by UV/Vis spectroscopy from 250 to 600 nm in DMF at room temperature. The comparison of the UV spectra of PCL, PCL-I and PCL-*g*-PDA are presented **Figure 39**. PCL does not absorb in the range of 250 to 600 nm and PCL-I absorbs from 250 to 400 nm – due to the presence of the iodine atom, as already observed in THF SEC analysis. The spectra also showed that PCL-*g*-PDA absorbs from 250 to 600 nm, which confirmed the presence of PDA in the copolymer. Therefore, the characteristic wavelengths of PDA are from 400 to 600 nm and λ = 450 nm was selected for further analyses. At λ = 450 nm and at a concentration of 3 mg.mL^{-1} in DMF , the absorbances of PCL and PCL-I were negligible (0.02 A.U) whereas clearly measurable for PCL-*g*-PDA (0.23 A.U.).

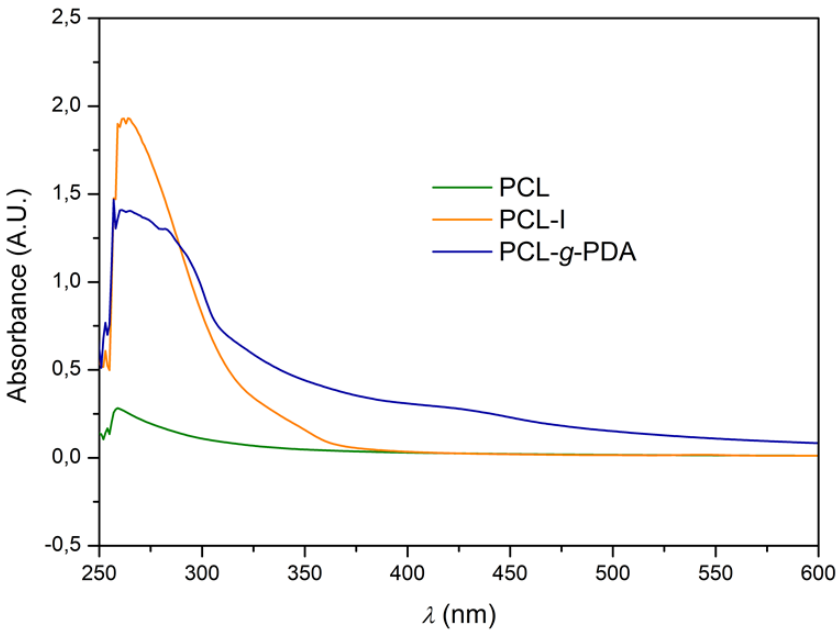

Figure 39. UV spectra of PCL, PCL-I and PCL-*g*-PDA at a concentration of 3 mg/mL in DMF

As a consequence, SEC analyses using a UV detection at λ = 450nm were performed. At 450 nm, only the PDA moiety absorbs. The chromatograms (**Figure 40**-B) showed a monomodal distribution indicating a single population, and a strong absorbance at the retention time of the PCL-*g*-PDA copolymer. The SEC analysis is another method that strengthens the proof of the grafting of PDA on the PCL backbone.

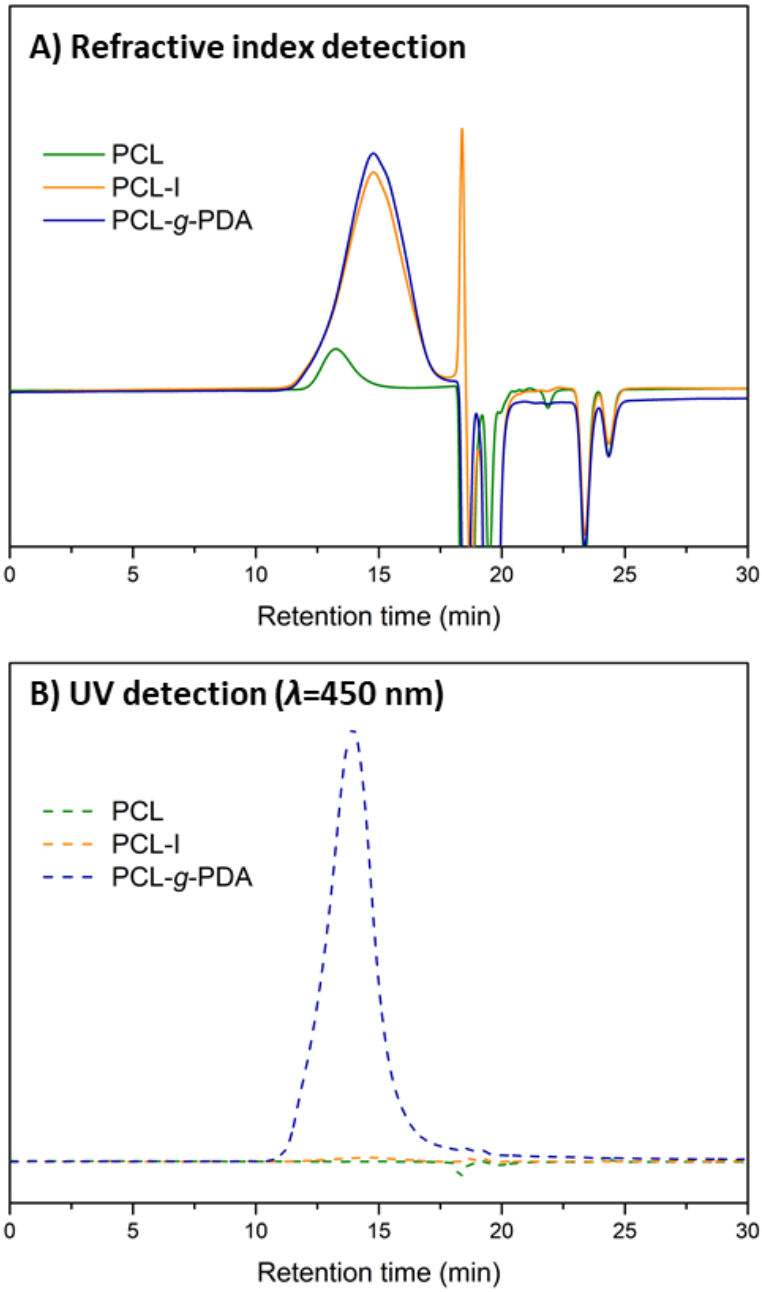

Figure 40. SEC analysis of PCL, PCL-I and PCL-*g*-PDA in DMF

3.1.3 Properties of PCL and PCL-*g*-PDA copolymers

3.1.3.1 Thermal stability

The polymers have been characterized before and after each chemical modification step. The thermogram and the derived curve (dTG, first derivate) of the PCL, **Figure 41**-A, showed a unique thermal event (minimum of dTG at 424 °C). In the case of PCL-I, **Figure 41**-B, the thermogram showed a major thermal event (minimum of dTG at 404°C) corresponding to the degradation of the non-modified units of the PCL backbone. Finally, in the case of the PCL-*g*-PDA copolymer, **Figure 41**-C, a unique thermal event is observed (minimum of dTG at 422 °C). These data highlight a 20°C decrease of the temperature of degradation for PCL-I compared to PCL, with a two-step degradation profile for PCL-I. Replacing iodine by PDA side chains almost restores the initial thermal properties, which is consistent with the work of Cho *et al.* [118], who observed a switch from a two-step to a one-step degradation profile and an enhancement of thermal stability when passing from PMMA-Br to PMMA-PDA.

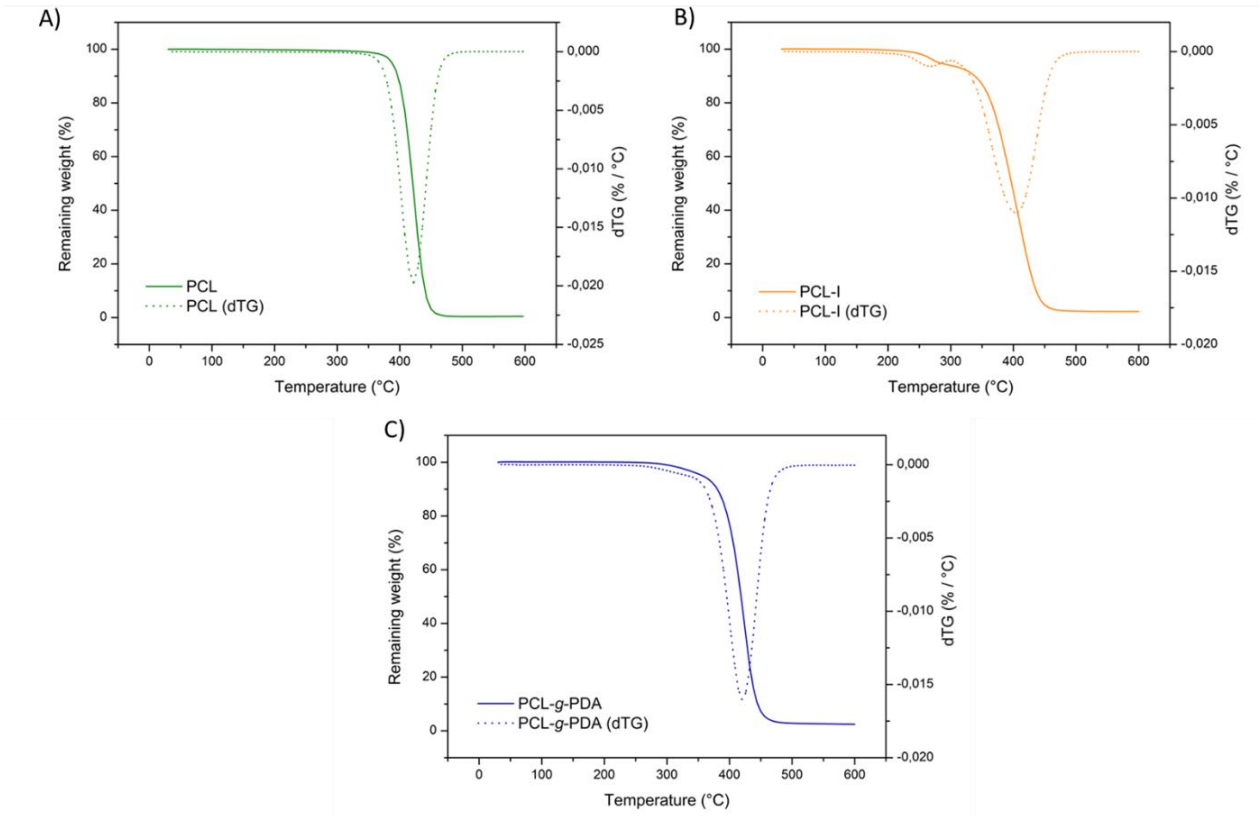

Figure 41. Thermogravimetric analyses of A) PCL, B) PCL-I and C) PCL-g-PDA after three successive purifications

3.1.3.2 Thermal properties

With the aim of comparing the change in enthalpy (*ΔH*) and the characteristic temperatures of PCL and PCL-*g*-PDA copolymers, the thermal history must first be erased. A first ramp of temperature was established from -80 °C to 100°C (stop à 100°C to avoid polymer degradation), then a second one was established from -80 to 300°C. The thermograms are shown in **Figure 42**.

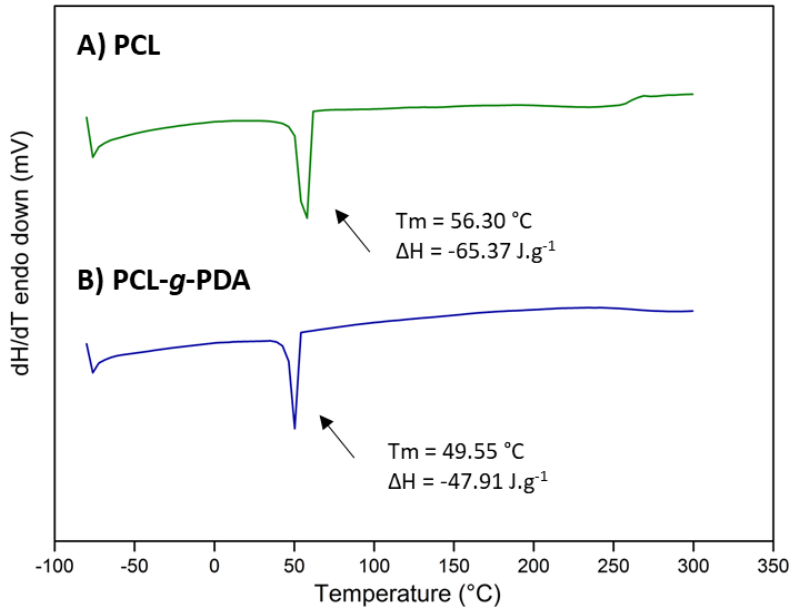

Figure 42. DSC analyses of PCL and PCL-*g*-PDA

The glass transition temperature (*Tg*) refers to the temperature at which the transition from a glassy state into viscous/rubbery state occurs in the amorphous regions of the material. In order to observe the *Tg* of polymers, the proportion of amorphous regions should be sufficient, the chain length should be long enough and, in the case of grafted copolymer, the chain length of the side chains should be long enough as well. Moreover, the starting temperature of analysis may be at least 20°C under the expected *Tg*. The glass transition temperature of PCL, theoretically around -63°C, was not observed in the conditions of analysis, probably due to the high degree of crystallinity of PCL and the difficulty for the cryostat to go below -80°C. Similarly, the glass transition temperature of PDA – between 97 °C [118] and 131 °C [93] – was not observed in PCL-*g*-PDA. As discussed, it is probably due to the short size of the PDA side chains distributed along the PCL backbone and the low proportion of PDA in the copolymer.

A slight decrease of the melting temperature (*Tm*) from 56.3 °C (PCL) to 49.5 °C (PCL-*g*-PDA) was observed in addition to a decrease of the melting enthalpy from -65.4 to -47.9 J.g^{-1}. Crystallinity degree

was assumed to be proportional to the experimental heat of fusion of 135 $J \cdot g^{-1}$ for the 100% crystalline PCL (theoretical value) [295,296]. The degree of crystallinity decreased from 48% for PCL to 35% for PCL-g-PDA. The decrease in melting temperature and crystallinity are due to the decrease of the molecular weight during the iodination and the addition of PDA affecting the spatial organization of the PCL chain. Moreover PDA is amorphous [93] as previously reported in Chapter I.

3.1.4 Quantification of the content of PDA in the copolymers

In order to quantify the amount of PDA in PCL-*g*-PDA, two methods have been used: UV spectroscopy and TG analysis. The first method is based on the UV/vis absorbance of the PDA moiety, the second method is based on the remaining weight of the degraded product.

3.1.4.1 Synthesis and characterization of oligomers of PDA: establishment of a model for the quantification of PDA in the PCL-g-PDA copolymers

In the previous parts, a method was developed to synthesize PCL-*g*-PDA copolymers in organic medium. In order to identify the signals obtained in NMR and to quantify the content of PDA in PCL-*g*-PDA, the synthesis of PDA is required.

Typically, the synthesis of nanoparticles of PDA are carried out in aqueous solution in oxidative conditions described in Chapter I. However, and in order to obtain PDA oligomers similar to the ones grafted on PCL-*g*-PDA, we chose to prepare PDA oligomers under our previous conditions. For that purpose, a halogenated initiator was synthesized to replace/act like the PCL-I macroinitiator.

The selected initiator diethylene glycol bis(2-bromoisobutyrate) was obtained from the reaction of diethylene glycol with bromoisobutyryl bromide in the presence of triethylamine in dry THF (**Scheme 20** in Appendix). The initiator is functionalized with a bromide group to act as a grafting site for the further chemical step. ^{1}H NMR spectrum in $CDCl_3$ of the initiator is shown in **Figure 61** in Appendix. The peak at 1.89 ppm (peak a) is a singlet which corresponds to the R-C*H*3 and the peaks at 3.73 ppm (peak c) and at 4.28 ppm (peak b) are triplets which correspond respectively to the signals of the protons O-CH_2-R and R-CH_2-O-CO. The PDA oligomers were prepared in the same conditions as PCL-*g*-PDA with adjustment of the quantities of reactants to account for the molecular weight and the number of

grafting sites of the initiator diethylene glycol bis(2-bromoisobutyrate) (**Scheme 19**). The product was collected by precipitation in THF and dried.

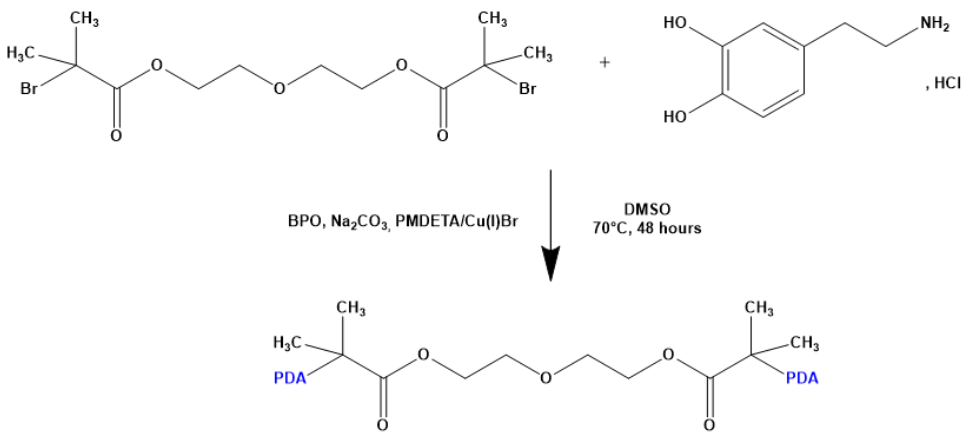

Scheme 19. Synthesis of PDA oligomers

The ^{1}H-NMR spectrum of the oligo-PDA in DMSO-d_6 is presented in **Figure 43**-A. Peaks are observed at 7.49 ppm, 7.59 ppm and 7.94 ppm whereas a large band containing several peaks is observed from 6.30 to 7.00 ppm. This band might be attributed to the chemical modification of dopamine (**Figure 43**-B) induced during the reaction and the hypothesis in supported by the work of Ma *et al.* [297] (**Figure 63**). Concerning the peaks at 7.49 ppm, 7.59 ppm and at 7.94 ppm, they might be attributed to the by-products of BPO (**Figure 43**-C). The DOSY-NMR spectra of oligo-PDA, dopamine and BPO are presented on the right side of **Figure 43**. PDA exhibit a diffusion coefficient of 1.48 x 10^{-10} $m^2.s^{-1}$ for the peaks located in the range from 6.30 to 7.00 ppm attributed to the moieties of dopamine modified during the reaction of polymerization, and a diffusion coefficient of -3.24 x 10^{-10} $m^2.s^{-1}$ for the peak located in the range of 7.00 to 8.00 ppm attributed to the by-product of BPO. The chemical shifts and the coefficient of diffusion of impurities of PCL-g-PDA (p1) (D = 3.98 x 10^{-10} $m^2.s^{-1}$ for the peaks in the range of 7-8 ppm | D = 1.62 x 10^{-10} $m^2.s^{-1}$ for the peaks in the range of 6-7 ppm, Chapter II part 3.1.2, **Figure 34**) were close the oligo-PDA ones, confirming that the impurities observed by NMR in PCL-g-PDA (p1) and removed after 3 purification steps were actually oligo-PDA.

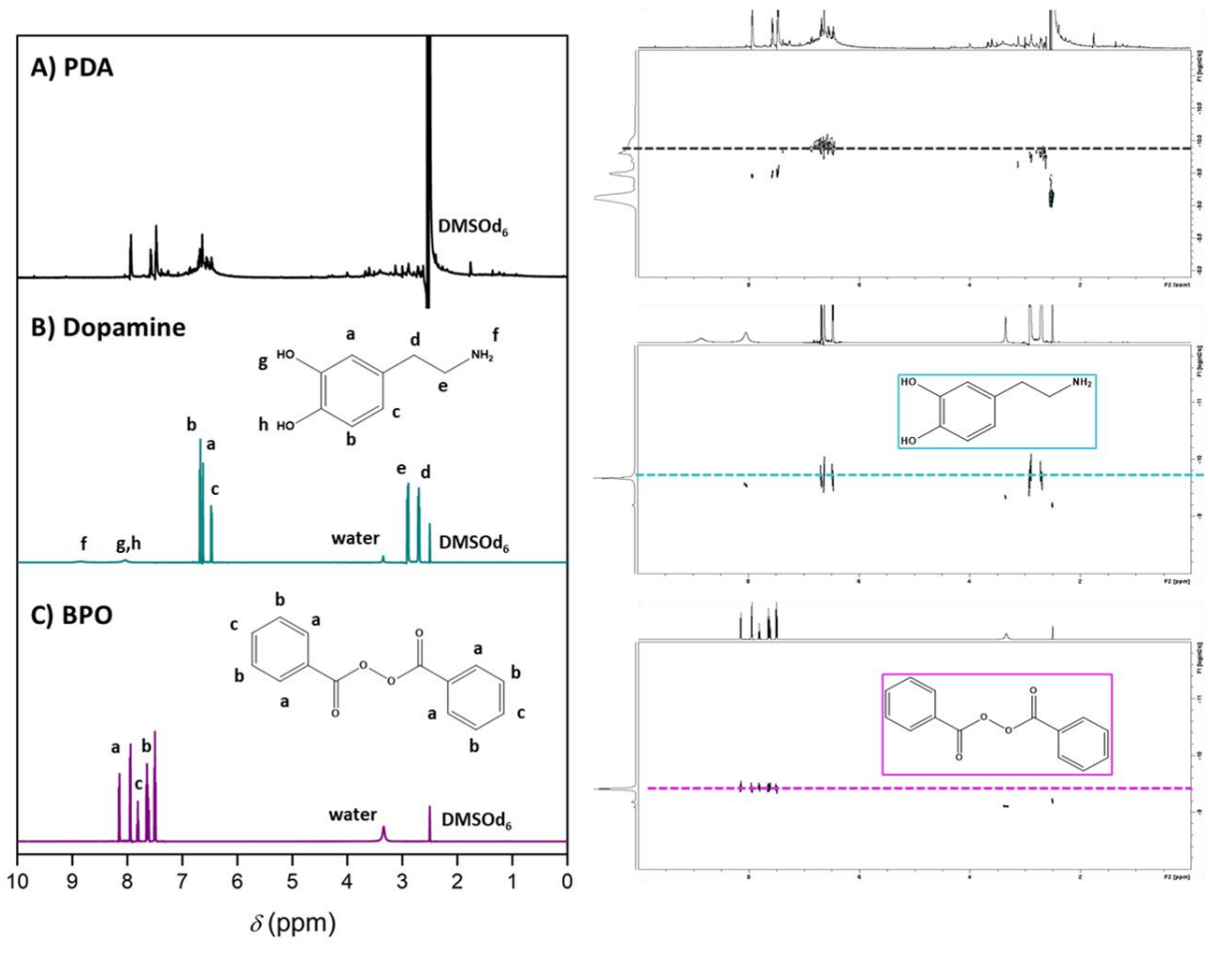

Figure 43. ^{1}H-NMR spectra on the left and DOSY-NMR spectra on the right of A) PDA, B) Dopamine and C) BPO in DMSO-d_6

The UV spectrum of oligo-PDA in DMF at a concentration of 0.1 mg.mL^{-1} is presented **Figure 44** and showed a broad absorption from 250 to 600 nm. At λ=450 nm – the selected specific wavelength for the UV detection of the copolymer PCL-*g*-PDA – the absorption was 0.49. The profile of UV absorbance of PDA is similar to the UV absorbance spectrum described by Tian Lei *et al.* [92] reported in Chapter I in **Figure 8**.

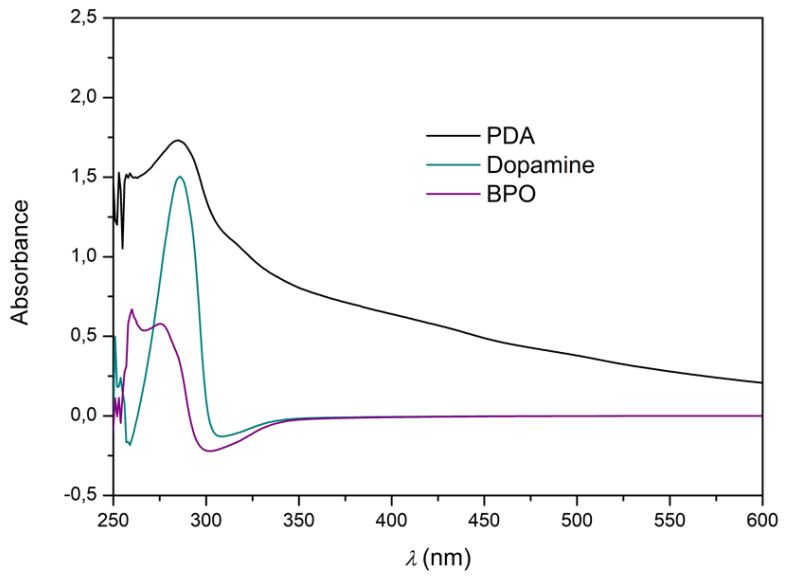

Figure 44. UV spectra of BPO, dopamine and oligo-PDA prepared at a concentration of 0.1 mg.mL^{-1} in DMF

The thermal decompositions and stabilities of the components of the reaction measured by TGA are presented in **Figure 45**. Dopamine (**Figure 45**-B) presents a unique thermal event (minimum of dTG at 330 °C). The thermal stability of BPO was not realized in the lab for safety reasons. Huang *et al.* [298] studied the thermal stability of BPO up to 300 °C and showed two thermal phenomena (**Figure 45**-C). The first thermal event occurring from 30 to 100°C corresponds to the thermal decomposition of BPO, and the second thermal event occurring from 100 to 300°C, corresponding to the progressive mass loss of the decomposed BPO. Besides, during the reaction of polymerization, the reactive medium is heated at 70°C and the half-life of BPO is 7.3 hours at this temperature [299]. As a result, there is no BPO anymore in the reaction medium at the end of the reaction and after precipitation, only the by-products of BPO remain – as observed previously in NMR analysis. In the oligo-PDA (**Figure 45**-A), a first thermal event (domain I) was observed from 30 to 100°C attributable to the elimination of the moisture and thermolabile residues. A second thermal event (domain II) occurred from 100 to 500 °C with a progressive mass loss of the product, which was attributed to the decomposition of oligo-PDA chain and impurities (dopamine and decomposed BPO). The third thermal decomposition (domain III) from 500 to 700°C was attributed to the decomposition of oligo-PDA only. The remaining weight of the product is around 64% at 600°C. The thermal decomposition profile of the oligo-PDA prepared with the diethylene glycol bis(2-bromoisobutyrate) initiator in organic conditions looked completely similar to the one obtained in aqueous conditions obtained by Tiwari *et al.* [93] and presented in Chapter I in **Figure 9**. Therefore, the synthesis procedure we developed might be an alternative.

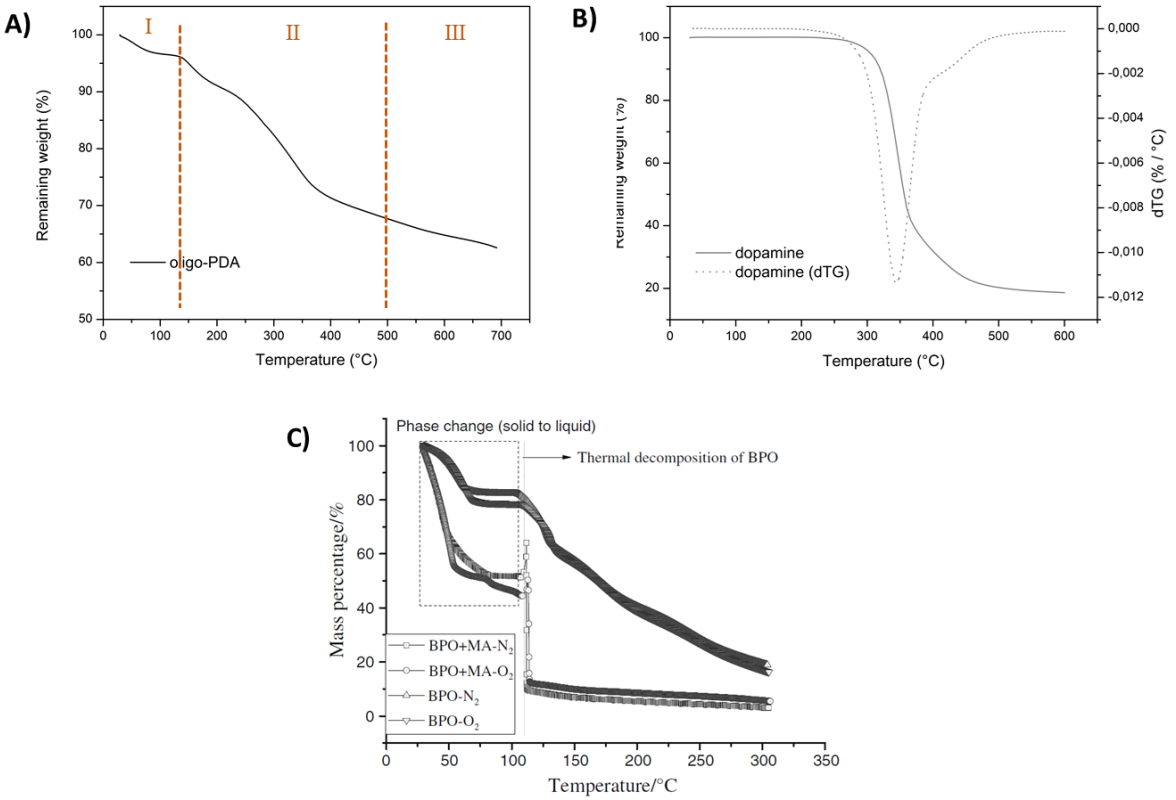

Figure 45. TG analysis of A) oligo-PDA, B) dopamine and C) BPO [298]

3.1.4.2 Quantification of PDA

<u>By UV spectroscopy</u>

As previously described, oligo-PDA and PCL-*g*-PDA absorbed in UV from 250 to 600nm and the characteristic wavelengths were established above 400 nm. In order to quantify the amount of PDA in PCL-*g*-PDA by UV spectroscopy, a calibration curve was established (**Figure 46**) reporting the absorbance with respect to the concentration of PDA in DMF in a range from 5 to 200 µg.mL^{-1}. As a reminder, the absorbance of the PCL-*g*-PDA at 450 nm in DMF was 0.23 (C= 3 mg.mL^{-1}). By application of the equation of the calibration curve, the concentration of PDA was 47 µg.mL^{-1} in the 3 mg.mL^{-1} PCL-*g*-PDA solution corresponding to 47 µg of PDA in 3 mg of PCL-g-PDA. The PDA content in PCL-*g*-PDA purified three times was estimated to be 1.6 wt.%.

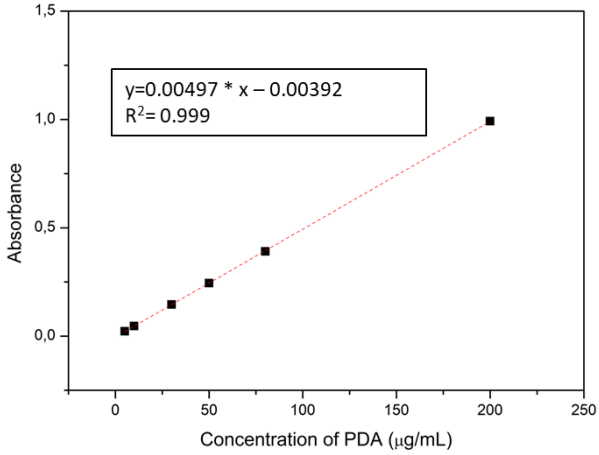

Figure 46. Calibration curve of oligo-PDA in DMF by UV spectrometry at λ =450 nm

By TG analysis

The second method of quantification of PDA content is based on the remaining masses at 600°C of PCL, PCL-g-PDA and oligo-PDA. The remaining weights of PCL, PCL-I and PCL-g-PDA purified three times are shown in **Table 9**. The remaining weight of PCL was 0.44% at 600°C, 2.46% for PCL-g-PDA (**Figure 41**) and 64% for oligo-PDA (**Figure 45**-C). By application of equation (9), the proportion of PDA in the PCL-g-PDA copolymer purified three times was estimated to be 3 wt.%.

Table 9. Mass loss and remaining weight of PCL, PCL-I and PCL-g-PDA copolymer from 30 to 600°C

Temperature range	Remaining weight at 600°C
PCL	0.44%
PCL-I	2.24%
PCL-g-PDA	2.46%

$$W\%_{\text{PDA in copolymer}} = \frac{\%_{\text{remaining weight in PCL-}g\text{-PDA at 600°C}} - \%_{\text{remaining weight in starting PCL at 600°C}}}{\%_{\text{remaining weight in oligo-PDA at 600°C}}} * 100 \qquad (9)$$

Comparison and conclusion

This value obtained in TGA (3wt.%) was in relatively good agreement with the value obtained the UV (1.6 wt.%) detection. The amount of PDA calculated confirmed the hypothesis made previously in DSC where the decrease in crystallinities and the absence of detection of the *Tg* were related to a low proportion of PDA in PCL-*g*-PDA copolymer.

3.2 Preparation and properties of PCL and PCL-*g*-PDA films, discs and implants

According to the temperatures of degradation of PCL and PCL-*g*-PDA, films were hot pressed at 100°C by processing quantities of polymer allowing the preparation of films with a thickness around 400 ± 50 µm. (**Figure 47**)

Figure 47. Preparation process for the PCL and PCL-*g*-PDA films by melting compression

3.2.1 Physical and chemical properties of PCL and PCL-*g*-PDA implants

3.2.1.1 Thermal properties

In order to evaluate the impact of the manufacturing process on the crystallinity properties, three processes were compared: i) genuine polymer as a powder (process 1) – already presented in Chapter II part 3.1.3.2, ii) polymer processed as a film directly made by hot compression of the powder (process 2), iii) polymer processed as a film made by hot compression of the powder previously dissolved in DMSO and dried (process 3). the thermograms are represented in **Figure 48**.

The melting temperature of PCL for each process was around 56°C and the degree of crystallinity was calculated between 46 and 50%, considering a melting enthalpy of -135 $J.g^{-1}$ for a 100 % crystalline PCL

(theoretical value) [295,296] . This study showed that the process had a low impact on the characteristics of PCL. The same study was performed on PCL-*g*-PDA copolymers. The melting temperature was around 49°C and the degree of crystallinity was 35%. The process 3 was not performed on PCL-*g*-PDA copolymer because of lack of material, but we can reasonably consider that, like for PCL, there is little if any influence of the process. Consequently, this study demonstrates that the manufacturing process had a negligeable impact on the thermal properties (*Tm* and *ΔH*) of the PCL and PCL-*g*-PDA.

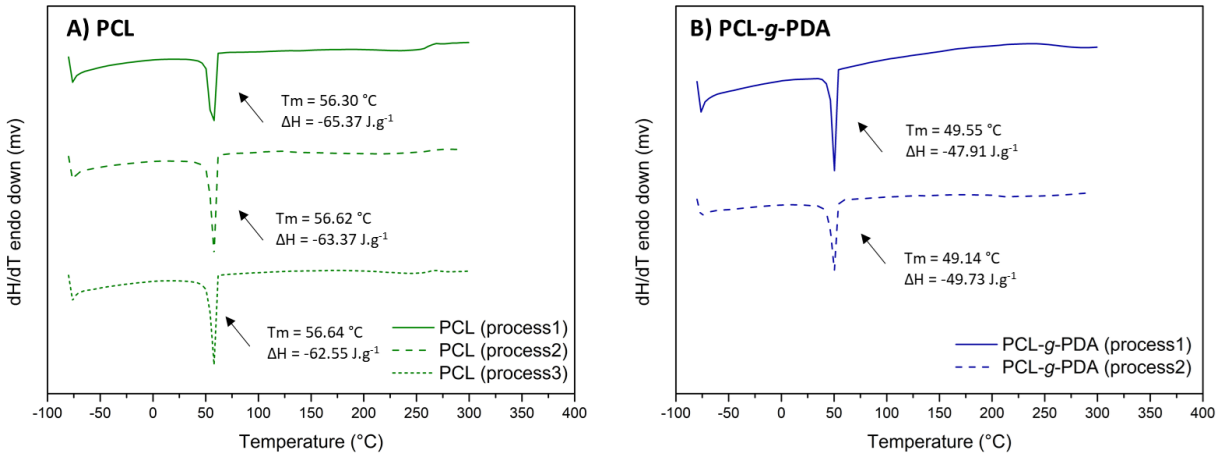

Figure 48. DSC of A) PCL and B) PCL-g-PDA under powder form (process1), film prepared by hot compression (process2) and film prepared by solvent casting followed by hot compression (process3)

3.2.1.2 Surface properties

In addition to the thermal properties, the properties of the surfaces of the films, especially the surface tension, were evaluated using the water static contact angle (Θ) method. By definition, a contact angle below 90° indicates a hydrophilic nature of the surface, between 90-120° a hydrophobic surface, between 120-180° a super hydrophobic surface.

Table 10 shows the contact angle values for PCL and PCL-*g*-PDA films made by hot compression (process 2). The surface of PCL exhibited a contact angle around 72°. However, PCL is a hydrophobic material with a contact angle around 97° according to the work of Basile *et al.* [300], which makes the value of the surface angle surprising. In fact, the method of the preparation of the film might impact the roughness of the surface thus impacting the contact angle value [301]. However, in our case sheets of Teflon®, inert material, were put on both sides of the mold during compression. Despite the surprising values of contact angle, the films of PCL and PCL-*g*-PDA exhibited similar values (around 72-73°) which suggest a similar surface composition. Indeed, in the literature, the coating of surfaces with

PDA deposit provides a decrease in the contact angle (*eg.* for PMMA-based surface [118], PDA content = 0 % | Θ = 74.6° *vs*. PDA content = 9.3 % | Θ = 64.7°) sign of a more pronounced hydrophilicity probably due to some free phenol or amine groups at the surface. The similar contact angle between PCL and the PCL-*g*-PDA were in agreement with the low content of PDA quantified previously (1.6-3 wt%).

Table 10. Contact angles of PCL and PCL-*g*-PDA films obtained by hot melt compression.

	Polymer	Contact angle Θ (°)
Literature	PCL [300]	94
PhD work	PCL	73
	PCL-*g*-PDA	72

3.2.2 *In vitro* degradation of PCL and PCL-*g*-PDA implant

The *in vitro* hydrolytic degradation of a polymer is a first insight towards its *in vivo* degradation behaviour, which is critical in most medical applications. The hydrolytic degradation of PCL and PCL-*g*-PDA implants was studied over 110 days. We focused on the evolution of the swelling ratio, the remaining weight and the number average molecular weight (M_n) over time according to the equations (1)-(3)

We aimed at evaluating the influence of the PDA side chains and the conditions of degradation on the degradation kinetics. We selected a commercial PCL (M_n= 45 000 g.mol^{-1}, data given by the manufacturer) because the molecular weight of PCL (M_n = 63 000 g.mol^{-1} | $Đ$ = 1.40 by SEC in DMF) is close to the molecular weight of PCL-*g*-PDA (M_n = 51 000 g.mol^{-1} | $Đ$ = 2.07 by SEC in DMF). Moreover, the 45 000 g.mol^{-1} PCL was used as reference in the drug release assays. Hydrolytic degradations were performed under two conditions, namely standard (neutral pH) or accelerated conditions (acidic pH).

3.2.2.1 *In vitro* degradation under standard conditions

The degradation of the films was evaluated in PBS at physiological pH =7.4 and at 37°C according to ISO 10993-13.

The evolution of water uptake over 110 days is represented in **Figure 49**-A. The water uptake values ranged between 0-3% for PCL implants and from 0 to 10% for the PCL-*g*-PDA. The higher values for PCL-*g*-PDA implants may be attributed either to an increase of hydrophilicity (not supported by the values of contact angle) or more likely to a decrease in the crystallinity (χ = 35 % for PCL-*g*-PDA *vs.* χ = 48 % for PCL). Indeed, water penetrates easier in the amorphous structures. [302]

The evolution of the residual mass of the implant is presented in **Figure 49**-B. No mass loss is observed for both PCL and PCL-*g*-PDA films during the 110 days of immersion. This result indicates that no soluble oligomers are released from the films in the course of this study.

The evolution of the residual M_n is presented in **Figure 49**-C. PCL films showed a decrease in molecular weight from 63 400 to 41 300 g.mol^{-1} (residual molecular weight = 76%) and a constant dispersity of 1.4. PCL-*g*-PDA films showed a slight decrease in molecular weight from 51 000 to 41 600 g.mol^{-1} (residual molecular weight = 79 %). The residual M_n were similar for PCL and PCL-*g*-PDA implants after 110 days of immersion, thus the presence of PDA barely impacts the degradation.

The variation of the pH over degradation of PCL or PCL-*g*-PDA is shown in **Figure 49**-D. A slight decrease of pH from 7.2 to 6.8 is observed at the early stage (5 days) for PCL films, and then remained stable until the end of the study, suggesting that some leachable could be contained in the commercial PCL or that surface impurities may have been added upon the moulding process. The pH remained stable around 7.2 for PCL-*g*-PDA films. The pH of the media containing PCL and PCL-g-PDA implants were in the range of the pH of the vitreous humour 7.0-7.4.

With the aim to limit the risk of obstructing the vision, it is preferable that implants keep their initial shape without breaking apart, once implanted/injected into the vitreous of the patient eye. Moreover, the vitreous humour should remain transparent. The physiological degradation medium and the photograph of the implants at day 0 and at day 110 are shown in **Figure 49**-E and **Figure 49**-F respectively. Macroscopically, the films looked similar and intact at day 0 and day 110, and no coloration of the degradation medium was observed.

Thermal characteristics and degree of crystallinity of the films over time during the degradation process were evaluated at days 0, 7, 45 and 110 and reported **Table 11**. The temperature of melting and the enthalpies of fusion of each film after immersion were all similar to the ones before immersion, suggesting a stability of the films in the *in vitro* standard conditions over 110 days.

Based on these results, PCL and PCL-*g*-PDA films (i) do not degrade *in vitro* in standard conditions and (ii) do not induce change in the local pH value. The presence of PDA units in the copolymer does not influence the degradation of the implant during 110 days.

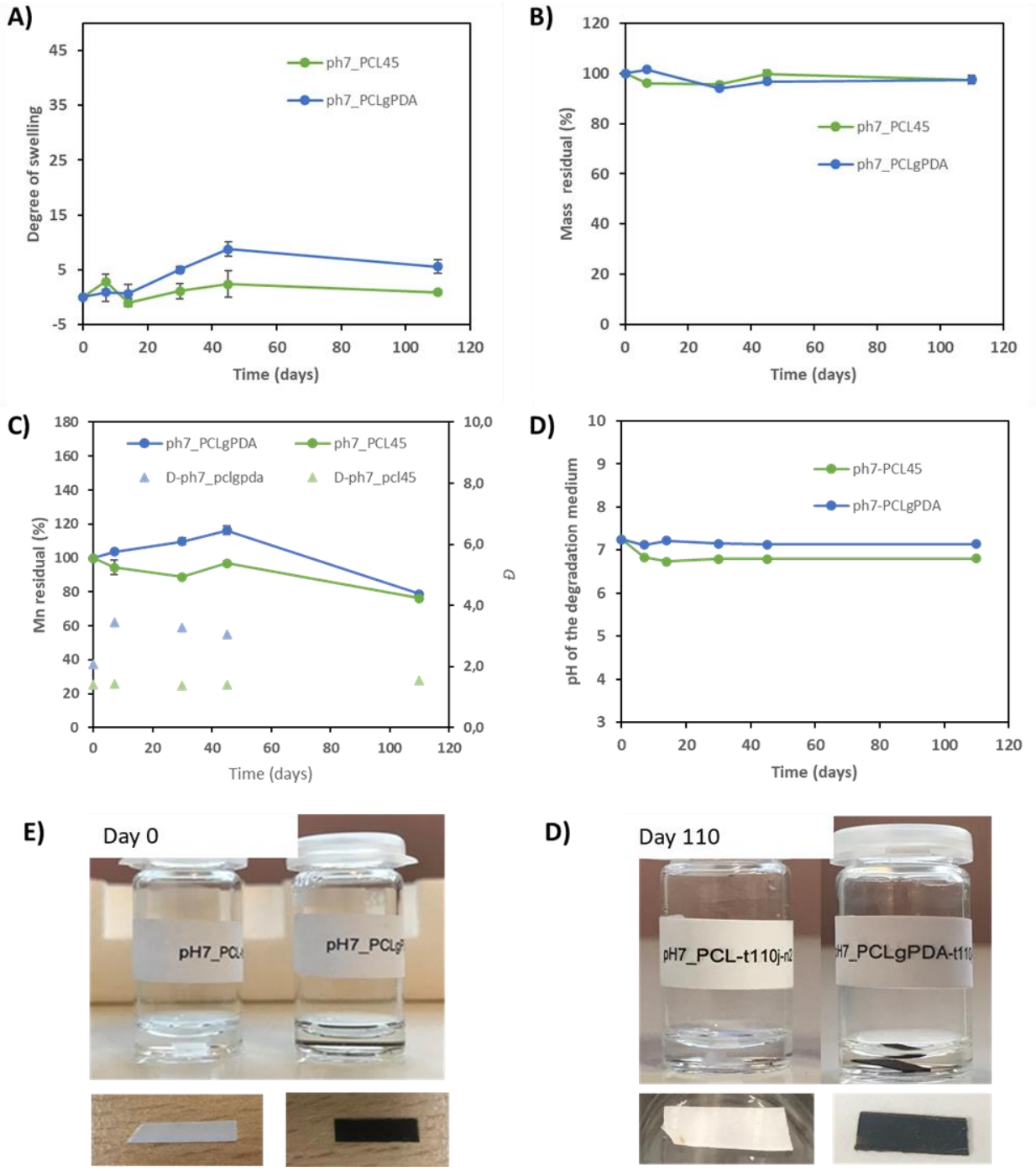

Figure 49. In vitro degradation of PCL and PCL-*g*-PDA in standard conditions (PBS, 37°C, pH=7.4) A) Degree of swelling, B) Residual mass, C) Dispersity and residual molecular weight, D) pH of the degradation medium, and photographs of the implant after E) 0 and F) 110 days of immersion.

Table 11. Thermal characteristics and degree of crystallinity of PCL and PCL-*g*-PDA films during the in vitro degradation study in standard conditions (PBS, pH 7.4, 37°C).

Polymer film	Time (days)	*Tm* (°C)	*ΔH* (J.g^{-1})	*χ* (%)
PCL	0	57	-69	51
	7	57	-65	48
	45	57	-69	51
	110	57	-67	49
PCL-g-PDA	0	49	-50	36
	7	47	-51	37
	45	46.	-49	36
	110	47	-49	36

3.2.2.2 In vitro *degradation* under accelerated conditions

The degradation of implants has also been investigated in accelerated conditions according to the ISO 10993-13. Increasing the temperature (preferentially at 70°C) is the method of choice for the study of the biomedical solid formulations in accelerated conditions. However, the thermal characteristic of the films showed that PCL and PCL-*g*-PDA exhibit a melting temperature around 57°C and 49°C respectively. A working temperature at 45°C is compatible with our polymers, but would have led to too long degradation times in the frame of this work. As described in Chapter I, the degradation of polyester –PCL in this case – can be radical-mediated, enzymatic, intracellular, pH-mediated [303] and the degradation of PDA is assumed to be radical-mediated [4,89], alkaline-mediated [95] and induced by micro-organism [96]. For practical reasons, the pH-mediated conditions were chosen because PCL is the major component of the copolymers.

We selected an acidic pH value (pH=1) according to Sailema *et al*. [169] who reported that the degradation of PCL in acidic conditions was consistent with a bulk degradation mechanism, which is representative of the hydrolytic degradation of PCL at physiological pH. Contrary to the thermal-induced degradation where the accelerated and the standard conditions are related with the Arrhenius equation, no correlation or equation has been described in the literature for the pH-induced degradation process. In other words, the pH-induced degradation process permits only to determine the type of mechanism of degradation of a polymeric system (bulk vs. surface erosion). The results are presented in **Figure 50**.

Due to the disintegration of the films and the need to remove the medium in the sampling glass, which could bias the data, the study of the water uptake content was not performed.

The evolution of the residual M_n and the dispersity $Đ$ are shown in **Figure 50**-B. From day 0 to day 7, the PCL films showed a decrease in the molecular weight from 63 300 to 28 300 g.mol^{-1} (residual molecular weight = 45%) with a relative constant dispersity around 1.4-1.5. From day 7 to day 45, the PCL films continued to degrade from 28 300 to 7 500 g.mol^{-1} (residual molecular weight = 12%). Concerning the PCL-*g*-PDA films, the molecular weight decreased from 51 000 to 17 800 g.mol^{-1} (residual molecular weight = 35%) with a decrease in the dispersity from 2.07 to 1.57. From day 7 to day 60, the molecular weight slowly decreased, and in lower proportion than PCL films, from 17 800 to 13 200 g.mol^{-1} (residual molecular weight = 25%). To resume, PCL and PCL-*g*-PDA films showed similar M_n evolution profiles.

The evolution of the residual mass is shown in **Figure 50**-A. The residual mass profile matched the residual molecular weight profile for both PCL and PCL-*g*-PDA films, with a similar residual mass of 13% and 18% respectively at day 45. Due to the complete disintegration of PCL films after this time point, the comparative study was stopped.

In PCL films, the lag time before mass loss, the progressive decrease of molecular weight and the occurrence of a double distribution are characteristics of a bulk degradation process. In PCL-*g*-PDA, an immediate mass loss is characteristic of a surface erosion process. However, a rapid molecular weight loss and a double distribution showed also a bulk degradation process. The two mechanisms are probably concomitant in the degradation of PCL-*g*-PDA. Moreover, the rapid mass and Mn loss of PCL-*g*-PDA films supported the hypothesis of a higher hydrophilicity or confirmed the less crystalline structure compared to PCL films

The physiological degradation medium and the pictures of the implants at day 0 and day 60 are shown in **Figure 50**-C and **Figure 50**-D respectively. Macroscopically, the films were broken and extremely brittle (they broke in several pieces when a movement is induced) confirming -as expected- the degradation of the PCL backbone in these conditions. Moreover, the degradation medium turned from transparent to light brown due to the greying of the PCL-*g*-PDA films. The colour fading of the PCL-*g*-PDA, and the coloration of the media induced, suggest the possible presence of soluble oligo-PDA and/or the degradation of the PDA [4,97].

Based on these results it can be concluded that, (i) PCL and PCL-*g*-PDA showed similar kinetics of degradation, (ii) degradation of PCL and PCL-*g*-PDA is in good agreement with a bulk degradation process and (iii) the kinetics of degradation of PCL-*g*-PDA can be extrapolated to the kinetics of PCL for in vitro standard conditions. In other words, PCL-*g*-PDA – containing 1.6-3 wt.% of PDA in the present

case – would probably degrade at the same rate as PCL, whose total resorption is estimated between 2 and 8 years [189] .

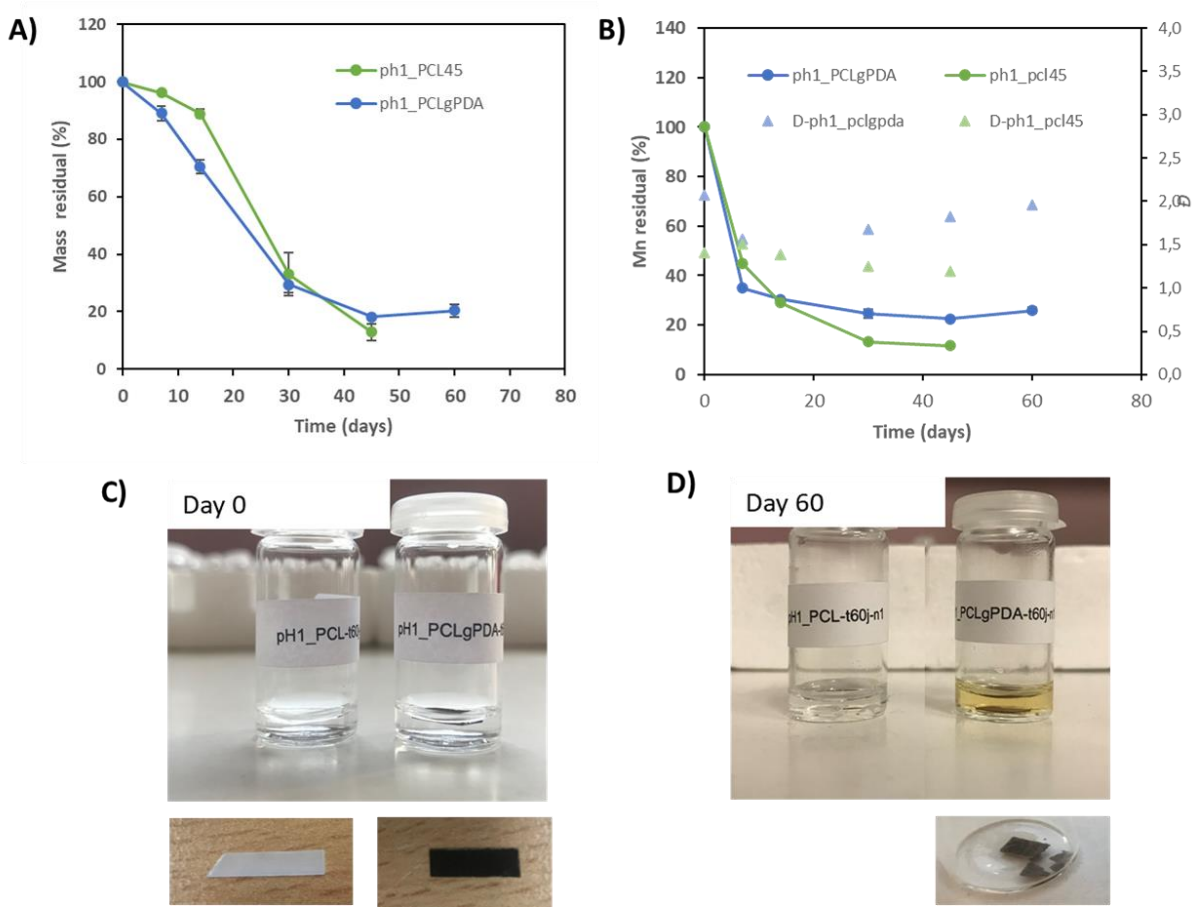

Figure 50. *In vitro* degradation of PCL and PCL-g-PDA in accelerated conditions (37°C, pH=1). A) Residual mass, B) Dispersity and residual molecular weight, and photographs of the implants after C) 0 and D) 60 days of immersion.

3.2.3 *In vitro* cytotoxicity studies of PCL and PCL-*g*-PDA discs

To confirm the potential use of PCL-*g*-PDA copolymers in injectable ocular implants, the cytotoxicity of PCL and PCL-*g*-PDA was investigated on mouse fibroblast cell line (L929) and human retinal epithelial cell line (ARPE-19) using extraction methods according to the ISO 10993-5.

The *in vitro* cytotoxicity results, presented in **Figure 51** showed the cell viability of PCL and PCL-*g*-PDA – with different numbers of purification steps – relative to the cell viability control (cells in the medium

free of discs). The compound is considered as non-toxic when a relative cell viability is above 70%. The negative control and the positive control induce cell viability and cell mortality, respectively.

The *in vitro* cytotoxicity results on the L929 cells line showed the complete cell viability of PCL (100%). PCL-*g*-PDA purified one time is named PCL-*g*-PDA (p1), and three times is named PCL-*g*-PDA (p3). The relative cell viability increased from 50 % to almost 100% when purifying the copolymer once or three times respectively, highlighting the importance of the purification step for PCL-*g*-PDA. The cell mortality possibly comes from the residual chemical products used during synthesis, like copper or by-products as described previously, which are removed upon purification (see Chapter II part 3.1.2 and 3.1.4.1).

Similarly, the cytotoxicity results on the ARPE-19 cells line showed the excellent relative cell viability for PCL discs (95%) and PCL-g-PDA discs purified three times (87%).

Based on these results, PCL and PCL-*g*-PDA p3 are not cytotoxic on L929 and ARPE-19 cell lines. These results are consistent with the work of Ku *et al.* [90] who reported that originally biocompatible surface modified/coated by PDA showed no cytotoxic effect on osteoblast, fibroblast and endothelial cells.

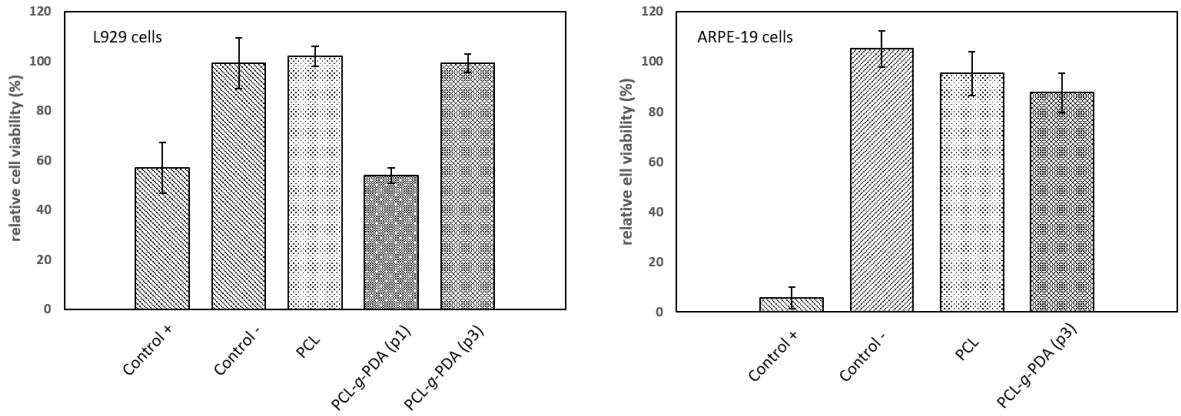

Figure 51. Cells viability on L929 after a 24h treatment and on ARPE-19 after a 48h treatment with direct contact with PCL and PCL-g-PDA films. Results are presented as means and error bars represent standard deviation (n=4).

3.3 Conclusion

In this part, we successfully synthesized a grafted copolymer based on PCL and PDA (PCL-*g*-PDA). The selected commercial PCL had a M_n of 190 000 g.mol^{-1} by SEC analysis in DMF. PCL was functionalized with iodine at a ratio of 10 mol.% and the resulting PCL-I had a molecular weight of M_n 49 000 g.mol^{-1}. The second step of synthesis involved simultaneously: the oxidative polymerization of dopamine, the grafting of dopamine units and/or oligo-PDA via ATRP-like conditions or on PCL-I, and the further growth PDA. The resulting PCL-*g*-PDA copolymer has a M_n of 46 000 g.mol^{-1}. The presence of PDA in the copolymer was shown by UV spectroscopy and TG analyses and the success of the grafting was proven by a combination of DOSY-NMR and SEC analysis. The content of PDA in the copolymer was estimated to be around 1.6-3 wt.%. The processability of PCL and PCL-*g*-PDA by hot melt compression was confirmed and yielded thin films (thickness = 300-500 µm) cut into discs (diameter = 6-7 mm) or implants (length = 10 mm, width = 4 mm). The crystallinity of the PCL-*g*-PDA implants (35%) was lower than the one of PCL implants (68%). Both implants had the same contact angle of 73°, lower than expected but supporting the low proportion of PDA in the copolymer. The *in vitro* degradation of PCL-*g*-PDA corresponded to a typical mechanism of bulk degradation similar to PCL – probably due to the low proportion of PDA – without water uptake, mass loss or significant molecular weight decrease after 110 days under physiological conditions. Importantly, the PCL and PCL-*g*-PDA discs were cyto-compatible towards L929 fibroblasts and ARPE-19 human retinal epithelial cells, when purified accordingly.

4. Section 2: Impact of PDA on the delivery of small molecules active pharmaceutical ingredients

4.1 Shaping and properties of drug-loaded PCL-*g*-PDA films

4.1.1 Selection and properties of relevant drug candidates

Dexamethasone (DEX) (M = 392.46 g.mol^{-1} | logP = 1.93 | water solubility < 1 mg/mL according to DrugBank data) is a synthetic drug which belongs to the corticosteroid class. As for all steroid hormones, it is efficient in suppressing intraocular inflammations, chronic or non-chronic, infectious or non-infectious, uveitis and diabetic macular edema [140,304–307] in concentration ranges between 0.15-4 µg/mL [140,308–310] in the vitreous cavity. Dexamethasone (0.7 mg) is the pharmaceutical active component contained in the commercial biodegradable intravitreal implant Ozurdex™ [148] described in Chapter I. Dexamethasone is a low binder to melanin (t-score = 0.6). [49]

Ciprofloxacin (M = 331.35 g.mol^{-1}) is a synthetic antibiotic which belongs to the fluoroquinolones class, and ciprofloxacin hydrochloride is its salt form (water-soluble form). While not approved yet for the treatment of ocular diseases, ciprofloxacin, as presented in Chapter I, was selected because of strong binding properties (t-score =-0.6) toward melanin [49], a major component of the pigment cells in the eye. As melanin and PDA share similar properties [3,4,87], ciprofloxacin and its salt version (logP = -1.85| water solubility <1 mg/mL according to Chemspider data) are drugs of choice to study the influence of the PDA contained in the copolymer on the in vitro drug release profiles. In the following study, only the hydrochloride ciprofloxacin was used.

The structures of the drugs are shown in **Figure 52**.

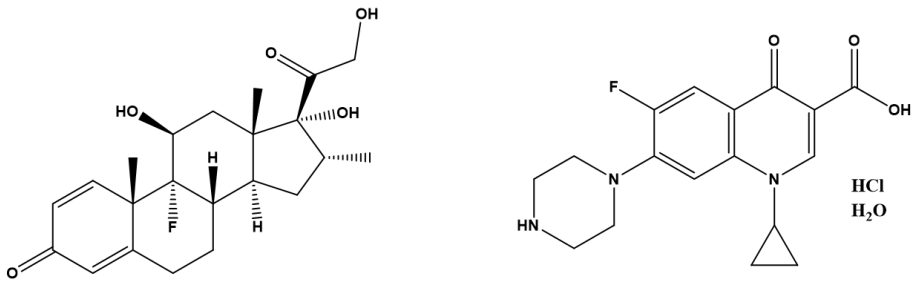

Dexamethasone (DEX) **Ciprofloxacin hydrochloride (CIP.HCl)**

Figure 52. Chemical structures of dexamethasone (DEX) and ciprofloxacin hydrochloride (CIP.HCl)

Since films are obtained via a hot melting process, we first analysed the thermal behaviour of the drugs to establish the parameters of the fabrication process. The thermogram and the derived curve (dTG, first derivate) obtained by TG analysis of DEX, **Figure 53**-A showed a unique thermal event (onset temperature = 268 °C). In the case of CIP.HCl, **Figure 53**-B, the thermogram showed a first thermal event from 30 to 300°C (minimum of dTG at 151°C) corresponding to the elimination of HCl and water, then a major second thermal event was observed from 300 to 600°C corresponding to the degradation of the ciprofloxacin.

The thermograms and thermal characteristics of the drug analysed by DSC are shown in **Figure 54**. Both drugs are crystalline white powders. DEX exhibits a melting temperature at 268°C and an enthalpy of fusion around -170 J.g^{-1}. CIP.HCl exhibits a melting temperature at 150°C and an enthalpy of fusion around -139 J.g^{-1}.

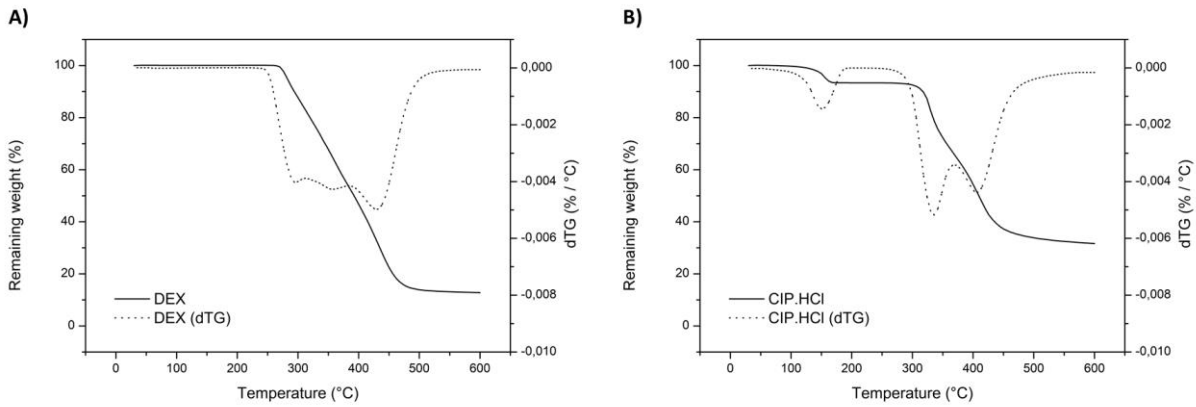

Figure 53. TG analysis of A) dexamethasone and B) ciprofloxacin hydrochloride

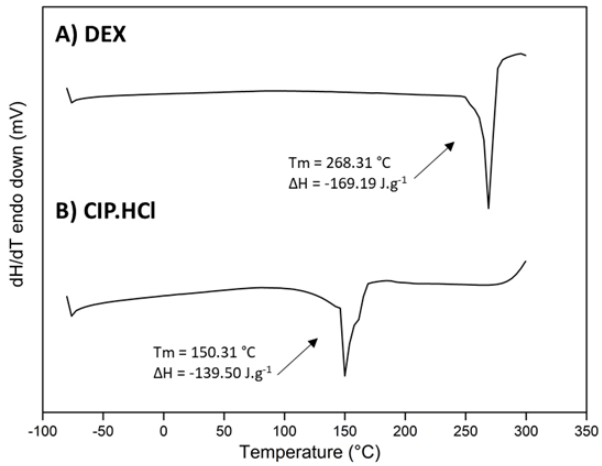

Figure 54. DSC analysis of A) dexamethasone and B) ciprofloxacin hydrochloride

4.1.2 Fabrication process of the drug-loaded films

The drug loading is set at 30 wt.% with respect to the total mass of the implant. This drug/polymer (30/70) ratio was selected to obtain the minimal and sufficient concentration of polymer to form an implant and a concentration of drug to be competitive with the existing biodegradable implant (Ozurdex™). The implants were composed of PCL, PCL-*g*-PDA or a (50/50) mix of PCL and PCL-*g*-PDA in order to study the impact of the presence and the concentration of the PDA units on the kinetics of release. For DEX, the three polymer compositions were tested. For CIP.HCl, only the two first compositions (PCL and PCL-*g*-PDA) were tested, the third composition was not performed due to lack of products.

According to the temperatures of fusion (PCL = 63°C | PCL-g-PDA = 49°C) and degradation (PCL = 424°C | PCL-g-PDA = 424°C) of PCL and PCL-*g*-PDA powders, and to the temperature of fusion of the drugs (DEX = 268°C |CIP.HCL = 151°C), the manufacturing process can be realized between 75 and 100°C without degrading the materials. The films were hot pressed at 100°C by processing quantities of polymer and drugs, allowing the preparation of films with a thickness around 400 ± 50 µm. The films, presented **Figure 55**, were then cut into implant (10 mm x 4 mm).

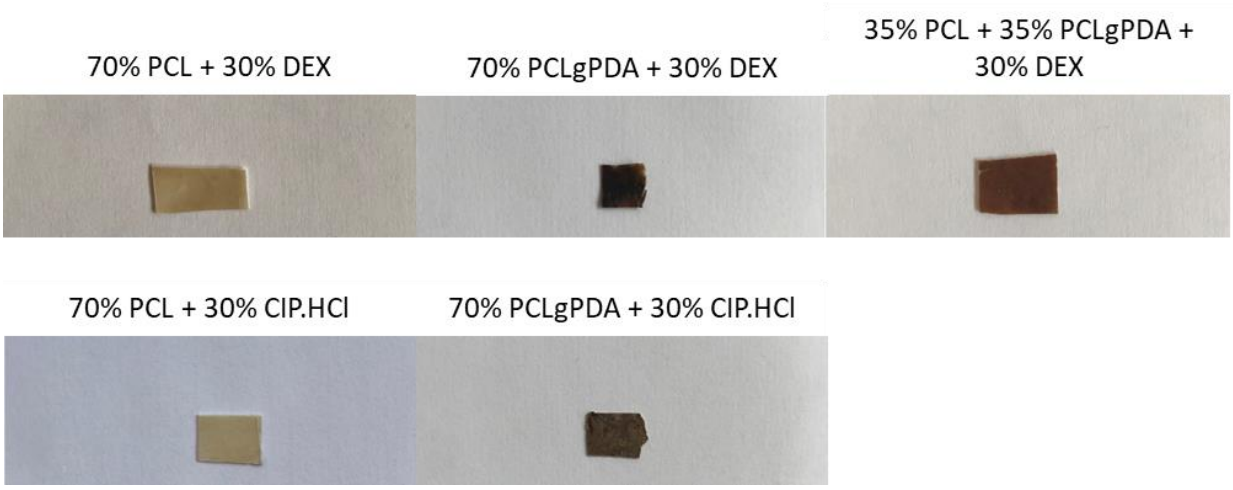

Figure 55. Pictures of the different films based on PCL or PCL-*g*-PDA, containing 30 wt.% dexamethasone (DEX) or ciprofloxacin hydrochloride (CIP.HCl)

4.1.3 Thermal properties of drug-loaded films

Crystallinity is a key factor for the aqueous solubility of the drug, which could have an impact on the drug release kinetics. Indeed, drug exists under amorphous, semi-crystalline and crystalline states, the latter existing under several physical forms (polymorph, hydrate, solvate and co-crystal for example). The crystalline state provides thermodynamically stable forms, the amorphous state provides on the opposite faster dissolution rate, enhanced solubility and bioavailability in dosage form. Therefore, DSC analysis provides interesting information regarding the solid-state form of DEX and CIP.HCl in the PCL, PCL-*g*-PDA and PCL/PCL-*g*-PDA (50/50) implants. It is noteworthy that DSC analyses can also give an insight in the possible interactions taking place between the API and the polymer, especially in the case of PDA for its binding affinity with drugs.

The thermal characteristics of the loaded implants are presented in **Figure 56**. Temperatures and enthalpies have been separated according to their belonging to the polymer zone or the API zone. Besides, the enthalpies originally expressed in mJ during analysis were recalculated in J/g according to the equation (10) and equation (11) using the theoretical feed ratio of polymer and drug (70:30 (w/w)).

$$\Delta H_{copolymer,loadedfilm} = \frac{\Delta H_{copolymer}\,(mJ)}{\%_{copolymer,theoretical} \times m_{loadedfilm}} \quad (10)$$

$$\Delta H_{drug,loadedfilm} = \frac{\Delta H_{drug}(mJ)}{\%_{drug,theoretical} \times m_{loadedfilm}} \quad (11)$$

The degree of crystallinity of PCL in the DEX loaded-PCL remained similar to the unloaded PCL (χ = 45% vs. χ = 46 % respectively). As expected, the crystallinity of the polymers in the implant of a blend (50/50) of PCL/PCL-*g*-PDA (χ = 42%) was between the one of PCL (χ = 45%) and the one of PCL-*g*-PDA (χ = 38%). Coming to the properties of the API mixed in the polymer matrix, the value of the relative crystallinity of DEX was reduced by 35%. Its melting temperature *Tm* is decreasing from 268°C to 245°C in the PCL implant, which suggests interactions between DEX and PCL. For PCL-*g*-PDA implants, DEX was no longer crystalline as shown by the absence of melting peak, which confirms stronger interactions in the presence of PDA. Finally, and surprisingly, almost all DEX incorporated in the blend matrix of PCL/PCL-g-PDA (50/50) remained in its crystalline form although a decrease of melting temperature similar to the one in PCL was observed (*Tm* = 241°C).

With the incorporation of CIP.HCl, similar values were observed for the degree of crystallinity of PCL (χ = 46 %) and PCL-*g*-PDA (χ = 33 %) implants compared with the unloaded implants (χ = 46 and 35 %

respectively). Surprisingly, in both implants, no melting peak of CIP.HCl was observed suggesting that the drug is fully amorphous or that a molecular dispersion is obtained.

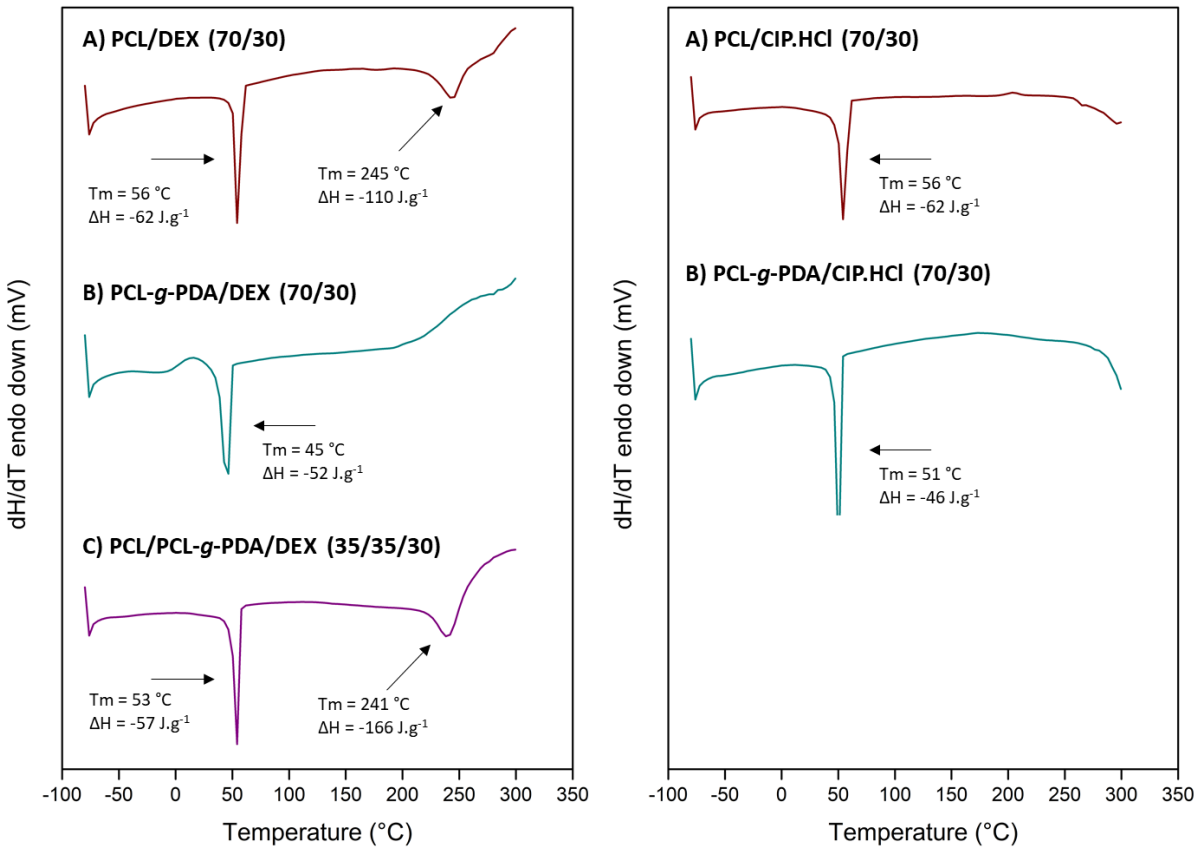

Figure 56. DSC analyses of the films of dexamethasone (left) loaded into A) PCL implant, B) PCL-*g*-PDA implant and C) PCL/PCL-g-PDA implant and of ciprofloxacin hydrochloride (right) A) PCL implant and B) PCL-*g*-PDA implant

Based on these results, (i) the incorporation of drug did not change the thermal properties (*Tm* and χ) of polymers but affected the drug properties and (ii) PDA seems to interact with the selected APIs that are no longer crystalline when incorporated in PCL-*g*-PDA films.

4.1.4 Determination of drug loading

We postulate that in the process of manufacturing the loaded films, the drug encapsulation efficiency is complete (100%). In other words, the mass of drug in the implant after all steps is equal to the mass of drug introduced into the solution of polymer/DMSO, which corresponds to the drug loading (DL) targeted. To test this hypothesis, a TG analysis method was developed. A calibration curve was

established reporting the drug percentage introduced with respect to the percentage of mass loss for several known ratios of polymer:drug in the domain of degradation of the drug – 340°C for DEX (**Figure 53**-A) and 204 °C for CIP.HCl (**Figure 53**-B). The calibration curves are shown in **Figure 64** in Appendix. The implants previously formed by hot melt compression were cut and pieces were taken at various locations. The drug content was calculated with respect to the calibration curve and the result are presented in **Table 12**. For implants containing DEX, the content of DEX was estimated at 29 wt.% for PCL-based implants, 32 wt.% for the PCL-*g*-PDA-based implants and 31 wt.% for the PCL/PCL-*g*-PDA-based implants. The calculated ratios were close to the feed ratios (30 wt.%) and the standard deviation was low, proving the homogeneity of the implants. For implants containing CIP, the amount of CIP was estimated at 34 wt.% for the PCL-*g*-PDA-based implants. The PCL-based implants were not analyzed due to the lack of material at the time of the study.

Table 12. Estimation of the drug content in PCL- and PCL-*g*-PDA-based implants using TG analysis.

Polymer/drug	Feed ratio (wt.%)	Measured ratio (wt.%)
PCL /DEX	70/30	71/29 (n=5, SD=2)
PCL-*g*-PDA /DEX	70/30	68/32 (n=4, SD=2)
(PCL/PCL-*g*-PDA) / DEX	(35/35)/30	67/31 (n=3, SD=3)
PCL /CIP.HCl	70/30	N/D
PCL-*g*-PDA / CIP.HCl	70/30	66/34 (n=3, SD=4)

4.2 *in vitro* evaluation of drug release and influence of the PDA content on the release kinetics

In vitro drug release studies of DEX- and CIP.HCl- loaded PCL and PCL-*g*-PDA implants (DL=30 wt.%) were carried out under classical simulated physiological conditions (PBS, pH 7.4, 37 °C). In doing so, we aimed at comparing the release profiles of the implants in the conditions used for the release of the commercial intravitreal implant Ozurdex ™ (0.7 mg of DEX in the implant). The mass of our loaded-implant (5 mg) introduced in the release medium (10 mL) corresponded to a total mass of drug released of 0.6 mg in 4 mL of medium, which is similar to Ozurdex ™ in the vitreous volume. Besides, the entire volume medium was removed and replaced by fresh release medium at predetermined

intervals of time to obtain a drug concentration at least 3 times under the aqueous limit of solubility to prevent drug saturation and biased results (sink conditions).

4.2.1.1 Detection and quantification of the drugs

DEX and CIP.HCl exhibit a maximum of absorbance at λ= 254 nm and λ= 278 nm respectively. Therefore, these two wavelengths were selected for HPLC detection. The typical chromatograms of the drugs are shown in **Figure 57** at a concentration of 50 mg.L^{-1} in PBS. The retention times of DEX and CIP.HCl were 2.2 min and 3.0 min respectively. Calibration curves have been established for each drug in a concentration range compatible with our systems – from 0.1 to 50 mg.L^{-1}. The calibration curves are represented in **Figure 65** in Appendix.

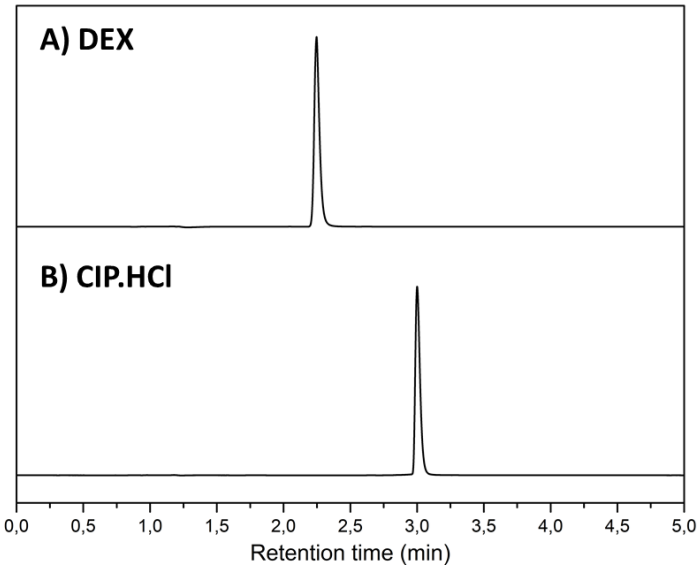

Figure 57. Chromatograms of A) dexamethasone and B) ciprofloxacin hydrochloride at a concentration of 50 mg.L^{-1} in PBS.

4.2.1.2 Release of drugs from the implants

Dexamethasone

In vitro drug release studies of DEX were carried out from PCL, PCL-*g*-PDA and PCL/PCL-*g*-PDA (50/50) blend implants.

Figure 58 shows that:

-no burst release occurred for the three implants

-At day 2 drug release (DR) was similar (around 5%) for the 3 implants.

-After 2 days, the kinetics of release started to differentiate for PCL and PCL-*g*-PDA implants. The cumulative release was 58% for PCL and 37% for PCL-*g*-PDA implants at day 42. As a reminder, the release of a drug from a polymeric implant can be influenced by the nature of the polymer chains, the molecular weight of the polymer, the crystallinity of the implants, the hydrophobic/hydrophobic balance of the implants, the type of drug and the drug loading. In our case, the molecular weights of the copolymers were similar (PCL M_n = 63 000 g.mol^{-1}, PCL-*g*-PDA M_n = 51 000 g.mol^{-1}). Both implants showed similar contact angles (~ 73°, **Table 10**) and a similar drug loadings (~30%, **Table 12**). The crystallinity of the PCL-*g*-PDA implants (χ ~ 36%, **Figure 48**) was lower than the one of PCL implants (χ ~ 50%, **Figure 48**) due to the presence of PDA. Therefore, we could expect the drug to be more rapidly removed from the implant by the penetration of water. However, the profiles showed that the release of DEX from the PCL implants was faster compared to the PCL-*g*-PDA implants. Therefore, this lower release rate was attributed to the presence of PDA in the systems. Drug-binding affinity of drug for PDA seems to be the predominant factor of the kinetics of release of DEX.

As previously described in the *in vitro* degradation study, both PCL and PCL-*g*-PDA implants were stable in physiological conditions for at least 110 days (**Figure 49**). Therefore, no burst release effect induced by the degradation of polymer was observed. At the end of the 155-day study, the cumulative release of dexamethasone was approximately quantitative.

Interestingly, and as further confirmation, the release kinetics of DEX in the implant made of PCL/PCL-*g*-PDA (50:50) blend was between PCL and PCL-*g*-PDA with a cumulative release of 44% at day 42. This result is interesting, as it shows that a mix of PCL and PCL-*g*-PDA could effectively control the release kinetics of DEX and that the ratio PCL/PCL-g-PDA could modulate the kinetics due to the drug-binding action of PDA. At day 84, the cumulative release reached 72% and, due to laboratory issue during the study, the analysis of the PCL/PCL-*g*-PDA (50:50) blend implant was stopped.

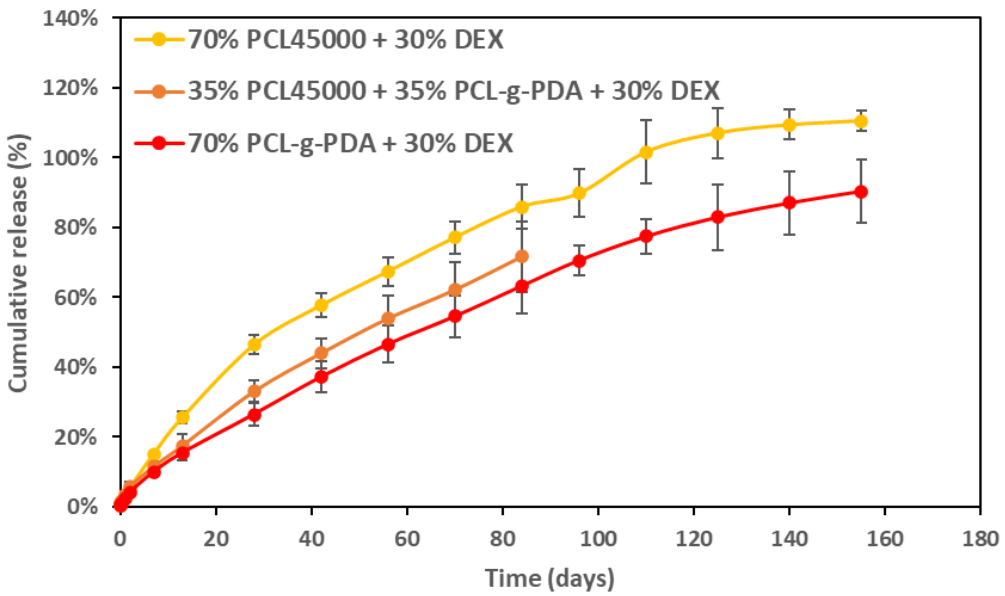

Figure 58. *In vitro* release of dexamethasone from PCL and PCL-g-PDA based implants (ratio drug to polymer 30:70 w/w). Data are expressed as an average of results obtained from measurements by HPCL (mean ± SD; n= 3).

To correlate these releases with existing models, 5 models of release kinetics were selected: the zero-order model, the first-order model, the Weibull model, the Higuchi model and the Korsmeyer-Peppas model (**Table 13**). The release of dexamethasone from PCL implants was closer to the Weibull (R^2 = 0.994), Higuchi (R^2 = 0.995) and Korsmeyer-Peppas (R^2 = 0.994) model. Weibull model describes the release from any matrix pharmaceutical dosage, Higushi model describes the release of soluble to low soluble drug from semi-solid and solid matrices, and Korsmeyer-Peppas describes the release of drug involving a non-fickian diffusion referring to a combination of diffusion and erosion (n=0.669). PCL being highly hydrophobic and stable over long period of time, diffusion is the predominant behaviour over erosion. In the case of PCL-g-PDA implants, the release rate of dexamethasone was closer to the Weibull (R^2 = 0.998) and Korsmeyer-Peppas model (R^2 = 0.996). In the case of the implant made of blend of PCL/PCL-g-PDA, the release of dexamethasone was closer to the Korsmeyer-Peppas (R^2 = 0.996). The curves were shown in **Figure 66** in Appendix

Table 13. Correlation coefficient and determination coefficient of models for the release of dexamethasone in *in vitro* conditions.

	Zero-order model		First-order model		Weibull model		Higuchi model		Korsmeyer-Peppas model	
Polymer/Plot values	**Slope**	**R^2**	**Slope**	**R^2**	**Slope**	**R^2**	**Slope**	**R^2**	**Slope**	**R^2**
PCL	1.237	0.956	0.0005	0.654	0.669	0.994	2.985	0.995	0.669	0.994
PCL-*g*-PDA	0.964	0.980	0.0005	0.670	0.688	0.998	2.345	0.985	0.688	0.996
PCL/PCL-*g*-PDA (50/50)	0.865	0.894	0.0007	0.674	0.631	0.996	2.386	0.987	0.631	0.996

As a result, the PCL, the PCL-*g*-PDA and the PCL/PCL-*g*-PDA implants showed sustained release of dexamethasone involving diffusion (major) and erosion (minor) release rates. By extrapolation of the release curves, it seems that a complete release of dexamethasone from PCL-*g*-PDA would be reached around day 160 (5.5 months).

Comparison with Ozurdex™

In Chapter I, Part 3.2.3.1, we described the Ozurdex™ (PLGA rod shaped intravitreal implant of 1.2 mg and containing 0.7 mg of dexamethasone) and aimed to enhance and extend the duration of release of the drug with our PCL-*g*-PDA-based systems. *In vitro*, Ozurdex™ (1.2 mg) – in one piece or fragmented into 3 pieces - was introduced in the release medium (30 mL) and showed a tri-phasic pattern, with a low amount of drug released (DR ~ 5%) in 7 days, then a linear release that reached DR ~ 80% at day 21 then the release slowed down to a plateau at DR ~ 90% until day 35 (**Figure 59**). [311]

By comparing the release profiles of the PCL-*g*-PDA based implants and the Ozurdex ™ it is clearly seen that the release patterns differs and that the PCL-*g*-PDA implants provide a slower and progressive release of dexamethasone without any lag time in *in vitro* conditions over a much longer time period.

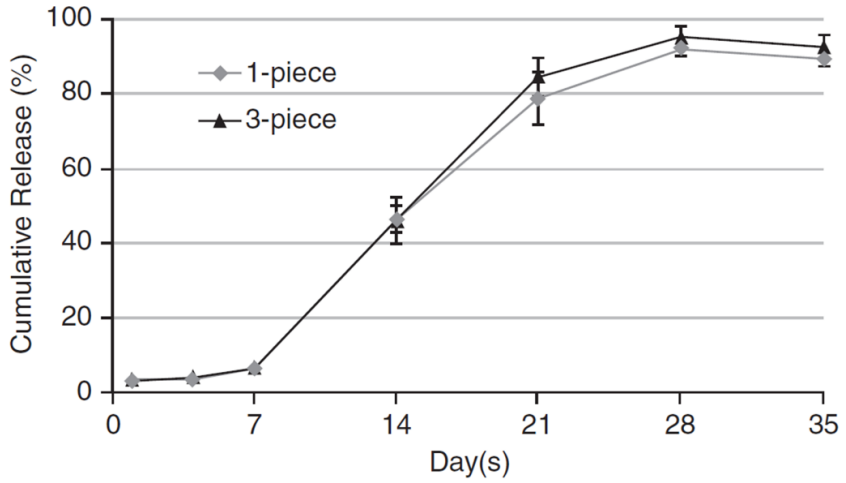

Figure 59. *In vitro* release of dexamethasone from Ozurdex™. Data are expressed selection as an average of results obtained from measurements by HPCL (mean ± SD; n= 6).

Ciprofloxacin hydrochloride

The release profile presented in **Figure 60** totally changed when CIP.HCl was used as drug. In the PCL implant, a massive burst was observed with more than 50% of the drug released at day 2. A plateau was reached after 60 days, with an almost complete drug release (89%) at day 155. Similarly, for PCL-*g*-PDA a burst effect was also observed but to a much lower extent with over 31% of the drug released at day 2, then a slow and constant release was observed after 7 days with a cumulative release of 80% at day 160. By extrapolation of the release curves, it seems that a complete release of dexamethasone would be reached in around 38 months.

The faster release of CIP.HCl from the implants might be attributed to the higher water solubility of CIP.HCl at pH 7 regarding the log P values (-1.85 *vs.* +1.93) and to its amorphous solid-state form compared to the crystalline DEX (**Figure 56**). Besides, the reduced release kinetics of CIP in PCL-*g*-PDA implants compared to the PCL implant might be attributed to the presence of PDA moiety in the systems. Indeed, CIP is an effective binder to melanin [49], therefore it is reasonable to think and expect that CIP.HCl would have the same binding affinity to PDA, the synthetic analogue of melanin [3,4,87] .

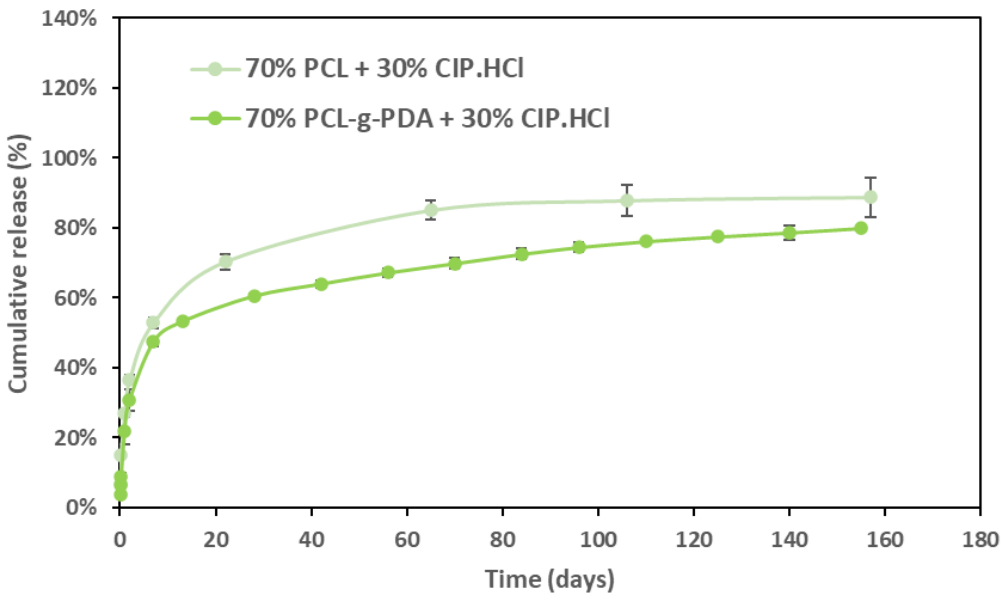

Figure 60. *In vitro* release of ciprofloxacin hydrochloride from PCL and PCL-*g*-PDA based implants (ratio drug to polymer 30:70 w/w). Data are expressed selection as an average of results obtained from measurements by HPCL (mean ± SD; n= 3).

The release rate of ciprofloxacin hydrochloride from both PCL and PCL-*g*-PDA implant didn't' fit any model described (**Table 14**). The curves were shown in **Figure 67** in Appendix.

Table 14. Correlation coefficient and determination coefficient of models for the release of ciprofloxacin hydrochloride in *in vitro* conditions.

	Zero-order model		First-order model		Weibull model		Higuchi model		Korsmeyer-Peppas model	
Polymer/Plot values	**Slope**	**R^2**	**Slope**	**R^2**	**Slope**	**R^2**	**Slope**	**R^2**	**Slope**	**R^2**
PCL	1.136	0.709	0.0002	0.436	0.298	0.949	1.947	0.854	0.014	0.636
PCL-*g*-PDA	1.138	0.815	0.0002	0.472	0.352	0.954	1.853	0.882	0.017	0.668

Conclusion

Based on these release studies we conclude that:

-PDA allows higher retention of the drug in the implants

-the release kinetics are lower and can be modulated by tuning the PCL/PCL-*g*-PDA ratio

-DEX (water-insoluble) progressively released from PCL-*g*-PDA without burst release or lag time

-CIP.HCl (water-soluble) is partly retained in the PCL-*g*-PDA implants after a massive burst release

4.3 Conclusion

In this part, we successfully designed PCL and PCL-*g*-PDA as thin implants containing either dexamethasone or ciprofloxacin hydrochloride in a mass ratio polymer/drug = 70/30. Thermal properties and drug loading efficiency were evaluated by DSC and TGA respectively. The kinetics of release of the drugs were evaluated *in vitro* under physiological mimicking conditions during 155 days.

The *in vitro* assays demonstrated that the grafting of PDA on PCL enables a higher retention of the drug compared to genuine PCL and that the kinetics may be modulated by the PCL/PCL-g-PDA ratio. The release of dexamethasone was sustained during 155 days ($DR_{PCL\text{-}g\text{-}PDA/DEX}$ = 90% and $DR_{PCL/DEX}$ = 110%) without any burst effect while the majority of ciprofloxacin hydrochloride was released in 14 days in an initial burst followed by a slow and constant release ($DR_{PCL\text{-}g\text{-}PDA/CIP.HCl}$ = 80 % and $DR_{PCL/CIP.HCl}$ = 89%). Therefore, after the initial burst effect, the release of ciprofloxacin was restrained in the presence of PDA, thus enhancing the sustained release behaviour over a long period, confirming the hypothesis that ciprofloxacin hydrochloride strongly interacts with PDA.

5. Conclusion

In this chapter our aim was to design and synthetize a new polymeric solid implant that could be used for intravitreal drug delivery applications. We chose to design a new polymer composed of PCL and PDA to combine biocompatibility, (bio)degradability, long-term storage stability and exploiting catechol binding properties toward selected APIs to further extend release of drugs.

The first part (section 1) of the study described the 2 steps synthesis of the grafted copolymer PCL-*g*-PDA. The first step was the functionalization of high molecular weight commercial PCL by iodine (PCL-I). The second step was the oxidative polymerization of dopamine and the grafting of dopamine and/or oligo-PDA under ATRP-like conditions. PCL-I acted as a macroinitiator to further grow PDA and generated PDA side chains (PCL-*g*-PDA). The confirmation of the grafting of PDA, the amount of PDA in PCL-*g*-PDA and the thermal properties of the copolymers were evaluated by NMR, SEC, UV, TGA and DSC. The PCL-*g*-PDA copolymer contained 1.6-3 wt.% of PDA, was stable *in vitro* under physiological mimicking conditions for at least 110 days and non-cytotoxic with L929 and ARPE-19 retinal epithelial cells.

The second part (section 2) of the study concerned the design of drug-loaded films to evaluate the ability of the PCL-*g*-PDA to retain hydrophobic drugs in the implants. The *in vitro* assays performed in physiological conditions showed the potency of PCL-*g*-PDA to slow down the release of dexamethasone and ciprofloxacin hydrochloride compared to PCL, thanks to the presence of PDA moiety in the copolymer.

As a conclusion, PCL-g-PDA is offering interesting perspectives (**Table 15**) for use as intravitreal implants for the release of small molecule drugs.

Table 15. Criterial for ocular long-acting delivery for PCL-*g*-PDA implants

Criterial for ocular long-acting delivery	DEX-loaded PCL-*g*-PDA implant	CIP.HCL-loaded PCL-*g*-PDA implant
high drug loading	Yes (DL=30 wt.%)	Yes (DL=30 wt.%)
Lag time	No	No
Limited burst	Yes (5%)	No (31%)
Sustained release	Yes (90% in 155 days)	Yes (77% in 125 days | extrapolation to 38 months)
Release kinetics	Weibull / Korsmeyer-Peppas model	Weibull model
Envisage manufacturing	Hot melt compression or extrusion (T≤130°C)	Hot melt compression or extrusion (T≤100°C)
Degradation	Yes (> after 3 months)	Yes (> after 3 months)
Ocular tolerability	Yes (unloaded)	Yes (unloaded)

6. Appendix

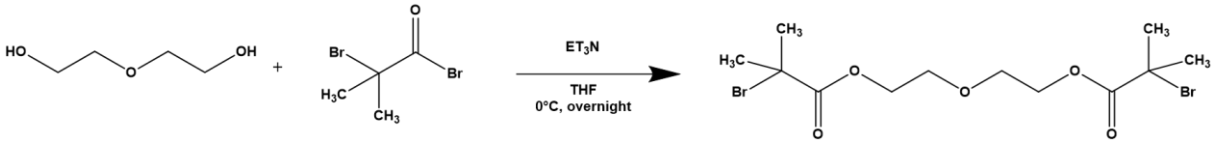

Scheme 20. Synthesis of the diethylene glycol bis(2-bromoisobutyrate)

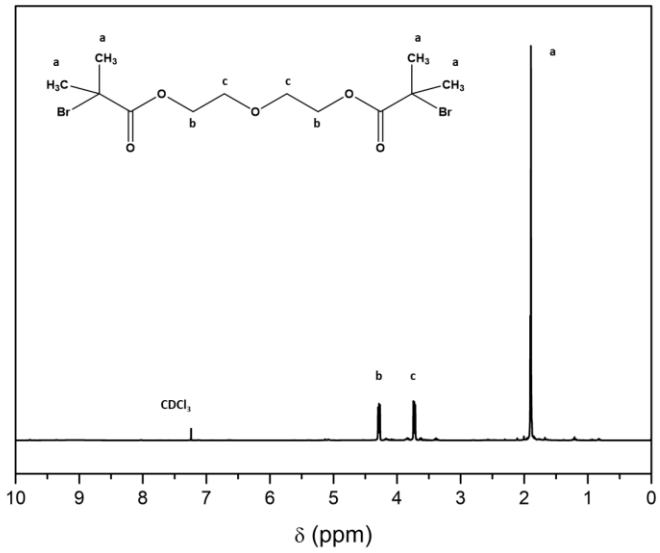

Figure 61. ^{1}H-NMR spectrum of diethylene glycol bis(2-bromoisobutyrate)

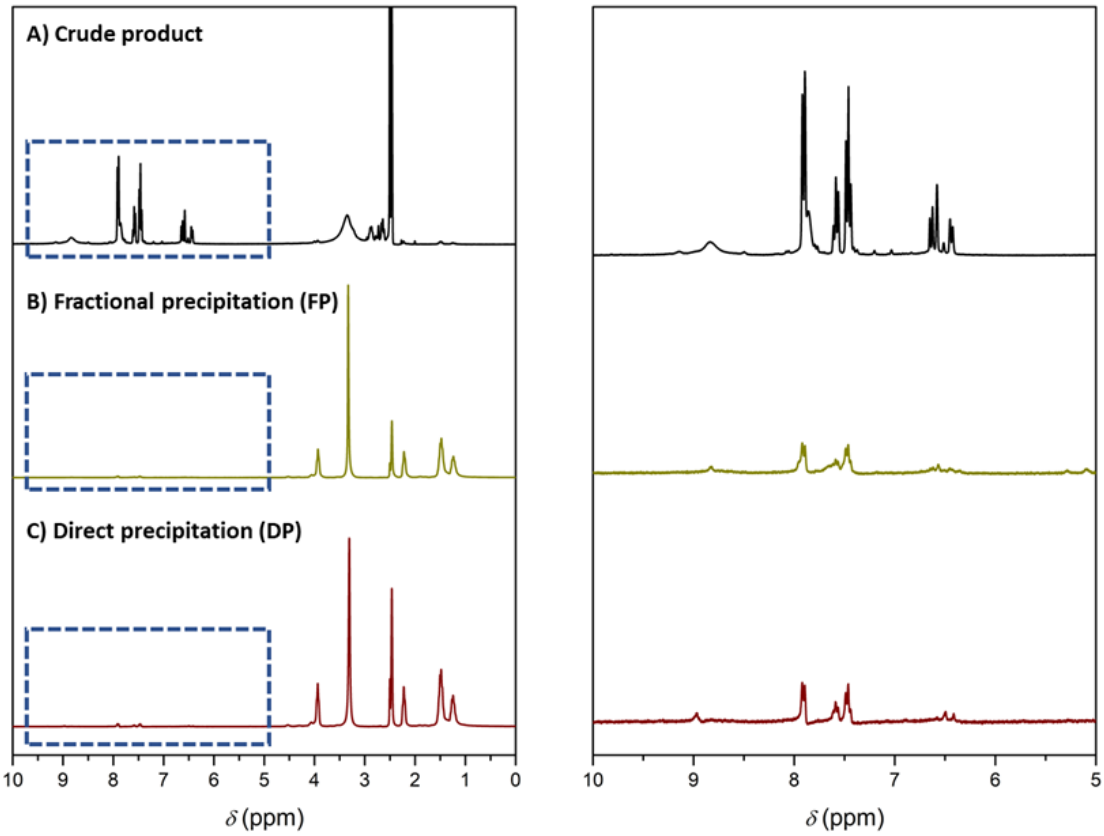

Figure 62. ^{1}H-NMR spectra of PCL-g-PDA A) without purification (crude product), B) after one purification using fractional precipitation and C) after one purification using direct precipitation.

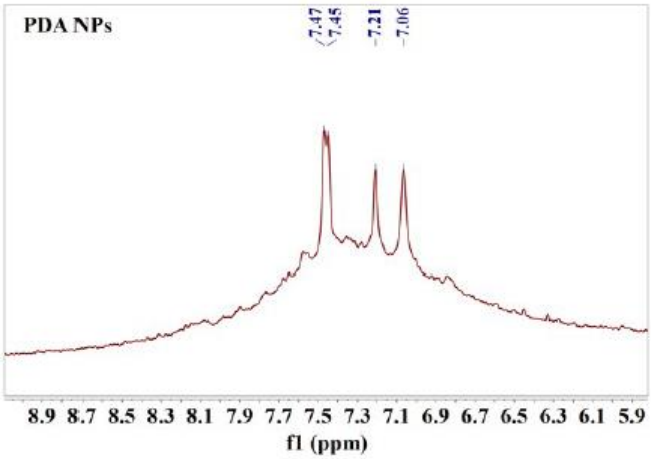

Figure 63. ^{1}H-NMR spectra of nanoparticles of PDA in $DMSOd_6$ obtained by the work of Ma *et al.* [297]

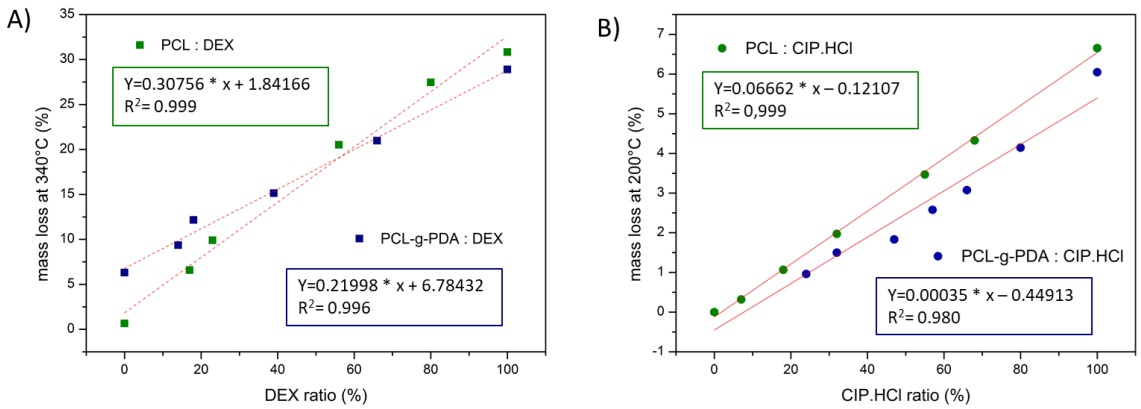

Figure 64. Calibration curves obtained from the mix of PCL and PCL-g-PDA with A) dexamethasone or with B) ciprofloxacin hydrochloride by TG analysis

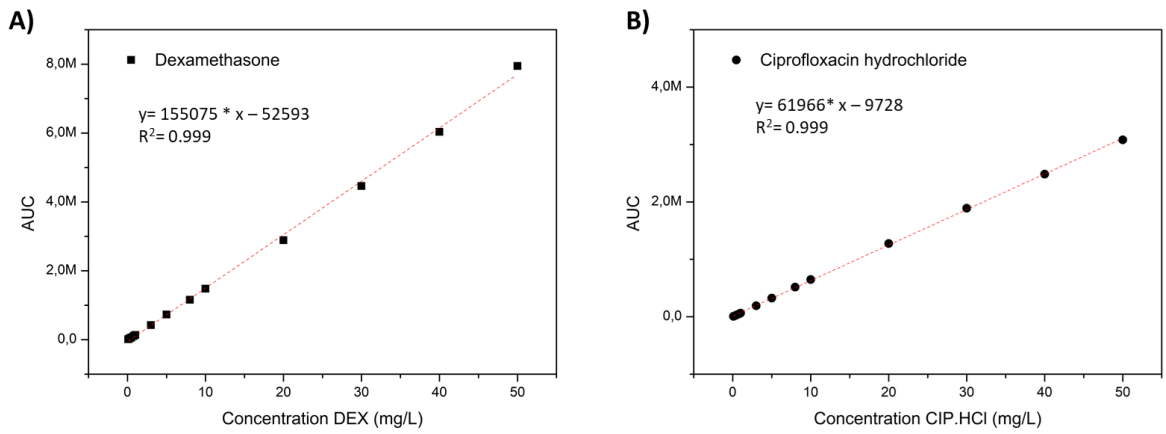

Figure 65. Calibration curves obtained from the dissolution of A) dexamethasone and B) ciprofloxacin hydrochloride in a mix of PBS:PS20(0.05%) by HPLC

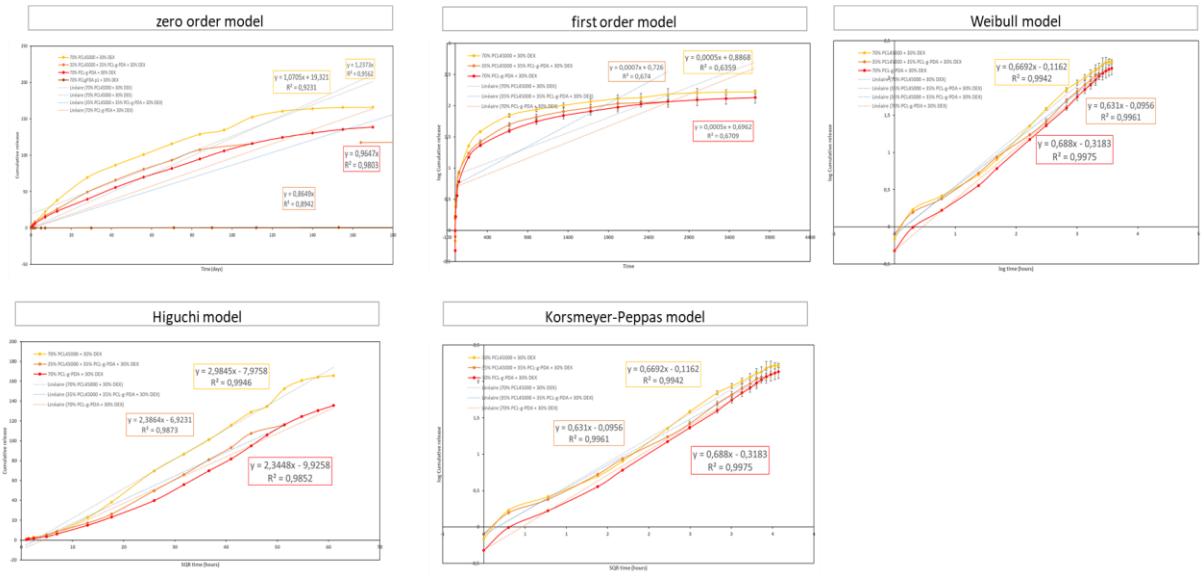

Figure 66. Determination of the appropriate model of kinetics of *in vitro* the release of dexamethasone from the PCL, PCL-*g*-PDA and PCL/PCL-*g*-PDA implants

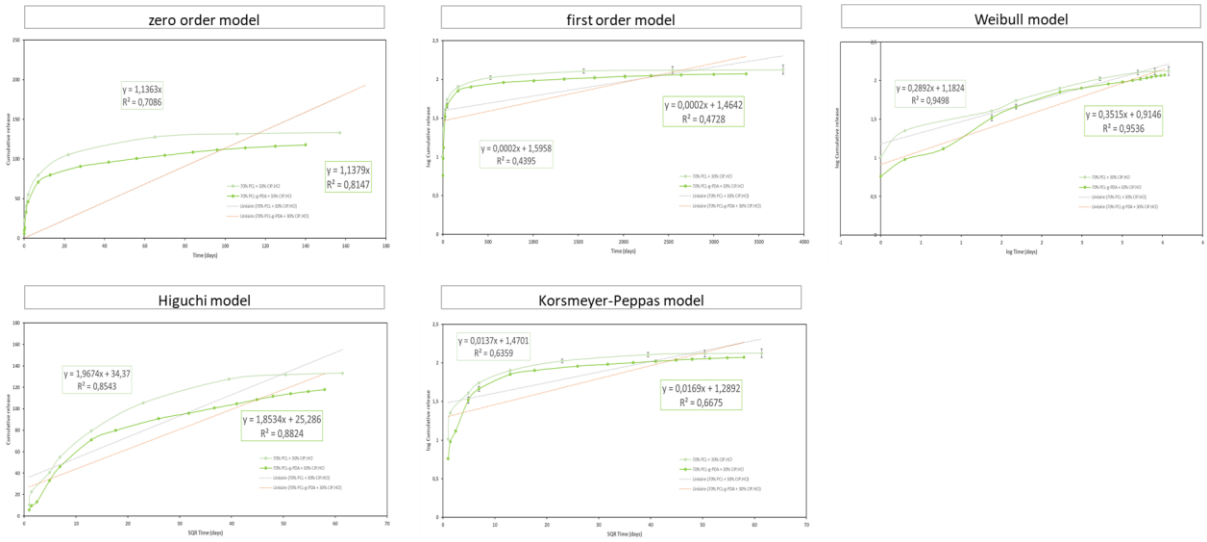

Figure 67. Determination of the appropriate model of kinetics of *in vitro* the release of ciprofloxacin hydrochloride from the PCL, PCL-*g*-PDA and PCL/PCL-*g*-PDA implants

CHAPTER III.

INJECTABLE GELLING SYSTEMS BASED ON COPOLYMERS CONTAINING PCL, PEG AND PDA ((PDA-*g*-PCL)-*b*-PEG-*b*-(PCL-*g*-PDA)) FOR SUSTAINED RELEASE OF BIOLOGICS

1. Introduction

As described in Chapter I, the investigations in the intravitreal ocular drug delivery field show interest for the development of (bio)degradable biomaterial providing sustained delivery of an active pharmaceutical ingredient (API) and minimizing surgical interventions. Particularly we described the two main families of polymeric formulations used for ophthalmic applications, namely the solid formulations and the in-situ forming depots. Among all the polymers – natural or synthetic – presenting biocompatibility and stimuli-responsiveness upon administration, PEG has shown particular interest in the design of chemically or physically cross-linked networks. Especially, the triblock copolymers composed of PEG and PCL [279–281,283,240,284] have shown promising properties for biocompatibility, thermal-responsiveness and injectability.

In Chapter II we reported the development of a biocompatible and degradable polymer to be used for the design of solid implants composed of PCL-*g*-PDA for the sustained delivery of small hydrophobic drugs and exploiting the drug/PDA interactions.

As an extension to this first strategy, the aim of this last chapter is to develop a drug delivery system based on an amphiphilic copolymer composed of PEG, PCL and PDA. This system would provide biocompatibility and (bio)degradability. Moreover, it is addressed to the long-term storage and controlled release of biological drugs thanks to the amphiphilicity of the copolymer and the 3D network formed allowing diffusion. This chapter will be subdivided into three parts.

The first part (**section 1**) consists of the design of an amphiphilic triblock copolymer composed of a central block of PEG with lateral PCL chains functionalized with grafted PDA chains ((PCL-*g*-PDA)-*b*-PEG-*b*-(PCL-*g*-PDA) (T-PDA)). A series of amphiphilic triblock copolymers (PCL-*b*-PEG-*b*-PCL (T)) are synthesized with different chains lengths in order to obtain different hydrophilic/hydrophobic balances. Then the PCL chains are functionalized with iodine as described in chapter II to obtain iodinated PCL ((PCL-I)-*b*-PEG-*b*-(PCL-I) (T-I)). In the last step, the lability of the carbon-iodine bond is exploited to initiate the polymerization of dopamine to yield poly(dopamine) side chains resulting in the targeted (PCL-*g*-PDA)-*b*-PEG-*b*-(PCL-*g*-PDA) construct. The grafting of PDA onto PCL is evaluated by NMR, UV spectrometry, SEC, DSC and TGA and the content of PDA in the T-PDA copolymer is evaluated by UV spectrometry and TGA. Also, the aqueous properties of the T and T-PDA are evaluated and compared. The second part (**section 2**) consists of the preparation of a formulation suitable for injection of 50-100 µL of solution through a 30G needle and providing stability of an antibody. PEG_{400} is used as co-solvent in the formulation to enhance solubility of the copolymers. The evaluation of the

injectability is performed by compression and the stability of the antibody is analyzed by SEC in order to draw the optimal formulation. The third and last part (**section 3**) consists of assessing the formation of the in-situ depot and the *in vitro* evaluation of the release of a monoclonal antibody in order to evaluate the ability of T-PDA to retain this type of biologics and its use as a potential delivery system for biologics.

2. Experimental section

2.1 Materials

Many of the materials mentioned in the Chapter II have been reused in Chapter III with addition of poly(ethylene glycol) (PEG, M_n 400 or 1 000 or 1 450 or 2 000 or 4 600 or 10 000 or 20 000 g.mol^{-1}), toluene, stannous octanoate ($Sn(Oct)_2$), ε-caprolactone (ε-CL), and diethyl ether that were purchased from Sigma-Aldrich. PEG was dried by azeotropic distillation of toluene solutions of PEG, and ε-CL was dried over calcium hydride (CaH2) for 48 h at room temperature and distilled under reduced pressure before use. PEG, ε-CL and $Sn(Oct)_2$ were kept under argon atmosphere.

2.2 Instrumentation

Nuclear magnetic resonance spectroscopy (NMR spectroscopy), Size Exclusion Chromatography (SEC) using THF as mobile phase, Differential Scanning Calorimetry (DSC), Thermogravimetric analysis (TGA) methods and instruments are similar to the ones described in Chapter II.

2.2.1 Size exclusion chromatography (SEC)

The number-average and weight-average molar masses (M_n and M_w, respectively) and dispersity ($Đ$, M_w/M_n) of the polymers were determined by SEC. The samples (5 mg.mL^{-1}) were filtrated through a 0.45 µm PTFE Millipore filter and analyzed using a Shimadzu (Japan) apparatus equipped with a RID-20A refractive index signal detector coupled to a SPD-20A UV/VIS detector and to a PLgel MIXED-C guard column (Agilent, 5µm, 50 x 7.5 mm) and two PLgel MIXED-C columns (Agilent, 5µm, 300 x 7.5 mm). The mobile phase was DMF + 0.1% LiBr. The flow rate was 1.0 mL.min^{-1} and the injection volume was 100 µL. The average molecular weight and dispersity ($Đ$) were express according to calibration using poly(ethylene glycol) (PEG) standards.

2.2.2 Aqueous size exclusion chromatography (Aqueous SEC)

The samples (1 $mg.mL^{-1}$) were filtrated through a 0.20 µm RC Millipore filter and analyzed using a Shimadzu (Japan) apparatus equipped with a RID-20A refractive index signal detector coupled to a SPD-40 UV/VIS detector and to a Biobasic SEC 300 guard column (Thermo Scientific, 5µm, 20 x 8 mm) and one Biobasic SEC 300 column (Thermo Scientific, 5µm, 150 x 7.8 mm). The mobile phase was an aqueous buffer solution composed of HK_2PO4/KH_2PO4 (0.1 M, pH=7). The flow rate was 0.80 $mL.min^{-1}$ and the injection volume was 100 µL.

2.2.3 Injectability testing by compression measurements

Injectability tests were carried out using a Instron 3344 with a 500N captor in compression mode. In the study, hypodermic needles (Sterican ® for special indications, B.Braun, Germany) in sizes 27G-30G and 1 mL disposable syringes (Omnifix®-F Luer, B.Braun, Gremany) were used. The syringes were filled with 1 mL of solution then the hypodermic needles were attached. The speed of injection was set at 0.5 or 1 $mm.s^{-1}$ and the volume of injection was 100 µL corresponding to a displacement of the plunger of 6 mm. The surrounding media was air.

2.3 Synthesis of copolymers

2.3.1 Synthesis of PCL-*b*-PEG-*b*-PCL

In a dry Schlenk flask, PEG (5.0 g, 2.5 mmol, M_n= 2 000 $g.mol^{-1}$) was solubilized in 55 mL of dry toluene under argon atmosphere. Then, $Sn(Oct)_2$ (0.20 g, 0.5 mmol) and ε-CL monomer (4.99 g, 43.8 mmol, 17.5 eq) were added, still under inert atmosphere. Water and oxygen were removed by three freeze-pump thaw cycles. Reaction was conducted at 100°C during 24 hours under argon flux and vigorous stirring. Reaction was stopped by adding few drops of HCl solution (0.1 M in methanol). The product was precipitated in cold diethyl ether, filtrated and dried under vacuum.

The molecular weights of triblock copolymers were calculated according to the following equations (12)-(15):

$$DP_{EG} = \frac{M_{n,PEG,th}}{44} \quad (12)$$

$$DP_{CL} = 2 \times DP_{EG} \times \frac{I_{3.99ppm}}{I_{3.50ppm}} \quad (13)$$

$$M_{n,NMR\ PCL} = DP_{CL} \times 114 \quad (14)$$

$$M_{n,NMR,PCL-PEG-PCL} = M_{n,PEG} + M_{n,PCL} \quad (15)$$

With 44 g.mol^{-1} the molecular weight of an ethylene glycol unit and 114 g.mol^{-1} the molecular weight of a ε-caprolactone unit.

The conversion is calculated by comparing the DP_{CL} obtained by NMR after purification with the theoretical value. The yield is calculated by comparing the mass of the polymer obtained with the theoretical mass value of polymer obtained taking into account the conversion calculated by NMR.

$$T_{conv} = \frac{DP_{CL,NMR}}{DP_{CL,feed}} * 100 \quad (16)$$

$$m_{th,PCL-PEG-PCL} = m_{PEG} + m_{PCL} \times T_{conv} \quad (17)$$

$$\eta = \frac{m_{PCL-PEG-PCL}}{m_{th,PCL-PEG-PCL}} \times 100 \quad (18)$$

Conversion: 86 %

Yield: 93%

^{1}H NMR (600 MHz, DMSOd$_6$): δ = 3.99 (t, R-C*H*$_2$-O-CO), 3.5 (m, R-C*H*$_2$-O), 2.27 (t, R-C*H*$_2$-CO-O), 1.54 (m, R-C*H*$_2$-CH$_2$-CO), 1.30 (m, R-C*H*$_2$-R)

SEC (THF, RI, PS): M_n = 6 143 g.mol^{-1}, *Đ* = 1.09

SEC (DMF, RI, PEG): M_n = 3 529 g.mol^{-1}, *Đ* = 1.07

2.3.2 Synthesis of iodinated (PCL-I)-*b*-PEG-*b*-(PCL-I)

In a typical experiment, PCL-*b*-PEG-*b*-PCL (4 g, $M_{n,NMR}$= 3 710 g.mol^{-1}, 1.08 mmol, 16.2 mmol of CL units) and anhydrous THF (200 mL) were introduced into a dry conic reactor and put under argon flux until complete dissolution. The solution was then cooled down at -50°C by diving it into a liquid nitrogen/ethanol mixture before addition of LDA (8.09 mL, 16.2 mmol) under argon. After 30 minutes

of reaction, a solution of iodine (4.10 g, 1.62 mmol) in a minimum amount of anhydrous THF was injected with a syringe through a septum and the mixture was kept at -50°C under stirring and argon atmosphere. After 30 minutes, the reaction was stopped by addition of an aqueous solution of NH_4Cl (2 M, 200 mL) and the temperature was increased to 0°C prior to addition of HCl(aq) (37%) to reach neutral pH. Then, the polymer was extracted from the solution by washing three times with dichloromethane (3×200 mL) in a separating funnel. Organic phases were collected, washed three times with a solution of $Na_2S_2O_3$ (0.3 M, 3×100 mL), dried using $MgSO_4$ powder, filtrated and concentrated under reduced pressure. The polymer was precipitated in cold diethyl ether, filtrated and dried under vacuum.

Substitution: 23 mol.%

Yield: 50 wt.%

^{1}H NMR (600 MHz, DMSOd$_6$): δ = 4.44 (m, R-C*H*I-CO-O), 3.99 (t, R-C*H*$_2$-O-CO), 3.50 (m, R-C*H*$_2$-O), 2.27 (t, R-C*H*$_2$-CO-O), 1.87 (m, R-C*H*$_2$-CHI), 1.54 (m, R-C*H*$_2$-CH$_2$-CO), 1.30 (m, R-C*H*$_2$-R)

SEC (THF, RI, PS): M_n = 5 760 g.mol^{-1}, $Đ$ = 1.28

SEC (DMF, RI, PEG): M_n = 3 500 g.mol^{-1}, $Đ$ = 1.24

2.3.3 Synthesis of (PCL-*g*-PDA)-*b*-PEG-*b*-(PCL-*g*-PDA)

In a typical experiment, in a Schlenk flask A, (PCL-I)-*b*-PEG-*b*-(PCL-I) (1.5 g, 1.07 mmol of iodinated CL units) and DMSO (20 mL) were added. In a Schlenk flask B, dopamine hydrochloride (5.09 g, 25 eq. with respect to iodinated CL unit, 26.8 mmol), PMDETA (340 µL, 1.5 eq. with respect to iodinated CL unit, 26.8 mmol), Na_2CO_3 (300.0 mg), BPO (6.49 g, 25 eq. with respect to iodinated CL unit, 26.8 mmol), and DMSO (37 mL) were added. Solutions were left under stirring and argon flux for 4 hours. Then, oxygen was removed by three freeze-pump thaw cycles. Iodinated PCL solution was transferred to the flask B and copper(I) bromide (0.23 g, 1.5 eq. with respect to iodinated CL, 1.61 mmol) was added. The flask was then dived in an oil bath at 70°C and vigorous stirring during 48 hours. Reaction was stopped by cooling in a liquid nitrogen bath. Solution was concentrated by evaporating DMSO at 70°C under vacuum. The polymer was dialyzed in water and freeze-dried.

PDA: 38-49 wt.%

^{1}H NMR (600 MHz, DMSOd$_6$): δ= 4.57 (m, R-C*H*(PDA)-CO), 3.99 (t, R-C*H*$_2$-O-CO), 3.5 (m, R-C*H*$_2$-O), 2.27 (t, R-C*H*$_2$-CO-O), 1.96 (m, R-CH$_2$-C*H*(PDA)), 1.84 (m, R-CH$_2$-C*H*(PDA)), 1.54 (m, R-C*H*$_2$-CH$_2$-CO), 1.30 (m, R-C*H*$_2$-R)

SEC (DMF, RI, PEG): M_n = 3 000 g.mol^{-1}, *Đ* = 1.24

2.4 Determination of sol-gel transitions

The sol-gel transition was determined by the test tube inverting method. The copolymer was introduced in water at concentrations ranging from 5 to 35 wt%. The sol-gel transition was investigated by raising temperature from 0 to 60 °C by increment of 5°C and stabilization a given temperature during 10 minutes. The copolymer solution was regarded as a ‘‘gel’’ in the case of no flow within 30 s by inverting the vial. In a first method, the copolymer solution was kept at 37°C during 24h prior the investigation of sol-gel transition. In a second method, the copolymer solution was kept at 0°C during 24h prior the investigation of sol-gel transition. In a third method, the copolymer solution was kept at 50°C during 15 minutes, then slowly cooled to room temperature, prior the investigation of sol-gel transition.

2.5 Protein loading, stability and release experiments

2.5.1 Stability of protein

The stability of mAb in pre-formulation or formulation studies was assessed in formulations composed of PBS, water:PEG$_{400}$, water:copolymer, HBS:PEG$_{400}$ or HBS:PEG$_{400}$:copolymer. The amount of PEG$_{400}$ and the copolymer used were study-dependent.

mAb + PBS: mAb (20 mg) was solubilized in PBS (0.5 mL) at a concentration of 40 mg.mL^{-1}, at 40°C and was protected from light. Then, at predetermined time points, aquilots of the medium was sampled and mobile phase solution was added in order to reach the desired concentration of analysis. The samples were analysed by aqueous SEC in the conditions established in Chapter III part 2.2.2

mAb + water:PEG$_{400}$ and mAb + HBS:PEG$_{400}$: (20 mg) mAb was solubilized in water:PEG400 (0.5 mL) or HBS:PEG400 (0.5mL) at a concentration of 40 mg.mL^{-1}, at 4°C and was protected from light. Then, at

predetermined time points, aquilots of the medium was sampled and mobile phase solution was added in order to reach the desired concentration of analysis. The samples were analysed by aqueous SEC in the conditions established in Chapter III part 2.2.2

mAb + water:copolymer : mAb (40 mg) was solubilized in water (1 mL) at a concentration of 40 $mg.mL^{-1}$ then copolymer (50 mg) was added . The solutions were kept at 4°C, protected from light and stirred at 100 rpm to allow intimate contact of the copolymers with water. vials were centrifuged to induce the sedimentation of the copolymer and the supernatant sampled to collect the soluble fraction of mAb. Then a mobile phase solution was added in order to reach the desired concentration of analysis. The samples were analysed by aqueous SEC in the conditions established in Chapter III part 2.2.2

mAb + HBS:PEG_{400}:copolymer: mAb (40 mg) was solubilized in HBS (0.5 mL) in a first vial and the copolymers (50 mg) were solubilized in PEG_{400} (0.5 mL) in a second vial. Then, the vials were gathered into one, kept at 4°C and protected from light. At predeterminate timepoints, vials were centrifuged to induce the sedimentation of the copolymer and the supernatant sampled to collect the soluble fraction of mAb. Then a mobile phase solution was added in order to reach the desired concentration of analysis. The samples were analysed by aqueous SEC in the conditions established in Chapter III part 2.2.2

2.5.2 *In vitro* protein release evaluation and quantification

The formulation was prepared in a two-step process. The copolymer (100 mg) was solubilized into PEG_{400} (0.5 mL). Simultaneously, the mAb (80 mg) was solubilized in histidine buffer solution (HBS) (0.5 mL). The solutions were gathered, gently mixed for further use.

The *in vitro* release study of mAb from formulations composed of T and/or (PCL-*g*-PDA)-*b*-PEG-*b* was assessed in phosphate buffered saline (PBS, pH 7.4) at 37°C under constant orbital shaking (60 rpm). Typically, 200 µL of formulation were introduced into 8 mL of phosphate buffer solution at 37°C through a 22-gauge needle. At specific time points, 1/10th of the medium was sampled then replaced by fresh PBS in the release medium. The collected samples were analysed by aqueous SEC as previously described. The quantification of the drugs was calculated from a calibration curve previously established in PBS from 0 to 1500 $\mu g.mL^{-1}$.

3. Section 1: Synthesis and properties of PCL-*b*-PEG-*b*-PCL (T) and (PCL-*g*-PDA)-*b*-PEG-*b*-(PCL-*g*-PDA) (T-PDA)

3.1 Synthesis and characterisations of PCL-*b*-PEG-*b*-PCL (T)

PEG is a semi-crystalline polymer exhibiting a melting temperature ranging from 40 to 65°C depending on its molecular weight. PEG is soluble in numerous solvents including water and exhibits large water-uptake capacity. PEG is biocompatible, not biodegradable (hydrolytically or other) but bio-eliminable by renal filtration [255] if its molecular weight is under 20 000 g.mol^{-1}. In literature, PEG (studied from 200 to 10 000 g.mol^{-1}) generally shows low toxicity by all routes of administration [312] (parental, ocular, rectal, topical).

Our aim being to generate an in-situ forming gel, we initially targeted thermo-sensitive polymers able to gel at physiological temperature. The structures described in literature and showed in Chapter I are typically composed of a central block of PEG under 5 000 g.mol^{-1}. To fit with the literature and the relative toxicity, we selected PEG-diols of molecular weight from 1000 to 5000 g.mol^{-1} as central blocks. The triblock copolymers T were synthesized by ring opening polymerization (ROP) in anhydrous toluene of ε-CL using commercial PEG-diols as initiator (**Scheme 21**) and $Sn(Oct)_2$ as catalyst. The solution was stirred during 24 hours at 100°C and precipitated in cold diethyl ether, filtrated and dried under vacuum.

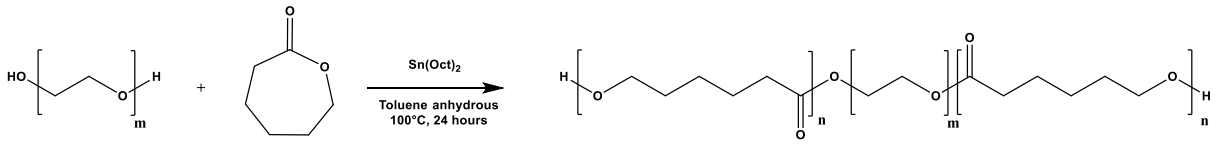

Scheme 21. Synthesis scheme of triblock copolymer T

According to the work of Liu *et al.* [313] , the gel to sol or sol to gel temperature of transition of PCL-PEG-PCL block copolymers depends on their chemical composition (CL/EG ratio) and their overall molecular weight. Therefore, in order to observe the influence of (i) the hydrophilic/hydrophobic balance and

(ii) the chain length of the block copolymers on the gelation various molecular weights of PEG and PCL blocks were tested. The CL/EG ratio ranged from 0.30 to 2.13 and the molecular weights from 4 300 to 9 400 g.mol^{-1}. The results are summarized in **Table 16**.

Along the study, the molecular weight of each polymer will be written in index number. For example, PEG of 1000 g.mol^{-1} will be defined as PEG_{1000} and PCL of 2000 g.mol^{-1} will be defined as PCL_{2000}. In the case of block copolymer of BAB-type (A refers to hydrophilic bloc, B refers to hydrophobic block), here PCL-*b*-PEG-*b*-PCL, PEG of 1000 g.mol^{-1} and PCL of 2000 g.mol^{-1} will be defined as 1000-2000-1000 in the entries of the tables of results. Moreover, PCL-*b*-PEG-*b*-PCL copolymer will be named T in the text.

Table 16. Characterizations of T

Entry	T theoretical	T obtained [a]	CL/EG	M_n [b] (g.mol^{-1})	$Đ$ [b]	yield (η_x) [c]
1	1800-4600-1800	1400-4600-1400	0.61	9 400	1.19	93
2	1000-4600-1000	700-4600-700	0.30	8 200	1.11	87
3	2000-2000-2000	2100-2000-2100	2.13	9 300	1.14	95
4	1200-2000-1200	1100-2000-1100	1.10	6 600	1.19	94
5	1000-2000-1000	855-2000-855	0.85	6 100	1,09	92
6	1000-2000-1000	890-2000-890	0.89	6 500	1.09	95
7	1000-2000-1000	846-2000-846	0.49	5 570	1.18	84
8	1100-1400-1100	1000-1400-1000	1.43	5 500	1.18	77
9	1000-1000-1000	940-1000-940	1.89	4 300	1.19	77

[a] determined by ^{1}H NMR in $CDCl_3$ using equation (15); [b] determined by SEC in THF using PS standards for calibration; [c] determined using equation (18).

A typical ^{1}H NMR spectrum in DMSO-d_6 of T is presented in **Figure 68**-A (entry 5 of **Table 16**). The peaks at 3.99 ppm (peak a) and at 2.27 ppm (peak d) correspond respectively to the signals of the protons R-C$\underline{H}_2$-O-CO and R-C$\underline{H}_2$-CO-O of PCL. The peaks at 1.54 ppm (peak b+b') and at 1.30 ppm (peak c) are multiplets, which correspond respectively to the signal of the protons R-C$\underline{H}_2$-CH_2-CO and R-C$\underline{H}_2$-R of PCL. The peak at 3.50 ppm (peak j) is a singlet, which corresponds to the signal of the proton R-$\underline{CH_2}$-O of the PEG. The mark "R" on the chemical formula of the triblock refers to the other side chain – symmetrical- of PCL.

The number average molecular weight of T can be calculated using ^{1}H NMR spectroscopy. The molecular weight of PEG is known and the molecular weight of PCL was calculated according to the series of equations (12)-(14). The total molecular weight was obtained by summing the molecular weight of each block according to equation (15) For all copolymers, the molecular weight calculated by ^{1}H NMR agreed with the theoretical values.

The yield was calculated by comparing the mass of the polymer obtained with the theoretical mass of polymer obtained taking into account the degree of polymerization of CL calculated by NMR according to the series of equation (16)-(18) The yield ranged from 77 to 95 %.

A typical SEC trace of the T in THF is shown in **Figure 68**-B (entry 5 of **Table 16**)The peak is well defined, exhibits a monomodal shape and the dispersity is around 1.1-1.2 which is a standard value for ROP, thus proving that the polymerization is well controlled. The difference in the molecular weights from NMR and SEC calculations is due to the amphiphilic nature of the copolymers leading to changes in the hydrodynamic volumes and to SEC calibrations using hydrophobic PS standards.

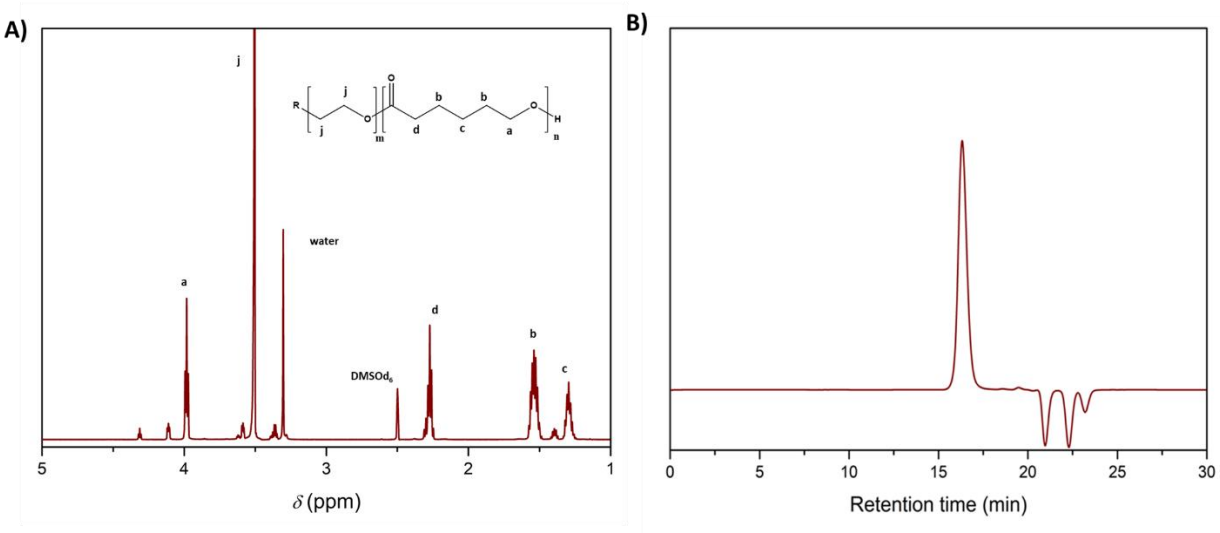

Figure 68. A) 1H-NMR spectrum of T in $DMSOd_6$ and B) SEC traces in THF for assay 5

3.2 Gelation behaviour of PCL-*b*-PEG-*b*-PCL in aqueous solution

As explained in chapter I, amphiphilic block copolymers form micelles above their critical micelle concentration and these micelles may pack and entangle in a certain range of temperature (thermo-responsive mechanism of micelle packing and entanglement). We aim to select the proper tri copolymer to get a thermo-responsive transition from sol to gel-like state compatible with the temperature of the eye (~ 35-37°C). We evaluated the properties of the T copolymers previously synthetized in aqueous solution at concentration ranging from 5 to 35 wt.% and a temperature ranging from 0 to 60 °C via the test tube inverting method (**Table 17**).

Table 17. Evaluation of the gelation properties of T in water at concentration ranging from 5 to 35 wt.% and a temperature ranging from 0 to 60 °C

Entry	T [a]	CL/EG	M_n (g.mol^{-1})	Đ [b]	In water		
					At 20°C	At 37°C	At 50°C
x	1400-4600-1400	0.61	9400	1.19	N/D	N/D	N/D
G2	700-4600-700	0.30	8200	1.11	Sol	Sol	Sol
G3	2100-2000-2100	2.13	9300	1.14	Insoluble	Insoluble	Insoluble
G4	1100-2000-1100	1.10	6600	1.19	Insoluble	Insoluble	Gel
G5	855-2000-855	0.85	6100	1,09	Gel	Gel	Gel
G6	890-2000-890	0.89	6500	1.09	Gel	Gel	Gel
G7	846-2000-846	0.49	5570	1.18	Sol	Sol	Sol
G8	1000-1400-1000	1.43	5500	1.18	Insoluble	Insoluble	Insoluble
G9	940-1000-940	1.89	4300	1.19	Insoluble	Insoluble	Insoluble

The gelation assays are written GX, the letter G refers to gelation and the X refers to the T copolymer. The typical aspect of the samples for entries G8, G4, G5, G6 and G2 are shown in **Figure 69** at a concentration of 30% (w/w) and at 37°C. For entries G3, G8 and G9, the T copolymers were insoluble into water at any concentration and at any temperature, due to their high hydrophobicity (CL/EG > 1.43). For entries G2 and G7, the T copolymers were water soluble but no sol-to-gel transitions were observed due to their high hydrophilicity (CL/EG < 0.49). For entry G4, T was nearly insoluble in water due to its hydrophobicity (CL/EG = 1.10) and showed a “sol”-to-gel transition above 50°C and for a concentration above 25 wt.%. The temperature of sol-to-gel transition was not compatible with the

medical application in the eye but it showed the possibility for T to undergo a thermal transition. For entries G5 and G6, T copolymers formed a strong gel at any concentration and no gel-to-sol transitions were observed (0.85 < CL/EG <0.89). The passage of the gel through a 30G diameter needle was impossible and thus was not compatible with the direct medical application in the eye.

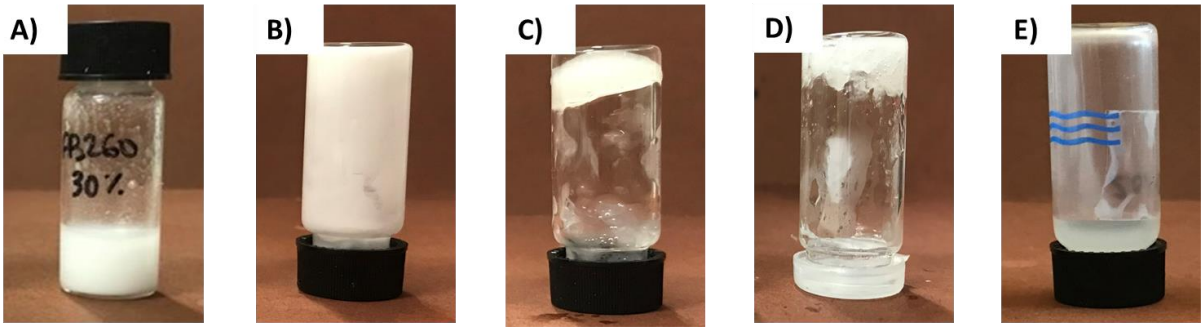

Figure 69. Visual aspects of the T copolymers in water at a concentration of 30 wt.% and at 37°C for A) G8 1000-1400-1000 (insoluble), B) G4 1100-2000-1100 (nearly insoluble but transition at high temperature), C) G5 855-2000-855 (gel) D) G6 890-2000-890 (gel) and D) G2 700-4600-700 (sol)

According to those results, it was clearly shown that the window to obtain a sol to gel-like aspect was small and that in most cases, no sol-gel transition induced by change in temperature was observed. We based our work and defined the targeted T structures regarding the structures encountered in the literature, but, surprisingly, our results do not corroborate what is described in the literature, despite the several methods tested. Especially, the copolymers 750-1000-750 (CL/EG = 1.5) and 1100-1500-1100 (CL/EG=1.46) described by Ma *et al.* [281]showed a transition from clear sol to gel around 25 and 32°C respectively at a concentration of 30%. Similarly, the copolymer 700-1000-700 (CL/EG = 1.4), 1000-1000-1000 (CL/EG = 2) and 1000-1500-1000 (CL/EG = 1.3) described by Gong *et al.* [280]showed sol to gel transition around 25, 22 and 42°C respectively. However, our copolymer 940-1000-940 (CL/EG = 1.88) was not even water soluble. At present, we do not know why the result from the literature are not reproductible. Considering the fact that PCL block need to be further functionalized by iodine and PDA, and that the first post-polymerization modification step is known to decrease the PCL blocks molecular weight, we hypothesized that these subsequent steps would change the aqueous properties of the final copolymers (change in the molecular weight, CL/EG ratio, hydrophilic/lipophilic balance).

In consequence, we did not further investigate the gelation behaviour of the T to fine tune their composition, but considering that G5 and G6 that form gel a room temperature looked promising, we kept the T corresponding to entries 5 and 6 for further chemical modification.

3.3 Synthesis and characterizations of iodinated PCL-*b*-PEG-*b*-PCL

The post-polymerization modification leading to the functionalisation of PCL is based on the work described by Nottelet *et al.* [293] and is similar to the method presented in Chapter II. The method consists of a two-step one-pot reaction described in **Scheme 22**. The first step is the anionic activation in presence of LDA of the most electrophilic proton of the PCL backbone, the second one is the electrophilic substitution with iodine.

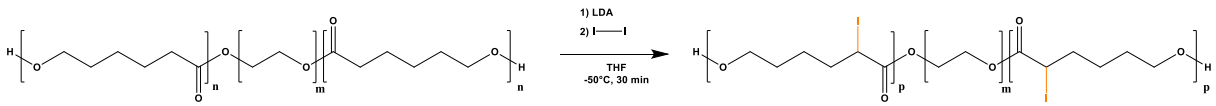

Scheme 22. Synthesis scheme of T-I ((PCL-I)-*b*-PEG-*b*-(PCL-I))

In agreement with the conclusion drawn in the previous part, the chemical modification with iodine was performed on the T entries 5 and 6, corresponding to compositions 855-2000-855 (CL/EG=0.85) and 890-2000-890 (CL/EG=0.89), respectively. The results are summarized in **Table 18**.

Table 18. Characterizations of (PCL-I)-*b*-PEG-*b*-(PCL-I) prepared in THF by anionic activation using LDA and electrophilic substitution using iodine.

	T				T-I					
Entry	Composition [a]	DP_{CL} [a]	M_n [b] (g.mol^{-1})	$Đ$ [b]	Composition [a]	DP_{CL*} [a]	T_I [a] (mol.%)	M_n [b] (g.mol^{-1})	$Đ$ [b]	Yield (%) [c]
I5	855-2000-850	15	**6 100**	**1.09**	790-2000-790	11	23	**5 800**	1.28	50
I6	890-2000-890	16	**6 500**	**1.09**	720-2000-720	10	24	**6 300**	1.31	51

[a] determined by ^{1}H NMR in $CDCl_3$ using equation (19) or (23); [b] determined by SEC in THF using PS standards for calibration; [c] determined using equation (25)

SEC chromatograms in THF of T and T-I for the entries 5 and I5 are presented **Figure 70**. A limited decrease in molecular weight of T-I (M_n = 5 800 g.mol^{-1}) compared to T (M_n = 6 100 g.mol^{-1}) and an increase in polydispersity from 1.09 to 1.28 were observed. These results are characteristic of the chain scission occurring during the anionic activation step. The grafting of iodine can be observed using UV detection in SEC analysis. Iodine exhibits a strong absorbance at 290 nm. The chromatogram clearly

showed a strong and large absorbance at 290 nm at the retention time of the polymer after functionalization, while no absorbance was observed before functionalisation, which confirmed the success of the functionalization of the PCL chains in the T copolymer.

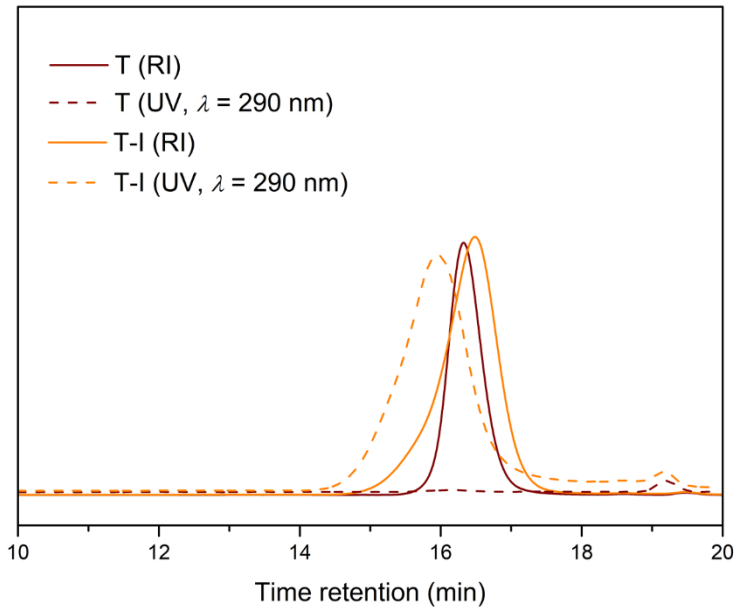

Figure 70. SEC traces of T (**Table 16**, entry 5) and T-I (**Table 18**, entry I5) using RI and UV detection (λ= 290 nm)

The ^{1}H NMR spectra of T and T-I for the entries 5 and I5 are presented in **Figure 71**. The attribution of the peaks (a, b, c, d, j) of T was established previously. The appearance of the peaks at 4.44 ppm (peak e) and at 1.87 ppm (peak f) correspond respectively to the signals of the proton R-C*H*I-CO-O and R-CH_2-CHI, which confirms the modification of the environment of the protons of the PCL backbone. The residual presence of the characteristic signal of R-CH_2-CO-O at 2.27 ppm (peak d) suggests that the functionalization is partial. The mark "R" on the chemical formula of the triblock refers to the other side chain – symmetrical – of PCL-I.

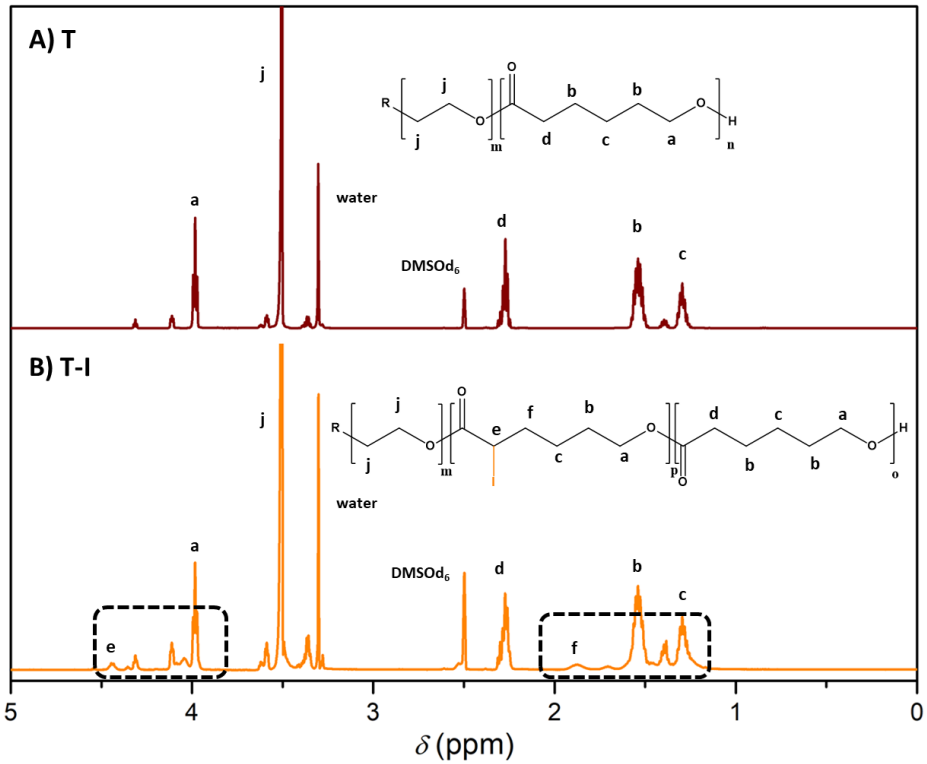

Figure 71. ^{1}H-NMR spectra of A) T (**Table 16** entry 5) and B) T-I (**Table 18** entry I5) in $DMSOd_6$.

The degree of substitution is calculated by comparing the intensity of the signal of the proton coupled with iodine (R-C*H*I-CO-O) at 4.44 ppm and the signal of (R-CH_2-O-CO) at 3.99 ppm, according to the equation (19). The degree of substitution was around 23% in each experiment with respect to the PCL chains.

$$T_I\,(\%) = 2 * \frac{I_{4.30\,ppm}}{I_{4.05\,ppm}} * 100 \qquad (19)$$

Moreover, the number average molecular weight of the T-I was calculated from the ^{1}H NMR spectra according to the series of equations described below. The molecular weight of the central PEG block does no vary. However, the DP_{CL} decreased due to the chain scission occurring during the chemical modification and was named DP_{CL*} where CL* is representative of the CL units non-functionalized and functionalized with iodine (equation (19)). Between entries 5 and I5, the DP_{CL} decreased from 15 to 11, which corresponds to compositions of 850-2000-850 and 790-2000-790 (calculated using equation (12) and (20)-(23)) in agreement with the results obtained by SEC analysis in THF.

$$DP_{EG} = \frac{M_{n,PEG,th}}{44} \tag{12}$$

$$DP_{CL*} = 2 \times DP_{EG} \times \frac{I_{3.99ppm}}{I_{3.50ppm}} \tag{20}$$

$$M_{CL*} = T_I \times 239.9 + (100 - T_I) \times 114 \tag{21}$$

$$M_{n,NMR\ PCL*} = DP_{CL*} \times M_{CL*} \tag{22}$$

$$M_{n,NMR,(PCL-I)-PEG-(PCL-I)} = M_{n,PEG} + M_{n,PCL*} \tag{23}$$

With 44 g.mol^{-1} the molecular weight of an ethylene glycol unit, 114 g.mol^{-1} the molecular weight of a ε-caprolactone unit and 239.9 g.mol^{-1} the molecular weight of an iodinated ε-caprolactone unit. CL* is representative of the CL units non-functionalized and functionalized with iodine

The yield is calculated by comparting the mass of the polymer obtained with the theoretical mass value of polymer obtained considering the degree of substitution calculated by NMR according to equation (24)-(25). The yield is around 50 wt.%.

$$m_{th,(PCL-I)-PEG-(PCL-I)} = m_{PCL-PEG-PCL} \times \frac{M_{CL*}}{M_{CL}} \tag{24}$$

$$\eta = \frac{m_{(PCL-I)-PEG-(PCL-I)}}{m_{th,(PCL-I)-PEG-(PCL-I)}} * 100 \tag{25}$$

3.4 Synthesis and characterizations of (PCL-*g*-PDA)-*b*-PEG-*b*-(PCL-*g*-PDA) (T-PDA), and thermal properties of the various copolymers

3.4.1 Synthesis and characterizations of (PCL-*g*-PDA)-*b*-PEG-*b*-(PCL-*g*-PDA) (T-PDA)

The functionalization of T-I with PDA was carried out in conditions similar to those described in Chapter II. As a reminder, we hypothesized that the carbon-iodine bond in PCL-I could play the role of the dormant macroinitiator, which, after removal of the iodine, could yield PCL radicals along the backbone

allowing the grafting of PDA side chains using conditions similar to those described by Cho et al. [118]. The reaction scheme is shown in **Scheme 23** and detailed conditions have been described in 2.3.3. T polymers containing PDA are new type of copolymers and have never been described (synthesis, purification or analysis) in the literature. In a first experiment, the solution of DMSO containing T-PDA was precipitated in cold diethyl ether but T-PDA was stuck to the bottom complicating the collection of the product. In a second experiment, the solution of DMSO containing T-PDA was introduced into a dialysis bag and DMSO was exchanged with water to collect T-PDA. Dialysis was kept as preferential purification method at this stage to collect T-PDA for further analysis.

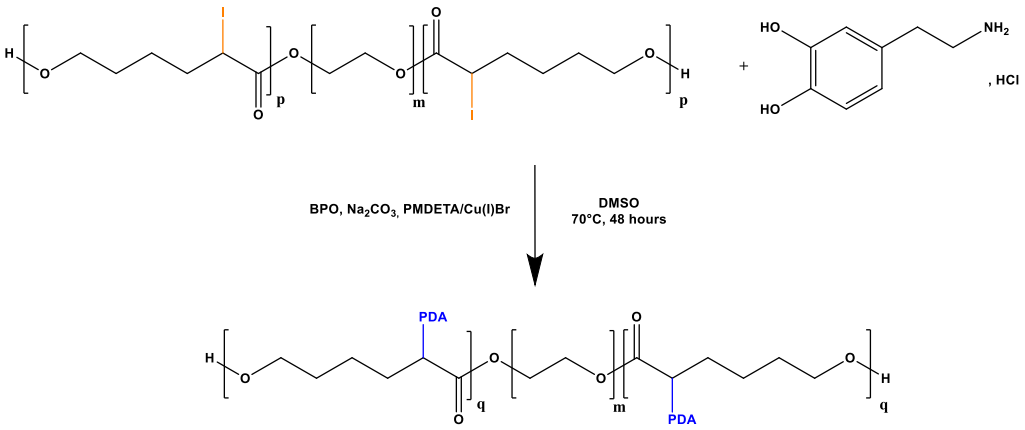

Scheme 23. Synthesis of T-PDA based according to the conditions adapted from Cho *et al.* [118]

The ^{1}H NMR spectra of T-I for the entry I5 and T-PDA in DMSO-d_6 are presented in **Figure 72**. The attribution of peaks (a, b, c, d, e, f, j) of T-I was established previously. The disappearance of the peak at 4.44 ppm (peak e) and at 1.87 ppm (peak f), characteristic signals from the functionalization of PCL by iodine, showed that the chemical environment of the polymer is modified after the introduction and the polymerization of dopamine. Moreover, the appearance of the peaks at 4.57 ppm, 1.96 ppm and 1.84 ppm also confirm this modification of the chemical environment. Moreover, the DP_{CL} in T-I and T-PDA respectively defined DP_{CL*} and DP_{CL**}, according to equation (26)) showed similar values (DP_{CL*} =DP_{CL**}= 8). To confirm that the changes of the chemical shifts could be attributed to an effective grafting of PDA side chains onto the PCL backbone, diffusion ordered NMR spectroscopy (DOSY NMR) analyses were performed. Peaks at 4.57 ppm, 1.96 ppm and 1.84 ppm display the same coefficient of diffusion (D = - 6.02 * 10^{-11} $m^2.s^{-1}$) than the peaks attributed to T, proving the grafting of PDA on the PCL chains (**Figure 73**). Those characteristic peaks of the modification of the chemical environment by PDA were represented by the black dotted rectangle with respective inserts and the bottom.

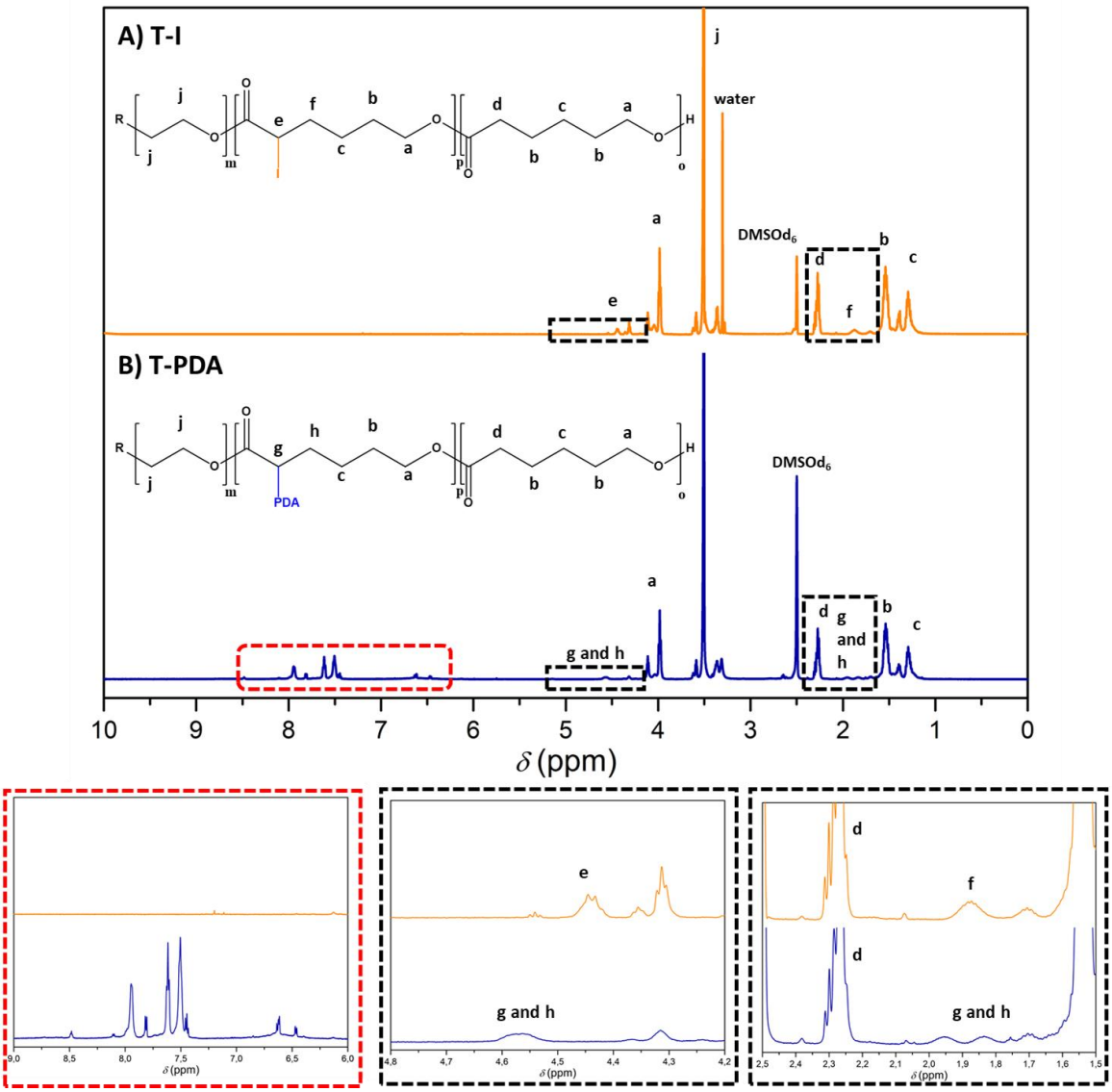

Figure 72. ^{1}H NMR spectra of A) T-I and B) T-PDA in DMSO-d6 (bottom row corresponds to insets)

The appearance of the signals at 7.95 ppm, 7.62 ppm, 7.51 ppm, 6.62 ppm, and 6.47 ppm represented with the red dotted rectangle corresponds to a combination of residual by-products of BPO, of dopamine and also of free-PDA according to the results obtained in chapter II part 3.1.2 and 3.1.4 in **Figure 43**. The peaks showed diffusion coefficients that differ from T-PDA, confirming the presence of non-grafted by-products of the reaction. Therefore, a fraction of free-PDA in the copolymer remained after dialysis, implying the possible necessity for another purification step or process.

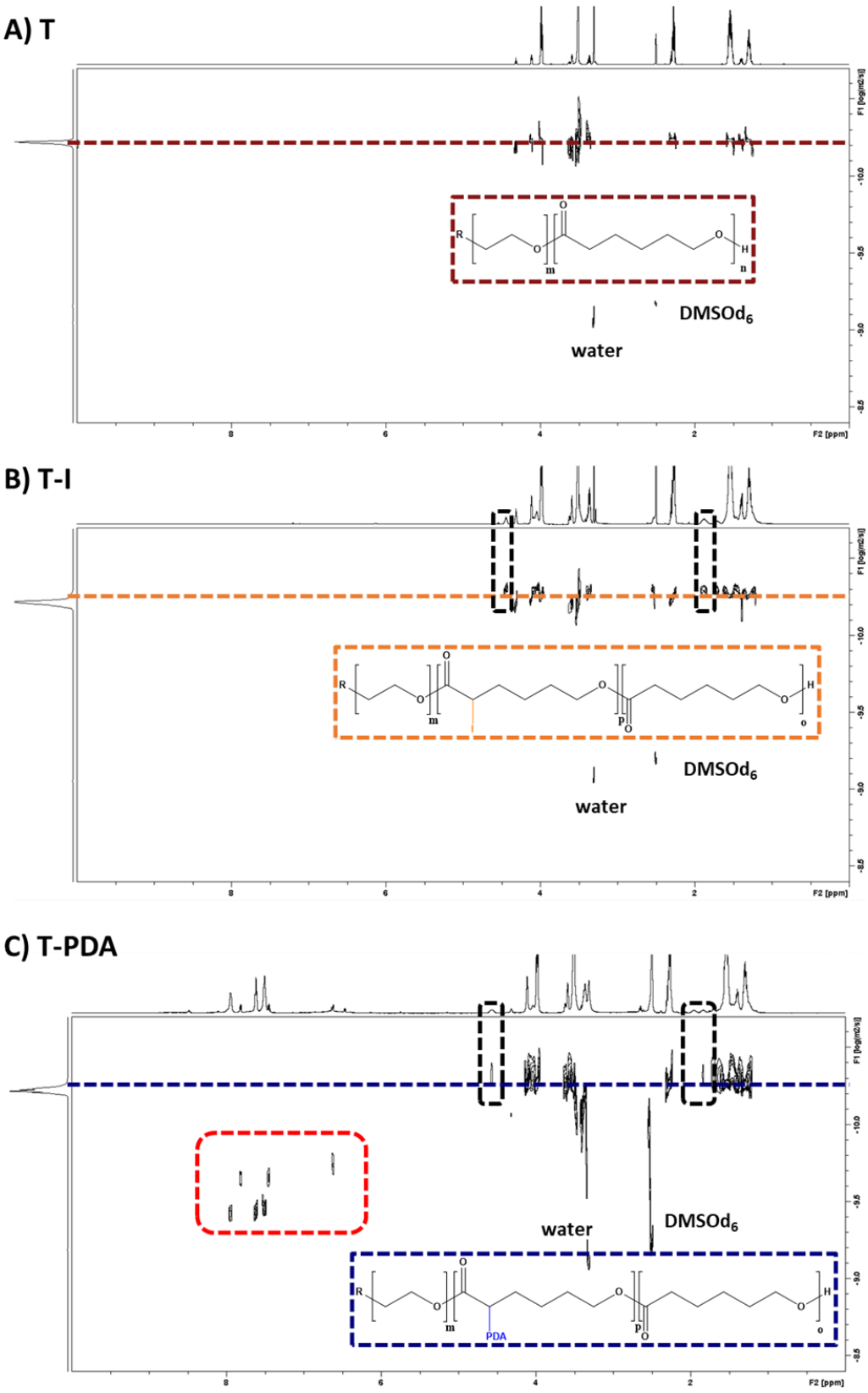

Figure 73. DOSY-NMR in $DMSOd_6$ of A) T, B) T-I and C) T-PDA

The copolymers were further analyzed by SEC in DMF. It is important to notice that the previous copolymers were analysed by SEC in THF, but copolymers containing PDA are not soluble in THF. Also, SEC traces in DMF of the different precursors and the T-PDA are shown in **Figure 74** and the molecular characteristics are reported in **Table 19**. The chromatograms using RI detection (**Figure 74**-A) showed a similar molecular weight of 3 500 g.mol^{-1} for T and T-I with an increase of polydispersity from 1.06 to 1.24, a classic phenomenon in the chemical modification step, quite similar to the previous results obtained with the THF SEC line. Chromatograms of T-PDA showed a slight decrease in molecular weight from 3 500 to 3 000 g.mol^{-1}) and in polydispersity index around 1.20. The addition of PDA in the polymer modified the chemical environment and affected also the properties of solubility, leading to changes in hydrodynamic radius that impacted the calculation of the molecular weight. According to the previous observation for oligo-PDA in Chapter II part 3.1.4.1, 450 nm is the preferential wavelength for the detection of PDA. The chromatograms using UV detection (**Figure 74**-B) at 450 nm clearly show an intense and large shape with a shift toward higher molecular weights. It may be due to the presence of T-PDA and of free oligo-PDA remaining in the product that stick to the SEC columns.

Table 19. Characteristics of polymers by SEC analysis

	In THF		**In DMF**	
	M_n (g.mol^{-1}) [a]	*Đ*	M_n (g.mol^{-1}) [b]	*Đ*
T	6 100	1.09	3 500	1.06
T-I	5 800	1.28	3 500	1.24
T-PDA	Not soluble		3 000	1.20

[a] determined by SEC in THF using PS standards for calibration, [b] determined by SEC in DMF using PEG standards for calibration

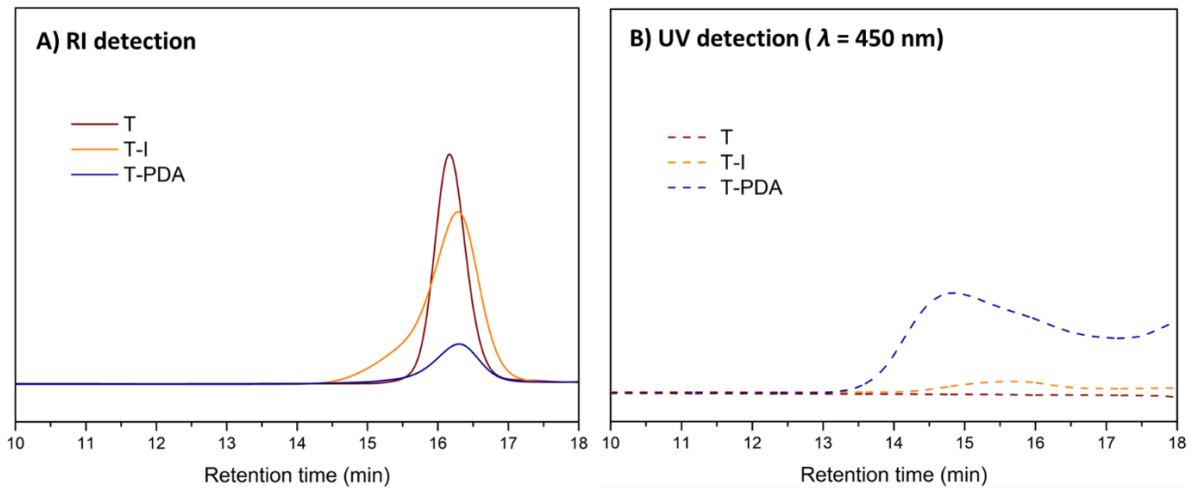

Figure 74. SEC analysis of T, T-I and T-PDA in DMF

3.4.2 Thermal stability of the copolymers

The polymers have been characterized by thermogravimetric analysis (TGA) before and after each chemical modification step. The thermogram and the derived curve (dTG, first derivate) of T, **Figure 75**-A showed a first thermal event from 30 to 370°C (minimum of dTG at 324°C) corresponding to the degradation of PCL chains, and a second thermal event from 370 to 450°C (minimum of dTG at 408°C) corresponding to the degradation of the PEG chain, leading to the almost complete degradation of the polymer. The two-step degradation profile is typical of linear block copolymers and is consistent with the work of Sun *et al* [314]. In the case of T-I, **Figure 75**-B, the thermogram showed a unique but broad thermal event from 30 to 600°C (minimum of dTG at 384°C) leading to the almost complete degradation of the polymer. Finally, in the case of T-PDA copolymers, **Figure 75**-C, the thermogram showed a first thermal event from 30 to 280°C (minimum of dTG at 170°C) possibly corresponding to the residues of synthesis and a second thermal event from 280 to 600°C (minimum of dTG at 402°C) referred to the degradation of the copolymer These data highlight an enhancement of thermal stability when passing from T or T-I to T-PDA, as previously observed in Chapter II and confirmed in the literature.

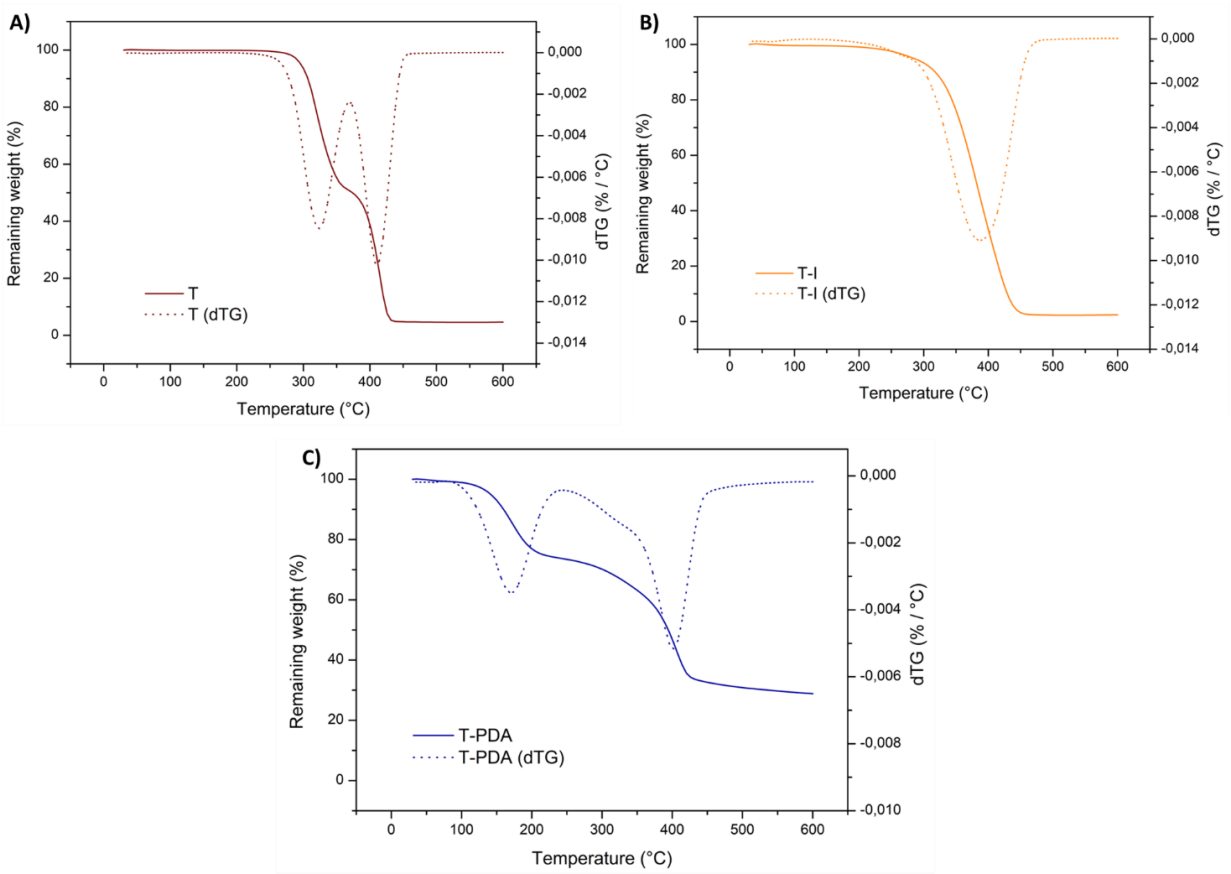

Figure 75. Thermogravimetric analyses of A) T, B) T-I and C) T-PDA

3.4.3 Quantification of total PDA in (PCL-*g*-PDA)-*b*-PEG-*b*-(PCL-*g*-PDA) (T-PDA)

In order to quantify the content of PDA present in T-PDA, the model of oligo-PDA, the methods used and the equation established in Chapter II were transferred and applied in Chapter III by adjusting the experimental values.

by UV spectroscopy

At λ = 450 nm and at a concentration of 0.1 mg.mL^{-1} in DMF, the absorbances of T and T-I were negligible (A < 0.01) whereas clearly measurable for T-PDA (A=0.24) and oligo-PDA (A=0.49, Chapter II). The UV spectra are represented in **Figure 76**. By application of the equation of the calibration curve of the oligo-PDA prepared in Chapter II part 3.1.4 and showed in **Figure 46**, the proportion of PDA in T-PDA was estimated to be of ca. 49 wt.%.

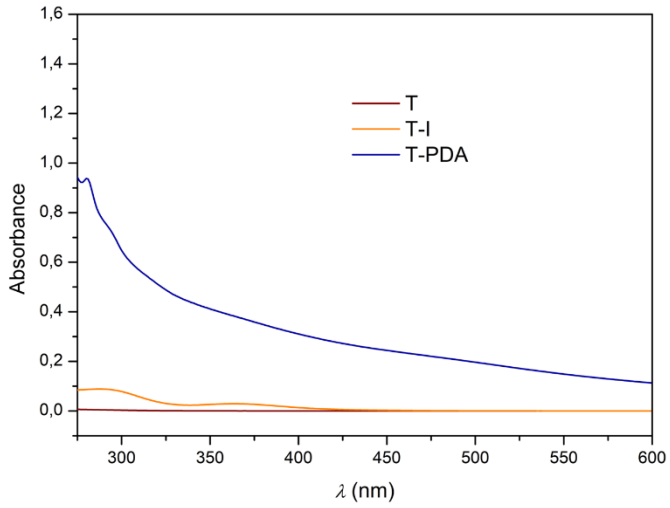

Figure 76 UV spectra of T, T-I, T-PDA and oligo-PDA at a concentration of 0.1 mg.mL^{-1} in DMF

by TG analysis

The second method of quantification of PDA content is based on the remaining masses at 600°C of PCL, PCL-*g*-PDA and oligo-PDA. The remaining weights of T, T-I and T-PDA are shown in **Table 20**.

Table 20. Mass loss and remaining weight of T, T-I and T-PDA copolymer from 30°C to 600°C

Temperature range	Remaining weight at 600°C
T	4.6%
T-I	2.4
T-PDA	28.9%

The remaining weight of T was ~5 % ~29 % for T-PDA and ~64% for oligo-PDA (chapter II). By application of equation (26), adapted from Chapter II part 3.1.4.3, the proportion of PDA in T-PDA copolymers is calculated to be 38 wt.%.

$$W\%_{\text{PDA in copolymer}} = \frac{\%_{\text{remaining weight in T-PDA at 600°C}} - \%_{\text{remaining weight in T at 600°C}}}{\%_{\text{remaining weight in oligo-PDA at 600°C}}} * 100 \quad (26)$$

<u>Comparison and conclusion</u>

The values of 38 and 49 wt.% obtained by UV and TG analysis were in relatively good agreement.

But, according to the fact that PDA chain only contained 3-4 units corresponding to ~ 620 g.mol^{-1} (according to the work of Chen *et al.* [85] described in Chapter I), and that only 2.5 PDA chains were grafted at maximum on each PCL chain (according to substitution ratio determined by NMR, **Table 18**), it is not possible that the 38-49 wt.% refer to the amount of grafted PDA. Therefore, these high values included the masses of free and grafted PDA in the copolymer which is consistent with the intensities of the peaks detected in NMR (**Figure 72** and **Figure 73**). The respective proportion of grafted PDA and free oligo-PDA are unknown. But, according to the calculation above, the proportion of free oligo-PDA is probably high, and resulted from the method of purification (dialysis) which is not sufficient to remove the last traces of by-product and residues.

3.4.4 Thermal properties of the copolymers

With the aim to compare the change in enthalpy (*ΔH*) and the characteristic temperatures of T and T-PDA copolymers, the thermal history must first be erased. A first ramp of temperature was performed from -80 °C to 100°C (100°C to avoid polymer degradation), then a second one was established from -80 to 300°C. The 2nd ramp thermograms are shown in **Figure 77**. The glass transition temperature (Tg) of PCL, theoretically around -63°C, was not observed in the conditions of analysis, as for DSC analysis in Chapter II part 3.1.3. On the opposite, the Tg of PDA was observed around 93°C, which is close to 97 °C determined in the literature [118]. It suggested that, unlike in the chapter II where the Tg of PDA in the implant was not observed due to the low amount of PDA (3wt.%), the proportion of PDA in T-PDA was high enough (38-49 wt.%) to be detected. T is semi-crystalline with a *Tm* around 33°C. However, no melting temperature was observed in T-PDA, showing a complete amorphous behaviour. The change in the crystallinity might be related to the modification of the spatial organization and the decrease of molecular weight after functionalization with PDA. Indeed, as shown in chapters I and II, the PDA is amorphous [93] and the grafting of PDA onto PCL backbone resulted in a decrease of melting temperature and melting enthalpy. In the present case, the complete amorphous behaviour might be related to a large amount of PDA present previously quantified in the copolymer (grafted or free) that prevented the structural arrangement of the chain, thus impairing the crystallization process.

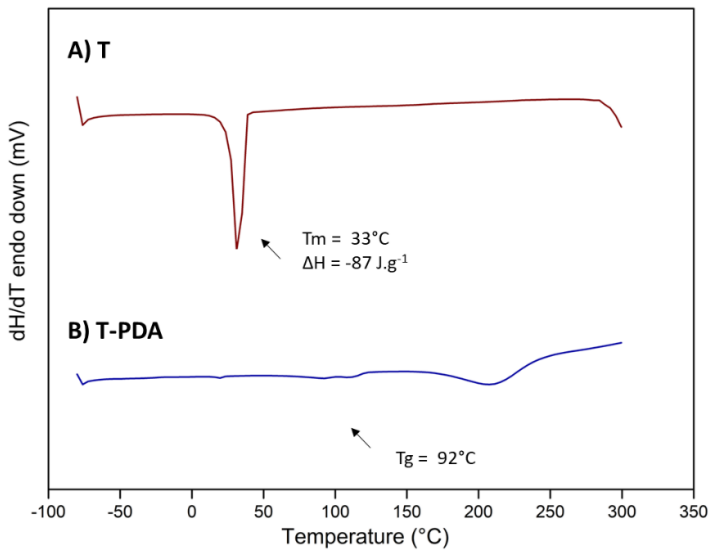

Figure 77. DSC analyses T and T-PDA

3.5 Gelation behaviour of (PCL-*g*-PDA)-*b*-PEG-*b*-(PCL-*g*-PDA) (T-PDA) in aqueous solution

The properties of aqueous solutions of T-PDA were evaluated. As a reminder, this copolymer was prepared from the T triblock that forms a gel in water (**Table 17**, entry G5). A typical aspect of the sample is shown in **Figure 78**, at a 30 w% concentration and at 37°C. It is clearly seen that a fraction of the T-PDA is soluble in water according to the coloration of the aqueous phase and that a fraction remained insoluble in water according to the presence of black chunks on the glass wall, thus making difficult the formation of a gel by direct dissolution of T-PDA in water.

Figure 78. Solubility of T-PDA in water

To overcome this limitation, and with the aim to obtain a gel-like T-PDA, a possibility is to mix T-PDA with the gel forming T. Moreover, to obtain an injectable solution containing either T or a mix of T and T-PDA, both copolymers should be solubilized in a co-solvent. Therefore, we will develop an injectable formulation for in-situ depot formation based on a solvent-exchange mechanism (in opposition to our primary aiming to thermo-responsive formulations). The formulation will be detailed in Section 2 of this chapter.

3.6 Conclusion

We successfully synthesized graft copolymers based on T and PDA (T-PDA). We synthesized T triblock copolymer with different chain lengths of PEG and PCL in order to obtain EG/CL ratios ranging from 0.30 to 2.13 and molecular weights from 4 300 to 9 400 g.mol^{-1}. We evaluated aqueous properties and

thermal-responsiveness of the copolymers and selected the most promising T for the application. No sol-gel transition was evidenced, only changes in solubility depending on the triblock compositions. The selected PCL_{855}-PEG_{2000}-PCL_{855} was functionalized with iodine at a functionalization ratio of 23 mol. % and a molecular weight of 3 500 g.mol^{-1}. The third step of the synthesis involved the simultaneous oxidative polymerization of dopamine, the grafting of dopamine units and/or oligo-PDA via ATRP-like conditions on PCL-I and further growth of PDA. The resulting T-PDA copolymer had by SEC a M_n of 3 000 g.mol^{-1}. The success of the grafting and the presence of a fraction of free-PDA in the copolymer were proven by DOSY-NMR. The overall content of PDA in the copolymer was estimated around 40% by UV and TG analyses. The respective proportion of grafted-PDA and free oligo-PDA were unknown and, the probably high proportion of oligo-PDA resulted from a defect in the method of purification. The selected T spontaneously forms a gel in water and the T-PDA is insoluble in water. To design injectable liquid formulations, we highlighted the need of a co-solvent in the formulation to enhance the solubility of the copolymers before injection and to form a gel-like depot based on solvent-exchange mechanism.

4. Section 2: Development of a formulation suitable for in situ forming systems for intravitreal injection

4.1 Selection of a co-solvent and ability of the copolymer to form in situ depot by solvent-exchange mechanism

Due to the non-thermo-responsiveness and non-solubility in water of T and T-PDA, we had to modify the formulation approach. Thus, we developed a formulation based on the mechanism of solvent-exchange that forms in-situ depots upon injection (see Chapter I part 4.2.1.3). For this purpose, dissolution of T and T-PDA in an organic solvent is required.

4.1.1 Selection of the organic solvent

For the formulation of *in situ* forming depot, and more particularly for parental route (including intramuscular, intravenous, subcutaneous administration), ethyl acetate, NMP and DMSO are typical organic solvents. [285,315,316] However, toxicity studies lack for human ocular application, thus none of these solvents have been approved yet for ocular use. Moreover, the compatibility with proteins is a limiting parameter.

We selected polyethylene glycol 400 (PEG_{400}) for its water-soluble properties, its low cost and its excipient pharmaceutical approval. Particularly, PEG_{400} has been used as plasticizer, at a concentration range from 3 -10 % with respect to copolymer, for the development of drug-loaded scleral implants by Thilek Kuman *et al.* [317] . The in vivo observations showed not pathological and/or structural changes in the rabbit eyes. Also, PEG_{400} has been used at a concentration of 7% for the development of suspension of niosomes for topical drug delivery by El Menshawe [318]. More recently, PEG_{400} was injected into the vitreous of rabbits at a concentration of 500 mg/mL (corresponding to 0.62 mL of PEG_{400} in 1.4 mL of vitreous), and severe conjunctival redness plus mild presence of vitreous cellular debris were observed after one week of treatment according to the work of Aguirre *et al*. [319]Due to the fact that the volume of the human eye is around 4 mL (2.85-fold more compared to rabbit eye), the safety assessment might differ and a increase in tolerability could be excepted. Besides, PEG_{400} was used as the major component of liquid formulation, at a concentration range from 80 to 90%, for subconjunctival and

intravitreal administration to treat retinal and choroidal diseases for an extended period of time. [320] Thus, it is reasonable to used PEG_{400} as organic co-solvent for the development of our liquid formulation for the IVT administration in human eye.

4.1.2 PCL-*b*-PEG-*b*-PCL (T) as in situ-forming system

The suitability of T for the in-situ formation of depot by solvent-exchange mechanism was evaluated. For this, T (PCL_{855}-PEG_{2000}-PCL_{855}, entry 5, **Table 16**) was dissolved in a proportion of 30% (w/v) in 1 mL of PEG_{400} forming a viscous white solution. Then, 5 mL of PBS was added on the top and the vial was kept at 37°C. The proportion of the copolymer in PBS thus decreased to 6% (w/v). At this concentration, the copolymer was able to form a gel in water according to the previous gelation study performed. **Figure 79** shows the visual aspects of the copolymer during the solvent-exchange process. After 4 hours, first time point of the study, we obtained a smooth and jelly depot. After 4 days, the copolymer formed gel clusters – not a single entity of gel as obtained in **Figure 69**. These preliminary tests demonstrated the potential of T to form a gel from an injectable solution, thanks to the solvent-exchange between PEG_{400} and PBS. It should however be noted that under the tested conditions, this gelation may be too slow to retain biologics and avoid their fast release.

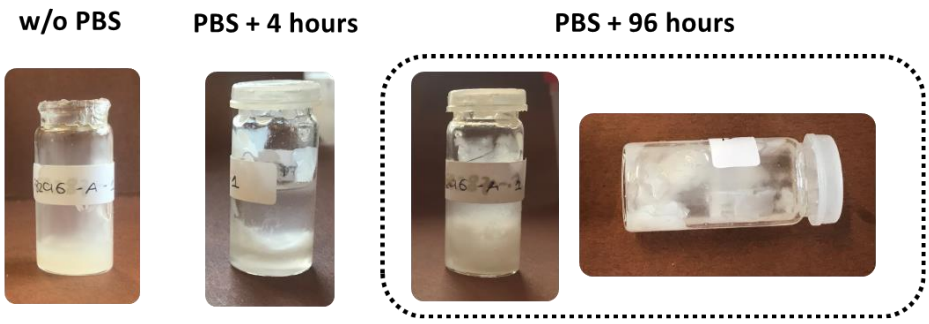

Figure 79. Formation of T gelling depots by solvent-exchange process between PEG_{400} and PBS at 37°C at different timepoints

Concerning the T-PDA, we previously concluded to the non-water solubility. Thus, T-PDA was dissolved in PEG_{400}. Moreover, due to the impossibility to obtain a gel-like aspect on his own in water, mixing T-PDA with T in PEG_{400} seemed suitable for the formation of gel clusters by solvent exchange process.

4.1.3 Selection of the protein

For the PhD purpose, the biologic provided by F.Hoffmann-La Roche is a powder containing a monoclonal antibody (mAb) (M_w=150 kDa, pI=8.0) spray-dried from 10 mM Histidine.HCl buffer and that contains also sucrose, NaCl and polysorbate 20 (PS20). The mAb is soluble in water, is reasonably stable at pH=7.4 and even more stable in the range 5.0-6.5. The maximum of absorbance of mAb in water is 280 nm according to the UV spectra presented in **Figure 80**.

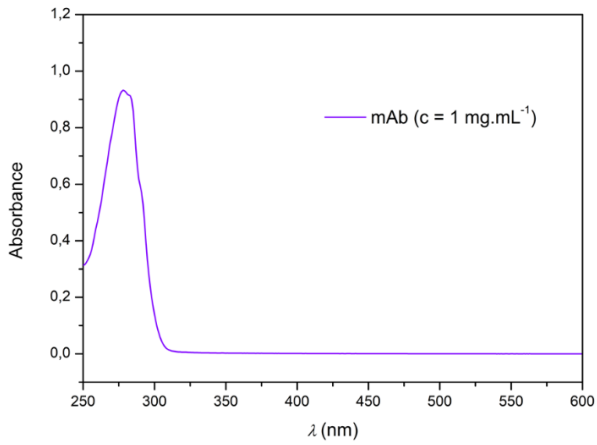

Figure 80. UV-Vis spectra of the mAb at a concentration of 1 mg.mL^{-1} in water

In a preliminary study, the mAb was added in water and in PEG 400 at a concentration of 12 mg.mL^{-1}. It was confirmed that mAb is fully soluble in water while insoluble in PEG_{400} as suggested by the presence of undissolved microparticles. In a second preliminary study, mAb was added at a concentration of 12 mg.mL^{-1} in a mix of PEG_{400} and T (20% w/v in PEG_{400}). It was not soluble in PEG_{400} and the addition of copolymer did not help its solubilisation.

4.1.4 Conclusion

According to the results obtained, water is the solvent of choice to solubilize the mAb, while PEG_{400} is the solvent of choice to solubilize the copolymers and is well tolerated by the eye after injection in the vitreous. Therefore, our formulation will be based on co-solvents and would be an interplay between injectability through a needle, and stability of the mAb during storage and release. These parameters are evaluated in the next parts.

4.2 Injectability of the polymeric formulation

Syringeability and injectability are key performance parameters of injectable formulations. Syringeability refers to the ability of a solution contained in a transfer vial to pass easily thought the hypodermic needle prior to injection. It includes factors such as ease of withdrawal, accuracy of dose measurement and risk of clogging. Injectability refers to the ability of the solution contained in the syringe to pass easily through the hypodermic needle and to the characteristics of the formulation during the injection. It includes the force of injection required, the evenness of the flow of the solution and the risk of clogging. Syringeability is not necessarily performed with the same needle as the one for injection. It is common for pharmaceutical products to provide two needles, and to change needle after transfer and prior to injection. In the present study, we focused on the injectability parameter with the perspective of an intravitreal injection.

4.2.1 Description of the factors studied for injectability

As described in Chapter I part 1.3.5.3, the intravitreal injection typically requires a needle length between 1.27 and 1.57 cm to reduce the risk of retinal injuries and a needle diameter between 27 and 30G even 31 and 32G to reduce patience pain and risk of injuries. [12] The typical injection volume is between 50 and 100 µL. [12] To the best of our knowledge, there is no description in the literature about the limit of speed and maximum force of injection of the product through the syringe into the target media. However, it is usually described that a speed of injection is set at 1 mm.s^{-1} which would reflect the manual standard of speed of injection [321] for the ophthalmologists. Besides, the force of injection should be as lower as possible in order for the ophthalmologists to easily inject the formulation and for the patients to reduce their pain and the risk of injuries. For example, Roche is using a force of injection under 15 N internally.

In the injectability study, a 1 mL syringe carefully filled with the selected formulations was used to avoid the presence of air bubbles. Then, the needle was fixed to the syringe with Parafilm® M and the whole system was placed in the configuration presented in **Figure 81** in a tensile-test machine. To test the injectability, we varied (i) the diameter of the needle (27G, 30G) and (ii) the composition of the formulation including the water:PEG$_{400}$ ratio (1:0, 1:1, 1:2 and 1:4) and the copolymer content (5,10 and 15% w/v). The speed of injection was kept constant at 1 mm s^{-1}, the temperature at 20°C and the volume of injection at 100 µL.

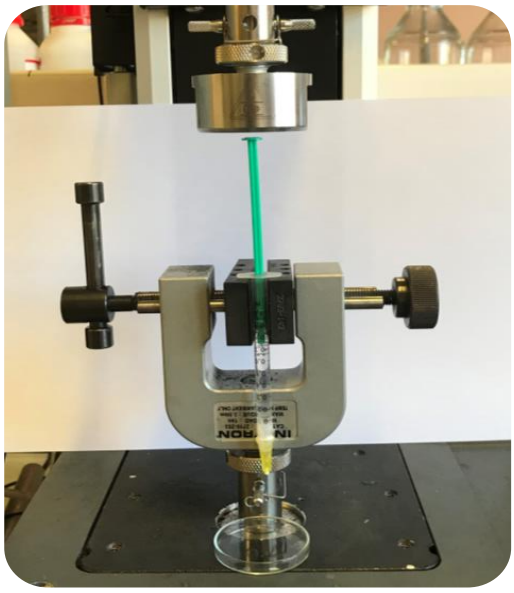

Figure 81. Set-up of injectability test in compression mode using 1mL-30G-syringe

4.2.2 Influence of the needle diameter and the composition of the formulation

As a reminder, the preferred formulation contains water and PEG_{400}. The influence of the ratio water:PEG_{400} on the force required for injection was evaluated. **Figure 82**-A shows that the higher the proportion of PEG_{400}, the higher the force required for injection due to the viscosity of PEG_{400}. Moreover, at equal speed of injection, the force required for the injection of PEG_{400} almost doubled when decreasing the internal diameter of the syringe from 27 to 30 G. We kept the water:PEG_{400} ratios 1:1 and 1:2 for further experiments because the force of injection obtained with the ratio 1:4 and the 30G needle was higher than the two others.

Due to the limited quantities of T-PDA copolymers available, the injectability tests were only performed on T copolymer. We hypothesized that, thanks to the close molecular weights and compositions between T and T-PDA, the behaviour of the formulation of the injectability tests will be similar. In order to form a strong gel-like depot upon injection, the amount of T should be the highest possible. Indeed, the higher the concentration of copolymer, the strongest is the physical cross-linking, and the slower the expected release of the protein. In the present study, we used PCL_{890}-PEG_{2000}-PCL_{890} (entry 6 **Table 16** and entry G6 **Table 18**)). For a 1:1 solvent ratio, **Figure 82**-B showed that the force of injection increased proportionally from 10 to 28 N with the increase in copolymer concentration from 5 to 15 wt.%. In the case of 1:2 solvent, the force of injection increased in the presence of copolymer

(10 wt.%) as well (**Figure 82**-C). Above 15 wt.%, the injection force would exceed the maximal value for both solvent ratios. We noted that the addition of mAb at a concentration of 40 mg.mL^{-1} in a solution composed of water:PEG$_{400}$ at a 1:1 and 5 % w/v T slightly increased the force of injection (**Figure 82**-D).

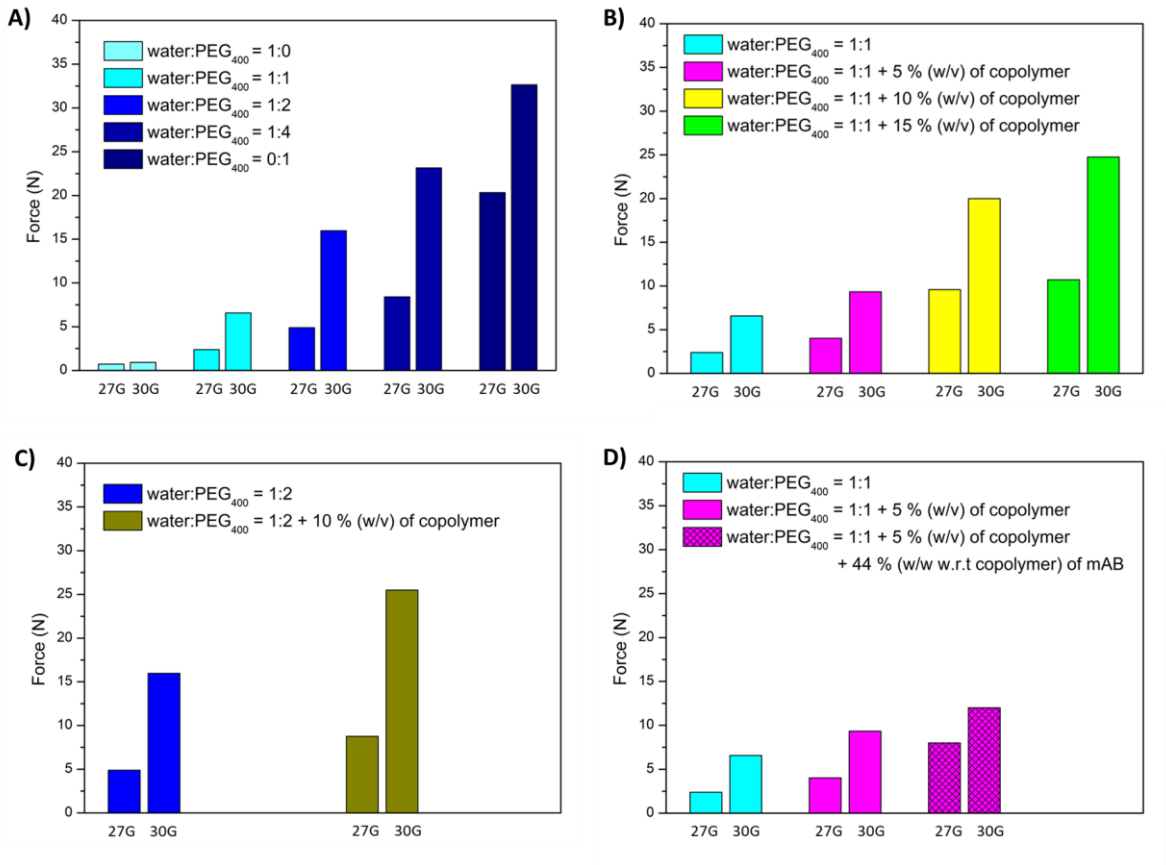

Figure 82. Maximal force reached upon injection of 100 µL performed at 20°C and 1 mm.s^{-1} with A) influence of the water:PEG$_{400}$ ratio without polymer, B)-C) influence of the proportion of T contained in the solution composed of water:PEG$_{400}$ at a 1:1 (B) or at a 1:2 ratio (C), and D) influence of the incorporation of mAb in the solution composed of water:PEG$_{400}$ at a 1:1 and T. T refers to assay I6/G6 (**Table 16** and **Table 18**)

4.2.3 Conclusion

The formulations based on water:PEG$_{400}$ mixtures at ratios 1:1 or 1:2 and containing 5% or 10 % (w/v) of T have the lower injection values and lower PEG$_{400}$ content, which make them suitable as injectable and tolerable formulations for the ocular application.

4.3 Stability of mAb in the pre-formulations

We aim to test the stability of the mAb provided by F.Hoffmann-La Roche in the formulations composed of water/PEG, water/copolymer and in HBS/PEG. HBS is the histidine buffer solution prepared to favour the stability of the mAb due to the presence of histidine in the mAb powder. These formulations are called pre-formulations and allow evaluating the influence of each component towards the stability of mAb. Afterward, the stability of the final formulation gathering all the components (mAb + HBS/PEG/copolymer) will be performed.

Aqueous SEC using UV detection is a common technique to study the protein denaturation (aggregation/fragmentation) when accompanied with a change in conformation and chain scissions, leading to:

- a change in retention time of the initial peak
- a change of area under curve (AUC)
- a change of intensity at 280 nm
- the appearance of additional peaks
- a change of in the aspect of the sample before injection (turbidity, precipitation)

In order to observe the degradation of the mAb, we performed a stability study of mAb under stress conditions to verify that under these conditions known to degrade mAb, we were able to visualize the degradation products. From day 0 to day 30, the samples were clear, transparent, without any precipitate visible in PBS before and after the addition of the mobile phase, suggesting a stability of the mAb in solution (**Figure 94**-A and B in Appendix). The same elution profiles have been obtained at day 0 and day 3 with a similar absorbance, a similar AUC and a similar wavelength ratio (**Figure 93** and **Figure 94**-C in Appendix). However, at day 15, the chromatograms showed a decrease in absorbance and an enlargement of the peak suggesting the appearance of populations of lower and higher molecular weights. The trend is confirmed at day 30. As a result, the chromatograms suggested a decrease in the amount of mAb and the possible scission and/or aggregation occurring in the samples let under stress conditions.

4.3.1 Stability of mAb in the presence of PEG_{400}

The stability of mAb in the presence of PEG_{400} was first studied in water:PEG mixtures at various PEG ratios. The evolution of the characteristic parameters of SEC (absorbance at 280 nm, the 280/254 nm wavelength ratio and the relative AUC at 280 nm) is shown in **Figure 83**. As a reminder, 280 nm is the selective wavelength of mAb, while 254 nm is representative of all the component in the media and is only used to calculate at wavelength ratio. The photographs of the water:PEG formulation before addition and after addition of the mobile phase are showed in **Figure 84**-A and **Figure 84**-B and the chromatograms are shown **Figure 84**-C.

In the formulations based on water:PEG_{400} = 1:0 and 1:1 the solutions were transparent, the absorbance at 280 nm, the relative wavelength ratio and the relative AUC were constant during 30 days.

However, in the formulation based on water:PEG_{400} = 1:2, the sample solutions were white but transparent after the addition of the mobile phase and detection of the mAb was observed at t=0. But from day 3, the solution turned turbid suggesting a destabilisation of mAb, which was confirmed by the SEC analysis where the relative AUC drastically decreased until mAb was not detected anymore.

The study clearly demonstrated that PEG_{400} at these hight concentrations affect the stability of mAb. Indeed, it is known that PEGs , depending on theirs molecular weights, their concentrations as solvent or co-solvent, have tendency to induce subtle perturbation of the protein's native structure (unfolding) affecting the long-term stability leading to a decrease of the thermodynamic stability and resulting in aggregation then precipitation of the proteins. [322–324]

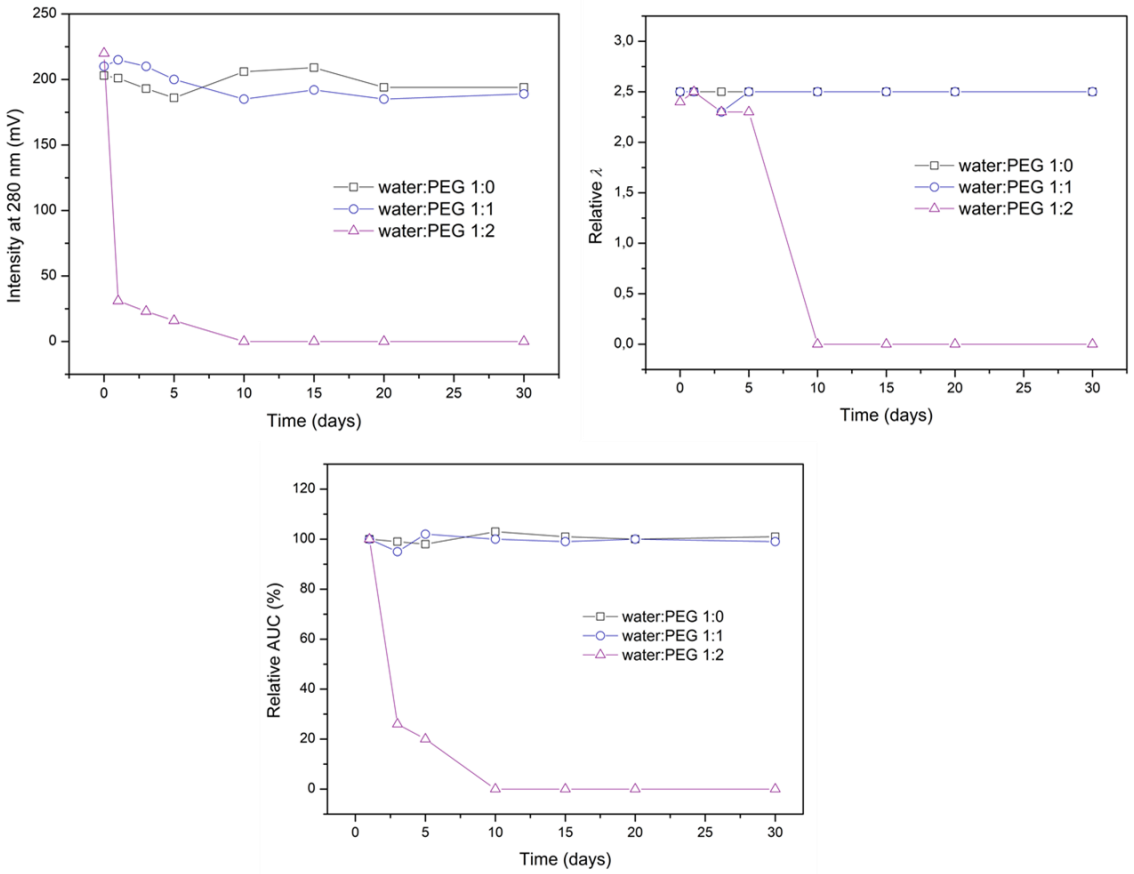

Figure 83. Evolution of the absorbances, wavelength ratio, and relative AUC of mAb detected at various water:PEG_{400} ratios

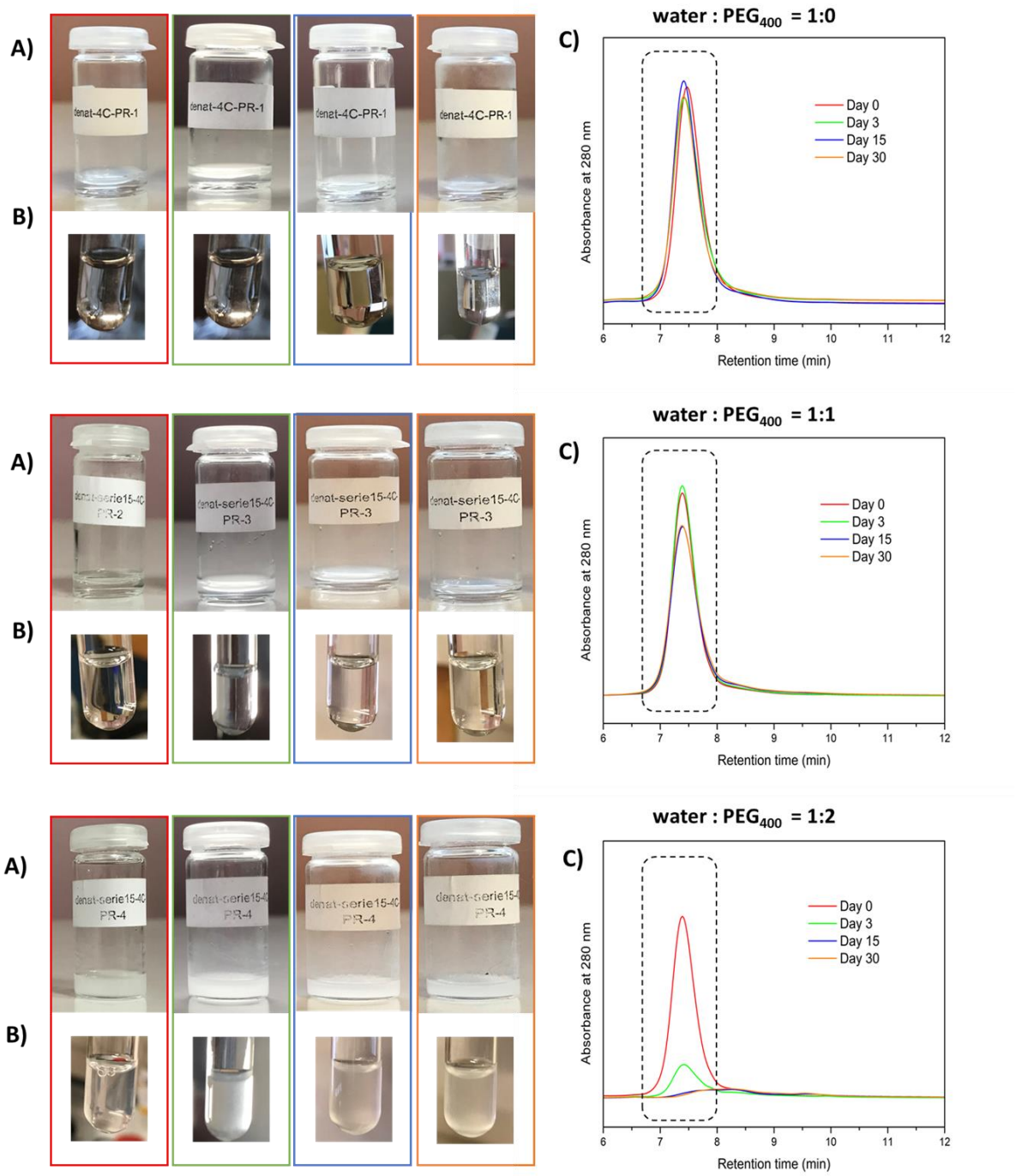

Figure 84. Stability study of mAb at various water:PEG_{400} ratio. Photographs of the samples A) before and B) after additions of the mobile phase and C) SEC chromatograms obtained at 280 nm.

In a similar way, the stability of mAb was studied in HBS:PEG at various PEG ratios, where HBS corresponds to a buffer solution of histidine (pH=6) in order to enhance the stabilization of the mAb. The results were consistent with those obtained with water during the 30-day study. The evolution of the SEC characteristics and the aspect of the solution are shown in **Figure 96** in Appendix.

As a consequence of these results, for further formulation development, we selected the ratio HBS:PEG_{400} = 1:1 to ensure solubility and stability of mAb and the solubilization of the copolymers.

4.3.2 Stability of mAb in presence of copolymers in water

The stability of mAb was then studied in the presence of copolymers – T and T-PDA – in water. Indeed, water provided stability of mAb during at least 30 days as previously shown. The stability was not studied using HBS as aqueous media due to the non-availability of the histidine at the time. For each formulation, the evolution of the characteristic parameters of SEC is shown in **Figure 85**. The photographs of the sample before addition and after addition of the mobile phase are shown in **Figure 86**-A and **Figure 86**-B respectively and the chromatograms of the detected mAb are presented **Figure 86**-C.

For the formulation containing T, the sample solutions were white due to the presence of the white powder of copolymer but transparent after the addition of the mobile phase and mAb was detected. At day 0 and day 3, the absorbance, the relative wavelength ratio and the relative AUC were nearly constant. At day 15, the amount of mAb decreased by two third. No additional peak appeared on the chromatogram. The relative wavelength ratio $\lambda_{dx,280/254nm}$ remained constant suggesting the interaction of the genuine mAb with the copolymer that decreases the amount of mAb in the supernatant. The study was stopped at day 15 because of the lack of product for aquiloting.

For the formulation containing T-PDA, the sample solutions were black due to the presence of the copolymer but transparent/light black after the addition of the mobile phase. As for T, the amount of mAb was nearly constant until day 3. The amount of mAb decreased by half at day 15 until complete disappearance at day 30. No additional peak appeared on the chromatogram. The relative wavelength ratio $\lambda_{dx,280/254nm}$ remained constant suggesting an interaction of mAb with the copolymer that decreases the amount of mAb in the supernatant. With T-PDA, an additional peak is observed at a retention time of 8.53 min. The absorbance and the relative AUC of the additional peak remained constant during the 30 days. The relative wavelength ratio drastically differed from the mAb value

(0.30 *vs.* 2.5 for mAb). This suggested that this additional peak was related to the presence of T-PDA. To confirm this hypothesis, T-PDA was added to water without mAb. The chromatograms of the formulation of T-PDA free of mAb clearly showed only the additional peak at the same retention time and the same absorbance value. This additional peak is therefore a water-soluble impurity of the T-PDA.

The study clearly demonstrated that both T and T-PDA copolymers interacted with mAb without denaturation of the soluble fraction of mAb in the supernatant, at least after 3 days.

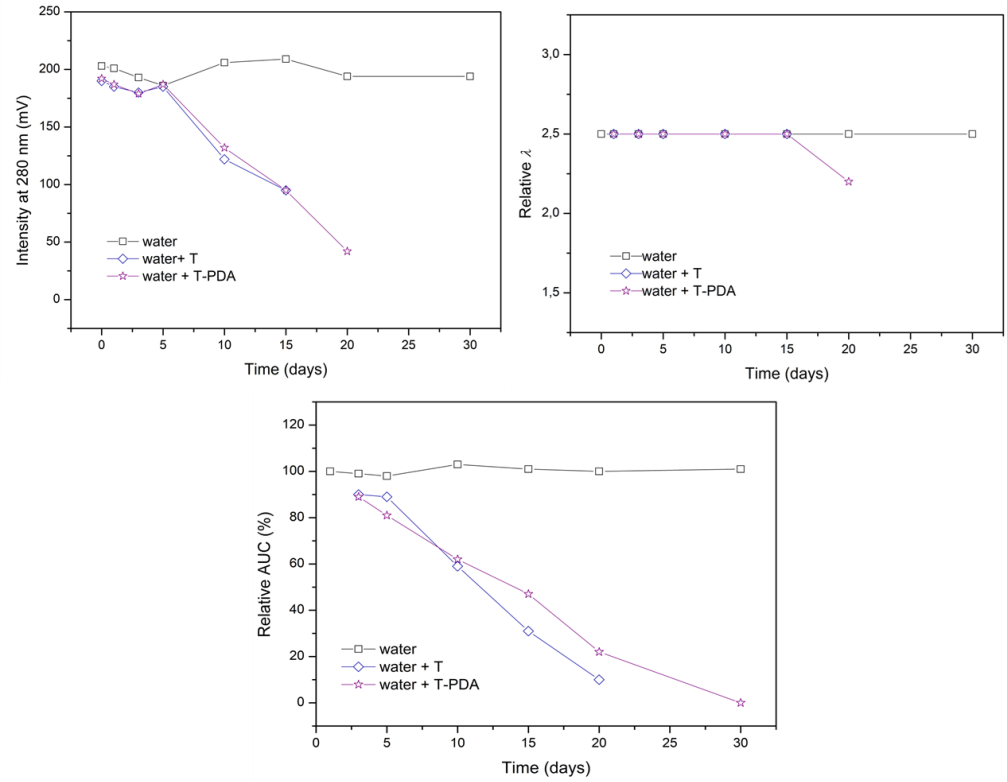

Figure 85. Evolution of the absorbances wavelength ratio, and relative AUC of mAb detected in the presence of T or T-PDA in water.

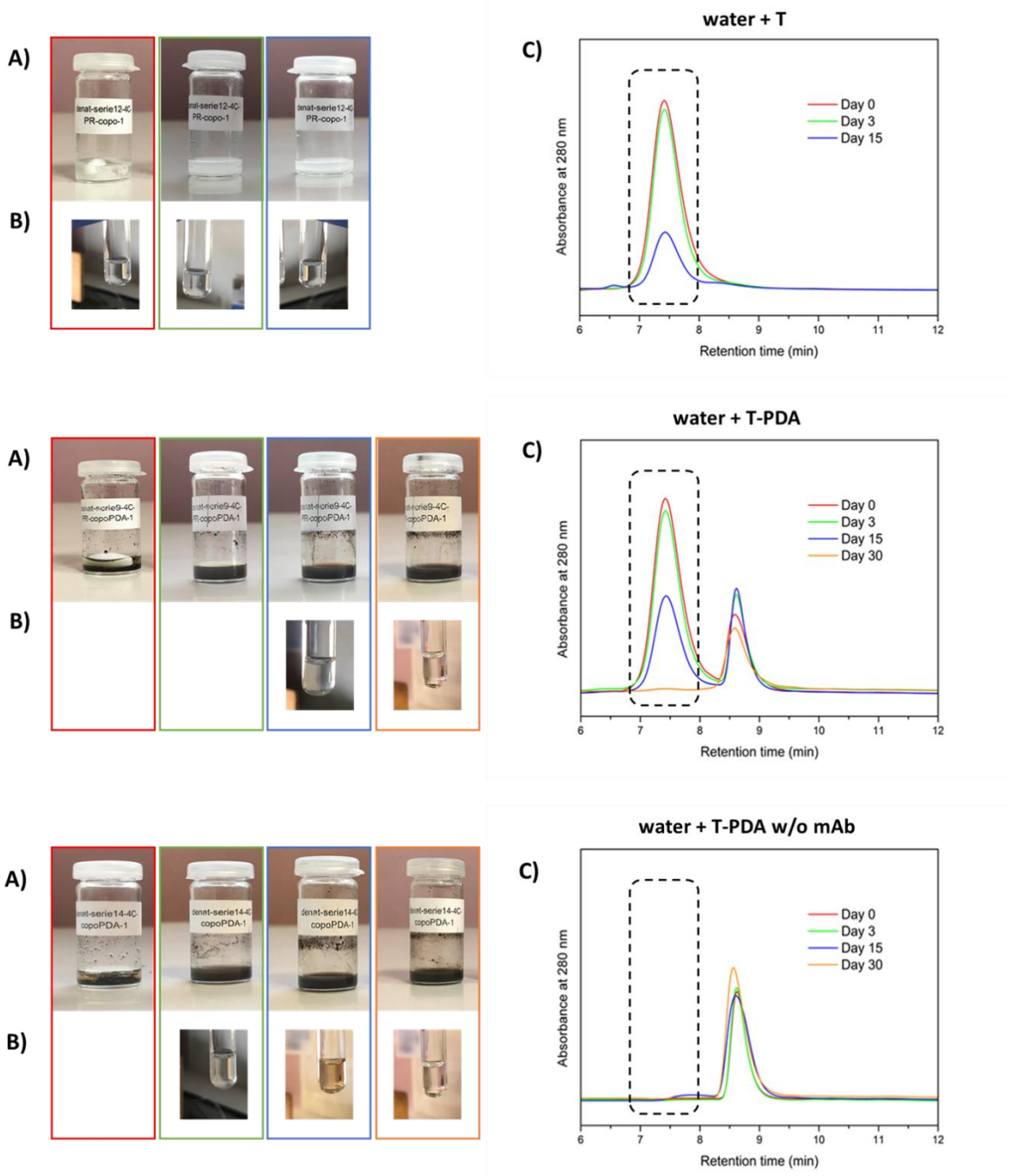

Figure 86. Stability study of mAb in the presence of T ((PCL$_{890}$-PEG$_{2000}$-PCL$_{890}$, entry 6, **Table 16**) or T-PDA (**Table 19**) in water. Photographs of the samples A) before and B) after additions of the mobile phase and C) SEC chromatograms obtained at 280 nm.

4.3.3 Conclusion

According to the study of the stability of the pre-formulation, high concentrations of PEG_{400} in the aqueous medium affect the stability of mAb. Moreover, the amount of mAb detected by SEC decreased in the presence of T and T-PDA copolymers, suggesting interactions between mAb and copolymers without inducing denaturation of mAb during 20 days in water. mAb is thus compatible with formulations containing T and T-PDA copolymers and PEG_{400} under ratio aqueous media:PEG_{400} not exceeding 1:1.

4.4 Conclusion and choice of the formulation suitable for *in vitro* release study

In this part, we developed a tentative formulation suitable for injectability through a 30G needle. The formulation was a compromise between the safety of the solvents, the solubility of the copolymers, the concentrations of polymers and mAb, and the stability of mAb in the formulation. mAb was solubilized in water or HBS T and T-PDA were solubilized in PEG_{400} to enhance their solubilities. We evaluated the force required for the injection of various formulations. The formulations based on water:PEG_{400} at ratio of 1:1 or 1:2 and containing 5%, 10 % and 15% (w/v) of T were promising for injection through a 30G needle under selected conditions of injection (20°C, 100 µL, 1 $mm.s^{-1}$). Meanwhile, we evaluated the stability of mAb in formulations by SEC. The water:PEG_{400} or HBS:PEG_{400} ratios ≥ 1:1 provided stability of mAb unlike the ratio 1:2. Typically, the mAb is stored in its buffer (here HBS) and, as a consequence of these results, the ratio HBS:PEG_{400} = 1:1 will be used for further formulation development to ensure solubility and stability of mAb as well as the solubilization of the copolymers. The presence of copolymer at a concentration of 5% w/v in water decreased the amount of mAb detected and particularly in the case of T-PDA, suggesting a strong interaction between mAb and the copolymers. This strong interaction may slow down the kinetics of release of the biologic and extend the duration of the therapeutic effect compared to the current polymers in pre-clinical phases. Based on these results, the tentative formulation to be tested for mAb release will be composed of 5 % (w/v) of copolymer in an HBS:PEG_{400} ratio = 1:1 (v/v).

5. Section 3: Stability and in vitro release of mAb from in situ forming depots of PCL-*b*-PEG-*b*-PCL (T) and (PCL-*g*-PDA)-*b*-PEG-*b*-(PCL-*g*-PDA) (T-PDA)

As defined in the previous part, the final formulation will be composed of 5 % (w/v) of copolymers (T or T-PDA) in a HBS:PEG_{400} 1:1 (v/v). The formulation will either contain 40 $mg.mL^{-1}$ (high dose (HD)) or 13 $mg.mL^{-1}$ (low dose (LD)) of mAb. Along this section, the formulation will be defined as formulation X-Y, where X is a letter referring to the copolymer (T, T-PDA, T/T-PDA) and Y is a number referring to the mAb dose (LD, HD). The formulations are details in **Table 21**.

Table 21. Composition of the formulations for the stability and the release of mAb *in vitro*

Formulation code	Copolymer	Copolymer (wt.%)	mAb DL (%)
T-LD	T	5	21
T-HD			44
T/T-PDA-LD	T and T-PDA (2:1)		22
T/T-PDA-HD			44
T-PDA-LD	T-PDA		22
T-PDA-HD			44

5.1 Stability of mAb in the formulations

The stability of mAb in the final formulations was studied. The T refers to assay I6/G6 (**Table 16** and **Table 18**) and T-PDA refers to the one presented and characterized (**Table 19**). For each formulation, the evolution of the characteristic parameters of SEC is shown in **Figure 87**. The photographs of the formulations before addition and after addition of the mobile phase are showed in **Figure 88**-A and **Figure 88**-B, and the chromatograms are shown in **Figure 88**-C. As for the pre-formulation studies, the concentration of mAb in 40 $mg.mL^{-1}$ (HD).

For the formulation T-HD, the sample solutions were white due to the presence of the white powder of copolymer but turned limpid after the addition of the mobile phase. At day 0 and day 3, the absorbance at 280 nm, the relative wavelength ratio and the relative AUC were nearly constant. Then, from day 3, the intensity and the relative AUC of mAb progressively decreased but the relative wavelength ratio remained constant. These results suggested the interaction of mAb with the copolymer that decreases the amount of mAb detected, which is consistent with the results of the pre-formulations study.

For the formulation T/T-PDA-HD, the sample solutions were black then blurred after the addition of the mobile phase. From day 0 to day 30, the absorbance and the relative AUC of the mAb detected progressively decreased but the relative wavelength ratio remained constant suggesting an interaction of mAb with the copolymer. It should be noted that the absorbance at day 0 of T/T-PDA-HD is divided by 2 compared to formulation of T-HD, showing a stronger initial interaction of mAb towards the mix of T and T-PDA. Besides, the decrease of the amount of mAb detected from day 0 to day 30 is higher in formulation T/T-PDA-HD (93% of mAb detection loss) than in formulation T-HD (63% of mAb detection loss).

For the formulation T-PDA-HD, the absorbance was around 5% at 280 nm but not sufficient at 254nm to calculate the wavelength ratio at day 0. Then, no mAb was detected from day 3 to day 30. This suggests a strong interaction between mAb and T-PDA. Regarding the pre-formulation stability study, it was shown that a progressive decrease of mAb was observed in the presence of copolymers. These results confirm that our PDA-based copolymers show a strong affinity towards mAb, which is in agreement with data of literature indicating immobilization of biomolecules, such as proteins, at the surface of PDA-based materials, thanks to the catechol, quinone and amine units [103–105].

As a result, the comparisons of SEC-UV spectra demonstrate that the 3 formulations composed of HBS:PEG_{400} (1:1) and 10% (w/v) of copolymer – T , T/T-PDA, and T-PDA – interacted with mAb without denaturation of the mAb. The highest decrease in the amount of mAb was observed in the presence of T-PDA, proving the high affinity of mAb towards PDA.

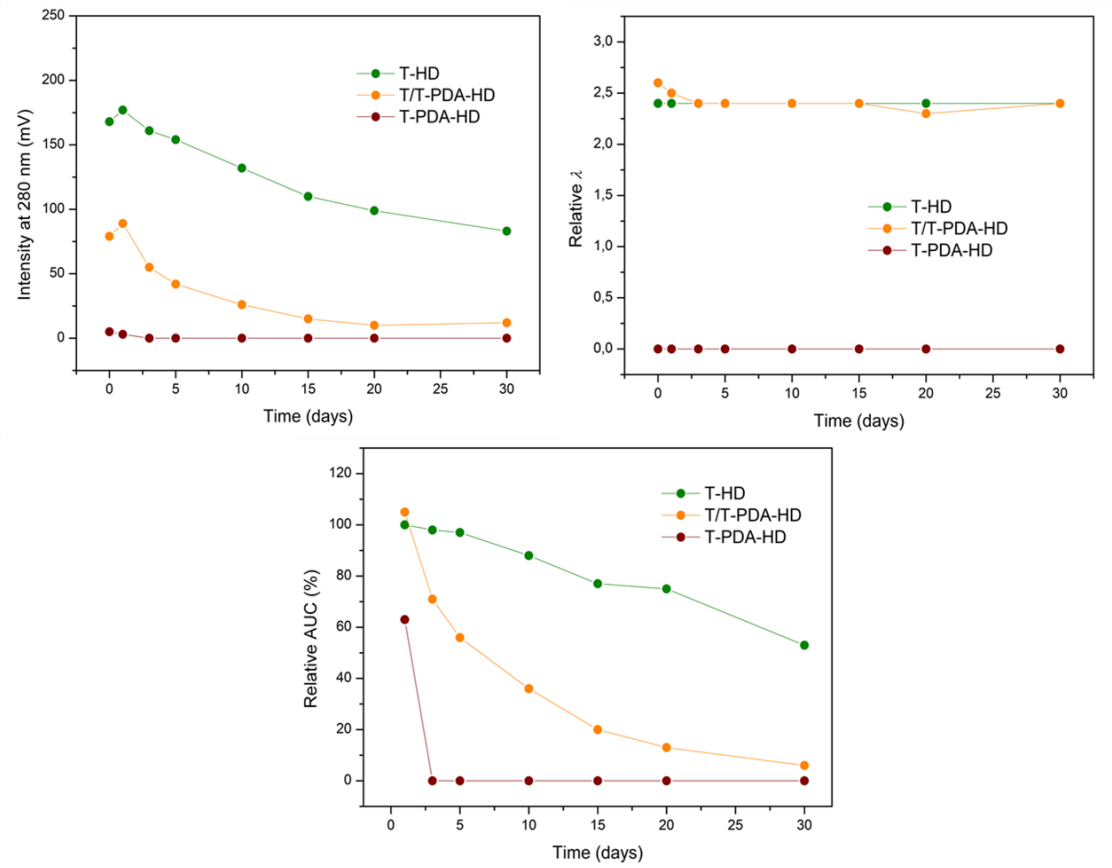

Figure 87. Evolution of the absorbances, wavelength ratio, and relative AUC of mAb detected in the formulation T-HD, T/T-PDA-HD and T-PDA-HD

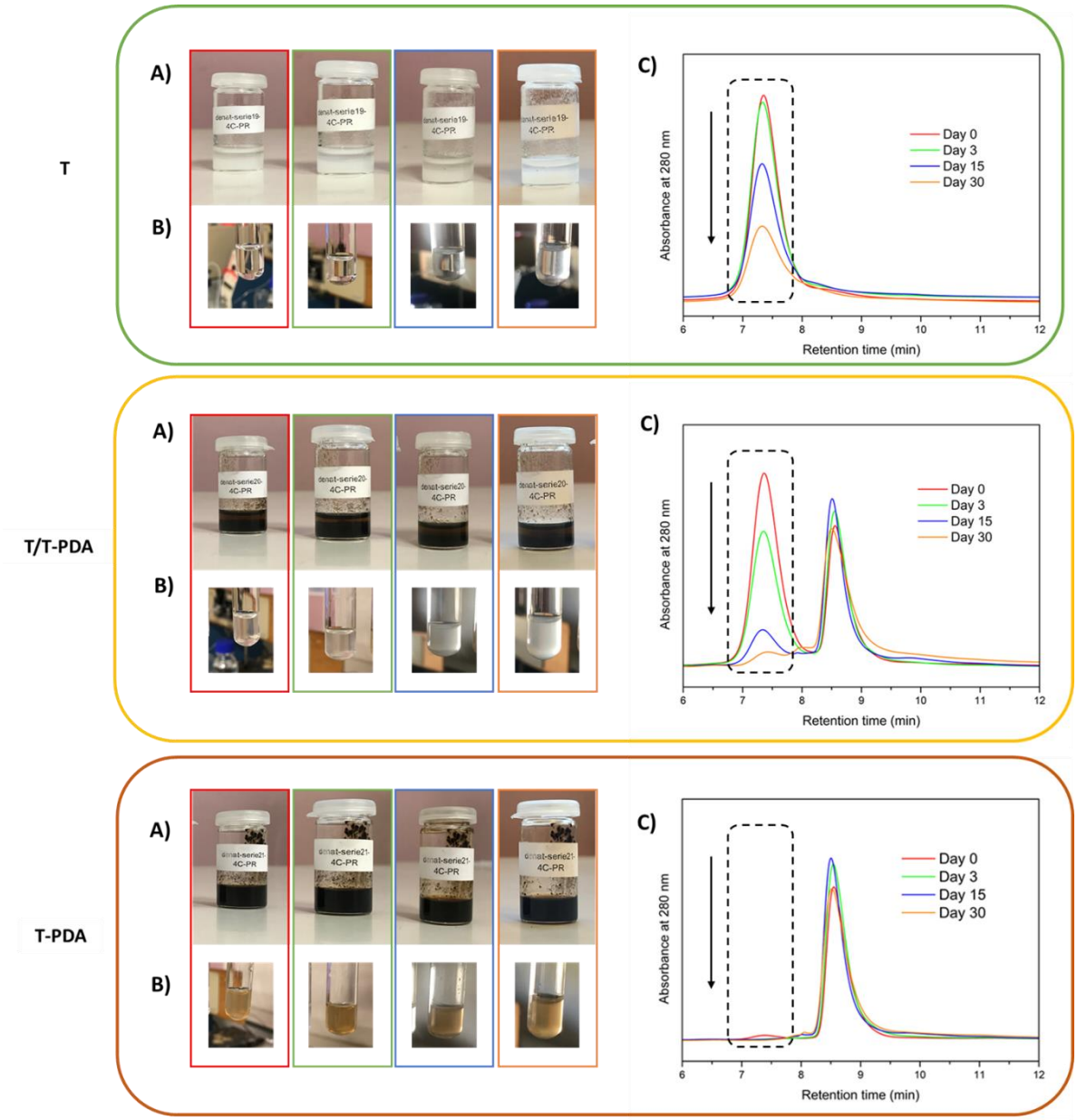

Figure 88. Stability study of mAb in formulations composed of T-HD, T/T-PDA-HD, and T-PDA-HD in HBS:PEG_{400} = 1:1. Photographs of the samples A) before and B) after additions of the mobile phase and C) SEC chromatograms obtained at 280 nm. T refers to assay I6/G6 (**Table 16** and **Table 18**) and T-PDA refers to **Table 19**

5.2 In vitro release of mAb

5.2.1 Description of the experiment

The aim was to study the impact of the presence of PDA units in the copolymer over the formation of the *in situ* depots and if it modifies the release of mAb. The, three final formulations selected for mAb stability were also used for the *in vitro* release experiments at two concentration of mAb at 40 $mg.mL^{-1}$ (HD) or 13 $mg.mL^{-1}$ (LD) corresponding respectively to DL= 44 % and 21% (w/w with respect to copolymer). By selecting those amounts of incorporated mAb we aim to deliver enough mAb to reach the therapeutic level after administration, which is a major concern for the application (Chapter I). The formulations were prepared and used straight afterwards in order to limit the progressive complexation of mAb with copolymers observed during the stability studies (**Figure 87** and **Figure 88**).

A volume of 200 µL was sampled from the formulation and injected through a needle in 8 mL of PBS, which corresponded to the intravitreal administration of 100 µL in 4 mL of vitreous humour. Samples were analysed by SEC with UV detection. In order to quantify the amount of mAb released in PBS, a calibration curve was established in a concentration range compatible with our systems, 0 to 1500 $\mu g.mL^{-1}$, represented in **Figure 97** in Appendix.

5.2.2 The in-situ formation of the depots

The formation and the evolution of the aspect of the *in-situ* depots for the formulations T-HD, T/T-PDA-HD and T-PDA-HD are shown in **Figure 89**-A, **Figure 89**-B and **Figure 89**-C respectively. The respective LD formulation looked similar.

Immediately after injection (day 0), we observed the formation of *in-situ* depots at the bottom of the vials. The formulation T formed gel-like precipitated white chunks at day 3 due to the mechanism of solvent-exchange where PEG_{400} that diffused into PBS. The aggregates seemed to became smaller from day 5 to day 30. The formulation T/T-PDA formed smaller – due to the lower amount of T – and black – due to the T-PDA – chunks at day 3 and the aspect remained similar until day 30. A slight coloration of the release medium was observed probably due the release of PDA-based impurities (*e.g*. the ones detected in SEC-UV corresponding to the additional peak). The formulation T-PDA formed a thin film with a part adhering to the bottom at day 3 and the aspect remained similar until today 30, with a coloration of the medium induced for the reason described previously.

As described in Chapter I, we would like to develop injectable formulation able to form a gel-like depot to overtake the drawbacks related to the use of particulate formulations such as the spreading/suspension in the vitreous humour and to the front of the eye, and the aggregation that could blur the vision [214] or obstruct the vessels. Despite the fact that the vitreous humour is a very

viscous diffusion-limiting aqueous solution, the small chunks formed after administration of the formulations T and T/T-PDA (HD or LD) might present a risk of spreading/suspension/obstruction *in vivo*. The thin films obtained from formulation T-PDA are potentially less risky due to their much larger size that would hinder diffusion in the vitreous. However, the coloration of the medium induced by formulations T/T-PDA and T-PDA might be taken into consideration for the administration into the eye. However, and despite the distinct structures and properties (*e.g.* aqueous solubility and crystallinity), of the PCL-*g*-PDA implants compared to the T-PDA copolymers, no coloration of PBS was observed during the *in vitro* degradation and release experiments of PCL-*g*-PDA implants purified 3 times. This coloration issue induced by T-PDA may be solved by removing the impurities of synthesis.

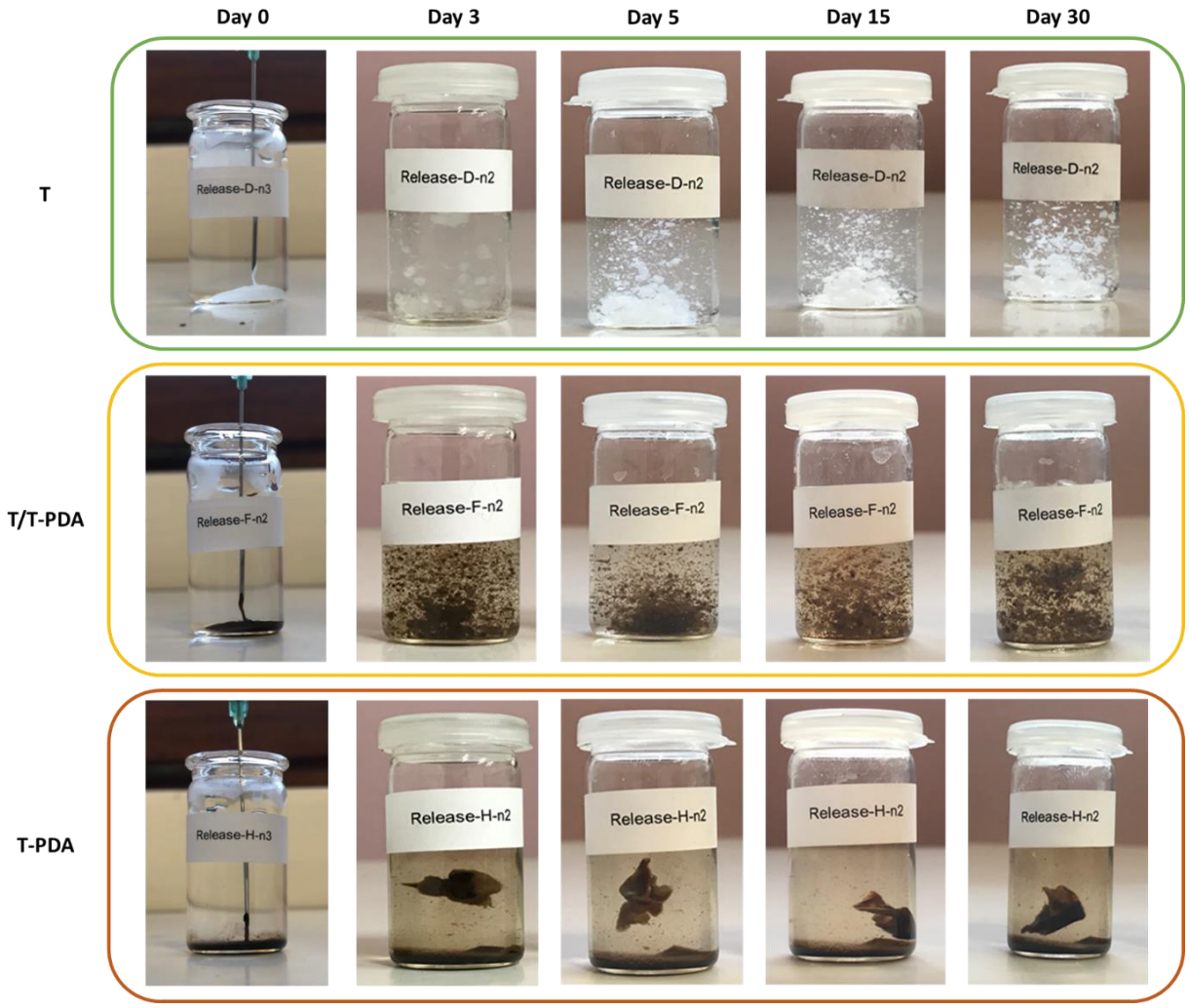

Figure 89. The formation and the evolution of the aspect during 30 days of the *in-situ* depots for the formulations T-HD or T/T-PDA-HD (2:1) and T-PDA-HD. T refers to assay I6/G6 (**Table 16** and **Table 18**) and T-PDA refers to **Table 19**.

5.2.3 Quantification of mAb released

Blank formulations (unloaded mAb formulation but containing polymers) and loaded formulations were prepared and studied under the same conditions. All samples were analyzed by SEC using UV detection (λ = 280 nm) and the curves obtained with blanks were subtracted to the curves of the loaded samples in order to compensate for the possible degradation of the polymer or the presence of impurities. The evolution of the characteristic parameters of SEC is shown in **Figure 90** and the SEC profiles are shown in **Figure 91**. The progressive decrease of detected mAb from T/T-PDA formulation suggested an interaction of the mAb with the polymers and the apparition of additional peaks at higher and lower retention time from day 15, similar to the peaks obtained during the stress test (**Figure 94** and **Figure 95** in Appendix), suggested the destabilisation of the mAb. The progressive decrease in wavelength also suggested a denaturation of mAb. In the case of T formulations, the detected mAb decreased but the wavelength ratio and profiles were similar, suggesting mAb-T interaction without denaturation. It seems that the formulations containing T-PDA favour the denaturation of the drug from day 15 in *in vitro* conditions. In the case of T-PDA formulation, no mAb peaks or denatured peaks were observed, suggesting the absence of mAb in the release medium.

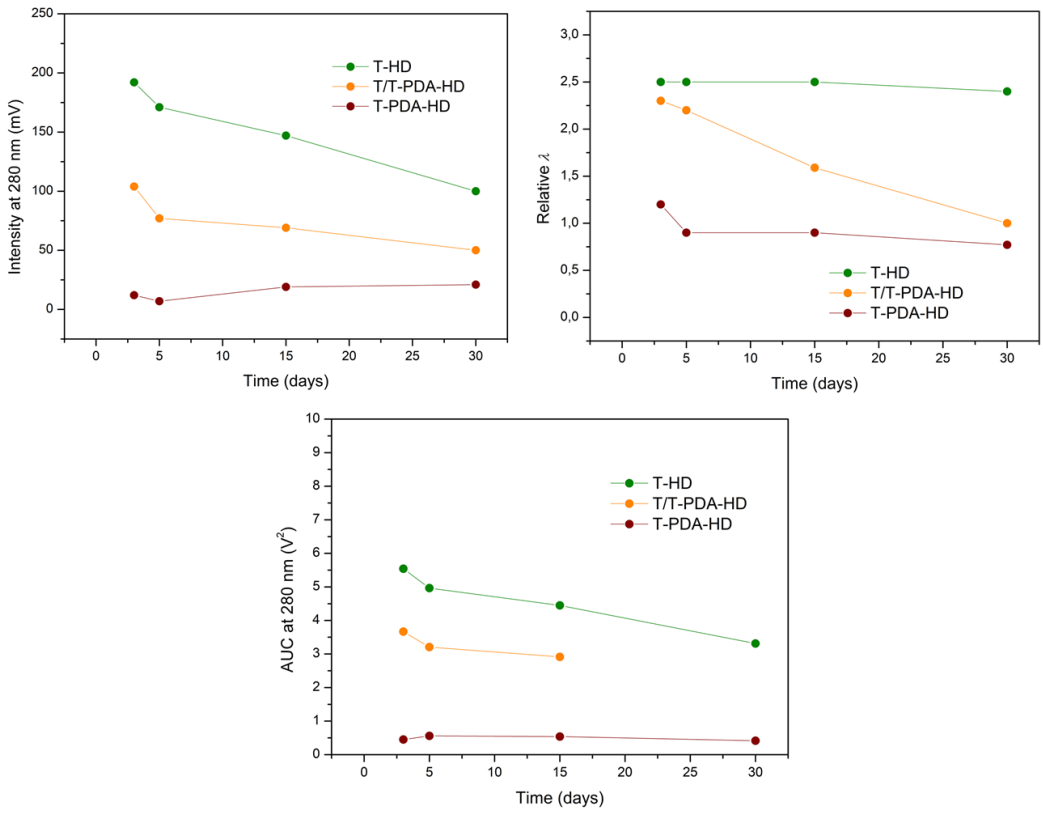

Figure 90. Evolution of the intensity, wavelength ratio, and AUC at 280 nm of mAb detected released in PBS from the formulation T-HD, T/T-PDA-HD and T-PDA-HD.

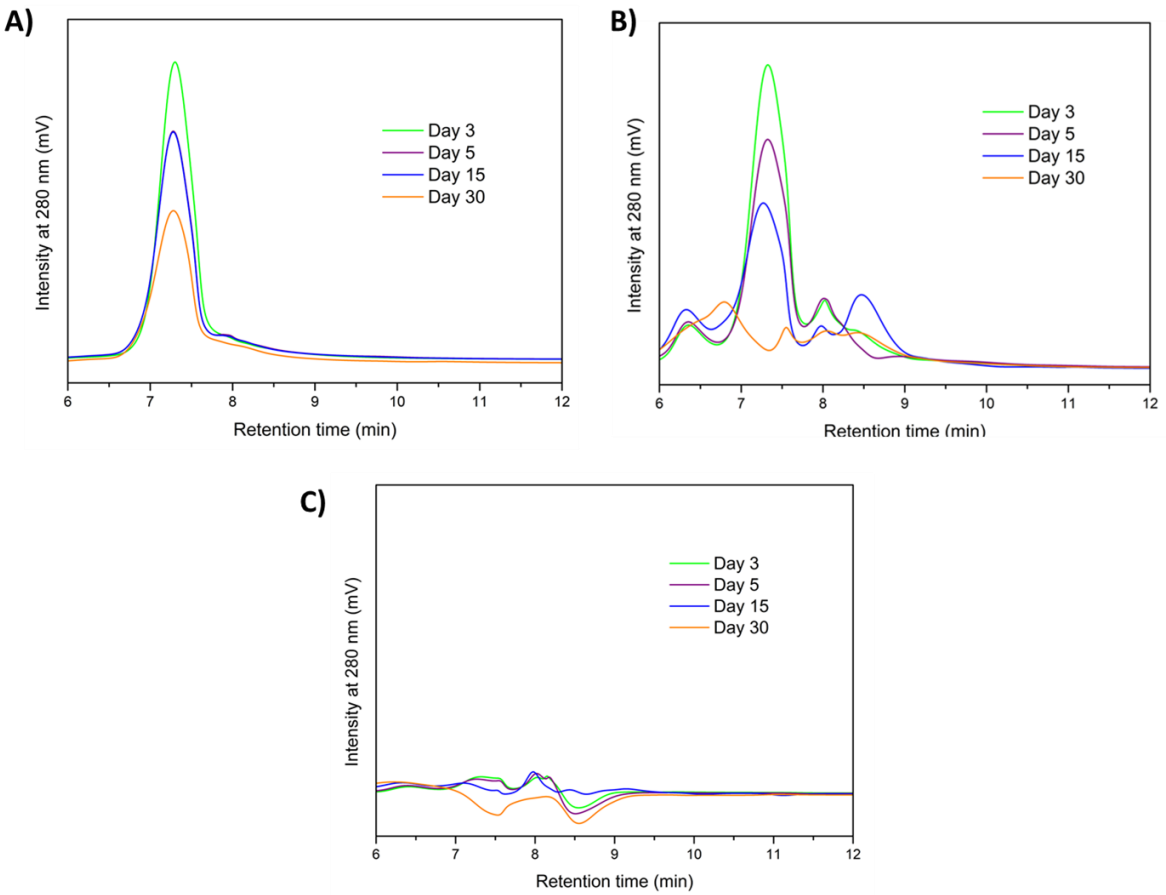

Figure 91. SEC chromatograms obtained at 280 nm from *in vitro* release from A) T-HD, B) T/T-PDA-HD and C) T-PDA-HD formulations. T refers to assay I6/G6 (**Table 16** and **Table 18**) and T-PDA refers to **Table 19**

The quantification of mAb release is based on the AUC at a specific range of retention times previously defined. Release profiles of mAb from each formulation are shown in **Figure 92**-A for HD formulations and in **Figure 92**-B for LD formulations. **Figure 92**-A shows the release profiles obtained with the different HD formulations. For the formulation T-HD, the release of mAb was almost completed at day 3 (DR=87%) due to a burst effect. The content of mAb remained nearly constant during 30 days of analysis. For the formulation T/T-PDA-HD, the cumulative release of mAb was lower at day 3 and 5 (DR=57%) than in formulation T-PDA-LD. For formulation T-PDA-LD, no release of mAb was observed during 30 days. The maximum of mAb released matched with the fraction of mAb detected – unbound fraction – during the study of the stability. Indeed, the intensities of the peak of the fraction of mAb detected were 158, 79 and 0 for formulations T-HD, T/T-PDA-HD and T-PDA-HD respectively corresponding by proportion to 84, 40 and 0 % taking account an intensity of 200 for the peak of mAb without copolymer. **Figure 92**-B showed similar release profiles for LD formulation (DR = 87% | 57% | 0% at day 3) compared to respective HD formulations.

Thus, release investigations showed that part of mAb does not interact with the copolymer and was released within 3 days in a burst effect, while the interacting mAb remained unreleased after 30 days. The complete release of mAb was probably due to the presence of mAb only at the surface, to the slow formation of depots due to the slow kinetics of solvent-exchange between PEG_{400} and PBS, or to the formation of a too distended polymer network. Moreover, the lower release rate and amount of T/T-PDA formulation and T-PDA formulation compared to T formulation were attributed to the addition of PDA in the systems whose drug-binding affinity seems to be the predominant factor for the regulation of the kinetics of release of mAb, as already encountered for the regulation of the hydrophobic drugs (Chapter II).

The release profile of APIs is generally composed of 1, 2 or 3 steps and the last step might be a burst effect due to the complete degradation of the (co)polymer releasing the remaining amount of drug entrapped in the depot. In our case, mAb seemed to be in strong interaction with the T-PDA copolymers due to the presence of catechol moieties. Therefore, the complete release of mAb (DR=100%) from the formulation would probably occur during the degradation of PDA (by oxygen-induced process, by alkalinity-driven process or by micro-organism as described in Chapter I).

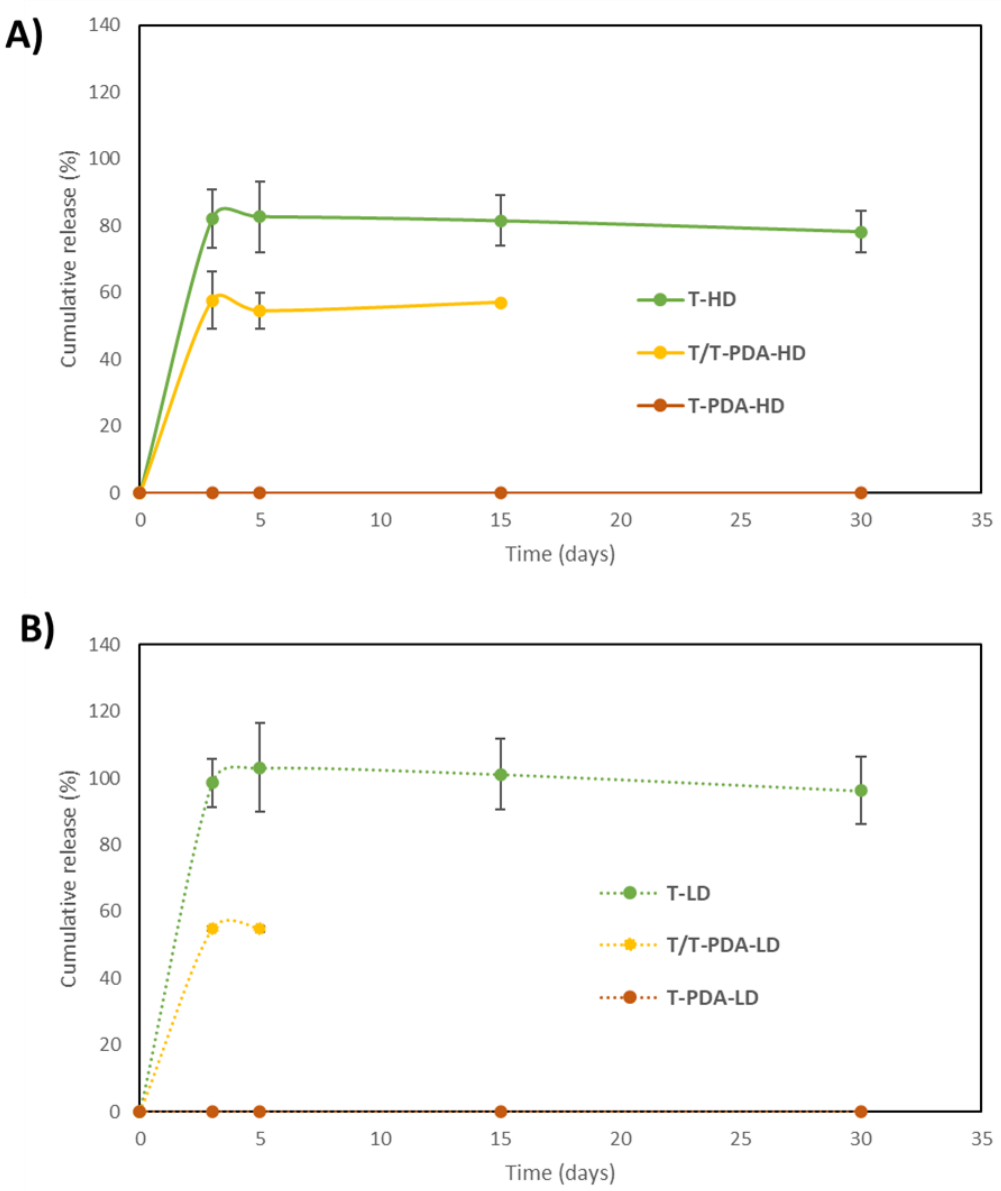

Figure 92. In vitro release of mAb from formulation T and T/T-PDA (2:1) loaded with A) 44% (HD) or B) 21% (LD) of mAb. T refers to assay I6/G6 (**Table 16** and **Table 18**) and T-PDA refers to **Table 19**.

5.3 Conclusion

In this part we developed a formulation composed of HBS:PEG_{400} of 1:1 (v/v) containing of 5 % (w/v) of i) T, ii) a mix of T and T-PDA at a ratio 2:1 and iii) T-PDA. The formulations were loaded with either 21 (LD) or 44% (HD) of mAb with respect to the amount of copolymer. The evaluation of mAb stability in the HD-formulation showed a progressive decrease of mAb detected without denaturation. The highest decrease of detected mAb is observed in the presence of T-PDA, proving the high affinity of mAb toward PDA moiety. The *in vitro* release assays demonstrate that PDA causes a higher retention of mAb. The whole content of unbound fraction of mAb to PDA was released in 3 days showing a burst release effect probably due to the slow formation of the depot upon solvent-exchange process, the location of mAb at the surface of the depot, or at a too distended network unable to retain t. The T formulation favoured the stability of mAb release while T-PDA based formulations tended to destabilize a fraction of mAb in the release medium.

6. Conclusion

In this chapter, our aim was to synthesize a new amphiphilic copolymer and design injectable liquid formulations that can be used for intravitreal drug delivery applications. We chose to design a new copolymer composed of amphiphilic copolymer PCL-*b*-PEG-*b*-PCL (T) on which PDA was grafted to combine biocompatibility, (bio)degradability, stimuli-responsiveness and binding properties toward the selected protein mAb.

The first part (section 1) of the study was dedicated to the 3 steps synthesis of the grafted amphiphilic copolymer T-PDA. The first step was the synthesis of the amphiphilic T triblock with different chain lengths. The evaluation of the aqueous properties showed no thermo-responsiveness but only changes in solubility regarding the compositions. A copolymer showing gelling propensity was selected. The second step was the functionalization of the PCL chains of T with iodine. The third step involved the simultaneous oxidative polymerization of dopamine, the grafting of dopamine units and/or oligo-PDA via ATRP-like conditions on iodinated PCL units of T and further growth PDA (T-PDA). The confirmation of the grafting of PDA, the content of PDA in copolymer and the thermal properties were evaluated by NMR, SEC, UV, TGA and DSC. The raw T-PDA copolymer contained around 40 wt% of PDA with a proportion of unbound PDA. The respective proportion of grafted-PDA and unbound PDA was unknown and, the high proportion of free oligo-PDA resulted from a defect in the method of purification.

The second part (section 2) of the study concerned the elaboration of the formulations suitable for IVT injection through a 30G needle and providing stability of mAb for the storage. A co-solvent process using water and PEG_{400} was required to solubilize mAb and the copolymers. The evaluation of the force of injection by compression technique and the evaluation of the stability of mAb by aqueous SEC showed the impact of each components in the formulation in order to draw the adequate formulation composed of HBS:PEG_{400} at a ratio 1:1 (v/v), 5% (w/v) of copolymer and loaded with 40 $mg.mL^{-1}$ of mAb.

The third part (section 3) of the study concerned the evaluation of the ability of T and T-PDA to retain mAb from the in situ forming depots. The stability study of various formulations showed the high affinity of mAb towards PDA without denaturation at 4°C. The *in vitro* release of mAb performed in physiological conditions showed the ability of T-PDA to make strong interactions with mAb. It is shown that mAb not bound with the copolymer was released before 3 days in a burst effect, while the bound mAb remained unreleased within 30 days. The T formulation favoured the stability of mAb released while T-PDA based formulations tended to destabilize a fraction of mAb in the release medium at 37°C.

As a conclusion, T-PDA is offering interesting perspectives (**Table 22**) in term of injectability for the IVT administration thought a 30G needle and stability of the mAb for the storage at 4°C. However, the influence of the PDA on the release of mAb in *in vitro* conditions was not really conclusive. Indeed, the proportion of remaining free-PDA in the formulation may strongly interact with the mAb, thus impacting the release of mAb from T-PDA based formulations. By removing the free-PDA, the release profile of mAb may differ and the duration of release may be extended in similar way PCL-*g*-PDA implant (Chapter II) offer.

Table 22. Criterial for ocular long-acting delivery for T-PDA in situ depots

Criterial for ocular long-acting delivery	**mAb-loaded T-PDA based in situ forming depots**
Formulation	Soluble (water and PEG_{400})
Injectability	Yes (30G needle)
Stability of mAb (storage at +4°C)	Yes (30 days)
Stability of mAb (release at +37°C)	Yes (<15 days)
High drug loading	Yes (DL=21 or 44 wt.% w.r.t copolymers)
Lag time	No
Limited burst	No
Sustained release	No (< 3 days) but the bounded mAb fraction to PDA not released
Degradation	Need to be performed
Ocular tolerability	Need to be performed

7. Appendix

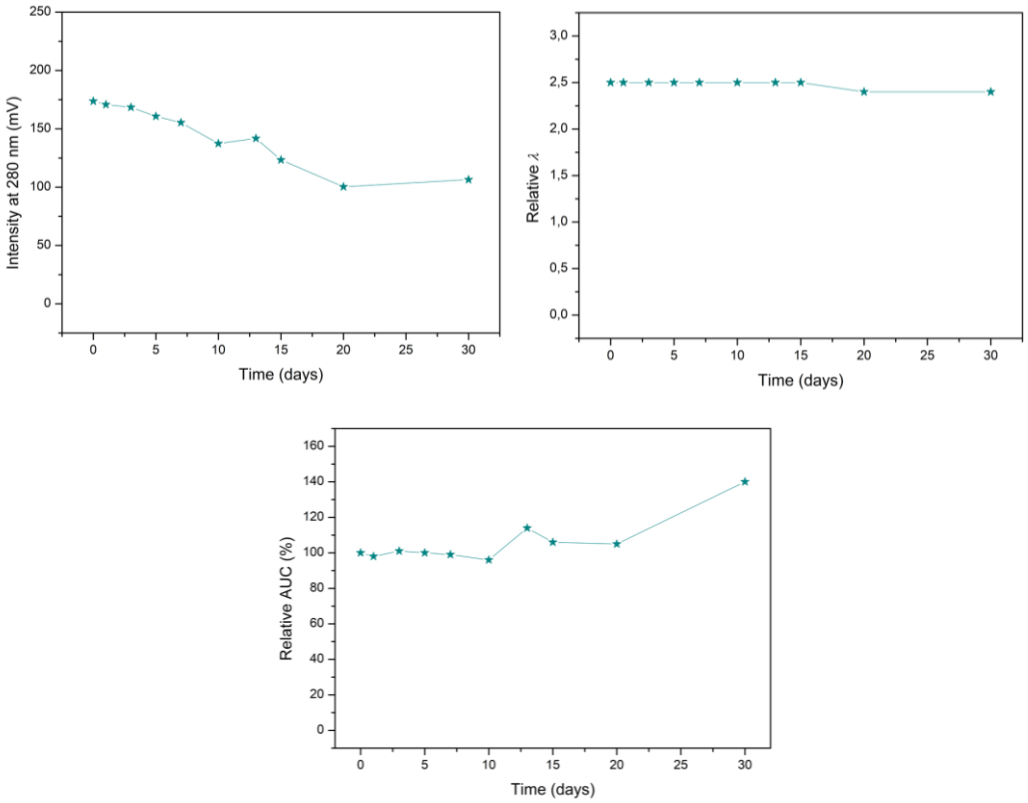

Figure 93. Evolution of the intensity, wavelength ratio, and relative AUC of mAb detected in stess conditions

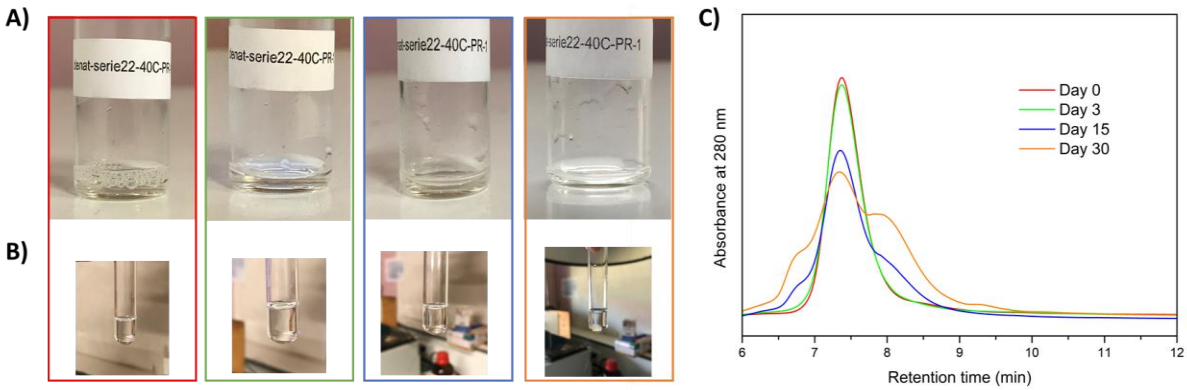

Figure 94. Stability study of mAb at 37°C in PBS (stress conditions). Photographs of the samples A) before and B) after additions of the mobile phase and C) SEC chromatograms obtained at 280 nm.

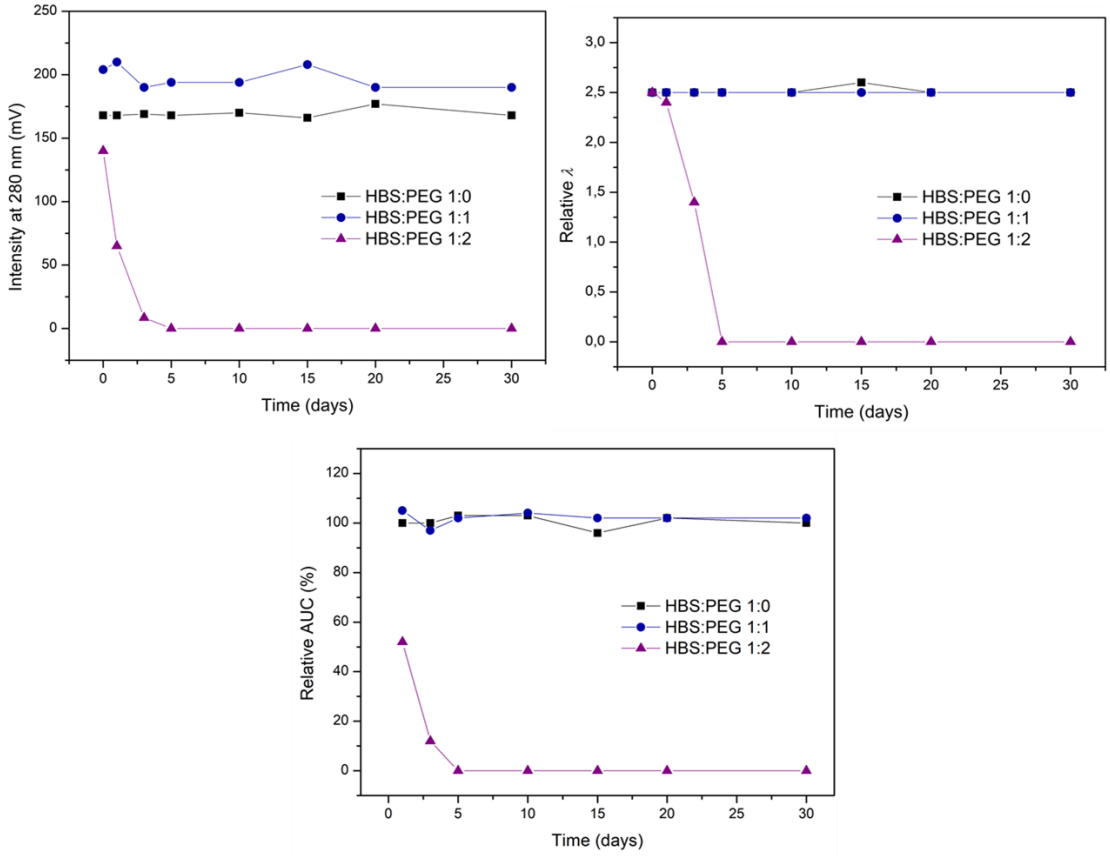

Figure 95. Evolution of the absorbances, wavelength ratio, and relative AUC of mAb detected at various HBS:PEG_{400} ratios

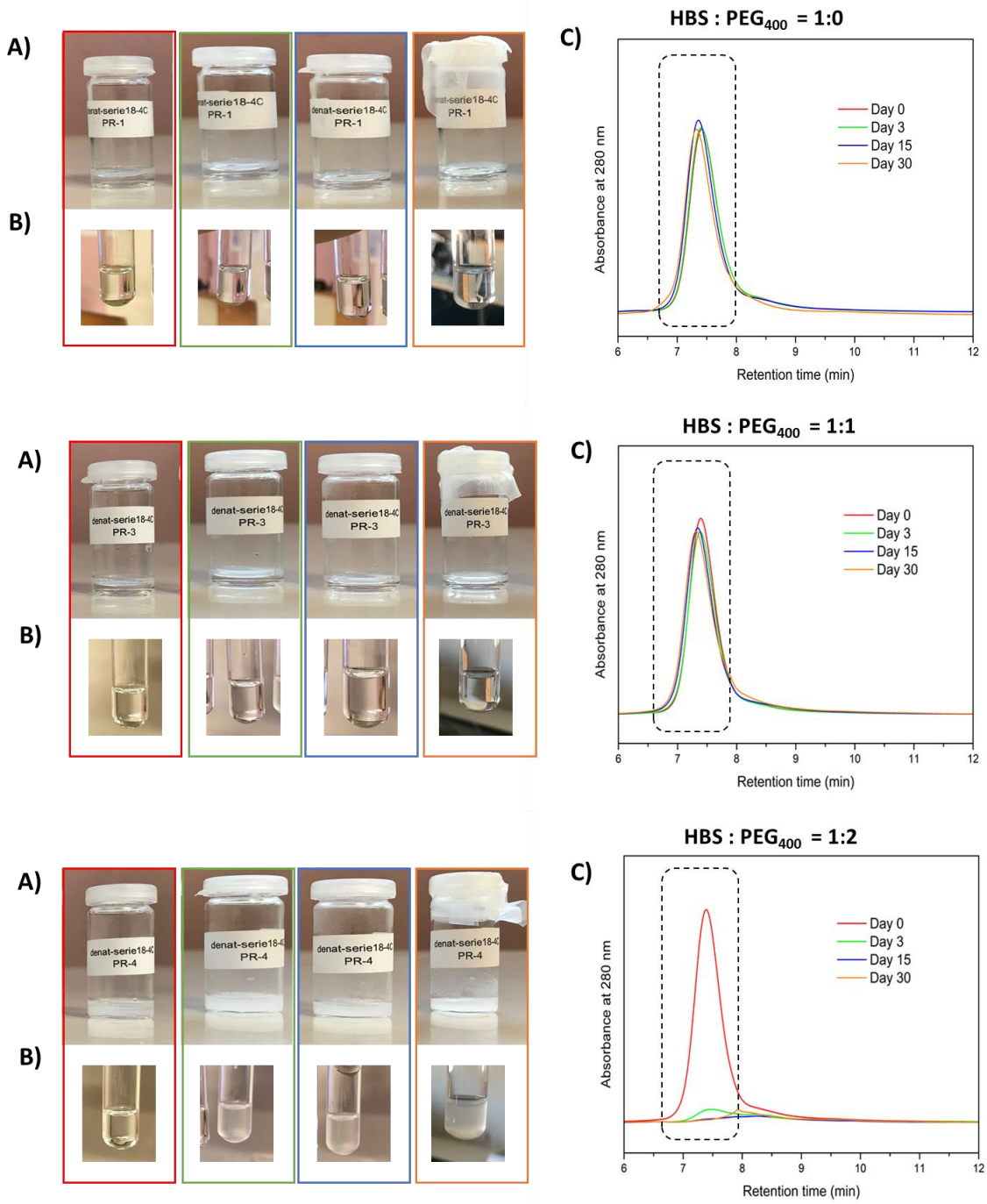

Figure 96. Stability study of mAb at various HBS:PEG_{400} ratio. Photographs of the samples A) before and B) after additions of the mobile phase and C) SEC chromatograms obtained at 280 nm.

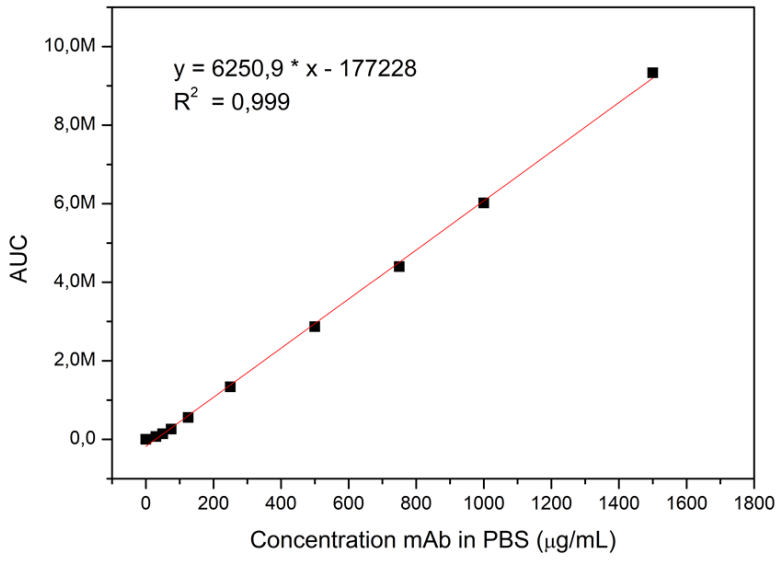

Figure 97. Calibration curves obtained from the dissolution of mAb in PBS by SEC

CONCLUSION AND OUTLOOKS

The ocular diseases refer to any condition or disorder that interferes with the ability of the eye to function properly and/or that negatively affects the visual clarity and are a major public health issue. The IVT administration – including implantation of medical devices or injection of suspensions, solutions or implant – is a routine method and is the most efficient one to deliver APIs to the retina. The main challenges of the IVT administration are the decrease in the frequency of injection to improve the patient compliance and adherence to the treatment, the ocular tolerability of the formulations and the stability of the biologics. At present, it is still challenging to satisfy all the specifications and the formulations based on polymer technology are marginal, recent but may solve those issues. Scientists are focusing their efforts on developing biocompatible, (bio)degradable or not, formulations providing long and sustained delivery of APIs with a minimal surgery operation in order to increase the well-being of patients and to reach therapeutic level to treat efficiently the ocular diseases.

The objective of this work was to evaluate the benefits of incorporation of PDA units in the design of novel copolymers for ophthalmology, with improved tolerability and superior sustained release features (of small or large molecules) thanks to preferential drug-PDA interactions. Among the polymers used in medical and/or drug delivery applications, the degradable synthetic-based formulations show interesting and promising properties. Particularly, PCL is biodegradable, degrades slowly, can be functionalized and is approved by the FDA for medical purpose (but not ophthalmic yet). Also, PEG is bio eliminable (function of its molecular weight), approved by the FDA for ophthalmic application and offer tunable gelation properties in combination with PCL. Two strategies were developed, one solid formulation for the delivery of small molecules, and the other one, a situ gelling system for the delivery of biologics.

The solid implant approach was achieved by designing a hydrophobic grafted copolymer PCL-*g*-PDA. The copolymer was synthesized in a two-step process. Firstly, the PCL (M_n=190 000 g.mol^{-1}) was post-functionalized by iodine via an electrophilic substitution to give an iodinated PCL (PCL-I). Secondly, PCL-I was functionalized by PDA under ATRP-like, oxidative and basic conditions to give a PCL-*g*-PDA copolymer containing ≅ 3 wt. % of grafted PDA. The *in vitro* cytotoxicity assays showed that the implants PCL-*g*-PDA were non-cytotoxic on mouse fibroblast cells and retinal cells and the importance of purification of the copolymer was highlighted. The first objective of ocular tolerance was reached. Besides, the implants were not degraded in physiological conditions over 110 days but degraded under accelerated conditions, proving the ability of PCL-*g*-PDA implant to degrade slowly which was the second objective of the project. *In vitro*, PCL-*g*-PDA implants showed a sustained, constant and complete release (zero-order kinetics) of water-insoluble dexamethasone (DL=30% w/w) during 155 days. In contrast PCL-*g*-PDA implants showed a burst effect followed by a sustained release of water-soluble ciprofloxacin hydrochloride (DL=30% w/w) during 125 days with an extrapolation of complete

release after around 500 days. In all cases, the kinetics of release for PCL-*g*-PDA implants were slower compared with PCL implants, thus showing the ability of PDA to retain the drug inside the implant, even with a low amount of grafted PDA, thanks to its interactions with the drug. The third objective of high drug loading and the fourth objective of superior sustained release properties of the PCL-g-PDA over PCL implants were reached. Moreover, PCL and PCL-*g*-PDA implants showed a longer release time of dexamethasone compared to the commercial PLGA-based implant (Ozurdex™).

Among the possible improvement/perspectives various points could be explored. It should be noted, however, that the *in vitro* release curve of DEX from PCL-g-PDA meets all the required criteria, in terms of release rate and biocompatibility. In any case, it would be interesting to first control and increase the percentage of grafted PDA in the PCL-*g*-PDA to study the impact of the proportion of PDA on the kinetics of release of small molecules. Due to the PDA-drug affinity, the release time is expected to be extended, thus improving the release performance of the implant. Second, the shift from lab scale to industrial scale should be evaluated which would require to adapt the synthesis procedure to improve the yield and the purification mode. Third, during this PhD work, the implants were obtained by hot melting compression and were considered as prototype. The shape and dimensions of the implant could be modified depending on the manufacture process, where extrusion or moulding techniques are the most frequently used in industry. Finally, it would be necessary to evaluate the PCL-*g*-PDA implants *in vivo* in the frame of pre-clinical studies to assess the ocular biocompatibility through histology of the ocular tissues, to evaluate the kinetics of release of the small molecule drugs and the amount released to ensure a therapeutical effect. Rabbits or monkeys are preferential animal models.

The in-situ gelling system approach was investigated by developing an amphiphilic grafted copolymer (PCL-*g*-PDA)-*b*-PEG-*b*-(PCL-*g*-PDA). Firstly, amphiphilic triblock PCL-*b*-PEG-*b*-PCL were synthesized at various PEG and PCL chain lengths to generate an in-situ forming gel at physiological temperature in water. Whatever the composition, no sol-gel transition was observed. Accordingly, a PCL-*b*-PEG-*b*-PCL showing gelling capacity at room temperature was selected. This PCL-*b*-PEG-*b*-PCL was functionalized via iodine by an electrophilic substitution to give (PCL-I)-*b*-PEG-*b*-(PCL-I), which was functionalized by PDA under ATRP-like, oxidative and basic conditions. The raw (PCL-*g*-PDA)-*b*-PEG-*b*-(PCL-*g*-PDA) contained 40 wt. % of PDA and was water-insoluble. Analyses showed the presence of bound and unbound PDA, but the respective proportions cannot be calculated due to unknown structure of PDA. We designed a soluble co-solvent formulation containing PCL-*b*-PEG-*b*-PCL, (PCL-*g*-PDA)-*b*-PEG-*b*-(PCL-*g*-PDA), PEG_{400}, water and mAb. A formulation composed of water and PEG_{400} (ratio water/PEG_{400}=1) as solvent, containing 5 wt.% of PCL-*b*-PEG-*b*-PCL copolymers and loaded with 40 $mg.mL^{-1}$ of mAb was

injectable through an 30G needle. The first objective of injectability with minimum of invasion was reached. The stability study of mAb showed the ability of (PCL-*g*-PDA)-*b*-PEG-*b*-(PCL-*g*-PDA) to interact with mAb without causing its denaturation during 30 days. The second objective of stability of the mAb in the formulation was reached. *In vitro*, this formulation formed an in-situ gelling depot by solvent-exchange process, as desired. Release investigations showed that part of mAb does not interact with the copolymer and was released within 3 days in a burst effect, while the interacting mAb remained unreleased after 30 days. The third objective of high drug loading was reached. The fourth objective of extended release was compromised but the release profiles achieved so far were not really conclusive because of the unbounded PDA. Indeed, F.Hoffmann-La Roche showed internally that pure PDA particles interact strongly with mAb and may, thus, may influence its release.

Among the possible improvement/perspectives, various points should be considered. It would be necessary to first establish an efficient purification method to remove the unbound fraction of PDA from the copolymer. Indeed, the role of the unbound PDA on the interaction with mAb as well as on the water insolubility of the PDA-functional copolymer may be important. Second, the *in vitro* evaluation of the cytotoxicity of the formulation should be performed prior to any consideration of in vivo ocular tolerability, and the activity of the mAb release should also be evaluated. The presence of by-products of the chemical reactions in the copolymer could induce a cytotoxic effect, as highlighted in the implant strategy, showing the importance of the purification process. Third, the shift from lab scale to industrial scale should be evaluated. Finally, the *in vitro* degradation rate of the copolymer should be evaluated and correlated with the expected kinetics of release of the fraction of mAb interacting with the copolymers. Additionally, other macromolecules or even small molecules could be loaded to study their interaction with PDA and their stability in formulations during storage and release.

Overall, this work has contributed to develop new PDA-based biomaterials to respond to the challenges of minimally invasive long-acting ocular delivery using biocompatible degradable synthetic copolymers. It succeeded in developing PDA-based implants suitable for the long-term delivery of small molecules and PDA-based injectable in situ gelling system promising for the formulation of biologics. The results generated open perspectives for the further industrial development of innovative ocular drug delivery systems.

Bibliography

(1) Flaxman, S. Global Causes of Blindness and Distance Vision Impairment 1990–2020: A Systematic Review and Meta-Analysis. *The Lancet Global Health* **2017**, *5* (12), e1221–e1234. https://doi.org/10.1016/S2214-109X(17)30393-5.

(2) Rimpelä, A.-K.; Reinisalo, M.; Hellinen, L.; Grazhdankin, E.; Kidron, H.; Urtti, A.; Del Amo, E. M. Implications of Melanin Binding in Ocular Drug Delivery. *Advanced drug delivery reviews* **2018**, *126*, 23–43. https://doi.org/10.1016/j.addr.2017.12.008.

(3) Wang, Z.; Duan, Y.; Duan, Y. Application of Polydopamine in Tumor Targeted Drug Delivery System and Its Drug Release Behavior. *Journal of Controlled Release* **2018**, *290*, 56–74. https://doi.org/10.1016/j.jconrel.2018.10.009.

(4) Liu, Y.; Ai, K.; Lu, L. Polydopamine and Its Derivative Materials: Synthesis and Promising Applications in Energy, Environmental, and Biomedical Fields. *Chemical reviews* **2014**, *114* (9), 5057–5115. https://doi.org/10.1021/cr400407a.

(5) Smith, T. J. Intravitreal Sustained-Release Ganciclovir. *Arch Ophthalmol* **1992**, *110* (2), 255. https://doi.org/10.1001/archopht.1992.01080140111037.

(6) Auritec Pharmaceuticals - Vitrsert® and Retisert ® http://www.auritecpharma.com/vitrasert-retisert (accessed 2020 -04 -28).

(7) Haghjou, N.; Soheilian, M.; Abdekhodaie, M. J. Sustained Release Intraocular Drug Delivery Devices for Treatment of Uveitis. *JOURNAL OF OPHTHALMIC AND VISION RESEARCH 6* (4), 14.

(8) Kane, F. E.; Burdan, J.; Cutino, A.; Green, K. E. Iluvien ™ : A New Sustained Delivery Technology for Posterior Eye Disease. *Expert Opinion on Drug Delivery* **2008**, *5* (9), 1039–1046. https://doi.org/10.1517/17425247.5.9.1039.

(9) Administration. *Iluvien*.

(10) Campochiaro, P. A.; Marcus, D. M.; Awh, C. C.; Regillo, C.; Adamis, A. P.; Bantseev, V.; Chiang, Y.; Ehrlich, J. S.; Erickson, S.; Hanley, W. D.; Horvath, J.; Maass, K. F.; Singh, N.; Tang, F.; Barteselli, G. The Port Delivery System with Ranibizumab for Neovascular Age-Related Macular Degeneration. *Ophthalmology* **2019**, *126* (8), 1141–1154. https://doi.org/10.1016/j.ophtha.2019.03.036.

(11) Chang-Lin, J.-E.; Attar, M.; Acheampong, A. A.; Robinson, M. R.; Whitcup, S. M.; Kuppermann, B. D.; Welty, D. Pharmacokinetics and Pharmacodynamics of a Sustained-Release Dexamethasone Intravitreal Implant. *Invest. Ophthalmol. Vis. Sci.* **2011**, *52* (1), 80. https://doi.org/10.1167/iovs.10-5285.

(12) Grzybowski, A.; Told, R.; Sacu, S.; Bandello, F.; Moisseiev, E.; Loewenstein, A.; Schmidt-Erfurth, U.; on behalf of the Euretina Board. 2018 Update on Intravitreal Injections: Euretina Expert Consensus Recommendations. *Ophthalmologica* **2018**, *239* (4), 181–193. https://doi.org/10.1159/000486145.

(13) Wong, W. L.; Su, X.; Li, X.; Cheung, C. M. G.; Klein, R.; Cheng, C.-Y.; Wong, T. Y. Global Prevalence of Age-Related Macular Degeneration and Disease Burden Projection for 2020 and 2040: A Systematic Review and Meta-Analysis. *The Lancet Global Health* **2014**, *2* (2), e106–e116. https://doi.org/10.1016/S2214-109X(13)70145-1.

(14) Wet Age-Related Macular Degeneration: Treatment Advances to Reduce the Injection Burden https://www.ajmc.com/view/wet-agerelated-macular-degeneration-treatment-advances-to-reduce-the-injection-burden (accessed 2021 -02 -05).

(15) Chader, G. J.; Taylor, A. Preface: The Aging Eye: Normal Changes, Age-Related Diseases, and Sight-Saving Approaches. *Invest. Ophthalmol. Vis. Sci.* **2013**, *54* (14), ORSF1. https://doi.org/10.1167/iovs.13-12993.

(16) Pascolini, D.; Mariotti, S. P. Global Estimates of Visual Impairment: 2010. *Br J Ophthalmol* **2012**, *96* (5), 614–618. https://doi.org/10.1136/bjophthalmol-2011-300539.

(17) Gaudana, R.; Ananthula, H. K.; Parenky, A.; Mitra, A. K. Ocular Drug Delivery. *The AAPS journal* **2010**, *12* (3), 348–360. https://doi.org/10.1208/s12248-010-9183-3.

(18) Kupferman, A.; Pratt, M. V.; Suckewer, K.; Leibowitz, H. M. Topically Applied Steroids in Corneal Disease. 3. The Role of Drug Derivative in Stromal Absorption of Dexamethasone. *Archives of ophthalmology (Chicago, Ill. : 1960)* **1974**, *91* (5), 373–376. https://doi.org/10.1001/archopht.1974.03900060385008.

(19) Leibowitz, H. M.; Kupferman, A. Antiinflammatory Medications. *International ophthalmology clinics* **1980**, *20* (3), 117–134. https://doi.org/10.1097/00004397-198002030-00012.

(20) Schoenwald, R. D.; Stewart, P. Effect of Particle Size on Ophthalmic Bioavailability of Dexamethasone Suspensions in Rabbits. *Journal of pharmaceutical sciences* **1980**, *69* (4), 391–394. https://doi.org/10.1002/jps.2600690407.

(21) Mitra, A. K.; Mikkelson, T. J. Mechanism of Transcorneal Permeation of Pilocarpine. *Journal of pharmaceutical sciences* **1988**, *77* (9), 771–775. https://doi.org/10.1002/jps.2600770911.

(22) Brechue, W. F.; Maren, T. H. PH and Drug Ionization Affects Ocular Pressure Lowering of Topical Carbonic Anhydrase Inhibitors. *Investigative Ophthalmology* **1993**, *34* (8), 7.

(23) Ahmed, I.; Patton, T. F. Importance of the Noncorneal Absorption Route in Topical Ophthalmic Drug Delivery. *Investigative ophthalmology & visual science* **1985**, *26* (4), 584–587.

(24) Ahmed', I.; Thoma, D. Physicochemical Determinants of Drug Diffusion across the Conjunctiva, Sclera, and Cornea. **1987**, *76* (8), 4.

(25) Freddo, T. F. Shifting the Paradigm of the Blood–Aqueous Barrier. *Experimental Eye Research* **2001**, *73* (5), 581–592. https://doi.org/10.1006/exer.2001.1056.

(26) Bill, A. The Blood-Aqueous Barrier. *Transactions of the ophthalmological societies of the United Kingdom* **1986**, *105 (Pt 2)*, 149–155.

(27) Mannermaa, E.; Vellonen, K.-S.; Urtti, A. Drug Transport in Corneal Epithelium and Blood-Retina Barrier: Emerging Role of Transporters in Ocular Pharmacokinetics. *Advanced drug delivery reviews* **2006**, *58* (11), 1136–1163. https://doi.org/10.1016/j.addr.2006.07.024.

(28) Hosoya, K.; Tomi, M. Advances in the Cell Biology of Transport via the Inner Blood-Retinal Barrier: Establishment of Cell Lines and Transport Functions. *Biological & Pharmaceutical Bulletin* **2005**, *28* (1), 1–8. https://doi.org/10.1248/bpb.28.1.

(29) Sunkara, G.; Kompella, U. Membrane Transport Processes in the Eye. In *Ophthalmic drug delivery systems*; Mitra, A. K., Ed.; Drugs and the pharmaceutical sciences; M. Dekker: New York; Basel, 2003; Vol. 2, pp 13–58. https://doi.org/10.1201/9780203912072.ch2.

(30) *Ophthalmic Drug Delivery Systems*, 2nd ed. rev. and expanded.; Mitra, A. K., Ed.; Drugs and the pharmaceutical sciences; M. Dekker: New York; Basel, 2003; Vol. 130. https://doi.org/10.1201/9780203912072.

(31) Duvvuri, S.; Majumdar, S.; Mitra, A. K. Drug Delivery to the Retina: Challenges and Opportunities. *Expert opinion on biological therapy* **2003**, *3* (1), 45–56. https://doi.org/10.1517/14712598.3.1.45.

(32) Pitkänen, L.; Ranta, V.-P.; Moilanen, H.; Urtti, A. Permeability of Retinal Pigment Epithelium: Effects of Permeant Molecular Weight and Lipophilicity. *Investigative ophthalmology & visual science* **2005**, *46* (2), 641–646. https://doi.org/10.1167/iovs.04-1051.

(33) Ghate, D.; Edelhauser, H. F. Ocular Drug Delivery. *Expert Opinion on Drug Delivery* **2006**, *3* (2), 275–287. https://doi.org/10.1517/17425247.3.2.275.

(34) Weijtens, O.; Feron, E. J.; Schoemaker, R. C.; Cohen, A. F.; Lentjes, E. G. W. M.; Romijn, F. P. H. T. M.; van Meurs, J. C. High Concentration of Dexamethasone in Aqueous and Vitreous after Subconjunctival Injection. *American Journal of Ophthalmology* **1999**, *128* (2), 192–197. https://doi.org/10.1016/S0002-9394(99)00129-4.

(35) Conrad, J. M.; Robinson, J. R. Mechanisms of Anterior Segment Absorption of Pilocarpine Following Subconjunctival Injection in Albino Rabbits. *Journal of Pharmaceutical Sciences* **1980**, *69* (8), 875–884. https://doi.org/10.1002/jps.2600690806.

(36) Lee, T. W.-Y.; Robinson, J. R. Drug Delivery to the Posterior Segment of the Eye: Some Insights on the Penetration Pathways after Subconjunctival Injection. *Journal of Ocular Pharmacology and Therapeutics* **2001**, *17* (6), 565–572. https://doi.org/10.1089/10807680152729257.

(37) Prausnitz, M. R.; Noonan, J. S. Permeability of Cornea, Sclera, and Conjunctiva: A Literature Analysis for Drug Delivery to the Eye. *Journal of pharmaceutical sciences* **1998**, *87* (12), 1479–1488. https://doi.org/10.1021/js9802594.

(38) Hosseini, K.; Matsushima, D.; Johnson, J.; Widera, G.; Nyam, K.; Kim, L.; Xu, Y.; Yao, Y.; Cormier, M. Pharmacokinetic Study of Dexamethasone Disodium Phosphate Using Intravitreal, Subconjunctival, and Intravenous Delivery Routes in Rabbits. *Journal of ocular pharmacology and therapeutics : the official journal of the Association for Ocular Pharmacology and Therapeutics* **2008**, *24* (3), 301–308. https://doi.org/10.1089/jop.2007.0117.

(39) Ilochonwu, B. C.; Urtti, A.; Hennink, W. E.; Vermonden, T. Intravitreal Hydrogels for Sustained Release of Therapeutic Proteins. *Journal of Controlled Release* **2020**, *326*, 419–441. https://doi.org/10.1016/j.jconrel.2020.07.031.

(40) del Amo, E. M.; Rimpelä, A.-K.; Heikkinen, E.; Kari, O. K.; Ramsay, E.; Lajunen, T.; Schmitt, M.; Pelkonen, L.; Bhattacharya, M.; Richardson, D.; Subrizi, A.; Turunen, T.; Reinisalo, M.; Itkonen, J.; Toropainen, E.; Casteleijn, M.; Kidron, H.; Antopolsky, M.; Vellonen, K.-S.; Ruponen, M.; Urtti, A. Pharmacokinetic Aspects of Retinal Drug Delivery. *Progress in Retinal and Eye Research* **2017**, *57*, 134–185. https://doi.org/10.1016/j.preteyeres.2016.12.001.

(41) Peeters, L.; Sanders, N. N.; Braeckmans, K.; Boussery, K.; van de Voorde, J.; Smedt, S. C.; Demeester, J. Vitreous: A Barrier to Nonviral Ocular Gene Therapy. *Investigative ophthalmology & visual science* **2005**, *46* (10), 3553–3561. https://doi.org/10.1167/iovs.05-0165.

(42) Maurice, D. M.; Mishima, S. Ocular Pharmacokinetics. In *Pharmacology of the Eye*; Sears, M. L., Ed.; Handbook of Experimental Pharmacology, Continuation of Handbuch der experimentellen Pharmakologie, 0171-2004; Springer Berlin Heidelberg: Berlin, Heidelberg, 1984; Vol. 69, pp 19–116. https://doi.org/10.1007/978-3-642-69222-2_2.

(43) Maurice, D. Review: Practical Issues in Intravitreal Drug Delivery. *Journal of ocular pharmacology and therapeutics : the official journal of the Association for Ocular Pharmacology and Therapeutics* **2001**, *17* (4), 393–401. https://doi.org/10.1089/108076801753162807.

(44) Del Amo, E. M.; Urtti, A. Rabbit as an Animal Model for Intravitreal Pharmacokinetics: Clinical Predictability and Quality of the Published Data. *Experimental eye research* **2015**, *137*, 111–124. https://doi.org/10.1016/j.exer.2015.05.003.

(45) del Amo, E. M.; Vellonen, K.-S.; Kidron, H.; Urtti, A. Intravitreal Clearance and Volume of Distribution of Compounds in Rabbits: In Silico Prediction and Pharmacokinetic Simulations for Drug Development. *European Journal of Pharmaceutics and Biopharmaceutics* **2015**, *95*, 215–226. https://doi.org/10.1016/j.ejpb.2015.01.003.

(46) Henein, C.; Awwad, S.; Ibeanu, N.; Vlatakis, S.; Brocchini, S.; Khaw, P. T.; Bouremel, Y. Hydrodynamics of Intravitreal Injections into Liquid Vitreous Substitutes. **2019**, 19.

(47) Jiskoot, W.; Randolph, T. W.; Volkin, D. B.; Russell Middaugh, C.; Schöneich, C.; Winter, G.; Friess, W.; Crommelin, D. J. A.; Carpenter, J. F. Protein Instability and Immunogenicity: Roadblocks to Clinical Application of Injectable Protein Delivery Systems for Sustained Release. *Journal of Pharmaceutical Sciences* **2012**, *101* (3), 946–954. https://doi.org/10.1002/jps.23018.

(48) Menon, I. A.; Wakeham, D. C.; Persad, S. D.; Avaria, M.; Trope, G. E.; Basu, P. K. Quantitative Determination of the Melanin Contents in Ocular Tissues from Human Blue and Brown Eyes. *Journal of Ocular Pharmacology and Therapeutics* **1992**, *8* (1), 35–42. https://doi.org/10.1089/jop.1992.8.35.

(49) Rimpelä, A.-K.; Reinisalo, M.; Hellinen, L.; Grazhdankin, E.; Kidron, H.; Urtti, A.; Del Amo, E. M. Implications of Melanin Binding in Ocular Drug Delivery. *Advanced drug delivery reviews* **2018**, *126*, 23–43. https://doi.org/10.1016/j.addr.2017.12.008.

(50) Weirer, J. J. Retinal Pigment Epithelial Lipofuscin and Melanin and Choroidal Melanin in Human Eyes. *27* (2), 8.

(51) Prota, G.; Hu, D.-N.; Vincensi, M. R.; McCORMICK, S. A.; Napolitano, A. Characterization of Melanins in Human Irides and Cultured Uveal Melanocytes From Eyes of Different Colors. *Experimental Eye Research* **1998**, *67* (3), 293–299. https://doi.org/10.1006/exer.1998.0518.

(52) Wakamatsu, K.; Hu, D.-N.; McCormick, S. A.; Ito, S. ORIGINAL ARTICLE: Characterization of Melanin in Human Iridal and Choroidal Melanocytes from Eyes with Various Colored Irides: Melanin in Human Uveal Melanocytes. *Pigment Cell & Melanoma Research* **2007**, *21* (1), 97–105. https://doi.org/10.1111/j.1755-148X.2007.00415.x.

(53) Ozeki, H.; Ito, S.; Wakamatsu, K.; Hirobe, T. Chemical Characterization of Hair Melanins in Various Coat-Color Mutants of Mice. *Journal of Investigative Dermatology* **1995**, *105* (3), 361–366. https://doi.org/10.1111/1523-1747.ep12320792.

(54) Ito, S.; Wakamatsu, K. Quantitative Analysis of Eumelanin and Pheomelanin in Humans, Mice, and Other Animals: A Comparative Review. *Pigment Cell Res* **2003**, *16* (5), 523–531. https://doi.org/10.1034/j.1600-0749.2003.00072.x.

(55) Zajac, G. W.; Gallas, J. M.; Cheng, J.; Eisner, M.; Moss, S. C.; Alvarado-Swaisgood, A. E. The Fundamental Unit of Synthetic Melanin: A Verification by Tunneling Microscopy of X-Ray Scattering Results. *Biochimica et Biophysica Acta (BBA) - General Subjects* **1994**, *1199* (3), 271–278. https://doi.org/10.1016/0304-4165(94)90006-X.

(56) Watt, A. A. R.; Bothma, J. P.; Meredith, P. The Supramolecular Structure of Melanin. *Soft Matter* **2009**, *5* (19), 3754. https://doi.org/10.1039/b902507c.

(57) Pralea, I.-E.; Moldovan, R.-C.; Petrache, A.-M.; Ilieș, M.; Hegheș, S.-C.; Ielciu, I.; Nicoară, R.; Moldovan, M.; Ene, M.; Radu, M.; Uifălean, A.; Iuga, C.-A. From Extraction to Advanced Analytical Methods: The Challenges of Melanin Analysis. *IJMS* **2019**, *20* (16), 3943. https://doi.org/10.3390/ijms20163943.

(58) Hu, D.-N.; Simon, J. D.; Sarna, T. Role of Ocular Melanin in Ophthalmic Physiology and Pathology. *Photochem Photobiol* **2008**, *84* (3), 639–644. https://doi.org/10.1111/j.1751-1097.2008.00316.x.

(59) Bustamante, J.; Bredeston, L.; Malanga, G.; Mordoh, J. Role of Melanin as a Scavenger of Active Oxygen Species. *Pigment Cell Res.* **1993**, *6* (5), 348–353. https://doi.org/10.1111/j.1600-0749.1993.tb00612.x.

(60) Pilas, B.; Sarna, T.; Kalyanaraman, B.; Swartz, H. M. The Effect of Melanin on Iron Associated Decomposition of Hydrogen Peroxide. *Free Radical Biology and Medicine* **1988**, *4* (5), 285–293. https://doi.org/10.1016/0891-5849(88)90049-4.

(61) Potts, A. M. The Concentration of Phenothiazines in the Eye of Experimental Animals. *Investigative Ophthalmology* **1962**, *1* (4), 9.

(62) Salminen, L.; Urtti, A. Effect of Ocular Pigmentation on Pilocarpine Pharmacology in the Rabbit Eye. I. Drug Distribution Tid Metabolism. 8.

(63) Urtti, A.; Salminen, L.; Kujari, H.; Jäntti, V. Effect of Ocular Pigmentation on Pilocarpine Pharmacology in the Rabbit Eye. II. Drug Response. *International Journal of Pharmaceutics* **1984**, *19* (1), 53–61. https://doi.org/10.1016/0378-5173(84)90132-7.

(64) Nagata, A.; Mishima, H. K.; Kiuchi, Y.; Hirota, A.; Kurokawa, T.; Ishibashi, S. Binding of Antiglaucomatous Drugs to Synthetic Melanin and Their Hypotensive Effects on Pigmented and Nonpigmented Rabbit Eyes. *Jpn. J. Ophthalmol.* **1993**, *37* (1), 32–38.

(65) Jakubiak, P.; Reutlinger, M.; Mattei, P.; Schuler, F.; Urtti, A.; Alvarez-Sánchez, R. Understanding Molecular Drivers of Melanin Binding To Support Rational Design of Small Molecule Ophthalmic Drugs. *Journal of medicinal chemistry* **2018**, *61* (22), 10106–10115. https://doi.org/10.1021/acs.jmedchem.8b01281.

(66) Jakubiak, P.; Lack, F.; Thun, J.; Urtti, A.; Alvarez-Sánchez, R. Influence of Melanin Characteristics on Drug Binding Properties. *Mol. Pharmaceutics* **2019**, *16* (6), 2549–2556. https://doi.org/10.1021/acs.molpharmaceut.9b00157.

(67) Jakubiak, P.; Cantrill, C.; Urtti, A.; Alvarez-Sánchez, R. Establishment of an In Vitro–In Vivo Correlation for Melanin Binding and the Extension of the Ocular Half-Life of Small-Molecule Drugs. *Mol. Pharmaceutics* **2019**, *16* (12), acs.molpharmaceut.9b00769. https://doi.org/10.1021/acs.molpharmaceut.9b00769.

(68) Potts, A. M. The Reaction of Uveal Pigment in Vitro with Polycyclic Compounds. *Investigative Ophthalmology* **1964**, *3* (4), 12.

(69) Tjalve, N. STUDIES ON THE MECHANISM OF DRUG-BINDING TO MELANIN. 7.

(70) Ings, R. M. J. The Melanin Binding of Drugs and Its Implications. *Drug Metabolism Reviews* **1984**, *15* (5–6), 1183–1212. https://doi.org/10.3109/03602538409033561.

(71) Zane, P. A.; Brindle, S. D.; Gause, D. O.; O'Buck, A. J.; Raghavan, P. R. Physicochemical Factors Associated with Binding and Retention of Compounds in Ocular Melanin of Rats: Correlations Using Data from Whole-Body Autoradiography and Molecular Modeling for Multiple Linear Regression Analyses. 7.

(72) Salazar-Bookaman, M. M.; Wainer, I.; Patil, P. N. Relevance of Drug-Melanin Interactions to Ocular Pharmacology and Toxicology. *Journal of Ocular Pharmacology and Therapeutics* **1994**, *10* (1), 217–239. https://doi.org/10.1089/jop.1994.10.217.

(73) Raghavan, P. R.; Zane, P. A.; Tripp, S. L. Calculation of Drug-Melanin Binding Energy Using Molecular Modeling. *Experientia* **1990**, *46* (1), 77–80. https://doi.org/10.1007/BF01955422.

(74) Lowrey, A. H.; Fameini, G. R.; Loumbev, V.; Wilson, L. Y.; Tosk, J. M. Modeling Drug-Melanin Interaction With Theoretical Linear Solvation Energy Relationships. *Pigment Cell Res* **1997**, *10* (5), 251–256. https://doi.org/10.1111/j.1600-0749.1997.tb00684.x.

(75) Radwa, A.; Fr??ckowiak, T.; Ibrahim, H.; Aubry, A.-F.; Kaliszan, R. Chromatographic Modelling of Interactions between Melanin and Phenothiazine and Dibenzazepine Drugs. *Biomed. Chromatogr.* **1995**, *9* (5), 233–237. https://doi.org/10.1002/bmc.1130090509.

(76) Reilly, J.; Williams, S. L.; Forster, C. J.; Kansara, V.; End, P.; Serrano-Wu, M. H. High-Throughput Melanin-Binding Affinity and In Silico Methods to Aid in the Prediction of Drug Exposure in Ocular Tissue. *Journal of Pharmaceutical Sciences* **2015**, *104* (12), 3997–4001. https://doi.org/10.1002/jps.24680.

(77) Dong, W.; Wang, Y.; Huang, C.; Xiang, S.; Ma, P.; Ni, Z.; Chen, M. Enhanced Thermal Stability of Poly(Vinyl Alcohol) in Presence of Melanin. *J Therm Anal Calorim* **2014**, *115* (2), 1661–1668. https://doi.org/10.1007/s10973-013-3419-2.

(78) Lee, H.; Dellatore, S. M.; Miller, W. M.; Messersmith, P. B. Mussel-Inspired Surface Chemistry for Multifunctional Coatings. *Science (New York, N.Y.)* **2007**, *318* (5849), 426–430. https://doi.org/10.1126/science.1147241.

(79) Jin, A.; Wang, Y.; Lin, K.; Jiang, L. Nanoparticles Modified by Polydopamine: Working as "Drug" Carriers. *Bioactive Materials* **2020**, *5* (3), 522–541. https://doi.org/10.1016/j.bioactmat.2020.04.003.

(80) Ni, Y.; Chen, F.; Shi, L.; Tong, G.; Wang, J.; Li, H.; Yu, C.; Zhou, Y. Facile Preparation of Water-Soluble and Cytocompatible Small-Sized Chitosan-Polydopamine Nanoparticles. *Chinese Journal of Chemistry* **2017**, *35* (6), 931–937. https://doi.org/10.1002/cjoc.201600765.

(81) Tan, Y.; Deng, W.; Li, Y.; Huang, Z.; Meng, Y.; Xie, Q.; Ma, M.; Yao, S. Polymeric Bionanocomposite Cast Thin Films with In Situ Laccase-Catalyzed Polymerization of Dopamine for Biosensing and Biofuel Cell Applications. 9.

(82) Li, N.; Wang, H.-B.; Thia, L.; Wang, J.-Y.; Wang, X. Enzymatic-Reaction Induced Production of Polydopamine Nanoparticles for Sensitive and Visual Sensing of Urea. *Analyst* **2014**, *140* (2), 449–455. https://doi.org/10.1039/C4AN01900H.

(83) Dreyer, D. R.; Miller, D. J.; Freeman, B. D.; Paul, D. R.; Bielawski, C. W. Elucidating the Structure of Poly(Dopamine). *Langmuir : the ACS journal of surfaces and colloids* **2012**, *28* (15), 6428–6435. https://doi.org/10.1021/la204831b.

(84) Liebscher, J.; Mrówczyński, R.; Scheidt, H. A.; Filip, C.; Hădade, N. D.; Turcu, R.; Bende, A.; Beck, S. Structure of Polydopamine: A Never-Ending Story? *Langmuir : the ACS journal of surfaces and colloids* **2013**, *29* (33), 10539–10548. https://doi.org/10.1021/la4020288.

(85) Chen, C.-T.; Martin-Martinez, F. J.; Jung, G. S.; Buehler, M. J. Polydopamine and Eumelanin Molecular Structures Investigated with Ab Initio Calculations. *Chem. Sci.* **2017**, *8* (2), 1631–1641. https://doi.org/10.1039/C6SC04692D.

(86) Cîrcu, M.; Filip, C. Closer to the Polydopamine Structure: New Insights from a Combined ^{13}C/ ^{1}H/ ^{2}H Solid-State NMR Study on Deuterated Samples. *Polym. Chem.* **2018**, *9* (24), 3379–3387. https://doi.org/10.1039/C8PY00633D.

(87) Lynge, M. E.; van der Westen, R.; Postma, A.; Städler, B. Polydopamine—a Nature-Inspired Polymer Coating for Biomedical Science. *Nanoscale* **2011**, *3* (12), 4916. https://doi.org/10.1039/c1nr10969c.

(88) Liu, Y.; Ai, K.; Lu, L. Polydopamine and Its Derivative Materials: Synthesis and Promising Applications in Energy, Environmental, and Biomedical Fields. *Chemical reviews* **2014**, *114* (9), 5057–5115. https://doi.org/10.1021/cr400407a.

(89) Liu, Y.; Ai, K.; Liu, J.; Deng, M.; He, Y.; Lu, L. Dopamine-Melanin Colloidal Nanospheres: An Efficient near-Infrared Photothermal Therapeutic Agent for in Vivo Cancer Therapy. *Adv Mater* **2013**, *25* (9), 1353–1359. https://doi.org/10.1002/adma.201204683.

(90) Ku, S. H.; Ryu, J.; Hong, S. K.; Lee, H.; Park, C. B. General Functionalization Route for Cell Adhesion on Non-Wetting Surfaces. *Biomaterials* **2010**, *31* (9), 2535–2541. https://doi.org/10.1016/j.biomaterials.2009.12.020.

(91) Luo, R.; Tang, L.; Zhong, S.; Yang, Z.; Wang, J.; Weng, Y.; Tu, Q.; Jiang, C.; Huang, N. In Vitro Investigation of Enhanced Hemocompatibility and Endothelial Cell Proliferation Associated with Quinone-Rich Polydopamine Coating. *ACS Appl Mater Interfaces* **2013**, *5* (5), 1704–1714. https://doi.org/10.1021/am3027635.

(92) Tian, Y.; Lei, M. Polydopamine-Based Composite Nanoparticles with Redox-Labile Polymer Shells for Controlled Drug Release and Enhanced Chemo-Photothermal Therapy. *Nanoscale Res Lett* **2019**, *14* (1), 186. https://doi.org/10.1186/s11671-019-3027-6.

(93) Tiwari, A. P.; Bhattarai, D. P.; Maharjan, B.; Ko, S. W.; Kim, H. Y.; Park, C. H.; Kim, C. S. Polydopamine-Based Implantable Multifunctional Nanocarpet for Highly Efficient Photothermal-Chemo Therapy. *Sci Rep* **2019**, *9* (1), 2943. https://doi.org/10.1038/s41598-019-39457-y.

(94) Zhu, L.; Lu, Y.; Wang, Y.; Zhang, L.; Wang, W. Preparation and Characterization of Dopamine-Decorated Hydrophilic Carbon Black. *Applied Surface Science* **2012**, *258* (14), 5387–5393. https://doi.org/10.1016/j.apsusc.2012.02.016.

(95) Chen, X.; Yang, W.; Zhang, J.; Zhang, L.; Shen, H.; Shi, D. Alkalinity Triggered the Degradation of Polydopamine Nanoparticles. *Polym. Bull.* **2020**. https://doi.org/10.1007/s00289-020-03312-2.

(96) Jia, X.; Ma, Z.; Zhang, G.; Hu, J.; Liu, Z.; Wang, H.; Zhou, F. Polydopamine Film Coated Controlled-Release Multielement Compound Fertilizer Based on Mussel-Inspired Chemistry. *J. Agric. Food Chem.* **2013**, *61* (12), 2919–2924. https://doi.org/10.1021/jf3053059.

(97) Jiang, P.; Choi, A.; Swindle-Reilly, K. E. Controlled Release of Anti-VEGF by Redox-Responsive Polydopamine Nanoparticles. *Nanoscale* **2020**, *12* (33), 17298–17311. https://doi.org/10.1039/D0NR03710A.

(98) Bettinger, C. J.; Bruggeman, J. P.; Misra, A.; Borenstein, J. T.; Langer, R. Biocompatibility of Biodegradable Semiconducting Melanin Films for Nerve Tissue Engineering. *Biomaterials* **2009**, *30* (17), 3050–3057. https://doi.org/10.1016/j.biomaterials.2009.02.018.

(99) Cave, A. C.; Brewer, A. C.; Narayanapanicker, A.; Ray, R.; Grieve, D. J.; Walker, S.; Shah, A. M. NADPH Oxidases in Cardiovascular Health and Disease. *Antioxid Redox Signal* **2006**, *8* (5–6), 691–728. https://doi.org/10.1089/ars.2006.8.691.

(100) Ju, K.-Y.; Lee, Y.; Lee, S.; Park, S. B.; Lee, J.-K. Bioinspired Polymerization of Dopamine to Generate Melanin-Like Nanoparticles Having an Excellent Free-Radical-Scavenging Property. *Biomacromolecules* **2011**, *12* (3), 625–632. https://doi.org/10.1021/bm101281b.

(101) Yu, B.; Liu, J.; Liu, S.; Zhou, F. Pdop Layer Exhibiting Zwitterionicity: A Simple Electrochemical Interface for Governing Ion Permeability. *Chem. Commun.* **2010**, *46* (32), 5900. https://doi.org/10.1039/c0cc00596g.

(102) Liu, Q.; Yu, B.; Ye, W.; Zhou, F. Highly Selective Uptake and Release of Charged Molecules by PH-Responsive Polydopamine Microcapsules. *Macromol. Biosci.* **2011**, *11* (9), 1227–1234. https://doi.org/10.1002/mabi.201100061.

(103) Protein Adsorption on Dopamine–Melanin Films_ Role of Electrostatic Interactions Inferred from ζ-Potential Measurements versus Chemisorption.Pdf.

(104) Chen, D.; Zhao, L.; Hu, W. Protein Immobilization and Fluorescence Quenching on Polydopamine Thin Films. *Journal of Colloid and Interface Science* **2016**, *477*, 123–130. https://doi.org/10.1016/j.jcis.2016.05.042.

(105) Luo, R.; Tang, L.; Wang, J.; Zhao, Y.; Tu, Q.; Weng, Y.; Shen, R.; Huang, N. Improved Immobilization of Biomolecules to Quinone-Rich Polydopamine for Efficient Surface Functionalization. *Colloids and Surfaces B: Biointerfaces* **2013**, *106*, 66–73. https://doi.org/10.1016/j.colsurfb.2013.01.033.

(106) Liu, Y.; Meng, H.; Konst, S.; Sarmiento, R.; Rajachar, R.; Lee, B. P. Injectable Dopamine-Modified Poly(Ethylene Glycol) Nanocomposite Hydrogel with Enhanced Adhesive Property and Bioactivity. *ACS Appl. Mater. Interfaces* **2014**, *6* (19), 16982–16992. https://doi.org/10.1021/am504566v.

(107) Hou, S.; Ma, P. X. Stimuli-Responsive Supramolecular Hydrogels with High Extensibility and Fast Self-Healing via Precoordinated Mussel-Inspired Chemistry. *Chem. Mater.* **2015**, *27* (22), 7627–7635. https://doi.org/10.1021/acs.chemmater.5b02839.

(108) GhavamiNejad, A.; Park, C. H.; Kim, C. S. In Situ Synthesis of Antimicrobial Silver Nanoparticles within Antifouling Zwitterionic Hydrogels by Catecholic Redox Chemistry for Wound Healing Application. *Biomacromolecules* **2016**, *17* (3), 1213–1223. https://doi.org/10.1021/acs.biomac.6b00039.

(109) Huang, J.; Liao, J.; Wang, T.; Sun, W.; Tong, Z. Super Strong Dopamine Hydrogels with Shape Memory and Bioinspired Actuating Behaviours Modulated by Solvent Exchange. *Soft Matter* **2018**, *14* (13), 2500–2507. https://doi.org/10.1039/C8SM00297E.

(110) Huang, K.; Chen, J. S.; Liu, Y. Bioinspired Synthesis of Cross-Linking of Dopamine-Containing Block Copolymers to Form Thermosensitive Covalent Hydrogels. *KEM* **2012**, *531–532*, 238–241. https://doi.org/10.4028/www.scientific.net/KEM.531-532.238.

(111) Gao, B.; Chen, L.; Zhao, Y.; Yan, X.; Wang, X.; Zhou, C.; Shi, Y.; Xue, W. Methods to Prepare Dopamine/Polydopamine Modified Alginate Hydrogels and Their Special Improved Properties for Drug Delivery. *European Polymer Journal* **2019**, *110*, 192–201. https://doi.org/10.1016/j.eurpolymj.2018.11.025.

(112) Bernsmann, F.; Ball, V.; Addiego, F.; Ponche, A.; Michel, M.; Gracio, J. J. de A.; Toniazzo, V.; Ruch, D. Dopamine−Melanin Film Deposition Depends on the Used Oxidant and Buffer Solution. *Langmuir* **2011**, *27* (6), 2819–2825. https://doi.org/10.1021/la104981s.

(113) Ball, V.; Frari, D. D.; Toniazzo, V.; Ruch, D. Kinetics of Polydopamine FIlm Deposition as a Function of PH and Dopamine Concentration: Insights in the Polydopamine Deposition Mechanism. *Journal of Colloid and Interface Science* **2012**, 7.

(114) Sundaram, H. S.; Han, X.; Nowinski, A. K.; Ella-Menye, J.-R.; Wimbish, C.; Marek, P.; Senecal, K.; Jiang, S. One-Step Dip Coating of Zwitterionic Sulfobetaine Polymers on Hydrophobic and Hydrophilic Surfaces. *ACS Appl. Mater. Interfaces* **2014**, *6* (9), 6664–6671. https://doi.org/10.1021/am500362k.

(115) Sundaram, H. S.; Han, X.; Nowinski, A. K.; Brault, N. D.; Li, Y.; Ella-Menye, J.-R.; Amoaka, K. A.; Cook, K. E.; Marek, P.; Senecal, K.; Jiang, S. Achieving One-Step Surface Coating of Highly Hydrophilic

Poly(Carboxybetaine Methacrylate) Polymers on Hydrophobic and Hydrophilic Surfaces. *Adv. Mater. Interfaces* **2014**, *1* (6), 1400071. https://doi.org/10.1002/admi.201400071.

(116) Zhai, Y.; Chen, X.; Yuan, Z.; Han, X.; Liu, H. A Mussel-Inspired Catecholic ABA Triblock Copolymer Exhibits Better Antifouling Properties Compared to a Diblock Copolymer. *Polym. Chem.* **2020**, *11* (28), 4622–4629. https://doi.org/10.1039/D0PY00810A.

(117) Vatankhah-Varnosfaderani, M.; Hu, X.; Li, Q.; Adelnia, H.; Ina, M.; Sheiko, S. S. Universal Coatings Based on Zwitterionic–Dopamine Copolymer Microgels. *ACS Appl. Mater. Interfaces* **2018**, *10* (24), 20869–20875. https://doi.org/10.1021/acsami.8b05570.

(118) Cho, J. H.; Shanmuganathan, K.; Ellison, C. J. Bioinspired Catecholic Copolymers for Antifouling Surface Coatings. *ACS applied materials & interfaces* **2013**, *5* (9), 3794–3802. https://doi.org/10.1021/am400455p.

(119) Hauser, D.; Septiadi, D.; Turner, J.; Petri-Fink, A.; Rothen-Rutishauser, B. From Bioinspired Glue to Medicine: Polydopamine as a Biomedical Material. *Materials* **2020**, *13* (7), 1730. https://doi.org/10.3390/ma13071730.

(120) Wang, W.; Tang, Z.; Zhang, Y.; Wang, Q.; Liang, Z.; Zeng, X. Mussel-Inspired Polydopamine: The Bridge for Targeting Drug Delivery System and Synergistic Cancer Treatment. *Macromol. Biosci.* **2020**, 2000222. https://doi.org/10.1002/mabi.202000222.

(121) He, H.; Markoutsa, E.; Zhan, Y.; Zhang, J.; Xu, P. Mussel-Inspired PLGA/Polydopamine Core-Shell Nanoparticle for Light Induced Cancer Thermochemotherapy. *Acta Biomaterialia* **2017**, *59*, 181–191. https://doi.org/10.1016/j.actbio.2017.07.005.

(122) Zhang, R.; Su, S.; Hu, K.; Shao, L.; Deng, X.; Sheng, W.; Wu, Y. Smart Micelle@polydopamine Core–Shell Nanoparticles for Highly Effective Chemo–Photothermal Combination Therapy. *Nanoscale* **2015**, *7* (46), 19722–19731. https://doi.org/10.1039/C5NR04828A.

(123) Xue, P.; Sun, L.; Li, Q.; Zhang, L.; Guo, J.; Xu, Z.; Kang, Y. PEGylated Polydopamine-Coated Magnetic Nanoparticles for Combined Targeted Chemotherapy and Photothermal Ablation of Tumour Cells. *Colloids and Surfaces B: Biointerfaces* **2017**, *160*, 11–21. https://doi.org/10.1016/j.colsurfb.2017.09.012.

(124) Lei, W.; Sun, C.; Jiang, T.; Gao, Y.; Yang, Y.; Zhao, Q.; Wang, S. Polydopamine-Coated Mesoporous Silica Nanoparticles for Multi-Responsive Drug Delivery and Combined Chemo-Photothermal Therapy. *Materials Science and Engineering: C* **2019**, *105*, 110103. https://doi.org/10.1016/j.msec.2019.110103.

(125) Wang, S.; Zhao, X.; Wang, S.; Qian, J.; He, S. Biologically Inspired Polydopamine Capped Gold Nanorods for Drug Delivery and Light-Mediated Cancer Therapy. *ACS Appl. Mater. Interfaces* **2016**, *8* (37), 24368–24384. https://doi.org/10.1021/acsami.6b05907.

(126) Cui, J.; Wang, Y.; Postma, A.; Hao, J.; Hosta-Rigau, L.; Caruso, F. Monodisperse Polymer Capsules: Tailoring Size, Shell Thickness, and Hydrophobic Cargo Loading via Emulsion Templating. *Adv. Funct. Mater.* **2010**, *20* (10), 1625–1631. https://doi.org/10.1002/adfm.201000209.

(127) Cui, J.; Yan, Y.; Such, G. K.; Liang, K.; Ochs, C. J.; Postma, A.; Caruso, F. Immobilization and Intracellular Delivery of an Anticancer Drug Using Mussel-Inspired Polydopamine Capsules. *Biomacromolecules* **2012**, *13* (8), 2225–2228. https://doi.org/10.1021/bm300835r.

(128) Ho, C.-C.; Ding, S.-J. The PH-Controlled Nanoparticles Size of Polydopamine for Anti-Cancer Drug Delivery. *J Mater Sci: Mater Med* **2013**, *24* (10), 2381–2390. https://doi.org/10.1007/s10856-013-4994-2.

(129) Wang, X.; Zhang, J.; Wang, Y.; Wang, C.; Xiao, J.; Zhang, Q.; Cheng, Y. Multi-Responsive Photothermal-Chemotherapy with Drug-Loaded Melanin-like Nanoparticles for Synergetic Tumor Ablation. *Biomaterials* **2016**, *81*, 114–124. https://doi.org/10.1016/j.biomaterials.2015.11.037.

(130) Wang, L.; Dai, W.; Yang, M.; Wei, X.; Ma, K.; Song, B.; Jia, P.; Gong, Y.; Yang, J.; Zhao, J. Cell Membrane Mimetic Copolymer Coated Polydopamine Nanoparticles for Combined PH-Sensitive Drug Release and near-Infrared Photothermal Therapeutic. *Colloids and Surfaces B: Biointerfaces* **2019**, *176*, 1–8. https://doi.org/10.1016/j.colsurfb.2018.12.057.

(131) Liu, Y.; Sui, Y.; Liu, C.; Liu, C.; Wu, M.; Li, B.; Li, Y. A Physically Crosslinked Polydopamine/Nanocellulose Hydrogel as Potential Versatile Vehicles for Drug Delivery and Wound Healing. *Carbohydrate Polymers* **2018**, *188*, 27–36. https://doi.org/10.1016/j.carbpol.2018.01.093.

(132) Gao, B.; Chen, L.; Zhao, Y.; Yan, X.; Wang, X.; Zhou, C.; Shi, Y.; Xue, W. Methods to Prepare Dopamine/Polydopamine Modified Alginate Hydrogels and Their Special Improved Properties for Drug Delivery. *European Polymer Journal* **2019**, *110*, 192–201. https://doi.org/10.1016/j.eurpolymj.2018.11.025.

(133) Rezk, A. I.; Obiweluozor, F. O.; Choukrani, G.; Park, C. H.; Kim, C. S. Drug Release and Kinetic Models of Anticancer Drug (BTZ) from a PH-Responsive Alginate Polydopamine Hydrogel: Towards Cancer Chemotherapy. *International Journal of Biological Macromolecules* **2019**, *141*, 388–400. https://doi.org/10.1016/j.ijbiomac.2019.09.013.

(134) Han, L.; Zhang, Y.; Lu, X.; Wang, K.; Wang, Z.; Zhang, H. Polydopamine Nanoparticles Modulating Stimuli-Responsive PNIPAM Hydrogels with Cell/Tissue Adhesiveness. *ACS Appl. Mater. Interfaces* **2016**, *8* (42), 29088–29100. https://doi.org/10.1021/acsami.6b11043.

(135) Wang, X.; Wang, C.; Wang, X.; Wang, Y.; Zhang, Q.; Cheng, Y. A Polydopamine Nanoparticle-Knotted Poly(Ethylene Glycol) Hydrogel for On-Demand Drug Delivery and Chemo-Photothermal Therapy. *Chem. Mater.* **2017**, *29* (3), 1370–1376. https://doi.org/10.1021/acs.chemmater.6b05192.

(136) Wang, C.; Zhao, N.; Yuan, W. NIR/Thermoresponsive Injectable Self-Healing Hydrogels Containing Polydopamine Nanoparticles for Efficient Synergistic Cancer Thermochemotherapy. *ACS Appl. Mater. Interfaces* **2020**, *12* (8), 9118–9131. https://doi.org/10.1021/acsami.9b23536.

(137) Bourges, J. L.; Bloquel, C.; Thomas, A.; Froussart, F.; Bochot, A.; Azan, F.; Gurny, R.; BenEzra, D.; Behar-Cohen, F. Intraocular Implants for Extended Drug Delivery: Therapeutic Applications. *Advanced drug delivery reviews* **2006**, *58* (11), 1182–1202. https://doi.org/10.1016/j.addr.2006.07.026.

(138) Smith, T. J. Intravitreal Sustained-Release Ganciclovir. *Arch Ophthalmol* **1992**, *110* (2), 255. https://doi.org/10.1001/archopht.1992.01080140111037.

(139) Sanborn, G. E. Sustained-Release Ganciclovir Therapy for Treatment of Cytomegalovirus Retinitis: Use of an Intravitreal Device. *Arch Ophthalmol* **1992**, *110* (2), 188. https://doi.org/10.1001/archopht.1992.01080140044023.

(140) Cheng, C.-K.; Berger, A. S.; Pearson, P. A.; Ashton, P.; Jaffe, G. J. Intravitreal Sustained-Release Dexamethasone Device in the Treatment of Experimental Uveitis. 12.

(141) Hainsworth, D. P.; Pearson, P. A.; Conklin, J. D.; Ashton, P. Sustained Release Intravitreal Dexamethasone. *Journal of Ocular Pharmacology and Therapeutics* **1996**, *12* (1), 57–63. https://doi.org/10.1089/jop.1996.12.57.

(142) Pearson, P. A. Evaluation of a Delivery System Providing Long-Term Release of Cyclosporine. *Arch Ophthalmol* **1996**, *114* (3), 311. https://doi.org/10.1001/archopht.1996.01100130307014.

(143) Jaffe, G. J.; Yang, C.-S.; Wang, X.-C.; Cousins, S. W.; Gallemore, R. P.; Ashton, P. Intravitreal Sustained-Release Cyclosporine in the Treatment of Experimental Uveitis. *Ophthalmology* **1998**, *105* (1), 46–56. https://doi.org/10.1016/S0161-6420(98)91176-9.

(144) Okabe, K.; Kimura, H.; Okabe, J.; Kato, A.; Kunou, N.; Ogura, Y. Intraocular Tissue Distribution of Betamethasone after Intrascleral Administration Using a Non-Biodegradable Sustained Drug Delivery Device. *Invest. Ophthalmol. Vis. Sci.* **2003**, *44* (6), 2702. https://doi.org/10.1167/iovs.02-0956.

(145) Ranta, V.-P.; Urtti, A. Transscleral Drug Delivery to the Posterior Eye: Prospects of Pharmacokinetic Modeling. *Advanced Drug Delivery Reviews* **2006**, *58* (11), 1164–1181. https://doi.org/10.1016/j.addr.2006.07.025.

(146) Frokjaer, S.; Otzen, D. E. Protein Drug Stability: A Formulation Challenge. *Nat Rev Drug Discov* **2005**, *4* (4), 298–306. https://doi.org/10.1038/nrd1695.

(147) Auritec Pharmaceuticals - Vitrsert® and Retisert ® http://www.auritecpharma.com/vitrasert-retisert (accessed 2020 -04 -28).

(148) Haghjou, N.; Soheilian, M.; Abdekhodaie, M. J. Sustained Release Intraocular Drug Delivery Devices for Treatment of Uveitis. *JOURNAL OF OPHTHALMIC AND VISION RESEARCH 6* (4), 14.

(149) Jaffe, G. J.; Martin, D.; Callanan, D.; Pearson, P. A.; Levy, B.; Comstock, T. Fluocinolone Acetonide Implant (Retisert) for Noninfectious Posterior Uveitis. *Ophthalmology* **2006**, *113* (6), 1020–1027. https://doi.org/10.1016/j.ophtha.2006.02.021.

(150) Kane, F. E.; Burdan, J.; Cutino, A.; Green, K. E. Iluvien ™ : A New Sustained Delivery Technology for Posterior Eye Disease. *Expert Opinion on Drug Delivery* **2008**, *5* (9), 1039–1046. https://doi.org/10.1517/17425247.5.9.1039.

(151) Fusi-Rubiano, W.; Blow, R. R.; Lane, M.; Morjaria, R.; Denniston, A. K. Iluvien™ (Fluocinolone Acetonide 0.19 Mg Intravitreal Implant) in the Treatment of Diabetic Macular Edema: A Review. *Ophthalmol Ther* **2018**, *7* (2), 293–305. https://doi.org/10.1007/s40123-018-0145-7.

(152) Campochiaro, P. A.; Hafiz, G.; Shah, S. M.; Bloom, S.; Brown, D. M.; Busquets, M.; Ciulla, T.; Feiner, L.; Sabates, N.; Billman, K.; Kapik, B.; Green, K.; Kane, F. Sustained Ocular Delivery of Fluocinolone Acetonide by an Intravitreal Insert. *Ophthalmology* **2010**, *117* (7), 1393-1399.e3. https://doi.org/10.1016/j.ophtha.2009.11.024.

(153) Campochiaro, P. A.; Brown, D. M.; Pearson, A.; Chen, S.; Boyer, D.; Ruiz-Moreno, J.; Garretson, B.; Gupta, A.; Hariprasad, S. M.; Bailey, C.; Reichel, E.; Soubrane, G.; Kapik, B.; Billman, K.; Kane, F. E.; Green, K. Sustained Delivery Fluocinolone Acetonide Vitreous Inserts Provide Benefit for at Least 3 Years in Patients with Diabetic Macular Edema. *Ophthalmology* **2012**, *119* (10), 2125–2132. https://doi.org/10.1016/j.ophtha.2012.04.030.

(154) Sharma, A.; Kumar, N.; Parachuri, N.; Kuppermann, B. D.; Bandello, F.; Regillo, C. D. Ranibizumab Port Delivery System (RPDS): Realising Long Awaited Dream of Prolonged VEGF Suppression. *Eye* **2020**, *34* (3), 422–423. https://doi.org/10.1038/s41433-019-0479-y.

(155) Chang, D. P.; Burra, S.; Day, E. S.; Chan, J.; Comps-Agrar, L.; Nivaggioli, T.; Rajagopal, K. Long-Term Stability of Anti-Vascular Endothelial Growth Factor (a-VEGF) Biologics Under Physiologically Relevant Conditions and Its Impact on the Development of Long-Acting Delivery Systems. *Journal of Pharmaceutical Sciences* **2021**, *110* (2), 860–870. https://doi.org/10.1016/j.xphs.2020.09.043.

(156) Williams, D. F. Biodegradation of Surgical Polymers. *J Mater Sci* **1982**, *17* (5), 1233–1246. https://doi.org/10.1007/BF00752233.

(157) Brannigan, R. P.; Dove, A. P. Synthesis, Properties and Biomedical Applications of Hydrolytically Degradable Materials Based on Aliphatic Polyesters and Polycarbonates. *Biomater. Sci.* **2017**, *5* (1), 9–21. https://doi.org/10.1039/C6BM00584E.

(158) Bartnikowski, M.; Dargaville, T. R.; Ivanovski, S.; Hutmacher, D. W. Degradation Mechanisms of Polycaprolactone in the Context of Chemistry, Geometry and Environment. *Progress in Polymer Science* **2019**, *96*, 1–20. https://doi.org/10.1016/j.progpolymsci.2019.05.004.

(159) Pierre, T. S.; Chiellini, E. Biodegradability of Synthetic Polymers Used for Medical And. 31.

(160) Li, S. M.; Garreau, H.; Vert, M. Structure-Property Relationships in the Case of the Degradation of Massive Poly(-Hydroxy Acids) in Aqueous Media. 9.

(161) Burkersroda, F. von; Schedl, L.; Göpferich, A. Why Degradable Polymers Undergo Surface Erosion or Bulk Erosion. *Biomaterials* **2002**, *23* (21), 4221–4231. https://doi.org/10.1016/S0142-9612(02)00170-9.

(162) Pitt, C. G.; Chasalow, F. I.; Hibionada, Y. M.; Klimas, D. M.; Schindler, A. Aliphatic Polyesters. I. The Degradation of Poly(ϵ-Caprolactone) *in Vivo*. *J. Appl. Polym. Sci.* **1981**, *26* (11), 3779–3787. https://doi.org/10.1002/app.1981.070261124.

(163) Huang, M.-H.; Li, S.; Hutmacher, D. W.; Coudane, J.; Vert, M. Degradation Characteristics of Poly(ε-Caprolactone)-Based Copolymers and Blends. *J. Appl. Polym. Sci.* **2006**, *102* (2), 1681–1687. https://doi.org/10.1002/app.24196.

(164) Li, S. M.; Garreau, H.; Vert, M. Structure-Property Relationships in the Case of the Degradation of Massive Aliphatic Poly-(?-Hydroxy Acids) in Aqueous Media: Part 1: Poly(Dl-Lactic Acid). *J Mater Sci: Mater Med* **1990**, *1* (3), 123–130. https://doi.org/10.1007/BF00700871.

(165) Grizzi, I.; Garreau, H.; Li, S.; Vert, M. Hydrolytic Degradation of Devices Based on Poly[m-Lactic Acid) Size- Dependence. **1995**, *16* (4), 7.

(166) Reed, A. M.; Gilding, D. K. Biodegradable Polymers for Use in s u r g e r y - Poly(Glycolic)/Poly(Lactic Acid) Homo and Copolymers: 2. In Vitro Degradation. 5.

(167) Vert, M.; Li, S. M.; Garreau, H.; Cnrs, C.-U. Attempts to Map the Structure and Degradation Characteristics of Aliphatic Polyesters Derived from Lactic and Glycolic Acids. 13.

(168) Lyu, S.; Untereker, D. Degradability of Polymers for Implantable Biomedical Devices. *IJMS* **2009**, *10* (9), 4033–4065. https://doi.org/10.3390/ijms10094033.

(169) Sailema-Palate, G. P.; Vidaurre, A.; Campillo-Fernández, A. J.; Castilla-Cortázar, I. A Comparative Study on Poly(ε-Caprolactone) Film Degradation at Extreme PH Values. *Polymer Degradation and Stability* **2016**, *130*, 118–125. https://doi.org/10.1016/j.polymdegradstab.2016.06.005.

(170) Lam, C. X. F.; Savalani, M. M.; Teoh, S.-H.; Hutmacher, D. W. Dynamics of *in Vitro* Polymer Degradation of Polycaprolactone-Based Scaffolds: Accelerated versus Simulated Physiological Conditions. *Biomed. Mater.* **2008**, *3* (3), 034108. https://doi.org/10.1088/1748-6041/3/3/034108.

(171) Araque-Monrós, M. C.; Vidaurre, A.; Gil-Santos, L.; Gironés Bernabé, S.; Monleón-Pradas, M.; Más-Estellés, J. Study of the Degradation of a New PLA Braided Biomaterial in Buffer Phosphate Saline, Basic and Acid Media, Intended for the Regeneration of Tendons and Ligaments. *Polymer Degradation and Stability* **2013**, *98* (9), 1563–1570. https://doi.org/10.1016/j.polymdegradstab.2013.06.031.

(172) Lee, S. S.; Hughes, P.; Ross, A. D.; Robinson, M. R. Biodegradable Implants for Sustained Drug Release in the Eye. *Pharmaceutical research* **2010**, *27* (10), 2043–2053. https://doi.org/10.1007/s11095-010-0159-x.

(173) Natural and Synthetic Biomedical Polymers - 1st Edition https://www.elsevier.com/books/natural-and-synthetic-biomedical-polymers/kum-bar/978-0-12-396983-5 (accessed 2021 -02 -10).

(174) Nair, L. S.; Laurencin, C. T. Biodegradable Polymers as Biomaterials. *Progress in Polymer Science* **2007**, *32* (8–9), 762–798. https://doi.org/10.1016/j.progpolymsci.2007.05.017.

(175) Gupta, B.; Revagade, N.; Hilborn, J. Poly(Lactic Acid) Fiber: An Overview. *Progress in Polymer Science* **2007**, *32* (4), 455–482. https://doi.org/10.1016/j.progpolymsci.2007.01.005.

(176) Lasprilla, A. J. R.; Martinez, G. A. R.; Lunelli, B. H.; Jardini, A. L.; Filho, R. M. Poly-Lactic Acid Synthesis for Application in Biomedical Devices — A Review. *Biotechnology Advances* **2012**, *30* (1), 321–328. https://doi.org/10.1016/j.biotechadv.2011.06.019.

(177) Kunou, N.; Ogura, Y.; Hashizoe, M.; Honda, Y.; Hyon, S.-H.; Ikada, Y. Controlled Intraocular Delivery of Ganciclovir with Use of Biodegradable Scleral Implant in Rabbits. *Journal of Controlled Release* **1995**, *37* (1–2), 143–150. https://doi.org/10.1016/0168-3659(95)00074-I.

(178) Kunou, N.; Ogura, Y.; Yasukawa, T.; Kimura, H.; Miyamoto, H.; Honda, Y.; Ikada, Y. Long-Term Sustained Release of Ganciclovir from Biodegradable Scleral Implant for the Treatment of Cytomegalovirus Retinitis. *Journal of Controlled Release* **2000**, *68* (2), 263–271. https://doi.org/10.1016/S0168-3659(00)00267-4.

(179) Gilding, D. K.; Reed, A. M. Biodegradable Polymers for Use in Surgery—Polyglycolic/Poly(Actic Acid) Homo- and Copolymers: 1. *Polymer* **1979**, *20* (12), 1459–1464. https://doi.org/10.1016/0032-3861(79)90009-0.

(180) Reed, A. M.; Gilding, D. K. Biodegradable Polymers for Use in s u r g e r y - Poly(Glycolic)/Poly(Lactic Acid) Homo and Copolymers: 2. In Vitro Degradation. 5.

(181) Li, S. M.; Garreau, H.; Vert, M. Structure-Property Relationships in the Case of the Degradation of Massive Poly(-Hydroxy Acids) in Aqueous Media. 9.

(182) Bala, I.; Hariharan, S.; Kumar, M. N. V. R. PLGA Nanoparticles in Drug Delivery: The State of the Art. *Crit Rev Ther Drug Carrier Syst* **2004**, *21* (5), 387–422. https://doi.org/10.1615/critrevtherdrugcarriersyst.v21.i5.20.

(183) Molavi, F.; Barzegar-Jalali, M.; Hamishehkar, H. Polyester Based Polymeric Nano and Microparticles for Pharmaceutical Purposes: A Review on Formulation Approaches. *Journal of Controlled Release* **2020**, *320*, 265–282. https://doi.org/10.1016/j.jconrel.2020.01.028.

(184) Eslamian, M.; Khorrami, M.; Yi, N.; Majd, S.; Abidian, M. R. Electrospinning of Highly Aligned Fibers for Drug Delivery Applications. *J. Mater. Chem. B* **2019**, *7* (2), 224–232. https://doi.org/10.1039/C8TB01258J.

(185) Zare, E. N.; Jamaledin, R.; Naserzadeh, P.; Afjeh-Dana, E.; Ashtari, B.; Hosseinzadeh, M.; Vecchione, R.; Wu, A.; Tay, F. R.; Borzacchiello, A.; Makvandi, P. Metal-Based Nanostructures/PLGA Nanocomposites: Antimicrobial Activity, Cytotoxicity, and Their Biomedical Applications. *ACS Appl. Mater. Interfaces* **2020**, *12* (3), 3279–3300. https://doi.org/10.1021/acsami.9b19435.

(186) Rasoulianboroujeni, M.; Fahimipour, F.; Shah, P.; Khoshroo, K.; Tahriri, M.; Eslami, H.; Yadegari, A.; Dashtimoghadam, E.; Tayebi, L. Development of 3D-Printed PLGA/TiO2 Nanocomposite Scaffolds for Bone Tissue Engineering Applications. *Materials Science and Engineering: C* **2019**, *96*, 105–113. https://doi.org/10.1016/j.msec.2018.10.077.

(187) Zolnik, B. S.; Burgess, D. J. Effect of Acidic PH on PLGA Microsphere Degradation and Release. *J Control Release* **2007**, *122* (3), 338–344. https://doi.org/10.1016/j.jconrel.2007.05.034.

(188) Kim, M. S.; Ahn, H. H.; Shin, Y. N.; Cho, M. H.; Khang, G.; Lee, H. B. An in Vivo Study of the Host Tissue Response to Subcutaneous Implantation of PLGA- and/or Porcine Small Intestinal Submucosa-Based Scaffolds. *Biomaterials* **2007**, *28* (34), 5137–5143. https://doi.org/10.1016/j.biomaterials.2007.08.014.

(189) Ikada, Y.; Tsuji, H. Biodegradable Polyesters for Medical and Ecological Applications. 16.

(190) Sinha, V. R.; Bansal, K.; Kaushik, R.; Kumria, R.; Trehan, A. Poly-ϵ-Caprolactone Microspheres and Nanospheres: An Overview. *International Journal of Pharmaceutics* **2004**, *278* (1), 1–23. https://doi.org/10.1016/j.ijpharm.2004.01.044.

(191) Barbault-Foucher, S.; Gref, R.; Russo, P.; Guechot, J.; Bochot, A. Design of Poly-´-Caprolactone Nanospheres Coated with Bioadhesive Hyaluronic Acid for Ocular Delivery. *Journal of Controlled Release* **2002**, 11.

(192) Sun, S.; Li, J.; Li, X.; Lan, B.; Zhou, S.; Meng, Y.; Cheng, L. Episcleral Drug Film for Better-Targeted Ocular Drug Delivery and Controlled Release Using Multilayered Poly-ε-Caprolactone (PCL). *Acta Biomaterialia* **2016**, *37*, 143–154. https://doi.org/10.1016/j.actbio.2016.04.014.

(193) Kim, S. Y. Application of the Three-Dimensionally Printed Biodegradable Polycaprolactone (PCL) Mesh in Repair of Orbital Wall Fractures. *Journal of Cranio-Maxillofacial Surgery* **2019**, *47* (7), 1065–1071. https://doi.org/10.1016/j.jcms.2019.03.009.

(194) Hedayati, S. K.; Behravesh, A. H.; Hasannia, S.; Bagheri Saed, A.; Akhoundi, B. 3D Printed PCL Scaffold Reinforced with Continuous Biodegradable Fiber Yarn: A Study on Mechanical and Cell Viability Properties. *Polymer Testing* **2020**, *83*, 106347. https://doi.org/10.1016/j.polymertesting.2020.106347.

(195) Cao, Y.; Samy, K. E.; Bernards, D. A.; Desai, T. A. Recent Advances in Intraocular Sustained-Release Drug Delivery Devices. *Drug Discov Today* **2019**, *24* (8), 1694–1700. https://doi.org/10.1016/j.drudis.2019.05.031.

(196) Chang-Lin, J.-E.; Attar, M.; Acheampong, A. A.; Robinson, M. R.; Whitcup, S. M.; Kuppermann, B. D.; Welty, D. Pharmacokinetics and Pharmacodynamics of a Sustained-Release Dexamethasone Intravitreal Implant. *Invest. Ophthalmol. Vis. Sci.* **2011**, *52* (1), 80. https://doi.org/10.1167/iovs.10-5285.

(197) Kuppermann, B. D. Randomized Controlled Study of an Intravitreous Dexamethasone Drug Delivery System in Patients With Persistent Macular Edema. *Arch Ophthalmol* **2007**, *125* (3), 309. https://doi.org/10.1001/archopht.125.3.309.

(198) Blumenkranz, M. S.; Chan; Leung. Critical Appraisal of the Clinical Utility of the Dexamethasone Intravitreal Implant (Ozurdex®) for the Treatment of Macular Edema Related to Branch Retinal Vein Occlusion or Central Retinal Vein Occlusion. *OPTH* **2011**, 1043. https://doi.org/10.2147/OPTH.S13775.

(199) Haller, J. A.; Dugel, P.; Weinberg, D. V.; Chou, C.; Whitcup, S. M. EVALUATION OF THE SAFETY AND PERFORMANCE OF AN APPLICATOR FOR A NOVEL INTRAVITREAL DEXAMETHASONE DRUG DELIVERY SYSTEM FOR THE TREATMENT OF MACULAR EDEMA: *Retina* **2009**, *29* (1), 46–51. https://doi.org/10.1097/IAE.0b013e318188c814.

(200) Haller, J. A.; Bandello, F.; Belfort, R.; Blumenkranz, M. S.; Gillies, M.; Heier, J.; Loewenstein, A.; Yoon, Y.-H.; Jacques, M.-L.; Jiao, J.; Li, X.-Y.; Whitcup, S. M. Randomized, Sham-Controlled Trial of Dexamethasone Intravitreal Implant in Patients with Macular Edema Due to Retinal Vein Occlusion. *Ophthalmology* **2010**, *117* (6), 1134-1146.e3. https://doi.org/10.1016/j.ophtha.2010.03.032.

(201) Kuppermann, B. D.; Patel, S. S.; Boyer, D. S.; Augustin, A. J.; Freeman, W. R.; Kerr, K. J.; Guo, Q.; Schneider, S.; López, F. J.; Brimo DDS Gen 1 Study Group. PHASE 2 STUDY OF THE SAFETY AND EFFICACY OF BRIMONIDINE DRUG DELIVERY SYSTEM (BRIMO DDS) GENERATION 1 IN PATIENTS WITH GEOGRAPHIC ATROPHY SECONDARY TO AGE-RELATED MACULAR DEGENERATION. *Retina* **2021**, *41* (1), 144–155. https://doi.org/10.1097/IAE.0000000000002789.

(202) Hashizoe, M.; Ogura, Y.; Takanashi, T.; Kunou, N.; Honda, Y.; Ikada, Y. Biodegradable Polymeric Device for Sustained Intravitreal Release of Ganciclovir in Rabbits. *Current Eye Research* **1997**, *16* (7), 633–639. https://doi.org/10.1076/ceyr.16.7.633.5063.

(203) Fialho, S. L.; Silva Cunha, A. da. Manufacturing Techniques of Biodegradable Implants Intended for Intraocular Application. *Drug Delivery* **2005**, *12* (2), 109–116. https://doi.org/10.1080/10717540590921432.

(204) Fialho, S. L.; Rêgo, M. B.; Siqueira, R. C.; Jorge, R.; Haddad, A.; Rodrigues, A. L.; Maia-Filho, A.; Silva-Cunha, A. Safety and Pharmacokinetics of an Intravitreal Biodegradable Implant of Dexamethasone Acetate in Rabbit Eyes. *Current Eye Research* **2006**, *31* (6), 525–534. https://doi.org/10.1080/02713680600719036.

(205) Fialho, S. L.; Siqueira, R. C.; Jorge, R.; Silva-Cunha, A. Biodegradable Implants for Ocular Delivery of Anti-Inflammatory Drug. *Journal of Drug Delivery Science and Technology* **2007**, *17* (1), 93–97. https://doi.org/10.1016/S1773-2247(07)50013-4.

(206) Sakurai, E.; Nozaki, M.; Okabe, K.; Kunou, N.; Kimura, H.; Ogura, Y. Scleral Plug of Biodegradable Polymers Containing Tacrolimus (FK506) for Experimental Uveitis. *Invest. Ophthalmol. Vis. Sci.* **2003**, *44* (11), 4845. https://doi.org/10.1167/iovs.02-1228.

(207) Fialho, S. Dexamethasone-Loaded Poly(ε-Caprolactone) Intravitreal Implants: A Pilot Study. *European Journal of Pharmaceutics and Biopharmaceutics* **2008**, *68* (3), 637–646. https://doi.org/10.1016/j.ejpb.2007.08.004.

(208) Silva-Cunha, A.; Fialho, S. L.; Naud, M.-C.; Behar-Cohen, F. Poly-Epsilon-Caprolactone Intravitreous Devices: An in Vivo Study. *Investigative ophthalmology & visual science* **2009**, *50* (5), 2312–2318. https://doi.org/10.1167/iovs.08-2969.

(209) Bernards, D. A.; Lance, K. D.; Ciaccio, N. A.; Desai, T. A. Nanostructured Thin Film Polymer Devices for Constant-Rate Protein Delivery. *Nano Lett.* **2012**, *12* (10), 5355–5361. https://doi.org/10.1021/nl302747y.

(210) Lance, K. D.; Bernards, D. A.; Ciaccio, N. A.; Good, S. D.; Mendes, T. S.; Kudisch, M.; Chan, E.; Ishikiriyama, M.; Bhisitkul, R. B.; Desai, T. A. In Vivo and in Vitro Sustained Release of Ranibizumab from a Nanoporous Thin-Film Device. *Drug Deliv. and Transl. Res.* **2016**, *6* (6), 771–780. https://doi.org/10.1007/s13346-016-0298-7.

(211) Mandal, A.; Bisht, R.; Rupenthal, I. D.; Mitra, A. K. Polymeric Micelles for Ocular Drug Delivery: From Structural Frameworks to Recent Preclinical Studies. *Journal of Controlled Release* **2017**, *248*, 96–116. https://doi.org/10.1016/j.jconrel.2017.01.012.

(212) Omerović, N.; Vranić, E. Application of Nanoparticles in Ocular Drug Delivery Systems. *Health Technol.* **2020**, *10* (1), 61–78. https://doi.org/10.1007/s12553-019-00381-w.

(213) Gote, V.; Sikder, S.; Sicotte, J.; Pal, D. Ocular Drug Delivery: Present Innovations and Future Challenges. *J Pharmacol Exp Ther* **2019**, *370* (3), 602–624. https://doi.org/10.1124/jpet.119.256933.

(214) Meng, T.; Kulkarni, V.; Simmers, R.; Brar, V.; Xu, Q. Therapeutic Implications of Nanomedicine for Ocular Drug Delivery. *Drug Discovery Today* **2019**, *24* (8), 1524–1538. https://doi.org/10.1016/j.drudis.2019.05.006.

(215) Weng, Y.; Liu, J.; Jin, S.; Guo, W.; Liang, X.; Hu, Z. Nanotechnology-Based Strategies for Treatment of Ocular Disease. *Acta Pharmaceutica Sinica B* **2017**, *7* (3), 281–291. https://doi.org/10.1016/j.apsb.2016.09.001.

(216) Talelli, M.; Barz, M.; Rijcken, C. J. F.; Kiessling, F.; Hennink, W. E.; Lammers, T. Core-Crosslinked Polymeric Micelles: Principles, Preparation, Biomedical Applications and Clinical Translation. *Nano Today* **2015**, *10* (1), 93–117. https://doi.org/10.1016/j.nantod.2015.01.005.

(217) Herrero-Vanrell, R.; Bravo-Osuna, I.; Andrés-Guerrero, V.; Vicario-de-la-Torre, M.; Molina-Martínez, I. T. The Potential of Using Biodegradable Microspheres in Retinal Diseases and Other Intraocular Pathologies. *Progress in Retinal and Eye Research* **2014**, *42*, 27–43. https://doi.org/10.1016/j.preteyeres.2014.04.002.

(218) Thackaberry, E. A.; Farman, C.; Zhong, F.; Lorget, F.; Staflin, K.; Cercillieux, A.; Miller, P. E.; Schuetz, C.; Chang, D.; Famili, A.; Daugherty, A. L.; Rajagopal, K.; Bantseev, V. Evaluation of the Toxicity of Intravitreally Injected PLGA Microspheres and Rods in Monkeys and Rabbits: Effects of Depot Size on Inflammatory Response. *Invest. Ophthalmol. Vis. Sci.* **2017**, *58* (10), 4274. https://doi.org/10.1167/iovs.16-21334.

(219) Gorantla, S.; Rapalli, V. K.; Waghule, T.; Singh, P. P.; Dubey, S. K.; Saha, R. N.; Singhvi, G. Nanocarriers for Ocular Drug Delivery: Current Status and Translational Opportunity. *RSC Adv.* **2020**, *10* (46), 27835–27855. https://doi.org/10.1039/D0RA04971A.

(220) Khan, S.; Ullah, A.; Ullah, K.; Rehman, N. Insight into Hydrogels. *Designed Monomers and Polymers* **2016**, *19* (5), 456–478. https://doi.org/10.1080/15685551.2016.1169380.

(221) Koetting, M. C.; Peters, J. T.; Steichen, S. D.; Peppas, N. A. Stimulus-Responsive Hydrogels: Theory, Modern Advances, and Applications. *Materials Science and Engineering: R: Reports* **2015**, *93*, 1–49. https://doi.org/10.1016/j.mser.2015.04.001.

(222) Klouda, L.; Mikos, A. G. Thermoresponsive Hydrogels in Biomedical Applications. *European Journal of Pharmaceutics and Biopharmaceutics* **2008**, *68* (1), 34–45. https://doi.org/10.1016/j.ejpb.2007.02.025.

(223) Wang, K.; Han, Z. Injectable Hydrogels for Ophthalmic Applications. *J Control Release* **2017**, *268*, 212–224. https://doi.org/10.1016/j.jconrel.2017.10.031.

(224) de Groot, J. H.; van Beijma, F. J.; Haitjema, H. J.; Dillingham, K. A.; Hodd, K. A.; Koopmans, S. A.; Norrby, S. Injectable Intraocular Lens Materials Based upon Hydrogels. *Biomacromolecules* **2001**, *2* (3), 628–634. https://doi.org/10.1021/bm005622r.

(225) Aliyar, H. A.; Hamilton, P. D.; Ravi, N. Refilling of Ocular Lens Capsule with Copolymeric Hydrogel Containing Reversible Disulfide. *Biomacromolecules* **2005**, *6* (1), 204–211. https://doi.org/10.1021/bm049574c.

(226) Feng, S.; Chen, H.; Liu, Y.; Huang, Z.; Sun, X.; Zhou, L.; Lu, X.; Gao, Q. A Novel Vitreous Substitute of Using a Foldable Capsular Vitreous Body Injected with Polyvinylalcohol Hydrogel. *Scientific Reports* **2013**, *3* (1), 1838. https://doi.org/10.1038/srep01838.

(227) Annaka, M.; Mortensen, K.; Vigild, M. E.; Matsuura, T.; Tsuji, S.; Ueda, T.; Tsujinaka, H. Design of an Injectable in Situ Gelation Biomaterials for Vitreous Substitute. *Biomacromolecules* **2011**, *12* (11), 4011–4021. https://doi.org/10.1021/bm201012f.

(228) Schramm, C.; Spitzer, M. S.; Henke-Fahle, S.; Steinmetz, G.; Januschowski, K.; Heiduschka, P.; Geis-Gerstorfer, J.; Biedermann, T.; Bartz-Schmidt, K. U.; Szurman, P. The Cross-Linked Biopolymer Hyaluronic Acid as an Artificial Vitreous Substitute. *Invest. Ophthalmol. Vis. Sci.* **2012**, *53* (2), 613–621. https://doi.org/10.1167/iovs.11-7322.

(229) Kempe, S.; Mäder, K. In Situ Forming Implants — an Attractive Formulation Principle for Parenteral Depot Formulations. *Journal of Controlled Release* **2012**, *161* (2), 668–679. https://doi.org/10.1016/j.jconrel.2012.04.016.

(230) Thakur, R. R. S.; Fallows, S. J.; McMillan, H. L.; Donnelly, R. F.; Jones, D. S. Microneedle-Mediated Intrascleral Delivery of *in Situ* Forming Thermoresponsive Implants for Sustained Ocular Drug Delivery: Microneedle-Mediated Intrascleral Delivery. *J Pharm Pharmacol* **2014**, *66* (4), 584–595. https://doi.org/10.1111/jphp.12152.

(231) Lynch, C. R.; Kondiah, P. P. D.; Choonara, Y. E.; du Toit, L. C.; Ally, N.; Pillay, V. Hydrogel Biomaterials for Application in Ocular Drug Delivery. *Front. Bioeng. Biotechnol.* **2020**, *8*, 228. https://doi.org/10.3389/fbioe.2020.00228.

(232) Cooper, R. C.; Yang, H. Hydrogel-Based Ocular Drug Delivery Systems: Emerging Fabrication Strategies, Applications, and Bench-to-Bedside Manufacturing Considerations. *Journal of Controlled Release* **2019**, *306*, 29–39. https://doi.org/10.1016/j.jconrel.2019.05.034.

(233) Vermonden, T.; Censi, R.; Hennink, W. E. Hydrogels for Protein Delivery. *Chem. Rev.* **2012**, *112* (5), 2853–2888. https://doi.org/10.1021/cr200157d.

(234) Kanjickal, D.; Lopina, S.; Evancho-Chapman, M. M.; Schmidt, S.; Donovan, D. Effects of Sterilization on Poly(Ethylene Glycol) Hydrogels. *J Biomed Mater Res A* **2008**, *87* (3), 608–617. https://doi.org/10.1002/jbm.a.31811.

(235) Saher, O.; Ghorab, D. M.; Mursi, N. M. Preparation and in Vitro/in Vivo Evaluation of Antimicrobial Ocular in Situ Gels Containing a Disappearing Preservative for Topical Treatment of Bacterial Conjunctivitis. *Pharm Dev Technol* **2016**, *21* (5), 600–610. https://doi.org/10.3109/10837450.2015.1035728.

(236) Huynh, C. T.; Nguyen, M. K.; Lee, D. S. Injectable Block Copolymer Hydrogels: Achievements and Future Challenges for Biomedical Applications. *Macromolecules* **2011**, *44* (17), 6629–6636. https://doi.org/10.1021/ma201261m.

(237) Southall, N. T.; Dill, K. A.; Haymet, A. D. J. A View of the Hydrophobic Effect. *J. Phys. Chem. B* **2002**, *106* (3), 521–533. https://doi.org/10.1021/jp015514e.

(238) Matanović, M. R.; Kristl, J.; Grabnar, P. A. Thermoresponsive Polymers: Insights into Decisive Hydrogel Characteristics, Mechanisms of Gelation, and Promising Biomedical Applications. *International Journal of Pharmaceutics* **2014**, *472* (1–2), 262–275. https://doi.org/10.1016/j.ijpharm.2014.06.029.

(239) Bae, S. J.; Suh, J. M.; Sohn, Y. S.; Bae, Y. H.; Kim, S. W.; Jeong, B. Thermogelling Poly(Caprolactone- *b* -Ethylene Glycol- *b* -Caprolactone) Aqueous Solutions. *Macromolecules* **2005**, *38* (12), 5260–5265. https://doi.org/10.1021/ma050489m.

(240) Gong, C.; Qian, Z.; Liu, C.; Huang, M.; Gu, Y.; Wen, Y.; Kan, B.; Wang, K.; Dai, M.; Li, X.; Gou, M.; Tu, M.; Wei, Y. A Thermosensitive Hydrogel Based on Biodegradable Amphiphilic Poly(Ethylene Glycol)–Polycaprolactone–Poly(Ethylene Glycol) Block Copolymers. *Smart Mater. Struct.* **2007**, *16* (3), 927–933. https://doi.org/10.1088/0964-1726/16/3/043.

(241) Thakur, R. R. S.; McMillan, H. L.; Jones, D. S. Solvent Induced Phase Inversion-Based in Situ Forming Controlled Release Drug Delivery Implants. *Journal of Controlled Release* **2014**, *176*, 8–23. https://doi.org/10.1016/j.jconrel.2013.12.020.

(242) Cheng, Y.-H.; Hung, K.-H.; Tsai, T.-H.; Lee, C.-J.; Ku, R.-Y.; Chiu, A. W.; Chiou, S.-H.; Liu, C. J. Sustained Delivery of Latanoprost by Thermosensitive Chitosan–Gelatin-Based Hydrogel for

Controlling Ocular Hypertension. *Acta Biomaterialia* **2014**, *10* (10), 4360–4366. https://doi.org/10.1016/j.actbio.2014.05.031.

(243) Cheng, Y.-H.; Tsai, T.-H.; Jhan, Y.-Y.; Chiu, A. W.; Tsai, K.-L.; Chien, C.-S.; Chiou, S.-H.; Liu, C. J. Thermosensitive Chitosan-Based Hydrogel as a Topical Ocular Drug Delivery System of Latanoprost for Glaucoma Treatment. *Carbohydrate Polymers* **2016**, *144*, 390–399. https://doi.org/10.1016/j.carbpol.2016.02.080.

(244) Pakzad, Y.; Fathi, M.; Omidi, Y.; Mozafari, M.; Zamanian, A. Synthesis and Characterization of Timolol Maleate-Loaded Quaternized Chitosan-Based Thermosensitive Hydrogel: A Transparent Topical Ocular Delivery System for the Treatment of Glaucoma. *International Journal of Biological Macromolecules* **2020**, *159*, 117–128. https://doi.org/10.1016/j.ijbiomac.2020.04.274.

(245) Luo, Z.; Jin, L.; Xu, L.; Zhang, Z. L.; Yu, J.; Shi, S.; Li, X.; Chen, H. Thermosensitive PEG–PCL–PEG (PECE) Hydrogel as an *in Situ* Gelling System for Ocular Drug Delivery of Diclofenac Sodium. *Drug Delivery* **2016**, *23* (1), 63–68. https://doi.org/10.3109/10717544.2014.903535.

(246) Ma, W.-D.; Xu, H.; Wang, C.; Nie, S.-F.; Pan, W.-S. Pluronic F127-g-Poly(Acrylic Acid) Copolymers as in Situ Gelling Vehicle for Ophthalmic Drug Delivery System. *International Journal of Pharmaceutics* **2008**, *350* (1–2), 247–256. https://doi.org/10.1016/j.ijpharm.2007.09.005.

(247) Davaran, S.; Lotfipour, F.; Sedghipour, N.; Sedghipour, M. R.; Alimohammadi, S.; Salehi, R. Preparation and in Vivo Evaluation of in Situ Gel System as Dual Thermo-/PH-Responsive Nanocarriers for Sustained Ocular Drug Delivery. *J Microencapsul* 10.

(248) Gabriel, D.; Mugnier, T.; Courthion, H.; Kranidioti, K.; Karagianni, N.; Denis, M. C.; Lapteva, M.; Kalia, Y.; Möller, M.; Gurny, R. Improved Topical Delivery of Tacrolimus: A Novel Composite Hydrogel Formulation for the Treatment of Psoriasis. *Journal of Controlled Release* **2016**, *242*, 16–24. https://doi.org/10.1016/j.jconrel.2016.09.007.

(249) Salwowska, N. M.; Bebenek, K. A.; Żądło, D. A.; Wcisło-Dziadecka, D. L. Physiochemical Properties and Application of Hyaluronic Acid: A Systematic Review. *J Cosmet Dermatol* **2016**, *15* (4), 520–526. https://doi.org/10.1111/jocd.12237.

(250) Necas, J.; Bartosikova, L.; Brauner, P.; Kolar, J. Hyaluronic Acid (Hyaluronan): A Review. *Veterinarni Medicina* **2008**, *53* (No. 8), 397–411. https://doi.org/10.17221/1930-VETMED.

(251) Tomme, S. R. V.; Hennink, W. E. Biodegradable Dextran Hydrogels for Protein Delivery Applications. *Expert Review of Medical Devices* **2007**, *4* (2), 147–164. https://doi.org/10.1586/17434440.4.2.147.

(252) Yu, Y.; Lau, L. C. M.; Lo, A. C.; Chau, Y. Injectable Chemically Crosslinked Hydrogel for the Controlled Release of Bevacizumab in Vitreous: A 6-Month In Vivo Study. *Trans. Vis. Sci. Tech.* **2015**, *4* (2), 5. https://doi.org/10.1167/tvst.4.2.5.

(253) Ahmadi, F.; Oveisi, Z.; Samani, S. M.; Amoozgar, Z. Chitosan Based Hydrogels: Characteristics and Pharmaceutical Applications. *Res Pharm Sci* **2015**, *10* (1), 1–16.

(254) Shariatinia, Z.; Jalali, A. M. Chitosan-Based Hydrogels: Preparation, Properties and Applications. *International Journal of Biological Macromolecules* **2018**, *115*, 194–220. https://doi.org/10.1016/j.ijbiomac.2018.04.034.

(255) Yamaoka, T.; Tabata, Y.; Ikada, Y. Distribution and Tissue Uptake of Poly(Ethylene Glycol) with Different Molecular Weights after Intravenous Administration to Mice. *JPharmSci* **1994**, *83* (4), 601–606. https://doi.org/10.1002/jps.2600830432.

(256) Thassu, D.; Chader, G. J. *Ocular Drug Delivery Systems: Barriers and Application of Nanoparticulate Systems*; CRC Press, 2012.

(257) Lin, C.-C.; Anseth, K. S. PEG Hydrogels for the Controlled Release of Biomolecules in Regenerative Medicine. *Pharm Res* **2009**, *26* (3), 631–643. https://doi.org/10.1007/s11095-008-9801-2.

(258) Schild, H. G. Poly(N-Isopropylacrylamide): Experiment, Theory and Application. *Progress in Polymer Science* **1992**, *17* (2), 163–249. https://doi.org/10.1016/0079-6700(92)90023-R.

(259) Lanzalaco, S.; Armelin, E. Poly(N-Isopropylacrylamide) and Copolymers: A Review on Recent Progresses in Biomedical Applications. *Gels* **2017**, *3* (4), 36. https://doi.org/10.3390/gels3040036.

(260) Drapala, P. W.; Brey, E. M.; Mieler, W. F.; Venerus, D. C.; Kang Derwent, J. J.; Pérez-Luna, V. H. Role of Thermo-Responsiveness and Poly(Ethylene Glycol) Diacrylate Cross-Link Density on Protein Release from Poly(N-Isopropylacrylamide) Hydrogels. *Journal of Biomaterials Science, Polymer Edition* **2011**, *22* (1–3), 59–75. https://doi.org/10.1163/092050609X12578498952315.

(261) Turturro, S. B.; Guthrie, M. J.; Appel, A. A.; Drapala, P. W.; Brey, E. M.; Pérez-Luna, V. H.; Mieler, W. F.; Kang-Mieler, J. J. The Effects of Cross-Linked Thermo-Responsive PNIPAAm-Based Hydrogel Injection on Retinal Function. *Biomaterials* **2011**, *32* (14), 3620–3626. https://doi.org/10.1016/j.biomaterials.2011.01.058.

(262) Alexandridis, P.; Alan Hatton, T. Poly(Ethylene Oxide)poly(Propylene Oxide)poly(Ethylene Oxide) Block Copolymer Surfactants in Aqueous Solutions and at Interfaces: Thermodynamics, Structure, Dynamics, and Modeling. *Colloids and Surfaces A: Physicochemical and Engineering Aspects* **1995**, *96* (1–2), 1–46. https://doi.org/10.1016/0927-7757(94)03028-X.

(263) Kabanov, A. V.; Batrakova, E. V.; Alakhov, V. Y. Pluronic® Block Copolymers as Novel Polymer Therapeutics for Drug and Gene Delivery. *Journal of Controlled Release* **2002**, *82* (2–3), 189–212. https://doi.org/10.1016/S0168-3659(02)00009-3.

(264) Brown, W.; Schillen, K.; Hvidt, S. Triblock Copolymers in Aqueous Solution Studied by Static and Dynamic Light Scattering and Oscillatory Shear Measurements: Influence of Relative Block Sizes. *J. Phys. Chem.* **1992**, *96* (14), 6038–6044. https://doi.org/10.1021/j100193a072.

(265) Mortensen, K.; Pedersen, J. S. Structural Study on the Micelle Formation of Poly(Ethylene Oxide)-Poly(Propylene Oxide)-Poly(Ethylene Oxide) Triblock Copolymer in Aqueous Solution. *Macromolecules* **1993**, *26* (4), 805–812. https://doi.org/10.1021/ma00056a035.

(266) Hatton1995.Pdf.

(267) Pitto-Barry, A.; Barry, N. P. E. Pluronic® Block-Copolymers in Medicine: From Chemical and Biological Versatility to Rationalisation and Clinical Advances. *Polym. Chem.* **2014**, *5* (10), 3291–3297. https://doi.org/10.1039/C4PY00039K.

(268) Hwang, Y.-S.; Chiang, P.-R.; Hong, W.-H.; Chiao, C.-C.; Chu, I.-M.; Hsiue, H.; Shen, C.-R. Study In Vivo Intraocular Biocompatibility of In Situ Gelation Hydrogels: Poly(2-Ethyl Oxazoline)-Block-Poly(e-Caprolactone)-Block-Poly(2-Ethyl Oxazoline) Copolymer, Matrigel and Pluronic F127. *PLOS ONE* **2013**, *8* (7), 9.

(269) Su, D. H.; Luu, C. D.; Barathi, A.; Zhu, X.; Cheah, E. S.; Cheng, B. C.; Chee, S.-P. Evaluation of the Use of Pluronic F127 as an Intravitreal Ocular Drug Delivery Vehicle. *Invest. Ophthalmol. Vis. Sci.* **2006**, *47* (13), 5122–5122.

(270) Hwang, M. J.; Suh, J. M.; Bae, Y. H.; Kim, S. W.; Jeong, B. Caprolactonic Poloxamer Analog: PEG-PCL-PEG. *Biomacromolecules* **2005**, *6* (2), 885–890. https://doi.org/10.1021/bm049347a.

(271) Wang, P.; Chu, W.; Zhuo, X.; Zhang, Y.; Gou, J.; Ren, T.; He, H.; Yin, T.; Tang, X. Modified PLGA–PEG–PLGA Thermosensitive Hydrogels with Suitable Thermosensitivity and Properties for Use in a Drug Delivery System. *J. Mater. Chem. B* **2017**, *5* (8), 1551–1565. https://doi.org/10.1039/C6TB02158A.

(272) Qiao, M.; Chen, D.; Ma, X.; Liu, Y. Injectable Biodegradable Temperature-Responsive PLGA–PEG–PLGA Copolymers: Synthesis and Effect of Copolymer Composition on the Drug Release from the Copolymer-Based Hydrogels. *International Journal of Pharmaceutics* **2005**, *294* (1–2), 103–112. https://doi.org/10.1016/j.ijpharm.2005.01.017.

(273) Rieke, E. R.; Amaral, J.; Becerra, S. P.; Lutz, R. J. Sustained Subconjunctival Protein Delivery Using a Thermosetting Gel Delivery System. *J Ocul Pharmacol Ther* **2010**, *26* (1), 55–64. https://doi.org/10.1089/jop.2009.0059.

(274) Chan, P. S.; Xian, J. W.; Li, Q.; Chan, C. W.; Leung, S. S. Y.; To, K. K. W. Biodegradable Thermosensitive PLGA-PEG-PLGA Polymer for Non-Irritating and Sustained Ophthalmic Drug Delivery. *AAPS J* **2019**, *21* (4), 59. https://doi.org/10.1208/s12248-019-0326-x.

(275) Chan, P. S.; Li, Q.; Zhang, B.; To, K. K. W.; Leung, S. S. Y. In Vivo Biocompatibility and Efficacy of Dexamethasone-Loaded PLGA-PEG-PLGA Thermogel in an Alkali-Burn Induced Corneal Neovascularization Disease Model. *European Journal of Pharmaceutics and Biopharmaceutics* **2020**, *155*, 190–198. https://doi.org/10.1016/j.ejpb.2020.08.022.

(276) Dutta et al. - 2020 - In Situ Forming Injectable Thermoresponsive Hydrog.Pdf.

(277) Xie, B.; Jin, L.; Luo, Z.; Yu, J.; Shi, S.; Zhang, Z.; Shen, M.; Chen, H.; Li, X.; Song, Z. An Injectable Thermosensitive Polymeric Hydrogel for Sustained Release of Avastin® to Treat Posterior Segment Disease. *International Journal of Pharmaceutics* **2015**, *490* (1–2), 375–383. https://doi.org/10.1016/j.ijpharm.2015.05.071.

(278) Zhang, L.; Shen, W.; Luan, J.; Yang, D.; Wei, G.; Yu, L.; Lu, W.; Ding, J. Sustained Intravitreal Delivery of Dexamethasone Using an Injectable and Biodegradable Thermogel. *Acta Biomaterialia* **2015**, *23*, 271–281. https://doi.org/10.1016/j.actbio.2015.05.005.

(279) Gong, C. Y.; Shi, S.; Dong, P. W.; Yang, B.; Qi, X. R.; Guo, G.; Gu, Y. C.; Zhao, X.; Wei, Y. Q.; Qian, Z. Y. Biodegradable in Situ Gel-Forming Controlled Drug Delivery System Based on Thermosensitive PCL–PEG–PCL Hydrogel: Part 1—Synthesis, Characterization, and Acute Toxicity Evaluation. *Journal of Pharmaceutical Sciences* **2009**, *98* (12), 4684–4694. https://doi.org/10.1002/jps.21780.

(280) Gong, C.; Shi, S.; Wu, L.; Gou, M.; Yin, Q.; Guo, Q.; Dong, P.; Zhang, F.; Luo, F.; Zhao, X.; Wei, Y.; Qian, Z. Biodegradable in Situ Gel-Forming Controlled Drug Delivery System Based on Thermosensitive PCL–PEG–PCL Hydrogel. Part 2: Sol–Gel–Sol Transition and Drug Delivery Behavior. *Acta Biomaterialia* **2009**, *5* (9), 3358–3370. https://doi.org/10.1016/j.actbio.2009.05.025.

(281) Ma, G.; Miao, B.; Song, C. Thermosensitive PCL-PEG-PCL Hydrogels: Synthesis, Characterization, and Delivery of Proteins. *J. Appl. Polym. Sci.* **2010**, *37*, NA-NA. https://doi.org/10.1002/app.31654.

(282) Wang, C.-H.; Hwang, Y.-S.; Chiang, P.-R.; Shen, C.-R.; Hong, W.-H.; Hsiue, G.-H. Extended Release of Bevacizumab by Thermosensitive Biodegradable and Biocompatible Hydrogel. *Biomacromolecules* **2012**, *13* (1), 40–48. https://doi.org/10.1021/bm2009558.

(283) Gong, C.; Shi, S.; Dong, P.; Kan, B.; Gou, M.; Wang, X.; Li, X.; Luo, F.; Zhao, X.; Wei, Y.; Qian, Z. Synthesis and Characterization of PEG-PCL-PEG Thermosensitive Hydrogel. *International journal of pharmaceutics* **2009**, *365* (1–2), 89–99. https://doi.org/10.1016/j.ijpharm.2008.08.027.

(284) Yin, H.; Gong, C.; Shi, S.; Liu, X.; Wei, Y.; Qian, Z. Toxicity Evaluation of Biodegradable and Thermosensitive PEG-PCL-PEG Hydrogel as a Potential *in Situ* Sustained Ophthalmic Drug Delivery System. *J. Biomed. Mater. Res.* **2010**, *92B* (1), 129–137. https://doi.org/10.1002/jbm.b.31498.

(285) Liu, H.; Venkatraman, S. S. Effect of Polymer Type on the Dynamics of Phase Inversion and Drug Release in Injectable In Situ Gelling Systems. *Journal of Biomaterials Science, Polymer Edition* **2012**, *23* (1–4), 251–266. https://doi.org/10.1163/092050610X549171.

(286) Bode, C.; Kranz, H.; Siepmann, F.; Siepmann, J. In-Situ Forming PLGA Implants for Intraocular Dexamethasone Delivery. *International journal of pharmaceutics* **2018**, *548* (1), 337–348. https://doi.org/10.1016/j.ijpharm.2018.07.013.

(287) Asmus, L. R.; Tille, J.-C.; Kaufmann, B.; Melander, L.; Weiss, T.; Vessman, K.; Koechling, W.; Schwach, G.; Gurny, R.; Möller, M. In Vivo Biocompatibility, Sustained-Release and Stability of Triptorelin Formulations Based on a Liquid, Degradable Polymer. *Journal of Controlled Release* **2013**, *165* (3), 199–206. https://doi.org/10.1016/j.jconrel.2012.11.014.

(288) Asmus, L. R.; Grimshaw, J. P. A.; Richle, P.; Eicher, B.; Urech, D. M.; Gurny, R.; Möller, M. Injectable Formulations for an Intravitreal Sustained-Release Application of a Novel Single-Chain VEGF Antibody Fragment. *European Journal of Pharmaceutics and Biopharmaceutics* **2015**, *95*, 250–260. https://doi.org/10.1016/j.ejpb.2015.02.007.

(289) Dahmana, N.; Kowalczuk, L.; Gabriel, D.; Behar-Cohen, F.; Gurny, R.; Kalia, Y. N. Ocular Biodistribution of Spironolactone after a Single Intravitreal Injection of a Biodegradable Sustained-Release Polymer in Rats. *Mol. Pharmaceutics* **2020**, *17* (1), 59–69. https://doi.org/10.1021/acs.molpharmaceut.9b00707.

(290) Fialho, S. Dexamethasone-Loaded Poly(ε-Caprolactone) Intravitreal Implants: A Pilot Study. *European Journal of Pharmaceutics and Biopharmaceutics* **2008**, *68* (3), 637–646. https://doi.org/10.1016/j.ejpb.2007.08.004.

(291) Silva-Cunha, A.; Fialho, S. L.; Naud, M.-C.; Behar-Cohen, F. Poly-Epsilon-Caprolactone Intravitreous Devices: An in Vivo Study. *Investigative ophthalmology & visual science* **2009**, *50* (5), 2312–2318. https://doi.org/10.1167/iovs.08-2969.

(292) Sun, S.; Li, J.; Li, X.; Lan, B.; Zhou, S.; Meng, Y.; Cheng, L. Episcleral Drug Film for Better-Targeted Ocular Drug Delivery and Controlled Release Using Multilayered Poly-ε-Caprolactone (PCL). *Acta Biomaterialia* **2016**, *37*, 143–154. https://doi.org/10.1016/j.actbio.2016.04.014.

(293) Nottelet, B.; Coudane, J.; Vert, M. Synthesis of an X-Ray Opaque Biodegradable Copolyester by Chemical Modification of Poly (ε-Caprolactone). *Biomaterials* **2006**, *27* (28), 4948–4954. https://doi.org/10.1016/j.biomaterials.2006.05.032.

(294) Habnouni, S. E.; Darcos, V.; Coudane, J. Synthesis and Ring Opening Polymerization of a New Functional Lactone, *α* -Iodo- *ε* -Caprolactone: A Novel Route to Functionalized Aliphatic Polyesters. *Macromol. Rapid Commun.* **2009**, *30* (3), 165–169. https://doi.org/10.1002/marc.200800596.

(295) Nagata, M.; Sato, Y. Synthesis and Properties of Photocurable Biodegradable Multiblock Copolymers Based on Poly(ε-Caprolactone) and Poly(L-Lactide) Segments. *Journal of Polymer Science Part A: Polymer Chemistry* **2005**, *43* (11), 2426–2439. https://doi.org/10.1002/pola.20718.

(296) Nagata, M.; Yamamoto, Y. Synthesis and Characterization of Photocrosslinked Poly(ε-Caprolactone)s Showing Shape-Memory Properties. *J. Polym. Sci. A Polym. Chem.* **2009**, *47* (9), 2422–2433. https://doi.org/10.1002/pola.23333.

(297) Zhang, X.; Nie, Y.; Zhang, Q.; Liang, Z.; Ma, Q. A Novel L -Cysteine Regulated Polydopamine Nanoparticle-Based Electrochemiluminescence Image Application. *J. Mater. Chem. C* **2020**, *8* (25), 8592–8600. https://doi.org/10.1039/D0TC01499K.

(298) Huang, Y.-H.; I, Y.-P.; Chen, N.-C.; Wu, S.-H.; Horng, J.-J.; Wu, Y.-T.; Wen, I.-J. Thermal Runaway Reaction Evaluation of Benzoyl Peroxide Using Calorimetric Approaches. *J Therm Anal Calorim* **2013**, *113* (2), 595–598. https://doi.org/10.1007/s10973-012-2822-4.

(299) Su, W.-F. Radical Chain Polymerization. In *Principles of Polymer Design and Synthesis*; Su, W.-F., Ed.; Lecture Notes in Chemistry; Springer: Berlin, Heidelberg, 2013; pp 137–183. https://doi.org/10.1007/978-3-642-38730-2_7.

(300) Basile, M. A.; d'Ayala, G. G.; Malinconico, M.; Laurienzo, P.; Coudane, J.; Nottelet, B.; Ragione, F. D.; Oliva, A. Functionalized PCL/HA Nanocomposites as Microporous Membranes for Bone Regeneration. *Materials Science and Engineering: C* **2015**, *48*, 457–468. https://doi.org/10.1016/j.msec.2014.12.019.

(301) Tian, Y.; Jiang, L. Intrinsically Robust Hydrophobicity. *Nature Materials* **2013**, *12* (4), 291–292. https://doi.org/10.1038/nmat3610.

(302) Li, S. M.; Garreau, H.; Vert, M. Structure-Property Relationships in the Case of the Degradation of Massive Aliphatic Poly-(?-Hydroxy Acids) in Aqueous Media: Part 1: Poly(Dl-Lactic Acid). *J Mater Sci: Mater Med* **1990**, *1* (3), 123–130. https://doi.org/10.1007/BF00700871.

(303) Bartnikowski, M.; Dargaville, T. R.; Ivanovski, S.; Hutmacher, D. W. Degradation Mechanisms of Polycaprolactone in the Context of Chemistry, Geometry and Environment. *Progress in Polymer Science* **2019**, *96*, 1–20. https://doi.org/10.1016/j.progpolymsci.2019.05.004.

(304) Graham, R. O. Intravitreal Injection of Dexamethasone: Treatment of Experimentally Induced Endophthalmitis. *Arch Ophthalmol* **1974**, *92* (2), 149. https://doi.org/10.1001/archopht.1974.01010010155016.

(305) Kwak, H. W. Evaluation of the Retinal Toxicity and Pharmacokinetics of Dexamethasone After Intravitreal Injection. *Arch Ophthalmol* **1992**, *110* (2), 259. https://doi.org/10.1001/archopht.1992.01080140115038.

(306) Martidis, A.; Duker, J. S.; Greenberg, P. B.; Rogers, A. H.; Puliafito, C. A.; Reichel, E.; Baumal, C. Intravitreal Triamcinolone for Refractory Diabetic Macular Edema. *Ophthalmology* **2002**, *109* (5), 920–927. https://doi.org/10.1016/S0161-6420(02)00975-2.

(307) Wilson, C. A. Treatment With Intravitreal Steroid Reduces Blood-Retinal Barrier Breakdown Due to Retinal Photocoagulation. *Arch Ophthalmol* **1992**, *110* (8), 1155. https://doi.org/10.1001/archopht.1992.01080200135041.

(308) Culpepper, J. A.; Lee, F. Regulation of IL 3 Expression by Glucocorticoids in Cloned Murine T Lymphocytes. *J. Immunol.* **1985**, *135* (5), 3191–3197.

(309) Knudsen, P. J.; Dinarello, C. A.; Strom, T. B. Glucocorticoids Inhibit Transcriptional and Post-Transcriptional Expression of Interleukin 1 in U937 Cells. *J. Immunol.* **1987**, *139* (12), 4129–4134.

(310) Enyedi, L. B.; Pearson, P. A.; Ashton, P.; Jaffe, G. J. An Intravitreal Device Providing Sustained Release of Cyclosporine and Dexamethasone. *Current Eye Research* **1996**, *15* (5), 549–557. https://doi.org/10.3109/02713689609000766.

(311) Bhagat, R.; Zhang, J.; Farooq, S.; Li, X.-Y. Comparison of the Release Profile and Pharmacokinetics of Intact and Fragmented Dexamethasone Intravitreal Implants in Rabbit Eyes.

Journal of Ocular Pharmacology and Therapeutics **2014**, *30* (10), 854–858. https://doi.org/10.1089/jop.2014.0082.

(312) Webster, R.; Elliott, V.; Park, B. K.; Walker, D.; Hankin, M.; Taupin, P. PEG and PEG Conjugates Toxicity: Towards an Understanding of the Toxicity of PEG and Its Relevance to PEGylated Biologicals. In *PEGylated Protein Drugs: Basic Science and Clinical Applications*; Veronese, F. M., Ed.; Milestones in Drug Therapy; Birkhäuser: Basel, 2009; pp 127–146. https://doi.org/10.1007/978-3-7643-8679-5_8.

(313) Liu, C. B.; Gong, C. Y.; Huang, M. J.; Wang, J. W.; Pan, Y. F.; Zhang, Y. D.; Li, G. Z.; Gou, M. L.; Wang, K.; Tu, M. J.; Wei, Y. Q.; Qian, Z. Y. Thermoreversible Gel–Sol Behavior of Biodegradable PCL-PEG-PCL Triblock Copolymer in Aqueous Solutions. *J. Biomed. Mater. Res.* **2008**, *84B* (1), 165–175. https://doi.org/10.1002/jbm.b.30858.

(314) Sun, T.; Shuai, X.; Ren, K.; Jiang, X.; Chen, Y.; Zhao, X.; Song, Q.; Hu, S.; Cai, Z. Amphiphilic Block Copolymer PCL-PEG-PCL as Stationary Phase for Capillary Gas Chromatographic Separations. *Molecules* **2019**, *24* (17), 3158. https://doi.org/10.3390/molecules24173158.

(315) Bode, C.; Kranz, H.; Siepmann, F.; Siepmann, J. In-Situ Forming PLGA Implants for Intraocular Dexamethasone Delivery. *International journal of pharmaceutics* **2018**, *548* (1), 337–348. https://doi.org/10.1016/j.ijpharm.2018.07.013.

(316) Roberge, C.; Cros, J.-M.; Serindoux, J.; Cagnon, M.-E.; Samuel, R.; Vrlinic, T.; Berto, P.; Rech, A.; Richard, J.; Lopez-Noriega, A. BEPO®: Bioresorbable Diblock MPEG-PDLLA and Triblock PDLLA-PEG-PDLLA Based in Situ Forming Depots with Flexible Drug Delivery Kinetics Modulation. *Journal of Controlled Release* **2020**, *319*, 416–427. https://doi.org/10.1016/j.jconrel.2020.01.022.

(317) In Vitro and In Vivo Characterization of Scleral Implant of Indomethacin_ Role of Plasticizer and Cross-Linking Time_.Pdf.

(318) El-Menshawe, S. F. A Novel Approach to Topical Acetazolamide/PEG 400 Ocular Niosomes. *Journal of Drug Delivery Science and Technology* **2012**, *22* (4), 295–299. https://doi.org/10.1016/S1773-2247(12)50049-3.

(319) Aguirre, S. A.; Gukasyan, H. J.; Younis, H. S.; Huang, W. Safety Assessment of Formulation Vehicles Following Intravitreal Administration in Rabbits. *Pharm Res* **2018**, *35* (9), 173. https://doi.org/10.1007/s11095-018-2450-1.

(320) US20180311152 LIQUID FORMULATIONS FOR TREATMENT OF DISEASES OR CONDITIONS https://patentscope.wipo.int/search/en/detail.jsf?docId=US232561318&tab=PCTDESCRIPTION (accessed 2021 -05 -09).

(321) Cilurzo, F.; Selmin, F.; Minghetti, P.; Adami, M.; Bertoni, E.; Lauria, S.; Montanari, L. Injectability Evaluation: An Open Issue. *AAPS PharmSciTech* **2011**, *12* (2), 604–609. https://doi.org/10.1208/s12249-011-9625-y.

(322) Sharma, V. K.; Kalonia, D. S. Polyethylene Glycol-Induced Precipitation of Interferon Alpha-2a Followed by Vacuum Drying: Development of a Novel Process for Obtaining a Dry, Stable Powder. *AAPS J* **2004**, *6* (1), 31–44. https://doi.org/10.1208/ps060104.

(323) Shulgin, I. L.; Ruckenstein, E. Preferential Hydration and Solubility of Proteins in Aqueous Solutions of Polyethylene Glycol. *Biophysical Chemistry* **2006**, *120* (3), 188–198. https://doi.org/10.1016/j.bpc.2005.11.010.

(324) Kumar, V.; Sharma, V. K.; Kalonia, D. S. Effect of Polyols on Polyethylene Glycol (PEG)-Induced Precipitation of Proteins: Impact on Solubility, Stability and Conformation. *International Journal of Pharmaceutics* **2009**, *366* (1–2), 38–43. https://doi.org/10.1016/j.ijpharm.2008.08.037.

Résumé de la thèse

Les maladies oculaires désignent toute affection ou tout trouble qui nuit à la capacité de l'œil de fonctionner correctement et/ou qui nuit à la clarté visuelle. Et 2015 et à travers le monde, plus de 216 millions de personnes sont malvoyantes et plus de 36 millions de personnes sont aveugles. Les maladies oculaires sont donc un problème de santé majeur. Parmi elle, les maladies rétiniennes sont une classe de maladie du segment postérieur de l'œil telles que la dégénérescence maculaire liée à l'âge et la rétinopathie diabétique.

L'administration intravitréenne (IVT) désigne l'administration de formulations (solution, suspension, implant) ou de dispositifs médicaux directement dans l'humeur vitrée. Cette méthode permet de contourner les différentes barrières oculaires telles que la barrière hémato-rétinienne, la barrière hémato-aqueuse, les flux lymphatiques, conjonctifs ou corneaux qui limitent la perméation et/ou diminue la biodisponibilité des principes actifs –molécules de faible ou haute masse molaire. Elle est aujourd'hui la méthode la plus efficace pour le traitement des maladies rétiniennes. Cependant, les principaux défis sont la biocompatibilité des formulations, la stabilité des principes actifs, et la diminution des fréquences d'administration afin d'améliorer l'observance du patient et de limiter les risques potentiels liés à l'opération.

Ainsi, la communauté scientifique a concentré tous ses efforts quant à l'élaboration de dispositifs médicaux et formulations permettant la libération de ces molécules dans la cavité vitreuse et leur diffusion jusque dans les tissus de la rétine. Les formulations basées sur la technologie des polymères sont récentes, marginales, mais peuvent répondre aux problématiques énoncées. Un consensus sur la standardisation des injections intravitréennes a été adopté afin de limiter les risques d'augmentation de pression intraoculaire, de réduire la force appliquée lors de la pénétration des tissus et de prévenir les éventuels reflux.

L'agence américaine des produits alimentaires et médicamenteux (FDA) a approuvé l'utilisation de dispositif médicaux solides ou de formulations solides dégradables pour le traitement des maladies rétiniennes. Dans le cas des dispositifs, l'avantage majeur est qu'elles permettent la libération contrôlée et constante de petites molécules sur de très longues périodes (jusqu'à 3 ans). En revanche, les opérations répétées d'implantation ou d'injection pour placer et retirer le dispositif sont des méthodes invasives et augmentent les risques de la pression intraoculaire, d'infections et de décollement de la rétine. Actuellement, un seul dispositif médical constitué de polysulfone et de silicone est en phase clinique 3 pour la libération de produits biologiques, mais aucune formulation solide ou dispositif viable a été trouvée. La difficulté réside dans le fait que les agents biologiques ont

des structures complexes et ont tendance à se dénaturer (perte de la conformation tridimensionnelle et déploiement) en présence d'agents dénaturants d'origine chimiques ou d'origine physique comme l'augmentation de la température ou la modification du pH.

La seule formulation solide dégradable et approuvée est constituée de poly(acide lactique-*co*-glycolique) (PLGA), un polyester aliphatique linéaire et hydrophobe présentant une cinétique de dégradation lente. Il permet la libération contrôlée d'une petite molécule hydrophobe pour une durée d'efficacité de 3 à 6 mois. L'implant se dégrade progressivement ce qui évite une étape chirurgicale pour le retirer. En revanche, la fréquence d'administration est rapprochée compte tenu de la libération et le risque d'augmentation de la pression oculaire ainsi que du développement de cataracte est élevé.

Concernant l'élaboration de formulations liquides (solution ou suspension) ou semi-solides basées sur la technologie des polymères, il n'y a à ce jour aucune formulation viable et approuvée par la FDA. Cette stratégie est basée sur la modification des propriétés physico-chimique de la solution en réponse aux variations environnementales lors de l'administration dans l'humeur vitrée. Elle présente plusieurs avantages tels que la facilité d'administration à travers une fine aiguille permettant une augmentation du confort et de la sécurité du patient ainsi qu'une capacité de chargement de principes actifs bien supérieur aux systèmes solides. En revanche, la viscosité de la solution, la stabilité des principes actifs en solution ainsi que la capacité de la formulation à transiter d'un état liquide à un état semi-solide sont des paramètres clé. Les formulations sont basées sur un mécanisme de thermo-sensibilité des polymères – notamment des copolymères de poly(éthylène glycol) (PEG) et de PLGA ou de poly(ε-caprolactone) (PCL) – ou sur un mécanisme d'échange de solvant, dont la tolérance oculaire est discutable.

Nous nous sommes intéressés au potentiel et aux bénéfices que la poly(dopamine) (PDA) pouvait apporter à la synthèse de nouveaux copolymères pour l'ophtalmologie. La PDA est un analogue synthétique de la mélanine, une macromolécule naturelle présente dans les cellules de la peau, des cheveux et des yeux qui est notamment responsable de la pigmentation, de la photoprotection ainsi que de la modification de la pharmacologie des principes actifs dans les tissus oculaires. La PDA est synthétisée par polymérisation de la dopamine, un neurotransmetteur. Bien qu'actuellement toujours en débat, le mécanisme de polymérisation s'apparenterait à une série d'oxydations et de réarrangements intramoléculaires de la dopamine et la structure finale serait un arrangement agrégats supramoléculaires empilés par π-stacking d'un mélange d'oligomères d'environ 4 unités liés par covalence. Due à l'analogie des procédés de synthèses et de structures, la PDA présente des propriétés similaires à la mélanine telles que la biocompatibilité, la stabilité thermique, la dégradabilité, le caractère zwitterionique ainsi que la capacité de liaison physique ou chimique des principes actifs due

à la présence de fonctions amines et de groupements catéchols. Ainsi, l'ajout d'unités PDA dans un copolymère permettrait de ralentir les cinétiques de libération de principes actifs et par conséquent diminuer les fréquences d'injections des formulations.

Compte tenu des informations précédentes, et dans le cadre du développement de formulations solides dégradables, notre choix s'est ainsi porté sur un polymère synthétique, biodégradable et biocompatible tel que la PCL présentant une cinétique de dégradation encore plus lente (entre 2 et 8 ans selon la masse molaire sélectionnée) que les formulations biodégradables actuelles. Dans le cadre du développement de formulations liquides à capacité gélifiante *in situ*, notre choix s'est ainsi porté sur un copolymère synthétique, dégradable et biocompatible composé de PEG et de PCL.

Le travail de thèse a été réalisé au sein du laboratoire de l'IBMM-Polymer for Health and Biomaterials (Montpellier, France) et du département Pharmaceutical Development, PTD Biologics Europe in F.Hoffmann-La Roche (Bâle, Suisse). Cette collaboration a permis de mettre en commun les spécialités des deux laboratoires – synthèse, caractérisation et mise de forme de polymères pour l'IBMM ; synthèse de protéines et expertise industrielle pour F.Hoffmann-La Roche. Le cahier des charges a été établi en amont du projet : les formulations solides (implant) ou liquides (solution) doivent être injectables par une fine aiguille dans l'œil, être biocompatibles, être dégradables, contenir de la PDA et présenter des cinétiques de libération lente de 1 à 6 mois pour les agents chimiques ou biologiques.

Dans le cadre de la stratégie des implants, la synthèse du copolymère PCL-g-PDA a été effectuée en deux étapes. Tout d'abord, une PCL commerciale de haute masse molaire (M_n = 190 000 g.mol^{-1}) a été sélectionnée pour diminuer le risque de fragilité du matériau final. La PCL a été fonctionnalisée à hauteur de 10 mol.% avec l'introduction d'un atome d'iode en α de la fonction cétone par substitution électrophile pour générer une PCL iodée (PCL-I). Ensuite,-PCL-I est fonctionnalisée par de la PDA en conditions oxydative, basique et similaire à la polymérisation radicalaire par transfert d'atomes (ATRP). Cette étape met en jeu les réactions simultanées de la polymérisation de la dopamine, le greffage d'unité de dopamine et/ou de oligo-PDA et leur croissance en PDA. La présence de PDA dans le copolymère est confirmée par analyses UV et RMN, le greffage effectif de PDA sur le squelette de la PCL est confirmé par analyse RMN DOSY et SEC La quantification de la PDA dans le copolymère est effectuée par ATG et spectroscopie UV et la valeur est estimée entre 1 et 3 wt.%. Les analyses thermiques montrent une diminution de la cristallinité lors de fonctionnalisation. La mise en forme des polymères PCL-*g*-PDA est effectuée par compression à chaud pour générer un film d'épaisseur comprise en 400 entre 500 µm qui est par la suite coupé en forme de disques de diamètre de 0.6 mm ou d'implants rectangulaires de dimension 10 mm x 4 mm. Les études de dégradation *in vitro* montrent une dégradation lente et similaire des implants prototypes de PCL et PCL-*g*-PDA sur 110 jours. Enfin,

les études de cytotoxicités *in vitro* montrent la non-cytotoxicité des disques de PCL et PCL-*g*-PDA sur les cellules fibroblaste et rétinienne humaine. Les critères de dégradabilité et de biocompatibilité des implants de PCL-*g*-PDA sont ainsi validés. Les implants PCL et PCL-*g*-PDA ont été chargés avec de la dexaméthasone, un corticostéroïde approuvé par la FDA pour les applications oculaires, ou du chlorhydrate de ciprofloxacine, une fluoroquinolone. Le taux de chargement en actif a été défini à 30 % en masse par rapport à la quantité totale, et vérifié par analyse TGA qui a confirmé la teneur et l'homogénéité du film. Les études de libération *in vitro* montrent une libération prolongée de la dexaméthasone et du chlorhydrate de ciprofloxacine pendant 155 jours. Une amélioration de la rétention de la dexaméthasone est observée dans le cas de l'implant de PCL-*g*-PDA, et notamment par comparaison avec l'implant commercial Ozurdex™, et ce, malgré la faible proportion de PDA. Ceci confirme l'intérêt des implants PCL-*g*-PDA pour la libération prolongée de principes actifs dans le système oculaire. Les critères de haut taux de chargement d'actifs et de l'amélioration des propriétés des libérations par addition des unités PDA ont été validés. Les améliorations et perspectives concernent le contrôle et l'augmentation du pourcentage de PDA afin d'étudier les propriétés de libération, la transposition de l'échelle laboratoire à l'échelle industrielle comprenant l'étape de synthèse chimique et de fabrication des implants, ainsi que les études *in vivo.*

Dans le cadre de la stratégie des gélifications in situ, la synthèse a été effectuée en 3 étapes. Tout d'abord un copolymère à bloc amphiphile PCL-*b*-PEG-*b*-PCL a été synthétisé. Le bloc de PEG central est de masse molaire inférieure à 20 000 $g.mol^{-1}$ pour permettre la bio-élimination et les longueurs de chaînes de PCL-*b*-PEG-*b*-PCL influent sur la capacité de gélification du copolymère dans l'eau. Le ratio EG/CL s'étendait de 0,30 à 2,30 et les masses molaires de 4 300 à 9 400 $g.mol^{-1}$. Cependant aucune transition sol-gel n'avait été observée autour de 37°C. Un PCL-*b*-PEG-*b*-PCL gélifiant instantanément à température ambiante a été sélectionné et fonctionnalisé avec l'introduction de l'iode puis le PDA, dans les conditions similaires utilisées dans la stratégie précédente, pour obtenir (PDA-*g*-PCL)-*b*-PEG-*b*-(PCL-*g*-PDA). La proportion de PDA dans le copolymère brut est voisine de 40%, mais il reste de la PDA libre qu'il est très difficile d'éliminer. Les proportions respectives de PDA greffé et libre n'est pas calculable en raison de la structure inconnue de la PDA. Le (PDA-*g*-PCL)-*b*-PEG-*b*-(PCL-*g*-PDA) ainsi formé n'est pas soluble dans l'eau. Dans le but de concevoir des formulations solubles et injectables, les copolymères ont été solubilisés dans un solvant organique miscible à l'eau et non toxique pour l'œil, le PEG_{400}. La protéine (mAb) a été solubilisée dans de l'eau ou dans une solution tampon histidine dans lequel mAb est classiquement utilisée. Les formulations doivent assurer l'injectabilité à travers une aiguille ainsi que la stabilité de la protéine. Les études de compression montrent qu'une concentration en copolymère inférieure à 30% en masse est nécessaire pour permettre la solubilité et le passage à travers une aiguille de 30 gauges à température ambiante. Les études de stabilité

montrent que la proportion de PEG_{400} dans le mélange doit être inférieure ou égale à 50% en masse pour assurer la stabilité du mAb. Également, la protéine interagit, sans dénaturation, avec les copolymères (PDA-*g*-PCL)-*b*-PEG-*b*-(PCL-*g*-PDA). Les critères d'injectabilité la moins invasive possible et de stabilité du mAb dans les formulations sont validés. *In vitro,* des petits agrégats cotonneux sont formés en présence de PCL-*b*-PEG-*b*-PCL combiné ou non avec le (PDA-*g*-PCL)-*b*-PEG-*b*-(PCL-*g*-PDA). Les résultats de libération sont très différents de ceux obtenus avec PCL-g-PDA : en présence de (PDA-*g*-PCL)-*b*-PEG-*b*-(PCL-*g*-PDA) aucune libération n'est observée pendant 30 jours, alors que 80% de la protéine est libérée en 3 jours en présence de PCL-*b*-PEG-*b*-PCL, copolymère sans PDA. Ceci démontre la complexation de la protéine mAb avec la PDA. Cette proportion passe à 55% en présence d'un mélange PCL-*b*-PEG-*b*-PCL /(PDA-*g*-PCL)-*b*-PEG-*b*-(PCL-*g*-PDA) (2/1 w/w) où seule une partie de la protéine est complexée. Le critère de haut taux de chargement d'actifs est validé. En revanche, celui de la libération prolongée n'est pas concluant en raison de la présence des oligo-PDA libres qui interagissent probablement très fortement avec le mAb, modifiant ainsi les profils de libération. Les améliorations et perspectives possibles concernent la méthode de purification du copolymère (PDA-*g*-PCL)-*b*-PEG-*b*-(PCL-*g*-PDA) afin d'éliminer les résidus de sous-produit de synthèse et le PDA non greffé, les études de cytotoxicité *in vitro,* l'amélioration de la libération prolongée de la protéine ainsi que la transposition des synthèses et formulations à l'échelle industrielle.

Au cours de ce travail de thèse, des nouveaux copolymères à base de PDA ont été synthétisés afin de répondre aux défis de la délivrance prolongée de principes actifs dans le système intravitréen en administrant des polymères synthétiques, dégradables, et biocompatibles, par méthode la moins invasive possible. Ainsi, les implants solides de copolymères PCL-*g*-PDA sont utilisés et conviennent à la délivrance prolongée de petites molécules hydrophobes. Les formulations liquides à gélification *in situ* à base de (PDA-*g*-PCL)-*b*-PEG-*b*-(PCL-*g*-PDA) pour la libération de macromolécules telles que des protéines sont prometteuses. Les résultats obtenus ouvrent des perspectives pour la poursuite du développement industriel de systèmes d'administration novateurs pour la libération des principes actifs dans l'œil.

Nouveaux systèmes polymères à base de poly(dopamine) pour la délivrance prolongée de principes actifs par administration intravitréenne

Les maladies oculaires sont un problème de santé publique majeur. Actuellement, la recherche se focalise sur l'élaboration de formulations à base de polymère permettant la libération prolongée de principe actifs par administration intravitréenne pour le traitement des pathologies rétiniennes. A ce jour, un seul implant dégradable contenant une petite molécule est commercialisé, et aucune formulation polymère viable pour la libération de protéine n'est disponible sur le marché. L'objectif est de créer des implants solides et des solutions gélifiantes in-situ à base de poly(éthylène glycol) (PEG) et/ou poly(ε-caprolactone) (PCL) (approuvés par la Food and Drug Administration) fonctionnalisée par de la poly(dopamine) (PDA) (utilisé dans les traitements du cancer) en exploitant les interactions PDA – principe actif. Les implants à base de PCL et de PCL-*g*-PDA sont obtenus par compression à chaud. Les études *in vitro* montrent que les implants sont dégradables et sont non-cytotoxiques. Les cinétiques de libération sont modulées en ajustant le ratio entre la PCL et la PCL-*g*-PDA et en fonction de la nature de la molécule chargée. Les implants de PCL-*g*-PDA permettent une libération prolongée pendant plus de 5 mois sans retardement. Les solutions gélifiantes à base de PCL-*b*-PEG-*b*-PCL et/ou (PCL-*g*-PDA)-*b*-PEG-*b*-(PCL-*g*-PDA) sont formulées dans du PEG de faible masse molaire et de l'eau afin de solubiliser les copolymères et l'anticorps. Elles permettent l'injectabilité à travers une fine aiguille, la stabilité des composés. Les études de libération *in vitro* montrent une libération de l'anticorps en 3 jours. Ces deux stratégies ouvrent des perspectives quant à la poursuite du développement industriel de systèmes polymère novateur d'administration oculaire pour la libération des principes actifs.

Mots clés : poly(dopamine), poly(ε-caprolactone), poly(éthylène glycol), copolymère, délivrance prolongée, œil, administration intravitréenne, injection, implant, dépôts in situ, principe actif

New copolymers based on poly(dopamine) for the sustained delivery of active pharmaceutical ingredient to the eye by intravitreal administration

The ocular diseases are a major public health issue. Currently, research is focusing on formulations providing sustained delivery of active pharmaceutical ingredient (APIs) using intravitreal administration for the treatment of retinal pathologies. At present, only one biodegradable implant loaded with small API is commercially available, and no commercial polymeric formulation is found for the delivery of large API. Consequently, this project focuses on the development of new implants or in-situ gelling formulations based on poly(ethylene glycol) (PEG) and/or poly(ε-caprolactone) (PCL) (approved by the Food and Drug Administration) functionalized with poly(dopamine) (PDA) (already used in cancer treatment) by exploiting PDA-API interactions. The PCL and PCL-*g*-PDA implants are obtained by hot compression. The *in vitro* studies show the degradability and the non-cytotoxicity of the implants. To modulate the release kinetics, the PCL and PCL-g-PDA proportion and the nature of the small molecule are adjusted. The PCL-*g*-PDA implants allow the release over 5 months without lag time. The liquid formulations based on PCL-*b*-PEG-*b*-PCL and/or (PCL-*g*-PDA)-*b*-PEG-*b*-(PCL-*g*-PDA) are formulated in small molecular weight PEG and water to enhance the solubility of the components. They allow injectability through small needle, stability of the antibody. The *in vitro* release studies show the release of the antibody within 3 days. The two strategies open perspectives for the development of innovative ocular drug delivery copolymer systems.

Keywords: poly(dopamine), poly(ε-caprolactone), poly(ethylene glycol), copolymer, sustained delivery, eye, intravitreal administration, injection, implant, in situ depots, active pharmaceutical ingredient